

1994

Heat transfer and fluid flow in spray evaporators with application to reducing refrigerant inventory

Shane Alan Moeykens
Iowa State University

Follow this and additional works at: <https://lib.dr.iastate.edu/rtd>

 Part of the [Mechanical Engineering Commons](#)

Recommended Citation

Moeykens, Shane Alan, "Heat transfer and fluid flow in spray evaporators with application to reducing refrigerant inventory" (1994).
Retrospective Theses and Dissertations. 10498.
<https://lib.dr.iastate.edu/rtd/10498>

This Dissertation is brought to you for free and open access by the Iowa State University Capstones, Theses and Dissertations at Iowa State University Digital Repository. It has been accepted for inclusion in Retrospective Theses and Dissertations by an authorized administrator of Iowa State University Digital Repository. For more information, please contact digirep@iastate.edu.

INFORMATION TO USERS

This manuscript has been reproduced from the microfilm master. UMI films the text directly from the original or copy submitted. Thus, some thesis and dissertation copies are in typewriter face, while others may be from any type of computer printer.

The quality of this reproduction is dependent upon the quality of the copy submitted. Broken or indistinct print, colored or poor quality illustrations and photographs, print bleedthrough, substandard margins, and improper alignment can adversely affect reproduction.

In the unlikely event that the author did not send UMI a complete manuscript and there are missing pages, these will be noted. Also, if unauthorized copyright material had to be removed, a note will indicate the deletion.

Oversize materials (e.g., maps, drawings, charts) are reproduced by sectioning the original, beginning at the upper left-hand corner and continuing from left to right in equal sections with small overlaps. Each original is also photographed in one exposure and is included in reduced form at the back of the book.

Photographs included in the original manuscript have been reproduced xerographically in this copy. Higher quality 6" x 9" black and white photographic prints are available for any photographs or illustrations appearing in this copy for an additional charge. Contact UMI directly to order.

U·M·I

University Microfilms International
A Bell & Howell Information Company
300 North Zeeb Road, Ann Arbor, MI 48106-1346 USA
313/761-4700 800/521-0600

Order Number 9503583

**Heat transfer and fluid flow in spray evaporators with
application to reducing refrigerant inventory**

Moeykens, Shane Alan, Ph.D.

Iowa State University, 1994

U·M·I
300 N. Zeeb Rd.
Ann Arbor, MI 48106

**Heat transfer and fluid flow in spray evaporators with
application to reducing refrigerant inventory**

by

Shane Alan Moeykens

**A Dissertation Submitted to the
Graduate Faculty in Partial Fulfillment of the
Requirements for the Degree of
DOCTOR OF PHILOSOPHY**

**Department: Mechanical Engineering
Major: Mechanical Engineering**

Approved:

Signature was redacted for privacy.

**_____
In Charge of Major Work**

Signature was redacted for privacy.

**_____
For the Major Department**

Signature was redacted for privacy.

**_____
For the Graduate College**

**Iowa State University
Ames, Iowa**

1994

TABLE OF CONTENTS

| | |
|--|---------------|
| LIST OF FIGURES | vi |
| LIST OF TABLES | xi |
| NOMENCLATURE | xxiv |
| ABSTRACT..... | xxviii |
| CHAPTER 1. INTRODUCTION..... | 1 |
| Background..... | 1 |
| Research Program..... | 3 |
| CHAPTER 2. LITERATURE REVIEW | 9 |
| Single-Tube Heat Transfer Studies..... | 10 |
| Tube Bundle Heat Transfer Studies..... | 13 |
| Falling-Film Heat Transfer Models..... | 16 |
| Lubricant Effects | 24 |
| CHAPTER 3. MULTI-TUBE TEST FACILITY | 29 |
| Facility Description..... | 29 |
| Experimental Methods..... | 37 |
| CHAPTER 4. TUBE BUNDLE TEST FACILITY..... | 41 |
| Facility Description..... | 41 |
| Experimental Procedure..... | 50 |

| | |
|--|------------|
| CHAPTER 5. DATA ANALYSIS | 59 |
| Data Reduction..... | 59 |
| Experimental Uncertainty..... | 64 |
| Data Analysis..... | 70 |
| CHAPTER 6. SOLUBILITY ANALYSIS | 73 |
| Solubility Test Facility | 74 |
| Experimental Procedure..... | 75 |
| Solubility Data..... | 76 |
| CHAPTER 7. MULTI-TUBE TEST FACILITY | |
| PLAIN-SURFACE RESULTS..... | 81 |
| Multi-Tube Test Facility Accuracy..... | 81 |
| Heat Transfer Results | 85 |
| Conclusions | 90 |
| CHAPTER 8. MULTI-TUBE TEST FACILITY SURFACE | |
| ENHANCEMENT AND OIL EFFECTS | 95 |
| Heat Transfer Results | 96 |
| Conclusions | 108 |
| CHAPTER 9. BUNDLE TEST FACILITY NOZZLE | |
| CONFIGURATION GEOMETRY EFFECTS | 115 |
| Heat Transfer Results | 117 |
| Conclusions | 129 |
| CHAPTER 10. BUNDLE TEST FACILITY SURFACE | |
| ENHANCEMENT, BUNDLE GEOMETRY, | |
| AND SUPPLY RATE EFFECTS..... | 131 |
| Heat Transfer Results | 132 |
| Conclusions | 147 |

| | |
|--|------------|
| CHAPTER 11. BUNDLE TEST FACILITY HFC-134a AND HCFC-22 RESULTS INCLUDING LUBRICANT EFFECTS | 149 |
| Heat Transfer Results | 151 |
| Conclusions | 168 |
| CHAPTER 12. BUNDLE TEST FACILITY HCFC-123 RESULTS INCLUDING LUBRICANT EFFECTS | 171 |
| Heat Transfer Results | 173 |
| Conclusions | 189 |
| CHAPTER 13. DESIGN CORRELATION COMPARISON | 191 |
| Correlations Comparison | 192 |
| Conclusions | 198 |
| CHAPTER 14. CONCLUSIONS AND RECOMMENDATIONS | 201 |
| Conclusions | 201 |
| Recommendations | 207 |
| BIBLIOGRAPHY | 209 |
| ACKNOWLEDGMENTS | 214 |
| APPENDIX A. MULTI-TUBE TEST FACILITY TABULATED DATA | 215 |
| APPENDIX B. BUNDLE TEST FACILITY HFC-134a TABULATED DATA | 225 |
| APPENDIX C. BUNDLE TEST FACILITY HCFC-22 TABULATED DATA | 247 |
| APPENDIX D. BUNDLE TEST FACILITY HCFC-123 TABULATED DATA | 251 |

APPENDIX E. HEAT TRANSFER COEFFICIENT PREDICTION
MODEL DEVELOPMENT 261

LIST OF FIGURES

| | |
|--|----|
| Figure 3.1: Multi-tube test facility schematic | 30 |
| Figure 3.2: Thermocouple location diagram for the 19.1 mm diameter test-tubes..... | 33 |
| Figure 4.1: Bundle Test Facility Schematic..... | 42 |
| Figure 4.2: Triangular-pitch tube bundle geometry | 44 |
| Figure 4.3: Square-pitch tube bundle geometry..... | 45 |
| Figure 4.4: Wilson plot data for the Tu-B tube with turbulator installed..... | 55 |
| Figure 4.5: Wilson plot data for the plain tube with turbulator installed..... | 56 |
| Figure 6.1: HFC-134a/polyol ester oil solubility data | 77 |
| Figure 6.2: HCFC-22/alkyl-benzene oil solubility data | 78 |
| Figure 6.3: HCFC-123/naphthenic mineral oil solubility data | 79 |
| Figure 7.1: Heat flux vs. excess temperature (external free convection, flooded evaporator; $T_{\text{sat}} = 2.0 \text{ }^\circ\text{C}$, tube diameter = 19.1 mm)..... | 83 |
| Figure 7.2: Heat transfer coefficient vs. heat flux (flooded evaporator, tube diameter = 19.1 mm | 84 |
| Figure 7.3: Heat transfer coefficient vs. heat flux, single-tube test ($T_{\text{sat}} = 2.0 \text{ }^\circ\text{C}$; tube diameter = 12.7 mm) | 86 |
| Figure 7.4: Heat transfer coefficient vs. heat flux, multi-tube test ($T_{\text{sat}} = 2.0 \text{ }^\circ\text{C}$; tube diameter = 12.7 mm) | 87 |
| Figure 7.5: Heat transfer coefficient vs. heat flux ($T_{\text{sat}} = 2.0 \text{ }^\circ\text{C}$) | 89 |

| | |
|--|-----|
| Figure 7.6: Heat transfer coefficient vs. heat flux ($T_{\text{sat}} = 2.0$ °C; tube diameter = 19.1 mm) | 91 |
| Figure 7.7: Heat transfer coefficient vs. heat flux ($T_{\text{sat}} = -14.0$ °C; tube diameter = 12.7 mm) | 92 |
| Figure 8.1: Heat transfer coefficient vs. heat flux ($T_{\text{sat}} = 2.0$ °C; pure HFC-134a, enhanced surface results)..... | 98 |
| Figure 8.2: Heat transfer coefficient vs. heat flux ($T_{\text{sat}} = 2.0$ °C; pure HFC-134a, low-finned surface results)..... | 99 |
| Figure 8.3: Surface enhancement factor vs. heat flux ($T_{\text{sat}} = 2.0$ °C; pure HFC-134a)..... | 100 |
| Figure 8.4: Heat transfer coefficient vs. heat flux ($P_{\text{sat}} = 314.5$ kPa; 160 SUS oil, plain tube)..... | 102 |
| Figure 8.5: Lubricant enhancement factor vs. heat flux ($P_{\text{sat}} = 314.5$ kPa; 160 SUS oil, plain tube) | 103 |
| Figure 8.6: Heat transfer coefficient vs. heat flux ($P_{\text{sat}} = 314.5$ kPa; 160 SUS oil, W-40 fpi tube)..... | 104 |
| Figure 8.7: Lubricant enhancement factor vs. heat flux ($P_{\text{sat}} = 314.5$ kPa; 160 SUS oil, W-40 fpi tube)..... | 105 |
| Figure 8.8: Heat transfer coefficient vs. heat flux ($P_{\text{sat}} = 314.5$ kPa; 160 SUS oil, Tu-Cii tube) | 106 |
| Figure 8.9: Lubricant enhancement factor vs. heat flux ($P_{\text{sat}} = 314.5$ kPa; 160 SUS oil, Tu-Cii tube) | 107 |
| Figure 8.10: Heat transfer coefficient vs. heat flux ($P_{\text{sat}} = 314.5$ kPa; 340 SUS oil, W-40 fpi tube)..... | 109 |
| Figure 8.11: Lubricant enhancement factor vs. heat flux ($P_{\text{sat}} = 314.5$ kPa; 340 SUS oil, W-40 fpi tube)..... | 110 |
| Figure 8.12: Heat transfer coefficient vs. heat flux ($P_{\text{sat}} = 314.5$ kPa; 340 SUS oil, Tu-Cii tube) | 111 |

| | |
|--|-----|
| Figure 8.13: Lubricant enhancement factor vs. heat flux ($P_{\text{sat}} = 314.5$ kPa; 340 SUS oil, Tu-Cii tube) | 112 |
| Figure 9.1: Heat transfer coefficient vs. heat flux ($T_{\text{sat}} = 2.0$ °C; M.F.R. = 25 kg/min) | 118 |
| Figure 9.2: Heat transfer coefficient vs. heat flux ($T_{\text{sat}} = 2.0$ °C; square and circular nozzle plume comparison) | 119 |
| Figure 9.3: Row performance factor variation with row depth ($T_{\text{sat}} = 2.0$ °C; M.F.R. = 25 kg/min, 17WHCRC & 17WLCRC configurations)..... | 121 |
| Figure 9.4: Row performance factor variation with row depth ($T_{\text{sat}} = 2.0$ °C; M.F.R. = 25 kg/min, 24WHCRC & 24WLCRC configurations)..... | 122 |
| Figure 9.5: Row performance factor variation with row depth ($T_{\text{sat}} = 2.0$ °C; M.F.R. = 25 kg/min, 24WHSQR & 24WLSQR configurations)..... | 123 |
| Figure 9.6: Row performance factor variation with row depth ($T_{\text{sat}} = 2.0$ °C; M.F.R. = 25 kg/min, 30WHSQR & 30WHCRC configurations) | 124 |
| Figure 9.7: Row performance factor variation with row depth ($T_{\text{sat}} = 2.0$ °C; M.F.R. = 45 kg/min, 30WHSQR & 30WHCRC configurations) | 125 |
| Figure 9.8: Heat transfer coefficient vs. heat flux ($T_{\text{sat}} = 2.0$ °C; pool boiling comparison)..... | 128 |
| Figure 10.1: Heat transfer coefficient vs. heat flux ($T_{\text{sat}} = 2.0$ °C; W-40 fpi and plain surface, triangular-pitch bundles | 134 |
| Figure 10.2: Heat transfer coefficient vs. heat flux ($T_{\text{sat}} = 2.0$ °C; W-SC and plain surface, triangular-pitch bundles | 135 |
| Figure 10.3: Heat transfer coefficient vs. heat flux ($T_{\text{sat}} = 2.0$ °C; Tu-Cii and plain surface, triangular-pitch bundles | 136 |
| Figure 10.4: Heat transfer coefficient vs. heat flux ($T_{\text{sat}} = 2.0$ °C; Tu-B and plain surface, triangular-pitch bundles | 137 |
| Figure 10.5: Heat transfer coefficient vs. heat flux ($T_{\text{sat}} = 2.0$ °C; Tu-B, triangular and square-pitch bundles | 139 |

| | |
|---|-----|
| Figure 10.6: Heat transfer coefficient vs. heat flux ($T_{\text{sat}} = 2.0 \text{ }^\circ\text{C}$; pool boiling comparison, triangular-pitch geometry)..... | 145 |
| Figure 10.7: Heat flux vs. LMTD ($T_{\text{sat}} = 2.0 \text{ }^\circ\text{C}$; pool boiling comparison, triangular-pitch geometry)..... | 146 |
| Figure 11.1: Heat transfer coefficient vs. heat flux ($P_{\text{sat}} = 314.5 \text{ kPa}$; oil effects testing, plain surface bundle)..... | 152 |
| Figure 11.2: Heat transfer coefficient vs. heat flux ($P_{\text{sat}} = 314.5 \text{ kPa}$; oil effects testing, W-40 fpi bundle)..... | 153 |
| Figure 11.3: Heat transfer coefficient vs. heat flux ($P_{\text{sat}} = 314.5 \text{ kPa}$; oil effects testing, W-SC bundle)..... | 154 |
| Figure 11.4: Heat transfer coefficient vs. heat flux ($P_{\text{sat}} = 314.5 \text{ kPa}$; oil effects testing, Tu-B bundle)..... | 155 |
| Figure 11.5: Surface enhancement factor vs. bundle load ($P_{\text{sat}} = 314.5 \text{ kPa}$; oil effects testing, M.F.R. = 15 kg/min)..... | 157 |
| Figure 11.6: Surface enhancement factor vs. bundle load ($P_{\text{sat}} = 314.5 \text{ kPa}$; oil effects testing, M.F.R. = 35 kg/min)..... | 158 |
| Figure 11.7: Lubricant enhancement factor vs. bundle load ($P_{\text{sat}} = 314.5 \text{ kPa}$; oil effects testing, M.F.R. = 15 kg/min)..... | 159 |
| Figure 11.8: Lubricant enhancement factor vs. bundle load ($P_{\text{sat}} = 314.5 \text{ kPa}$; oil effects testing, M.F.R. = 35 kg/min)..... | 160 |
| Figure 11.9: Heat transfer coefficient vs. heat flux (plain surface bundle, HCFC-22 and HFC-134a results, M.F.R. = 15 kg/min)..... | 165 |
| Figure 11.10: Heat transfer coefficient vs. heat flux (Tu-B bundle, HCFC-22 and HFC-134a results, M.F.R. = 15 kg/min)..... | 166 |
| Figure 11.11: Lubricant enhancement factor vs. bundle load (HCFC-22 and HFC-134a results, M.F.R. = 15 kg/min)..... | 167 |
| Figure 12.1: Heat transfer coefficient vs. heat flux ($P_{\text{sat}} = 35.7 \text{ kPa}$; 24WDCRC & 30WDCRC configurations)..... | 175 |

| | |
|--|-----|
| Figure 12.2: Heat transfer coefficient vs. heat flux ($P_{\text{sat}} = 35.7$ kPa; lubricant effects testing, plain surface bundle) | 177 |
| Figure 12.3: Heat transfer coefficient vs. heat flux ($P_{\text{sat}} = 35.7$ kPa; lubricant effects testing, Tu-Cii bundle) | 178 |
| Figure 12.4: Heat transfer coefficient vs. heat flux ($P_{\text{sat}} = 35.7$ kPa; lubricant effects testing, Tu-B bundle) | 179 |
| Figure 12.5: Surface enhancement factor vs. bundle load ($P_{\text{sat}} = 35.7$ kPa; lubricant effects testing, Tu-Cii bundle) | 182 |
| Figure 12.6: Surface enhancement factor vs. bundle load ($P_{\text{sat}} = 35.7$ kPa; lubricant effects testing, Tu-B bundle) | 183 |
| Figure 12.7: Lubricant enhancement factor vs. bundle load ($P_{\text{sat}} = 35.7$ kPa; plain surface bundle) | 185 |
| Figure 12.8: Lubricant enhancement factor vs. bundle load ($P_{\text{sat}} = 35.7$ kPa; Tu-Cii bundle) | 186 |
| Figure 12.9: Lubricant enhancement factor vs. bundle load ($P_{\text{sat}} = 35.7$ kPa; Tu-B bundle) | 187 |
| Figure 13.1: Heat transfer coefficient vs. heat flux ($P_{\text{sat}} = 314.5$ kPa; plain-surface bundle data, HFC-134a, M.F.R. = 15 kg/min)..... | 194 |
| Figure 13.2: Heat transfer coefficient vs. heat flux ($P_{\text{sat}} = 314.5$ kPa; plain-surface bundle data, HFC-134a, M.F.R. = 35 kg/min)..... | 195 |
| Figure 13.3: Heat transfer coefficient vs. heat flux ($P_{\text{sat}} = 314.5$ kPa; plain-surface bundle data, HFC-134a) | 197 |
| Figure 13.4: Heat transfer coefficient vs. heat flux ($P_{\text{sat}} = 35.7$ kPa; plain-surface bundle data, HCFC-123) | 199 |

LIST OF TABLES

| | |
|---|----|
| Table 2.1: Correlation constants accompanying Equations 2.13 and 2.14 | 22 |
| Table 3.1: Geometric specifications for tubes tested on the multi-tube test facility | 34 |
| Table 4.1: Geometry specifications for the tubes tested on the bundle test facility | 46 |
| Table 4.2: Geometric specifications for the nozzle configurations used on the bundle test facility | 49 |
| Table 4.3: Bundle test facility, collector test results | 57 |
| Table 5.1: Multi-tube test facility shell-side heat transfer coefficient experimental uncertainty | 66 |
| Table 5.2: Pure HFC-134 testing shell-side heat transfer coefficient uncertainty, bundle test facility | 68 |
| Table 5.3: HFC-134a and HCFC-22 lubricant effects testing shell-side heat transfer coefficient uncertainty, bundle test facility | 69 |
| Table 5.4: HCFC-123 lubricant effects testing shell-side heat transfer coefficient uncertainty, bundle test facility | 69 |
| Table 6.1: Solubility data correlation constants accompanying Equation 6.1 | 80 |
| Table 6.2: Lubricant effects upon saturation temperature for each refrigerant | 80 |
| Table 8.1: Multi-tube test facility operating parameters | 96 |
| Table 8.2: Test-section recirculation ratios and tube overfeed ratios | 96 |

| | |
|--|-----|
| Table 9.1: Bundle test facility operating parameters, nozzle configuration geometry effects testing | 116 |
| Table 9.2: Bundle overfeed ratios for the tests conducted with known collector test fractions, nozzle configuration geometry effects testing..... | 116 |
| Table 9.3: Top and bottom row shell-side heat transfer coefficients from the 17WLCRC, 24WLCRC, and 30WHCRC nozzle configurations..... | 126 |
| Table 10.1: Bundle test facility operating parameters, HFC-134a testing..... | 132 |
| Table 10.2: Bundle overfeed ratios for the triangular and square-pitch bundle geometries and the 30WHCRC nozzle configuration, HFC-134a testing..... | 133 |
| Table 10.3: Surface enhancement factors for the triangular-pitch geometry tests, HFC-134a results | 138 |
| Table 10.4: Row performance factor variation with row depth, triangular-pitch geometry, HFC-134a results | 143 |
| Table 10.5: Row performance factor variation with row depth, square-pitch geometry, HFC-134a results | 144 |
| Table 11.1: Bundle test facility operating parameters, HFC-134a and HCFC-22 lubricant effects testing..... | 150 |
| Table 11.2: Bundle overfeed ratios for the 30WHCRC nozzle configuration with refrigerants HFC-134a and HCFC-22..... | 150 |
| Table 11.3: Row performance factor variation with row depth, HFC-134a lubricant effects results, 15 kg/min refrigerant supply rate | 162 |
| Table 11.4: Row performance factor variation with row depth, HFC-134a lubricant effects results, 35 kg/min refrigerant supply rate | 163 |
| Table 11.5: Row performance factor variation with row depth, HCFC-22 lubricant effects results, 15 kg/min refrigerant supply rate | 168 |
| Table 12.1: Bundle test facility operating parameters, HCFC-123 testing | 173 |
| Table 12.2: Bundle overfeed ratios for the 24WDCRC and 30WDCRC nozzle configurations, HCFC-123 testing | 173 |

| | | |
|-------------|---|-----|
| Table 12.3: | Row performance factor variation with row depth, pure HCFC-123 results | 188 |
| Table 12.4: | Row performance factor variation with row depth, HCFC-123 lubricant effects results | 188 |
| Table A.1 | Refrigerant: HFC-134a, Plain Surface, Diameter: 19.1 mm, Pool Boiling, T-sat: 2.0 °C, Pure Refrigerant Testing | 216 |
| Table A.2 | Refrigerant: HFC-134a, W-26 fpi Surface, Diameter: 19.1 mm, Film Feed Supply Rate: 1.26E-02 kg/(s*m), T-sat: 2.0 °C, Pure Refrigerant Testing..... | 216 |
| Table A.3 | Refrigerant: HFC-134a, Tu-B Surface, Diameter: 19.1 mm, Film Feed Supply Rate: 1.26E-02 kg/(s*m), T-sat: 2.0 °C, Pure Refrigerant Testing..... | 216 |
| Table A.4 | Refrigerant: HFC-134a, W-SE Surface, Diameter: 19.1 mm, Film Feed Supply Rate: 1.26E-02 kg/(s*m), T-sat: 2.0 °C, Pure Refrigerant Testing..... | 217 |
| Table A.5 | Refrigerant: HFC-134a, W-SC Surface, Diameter: 19.1 mm, Film Feed Supply Rate: 1.26E-02 kg/(s*m), T-sat: 2.0 °C, Pure Refrigerant Testing..... | 217 |
| Table A.6 | Refrigerant: HFC-134a, Plain Surface, Diameter: 19.1 mm, Film Feed Supply Rate: 1.26E-02 kg/(s*m), P-sat: 314.5 kPa, Lubricant Concentration: 0.0 % (160 SUS oil testing) | 217 |
| Table A.7 | Refrigerant: HFC-134a, Plain Surface, Diameter: 19.1 mm, Film Feed Supply Rate: 1.26E-02 kg/(s*m), P-sat: 314.5 kPa, Lubricant Concentration: 1.0 % (160 SUS oil testing) | 218 |
| Table A.8 | Refrigerant: HFC-134a, Plain Surface, Diameter: 19.1 mm, Film Feed Supply Rate: 1.26E-02 kg/(s*m), P-sat: 314.5 kPa, Lubricant Concentration: 2.0 % (160 SUS oil testing) | 218 |
| Table A.9 | Refrigerant: HFC-134a, Plain Surface, Diameter: 19.1 mm, Film Feed Supply Rate: 1.26E-02 kg/(s*m), P-sat: 314.5 kPa, Lubricant Concentration: 3.0 % (160 SUS oil testing) | 218 |

| | | |
|------------|--|-----|
| Table A.10 | Refrigerant: HFC-134a, W-40 fpi Surface, Diameter: 19.1 mm, Film Feed Supply Rate: 1.26E-02 kg/(s*m), P-sat: 314.5 kPa, Lubricant Concentration: 0.0 % (160 SUS oil testing) | 219 |
| Table A.11 | Refrigerant: HFC-134a, W-40 fpi Surface, Diameter: 19.1 mm, Film Feed Supply Rate: 1.26E-02 kg/(s*m), P-sat: 314.5 kPa, Lubricant Concentration: 1.0 % (160 SUS oil testing) | 219 |
| Table A.12 | Refrigerant: HFC-134a, W-40 fpi Surface, Diameter: 19.1 mm, Film Feed Supply Rate: 1.26E-02 kg/(s*m), P-sat: 314.5 kPa, Lubricant Concentration: 2.0 % (160 SUS oil testing) | 219 |
| Table A.13 | Refrigerant: HFC-134a, W-40 fpi Surface, Diameter: 19.1 mm, Film Feed Supply Rate: 1.26E-02 kg/(s*m), P-sat: 314.5 kPa, Lubricant Concentration: 3.0 % (160 SUS oil testing) | 220 |
| Table A.14 | Refrigerant: HFC-134a, Tu-Cii Surface, Diameter: 19.1 mm, Film Feed Supply Rate: 1.26E-02 kg/(s*m), P-sat: 314.5 kPa, Lubricant Concentration: 0.0 % (160 SUS oil testing) | 220 |
| Table A.15 | Refrigerant: HFC-134a, Tu-Cii Surface, Diameter: 19.1 mm, Film Feed Supply Rate: 1.26E-02 kg/(s*m), P-sat: 314.5 kPa, Lubricant Concentration: 1.0 % (160 SUS oil testing) | 220 |
| Table A.16 | Refrigerant: HFC-134a, Tu-Cii Surface, Diameter: 19.1 mm, Film Feed Supply Rate: 1.26E-02 kg/(s*m), P-sat: 314.5 kPa, Lubricant Concentration: 2.0 % (160 SUS oil testing) | 221 |
| Table A.17 | Refrigerant: HFC-134a, Tu-Cii Surface, Diameter: 19.1 mm, Film Feed Supply Rate: 1.26E-02 kg/(s*m), P-sat: 314.5 kPa, Lubricant Concentration: 3.0 % (160 SUS oil testing) | 221 |
| Table A.18 | Refrigerant: HFC-134a, W-40 fpi Surface, Diameter: 19.1 mm, Film Feed Supply Rate: 1.26E-02 kg/(s*m), P-sat: 314.5 kPa, Lubricant Concentration: 0.0 % (340 SUS oil testing) | 221 |
| Table A.19 | Refrigerant: HFC-134a, W-40 fpi Surface, Diameter: 19.1 mm, Film Feed Supply Rate: 1.26E-02 kg/(s*m), P-sat: 314.5 kPa, Lubricant Concentration: 0.5 % (340 SUS oil testing) | 222 |

| | | |
|------------|--|-----|
| Table A.20 | Refrigerant: HFC-134a, W-40 fpi Surface, Diameter: 19.1 mm, Film Feed Supply Rate: 1.26E-02 kg/(s*m), P-sat: 314.5 kPa, Lubricant Concentration: 1.0 % (340 SUS oil testing) | 222 |
| Table A.21 | Refrigerant: HFC-134a, W-40 fpi Surface, Diameter: 19.1 mm, Film Feed Supply Rate: 1.26E-02 kg/(s*m), P-sat: 314.5 kPa, Lubricant Concentration: 3.0 % (340 SUS oil testing) | 222 |
| Table A.22 | Refrigerant: HFC-134a, W-40 fpi Surface, Diameter: 19.1 mm, Film Feed Supply Rate: 1.26E-02 kg/(s*m), P-sat: 314.5 kPa, Lubricant Concentration: 5.0 % (340 SUS oil testing) | 223 |
| Table A.23 | Refrigerant: HFC-134a, Tu-Cii Surface, Diameter: 19.1 mm, Film Feed Supply Rate: 1.26E-02 kg/(s*m), P-sat: 314.5 kPa, Lubricant Concentration: 0.0 % (340 SUS oil testing) | 223 |
| Table A.24 | Refrigerant: HFC-134a, Tu-Cii Surface, Diameter: 19.1 mm, Film Feed Supply Rate: 1.26E-02 kg/(s*m), P-sat: 314.5 kPa, Lubricant Concentration: 0.5 % (340 SUS oil testing) | 223 |
| Table A.25 | Refrigerant: HFC-134a, Tu-Cii Surface, Diameter: 19.1 mm, Film Feed Supply Rate: 1.26E-02 kg/(s*m), P-sat: 314.5 kPa, Lubricant Concentration: 1.0 % (340 SUS oil testing) | 224 |
| Table A.26 | Refrigerant: HFC-134a, Tu-Cii Surface, Diameter: 19.1 mm, Film Feed Supply Rate: 1.26E-02 kg/(s*m), P-sat: 314.5 kPa, Lubricant Concentration: 3.0 % (340 SUS oil testing) | 224 |
| Table A.27 | Refrigerant: HFC-134a, Tu-Cii Surface, Diameter: 19.1 mm, Film Feed Supply Rate: 1.26E-02 kg/(s*m), P-sat: 314.5 kPa, Lubricant Concentration: 5.0 % (340 SUS oil testing) | 224 |
| Table B.1 | Refrigerant: HFC-134a, Plain Surface, Triangular Pitch, Nozzle Configuration: 30WHCRC, Refrigerant Supply Rate: 15 kg/min, Pure Refrigerant Data..... | 227 |
| Table B.2 | Refrigerant: HFC-134a, Plain Surface, Triangular Pitch, Nozzle Configuration: 30WHCRC, Refrigerant Supply Rate: 35 kg/min, Pure Refrigerant Data..... | 227 |

| | | |
|------------|--|-----|
| Table B.3 | Refrigerant: HFC-134a, W-40 fpi surface, Triangular Pitch, Nozzle Configuration: 30WHCRC, Refrigerant Supply Rate: 15 kg/min, Pure Refrigerant Data..... | 228 |
| Table B.4 | Refrigerant: HFC-134a, W-40 fpi surface, Triangular Pitch, Nozzle Configuration: 30WHCRC, Refrigerant Supply Rate: 25 kg/min, Pure Refrigerant Data..... | 228 |
| Table B.5 | Refrigerant: HFC-134a, W-40 fpi surface, Triangular Pitch, Nozzle Configuration: 30WHCRC, Refrigerant Supply Rate: 35 kg/min, Pure Refrigerant Data..... | 229 |
| Table B.6 | Refrigerant: HFC-134a, W-40 fpi surface, Triangular Pitch, Nozzle Configuration: 30WHCRC, Refrigerant Supply Rate: 45 kg/min, Pure Refrigerant Data..... | 229 |
| Table B.7 | Refrigerant: HFC-134a, W-SC surface, Triangular Pitch, Nozzle Configuration: 30WHCRC, Refrigerant Supply Rate: 15 kg/min, Pure Refrigerant Data..... | 230 |
| Table B.8 | Refrigerant: HFC-134a, W-SC surface, Triangular Pitch, Nozzle Configuration: 30WHCRC, Refrigerant Supply Rate: 25 kg/min, Pure Refrigerant Data..... | 230 |
| Table B.9 | Refrigerant: HFC-134a, W-SC surface, Triangular Pitch, Nozzle Configuration: 30WHCRC, Refrigerant Supply Rate: 35 kg/min, Pure Refrigerant Data..... | 231 |
| Table B.10 | Refrigerant: HFC-134a, W-SC surface, Triangular Pitch, Nozzle Configuration: 30WHCRC, Refrigerant Supply Rate: 45 kg/min, Pure Refrigerant Data..... | 231 |
| Table B.11 | Refrigerant: HFC-134a, Tu-Cii surface, Triangular Pitch, Nozzle Configuration: 30WHCRC, Refrigerant Supply Rate: 15 kg/min, Pure Refrigerant Data..... | 232 |
| Table B.12 | Refrigerant: HFC-134a, Tu-Cii surface, Triangular Pitch, Nozzle Configuration: 30WHCRC, Refrigerant Supply Rate: 25 kg/min, Pure Refrigerant Data..... | 232 |

| | | |
|------------|--|-----|
| Table B.13 | Refrigerant: HFC-134a, Tu-Cii surface, Triangular Pitch, Nozzle Configuration: 30WHCRC, Refrigerant Supply Rate: 35 kg/min, Pure Refrigerant Data..... | 233 |
| Table B.14 | Refrigerant: HFC-134a, Tu-Cii surface, Triangular Pitch, Nozzle Configuration: 30WHCRC, Refrigerant Supply Rate: 45 kg/min, Pure Refrigerant Data..... | 233 |
| Table B.15 | Refrigerant: HFC-134a, Tu-B surface, Triangular Pitch, Nozzle Configuration: 30WHCRC, Refrigerant Supply Rate: 15 kg/min, Pure Refrigerant Data..... | 234 |
| Table B.16 | Refrigerant: HFC-134a, Tu-B surface, Triangular Pitch, Nozzle Configuration: 30WHCRC, Refrigerant Supply Rate: 25 kg/min, Pure Refrigerant Data..... | 234 |
| Table B.17 | Refrigerant: HFC-134a, Tu-B surface, Triangular Pitch, Nozzle Configuration: 30WHCRC, Refrigerant Supply Rate: 35 kg/min, Pure Refrigerant Data..... | 235 |
| Table B.18 | Refrigerant: HFC-134a, Tu-B surface, Triangular Pitch, Nozzle Configuration: 30WHCRC, Refrigerant Supply Rate: 45 kg/min, Pure Refrigerant Data..... | 235 |
| Table B.19 | Refrigerant: HFC-134a, Tu-B surface, Square Pitch, Nozzle Configuration: 30WHCRC, Refrigerant Supply Rate: 15 kg/min, Pure Refrigerant Data..... | 236 |
| Table B.20 | Refrigerant: HFC-134a, Tu-B surface, Square Pitch, Nozzle Configuration: 30WHCRC, Refrigerant Supply Rate: 25 kg/min, Pure Refrigerant Data..... | 236 |
| Table B.21 | Refrigerant: HFC-134a, Tu-B surface, Square Pitch, Nozzle Configuration: 30WHCRC, Refrigerant Supply Rate: 35 kg/min, Pure Refrigerant Data..... | 237 |
| Table B.22 | Refrigerant: HFC-134a, Tu-B surface, Square Pitch, Nozzle Configuration: 30WHCRC, Refrigerant Supply Rate: 45 kg/min, Pure Refrigerant Data..... | 237 |

| | | |
|------------|--|-----|
| Table B.23 | Refrigerant: HFC-134a, W-40 fpi surface, Triangular Pitch, Nozzle Configuration: 17WHCRC, Refrigerant Supply Rate: 25 kg/min, Pure Refrigerant Data..... | 238 |
| Table B.24 | Refrigerant: HFC-134a, W-40 fpi surface, Triangular Pitch, Nozzle Configuration: 17WLCRC, Refrigerant Supply Rate: 25 kg/min, Pure Refrigerant Data..... | 238 |
| Table B.25 | Refrigerant: HFC-134a, W-40 fpi surface, Triangular Pitch, Nozzle Configuration: 24WHCRC, Refrigerant Supply Rate: 25 kg/min, Pure Refrigerant Data..... | 238 |
| Table B.26 | Refrigerant: HFC-134a, W-40 fpi surface, Triangular Pitch, Nozzle Configuration: 24WLCRC, Refrigerant Supply Rate: 25 kg/min, Pure Refrigerant Data..... | 239 |
| Table B.27 | Refrigerant: HFC-134a, W-40 fpi surface, Triangular Pitch, Nozzle Configuration: 24WHSQR, Refrigerant Supply Rate: 25 kg/min, Pure Refrigerant Data..... | 239 |
| Table B.28 | Refrigerant: HFC-134a, W-40 fpi surface, Triangular Pitch, Nozzle Configuration: 24WLSQR, Refrigerant Supply Rate: 25 kg/min, Pure Refrigerant Data..... | 239 |
| Table B.29 | Refrigerant: HFC-134a, W-40 fpi surface, Triangular Pitch, Nozzle Configuration: 30WHSQR, Refrigerant Supply Rate: 25 kg/min, Pure Refrigerant Data..... | 240 |
| Table B.30 | Refrigerant: HFC-134a, W-40 fpi surface, Triangular Pitch, Nozzle Configuration: 30WHSQR, Refrigerant Supply Rate: 45 kg/min, Pure Refrigerant Data..... | 240 |
| Table B.31 | Refrigerant: HFC-134a, W-40 fpi surface, Triangular Pitch, Pool Boiling, Pure Refrigerant Data | 240 |
| Table B.32 | Refrigerant: HFC-134a, Tu-B surface, Triangular Pitch, Pool Boiling, Pure Refrigerant Data | 241 |

| | | |
|------------|--|-----|
| Table B.33 | Refrigerant: HFC-134a, Plain surface, Triangular Pitch, Nozzle Configuration: 30WHCRC, Refrigerant Supply Rate: 15 kg/min, 1.0 % Oil Concentration..... | 241 |
| Table B.34 | Refrigerant: HFC-134a, Plain surface, Triangular Pitch, Nozzle Configuration: 30WHCRC, Refrigerant Supply Rate: 35 kg/min, 1.0 % Oil Concentration..... | 241 |
| Table B.35 | Refrigerant: HFC-134a, Plain surface, Triangular Pitch, Nozzle Configuration: 30WHCRC, Refrigerant Supply Rate: 15 kg/min, 2.5 % Oil Concentration..... | 242 |
| Table B.36 | Refrigerant: HFC-134a, Plain surface, Triangular Pitch, Nozzle Configuration: 30WHCRC, Refrigerant Supply Rate: 35 kg/min, 2.5 % Oil Concentration..... | 242 |
| Table B.37 | Refrigerant: HFC-134a, W-40 fpi surface, Triangular Pitch, Nozzle Configuration: 30WHCRC, Refrigerant Supply Rate: 15 kg/min, 1.0 % Oil Concentration..... | 242 |
| Table B.38 | Refrigerant: HFC-134a, W-40 fpi surface, Triangular Pitch, Nozzle Configuration: 30WHCRC, Refrigerant Supply Rate: 35 kg/min, 1.0 % Oil Concentration..... | 243 |
| Table B.39 | Refrigerant: HFC-134a, W-40 fpi surface, Triangular Pitch, Nozzle Configuration: 30WHCRC, Refrigerant Supply Rate: 15 kg/min, 2.5 % Oil Concentration..... | 243 |
| Table B.40 | Refrigerant: HFC-134a, W-40 fpi surface, Triangular Pitch, Nozzle Configuration: 30WHCRC, Refrigerant Supply Rate: 35 kg/min, 2.5 % Oil Concentration..... | 243 |
| Table B.41 | Refrigerant: HFC-134a, W-SC surface, Triangular Pitch, Nozzle Configuration: 30WHCRC, Refrigerant Supply Rate: 15 kg/min, 1.0 % Oil Concentration..... | 244 |
| Table B.42 | Refrigerant: HFC-134a, W-SC surface, Triangular Pitch, Nozzle Configuration: 30WHCRC, Refrigerant Supply Rate: 35 kg/min, 1.0 % Oil Concentration..... | 244 |

| | | |
|------------|--|-----|
| Table B.43 | Refrigerant: HFC-134a, W-SC surface, Triangular Pitch, Nozzle Configuration: 30WHCRC, Refrigerant Supply Rate: 15 kg/min, 2.5 % Oil Concentration..... | 244 |
| Table B.44 | Refrigerant: HFC-134a, W-SC surface, Triangular Pitch, Nozzle Configuration: 30WHCRC, Refrigerant Supply Rate: 35 kg/min, 2.5 % Oil Concentration..... | 245 |
| Table B.45 | Refrigerant: HFC-134a, Tu-B surface, Triangular Pitch, Nozzle Configuration: 30WHCRC, Refrigerant Supply Rate: 15 kg/min, 1.0 % Oil Concentration..... | 245 |
| Table B.46 | Refrigerant: HFC-134a, Tu-B surface, Triangular Pitch, Nozzle Configuration: 30WHCRC, Refrigerant Supply Rate: 35 kg/min, 1.0 % Oil Concentration..... | 245 |
| Table B.47 | Refrigerant: HFC-134a, Tu-B surface, Triangular Pitch, Nozzle Configuration: 30WHCRC, Refrigerant Supply Rate: 15 kg/min, 2.5 % Oil Concentration..... | 246 |
| Table B.48 | Refrigerant: HFC-134a, Tu-B surface, Triangular Pitch, Nozzle Configuration: 30WHCRC, Refrigerant Supply Rate: 35 kg/min, 2.5 % Oil Concentration..... | 246 |
| Table C.1 | Refrigerant: HCFC-22, Plain Surface, Triangular Pitch, Nozzle Configuration: 30WHCRC, Refrigerant Supply Rate: 15 kg/min, Pure Refrigerant Data..... | 248 |
| Table C.2 | Refrigerant: HCFC-22, Tu-B Surface, Triangular Pitch, Nozzle Configuration: 30WHCRC, Refrigerant Supply Rate: 15 kg/min, Pure Refrigerant Data..... | 249 |
| Table C.3 | Refrigerant: HCFC-22, Plain surface, Triangular Pitch, Nozzle Configuration: 30WHCRC, Refrigerant Supply Rate: 15 kg/min, 1.0 % Oil Concentration..... | 250 |
| Table C.4 | Refrigerant: HCFC-22, Tu-B surface, Triangular Pitch, Nozzle Configuration: 30WHCRC, Refrigerant Supply Rate: 15 kg/min, 1.0 % Oil Concentration..... | 250 |

| | | |
|------------|--|-----|
| Table D.1 | Refrigerant: HCFC-123, Plain Surface, Triangular Pitch, Nozzle Configuration: 24WDCRC, Refrigerant Supply Rate: 25 kg/min, Pure Refrigerant Data..... | 252 |
| Table D.2 | Refrigerant: HCFC-123, Plain Surface, Triangular Pitch, Nozzle Configuration: 24WDCRC, Refrigerant Supply Rate: 35 kg/min, Pure Refrigerant Data..... | 252 |
| Table D.3 | Refrigerant: HCFC-123, Plain surface, Triangular Pitch, Nozzle Configuration: 30WDCRC, Refrigerant Supply Rate: 25 kg/min, Pure Refrigerant Data..... | 253 |
| Table D.4 | Refrigerant: HCFC-123, Plain surface, Triangular Pitch, Nozzle Configuration: 30WDCRC, Refrigerant Supply Rate: 35 kg/min, Pure Refrigerant Data..... | 253 |
| Table D.5 | Refrigerant: HCFC-123, Tu-Cii surface, Triangular Pitch, Nozzle Configuration: 24WDCRC, Refrigerant Supply Rate: 25 kg/min, Pure Refrigerant Data..... | 254 |
| Table D.6 | Refrigerant: HCFC-123, Tu-Cii surface, Triangular Pitch, Nozzle Configuration: 24WDCRC, Refrigerant Supply Rate: 35 kg/min, Pure Refrigerant Data..... | 254 |
| Table D.7 | Refrigerant: HCFC-123, Tu-Cii surface, Triangular Pitch, Nozzle Configuration: 30WDCRC, Refrigerant Supply Rate: 25 kg/min, Pure Refrigerant Data..... | 255 |
| Table D.8 | Refrigerant: HCFC-123, Tu-Cii surface, Triangular Pitch, Nozzle Configuration: 30WDCRC, Refrigerant Supply Rate: 35 kg/min, Pure Refrigerant Data..... | 255 |
| Table D.9 | Refrigerant: HCFC-123, Tu-B surface, Triangular Pitch, Nozzle Configuration: 30WDCRC, Refrigerant Supply Rate: 25 kg/min, Pure Refrigerant Data..... | 256 |
| Table D.10 | Refrigerant: HCFC-123, Tu-B surface, Triangular Pitch, Nozzle Configuration: 30WDCRC, Refrigerant Supply Rate: 35 kg/min, Pure Refrigerant Data..... | 256 |

| | | |
|------------|--|-----|
| Table D.11 | Refrigerant: HCFC-123, Plain surface, Triangular Pitch, Nozzle Configuration: 30WDCRC, Refrigerant Supply Rate: 25 kg/min, 1.1 % Oil Concentration..... | 257 |
| Table D.12 | Refrigerant: HCFC-123, Plain surface, Triangular Pitch, Nozzle Configuration: 30WDCRC, Refrigerant Supply Rate: 25 kg/min, 2.5 % Oil Concentration..... | 257 |
| Table D.13 | Refrigerant: HCFC-123, Plain surface, Triangular Pitch, Nozzle Configuration: 30WDCRC, Refrigerant Supply Rate: 35 kg/min, 2.5 % Oil Concentration..... | 257 |
| Table D.14 | Refrigerant: HCFC-123, Tu-Cii surface, Triangular Pitch, Nozzle Configuration: 30WDCRC, Refrigerant Supply Rate: 25 kg/min, 1.1 % Oil Concentration..... | 258 |
| Table D.15 | Refrigerant: HCFC-123, Tu-Cii surface, Triangular Pitch, Nozzle Configuration: 30WDCRC, Refrigerant Supply Rate: 25 kg/min, 2.5 % Oil Concentration..... | 258 |
| Table D.16 | Refrigerant: HCFC-123, Tu-Cii surface, Triangular Pitch, Nozzle Configuration: 30WDCRC, Refrigerant Supply Rate: 35 kg/min, 2.5 % Oil Concentration..... | 258 |
| Table D.17 | Refrigerant: HCFC-123, Tu-B surface, Triangular Pitch, Nozzle Configuration: 30WDCRC, Refrigerant Supply Rate: 25 kg/min, 1.1 % Oil Concentration..... | 259 |
| Table D.18 | Refrigerant: HCFC-123, Tu-B surface, Triangular Pitch, Nozzle Configuration: 30WDCRC, Refrigerant Supply Rate: 25 kg/min, 2.5 % Oil Concentration..... | 259 |
| Table D.19 | Refrigerant: HCFC-123, Tu-B surface, Triangular Pitch, Nozzle Configuration: 30WDCRC, Refrigerant Supply Rate: 35 kg/min, 2.5 % Oil Concentration..... | 260 |
| Table E.1: | Models correlating the pure HFC-134a results..... | 264 |
| Table E.2: | Models correlating the HFC-134a lubricant effects results | 265 |
| Table E.3: | Models correlating the HCFC-123 lubricant effects results | 266 |

| | | |
|-------------|--|-----|
| Table E.4: | Pure HFC-134a, plain-surface, triangular-pitch tube bundle, correlation results summary (Model 1)..... | 268 |
| Table E.5: | Pure HFC-134a, W-40 fpi, triangular-pitch tube bundle, correlation results summary (Model 2)..... | 269 |
| Table E.6: | Pure HFC-134a, W-SC, triangular-pitch tube bundle, correlation results summary (Model 3)..... | 270 |
| Table E.7: | Pure HFC-134a, Tu-Cii, triangular-pitch tube bundle, correlation results summary (Model 4)..... | 271 |
| Table E.8: | Pure HFC-134a, Tu-B, triangular-pitch tube bundle, correlation results summary (Model 5)..... | 272 |
| Table E.9: | Pure HFC-134a, Tu-B, square-pitch tube bundle, correlation results summary (Model 6)..... | 273 |
| Table E.10: | HFC-134a lubricant effects testing, plain-surface, triangular-pitch tube bundle, correlation results summary (Model 7)..... | 274 |
| Table E.11: | HFC-134a lubricant effects testing, W-40 fpi, triangular-pitch tube bundle, correlation results summary (Model 8)..... | 275 |
| Table E.12: | HFC-134a lubricant effects testing, W-SC, triangular-pitch tube bundle, correlation results summary (Model 9)..... | 276 |
| Table E.13: | HFC-134a lubricant effects testing, Tu-B, triangular-pitch tube bundle, correlation results summary (Model 10)..... | 277 |
| Table E.14: | HCFC-123 lubricant effects testing, plain-surface, triangular-pitch tube bundle, correlation results summary (Model 11)..... | 278 |
| Table E.15: | HCFC-123 lubricant effects testing, Tu-Cii, triangular-pitch tube bundle, correlation results summary (Model 12)..... | 279 |
| Table E.16: | HCFC-123 lubricant effects testing, Tu-Bi, triangular-pitch tube bundle, correlation results summary (Model 13)..... | 280 |

NOMENCLATURE

| | | |
|-----------|---|---|
| A | = | area |
| C | = | constant used in the Rohsenow boiling equation |
| c | = | specific heat |
| CTF | = | collector test fraction |
| d | = | diameter |
| D | = | tube diameter |
| DF | = | dummy factor accounting for plugged tubes in the bundle |
| g | = | gravitational constant |
| h | = | heat transfer coefficient |
| i | = | latent heat of vaporization |
| k | = | thermal conductivity |
| L | = | circumferential length of heated surface; tube length |
| LEF | = | lubricant enhancement factor |
| $LMTD$ | = | log mean temperature difference |
| \dot{m} | = | mass flow rate |
| OFR | = | overfeed ratio which accounts for the CTF and DF if appropriate |
| P | = | pressure |
| q | = | thermal energy transfer rate |

| | | |
|-----|---|---|
| Q | = | single tube energy transfer rate |
| R | = | tube radius; wall thermal resistance term |
| RCR | = | recirculation ratio as calculated from energy balance |
| RPF | = | row performance factor |
| s | = | centerline to centerline distance |
| SEF | = | surface enhancement factor |
| STC | = | Seider-Tate coefficient |
| t | = | time |
| T | = | temperature |
| U | = | overall heat transfer coefficient |
| v | = | velocity |
| x | = | inverse of the recirculation ratio |

Symbols

| | | |
|----------|---|--|
| α | = | diffusivity of heat |
| δ | = | film thickness |
| ϕ | = | angular position |
| Γ | = | film feed supply rate [refrigerant supply rate per tube/(2*tube length)] |
| μ | = | dynamic viscosity |
| π | = | pi |
| ρ | = | density |
| σ | = | surface tension |
| ν | = | kinematic viscosity |

| | | |
|----------|---|--------------------|
| ω | = | velocity |
| ζ | = | irrigation density |
| ψ | = | volume fraction |

Superscripts

| | | |
|---|---|----------------------------|
| " | = | per unit area; vapor phase |
|---|---|----------------------------|

Subscripts

| | | |
|-----|---|--|
| b | = | boiling; bulk; bundle |
| c | = | convection |
| d | = | developing; diffusion |
| es | = | enhanced or finned surface |
| f | = | saturated liquid; film |
| g | = | saturated vapor |
| fd | = | fully developed |
| i | = | impingement; inside; in |
| l | = | lubricant; left; refrigerant/oil mixture |
| L | = | length |
| liq | = | test section liquid outlet |
| o | = | outside or shell-side; out |
| p | = | constant pressure; pure refrigerant |
| ps | = | plain surface |

| | | |
|-----|---|---------------------------------|
| r | = | root; row; refrigerant; right |
| s | = | saturation; stagnation; surface |
| sat | = | saturation |
| spr | = | spray manifold supply |
| tr | = | transition |
| vap | = | test section vapor outlet |
| w | = | wall; water |

Dimensionless Groups

| | | |
|----|---|--|
| Bo | = | Boiling number, $\left(\frac{\omega_B}{\omega}\right)$ |
| Nu | = | Nusselt number, $\frac{\bar{h}}{k} \left(\frac{v^2}{g}\right)^{1/3}$ |
| Pr | = | Prandtl number, $\left(\frac{c_p \mu}{k}\right)$ |
| Re | = | Reynolds number, $\left(\frac{4\Gamma}{\mu_f}\right)$ |
| Kp | = | dimensionless number for amount of superheat in the film, $\frac{\rho}{\sigma} \left(\frac{\sigma}{g(\rho - \rho'')}\right)^{1/2}$ |

ABSTRACT

As the phase-out of chlorofluorocarbons (CFC's) approaches, there is a current need for the development of new vapor compression chillers which can operate with non-CFC refrigerants while still maintaining high operating efficiencies. Redesign of the traditional flooded evaporator used in refrigeration chillers so as to incorporate a spray evaporation capability offers both a potential for increased heat transfer performance and a reduction in refrigerant inventory for a given chiller capacity relative to that found with existing industrial units.

This study is an evaluation of the spray evaporation heat transfer performance of refrigerants HFC-134a, HCFC-22, and HCFC-123 with commercially available copper alloy tubes. In addition, the effects of small concentrations of oil on the spray evaporation heat transfer process are also investigated.

Two different spray evaporation heat transfer facilities were designed and constructed, namely, a multi-tube facility and a large scale bundle facility. Testing of HFC-134a was conducted on the multi-tube test facility with six different enhanced and low-finned surface copper tubes. These initial tests indicated that enhanced condensation surfaces were better suited for the spray evaporation environment than enhanced boiling surfaces. The pure refrigerant work was followed by lubricant effects testing with two different viscosity polyol-

ester oils. It was found that oil concentrations through 5.0 % of a 340 SUS polyol-ester oil yielded heat transfer performances greater than those measured in the pure refrigerant testing.

Following the initial tests on the multi-tube test facility, large scale bundle work was conducted with all three refrigerants. The performance of HFC-134a was approximately 100 percent greater than that found with HCFC-123, and it was verified that pure HCFC-22 performed better than HFC-134a with two different tube surfaces. Small concentrations of a polyol-ester oil (through 2.5 %) increased the spray evaporation heat transfer performance of HFC-134a with all surfaces evaluated. Refrigerant HCFC-22 received less benefit from small concentrations of an alkyl-benzene oil than that seen in the HFC-134a testing with the polyol-ester oil. In a similar film-feed supply rate range as that used in the high-pressure refrigerant testing, small concentrations of a naphthenic mineral oil decreased the spray evaporation heat transfer performance of HCFC-123.

Limited-pool boiling testing was conducted with pure HFC-134a for comparison with spray evaporation heat transfer results. It was verified that the spray evaporation heat transfer performance of a low-finned tube bundle was better than that found in flooded evaporator testing with the same bundle. More importantly, it was found that the spray evaporation heat transfer performance of an enhanced condensation surface bundle surpassed the pool boiling performance of an enhanced convective boiling surface bundle.

CHAPTER 1. INTRODUCTION

The phase out of chlorofluorocarbons (CFC's), as mandated by the Montreal protocol, has created great interest in new refrigeration equipment and alternative designs to the conventional vapor compression systems. One area of this current research effort is seeking potential replacements for the shell-and-tube flooded evaporators found on virtually all large industrial chillers (over 400 ton capacity). Specifically, spray type evaporators offer high heat transfer performance greater than or equal to that found in conventional flooded evaporators [1].

Background

Over the past twenty-five years a significant amount of work has been conducted using both analytical and experimental techniques analyzing the film evaporation mechanism. Additional studies have been performed investigating the effects of nucleate boiling upon film heat transfer performance [1,2,3]. One of the primary goals of this research project was to analyze the film evaporation heat transfer process using commercially available enhanced and low-finned copper alloy tubes. Also, it was of interest to determine if any of the commercially available tubes could yield greater heat transfer coefficients in a spray evaporation

environment than those found with the leading nucleate boiling surfaces in the pool boiling environment. In this effort, a parametric study was conducted on the effects of nozzle configuration geometry on shell-side heat transfer performance.

This project makes a significant contribution to previous falling-film evaporation studies with the analysis of the effect of small concentrations of an oil upon film heat transfer performance. Refrigerant oil is present in all industrial chillers to provide lubrication for the compressor. The amount of oil circulated throughout the system varies from one design to another. If not recirculated back to the compressor excessive concentrations of the oil will collect in the evaporator. Similar to the conventional vapor compression systems equipped with a flooded evaporator, oil will collect in the evaporator of a spray evaporation unit if it is not recirculated back to the compressor. Although oil is removed from this heat exchanger, the amount of oil present during normal operation is enough to significantly influence the heat transfer mechanism whether it be pool boiling or film evaporation.

Most previous falling-film evaporation studies were conducted with single tubes. The current effort has focused predominantly on tube-bundle performance with geometries similar to those found in industry. It is of interest to determine how a given tube surface performs within a tube bundle. The degree of performance can be quite different than that found in single-tube experiments.

One of the greatest challenges in developing a falling-film evaporator is the distribution of liquid evenly throughout the bundle to prevent localized dry spots at relatively low overfeed ratios [2]. For a liquid distribution system to be deemed acceptable it must satisfy two main requirements. First, as much of the liquid circulated to the distributor manifold as possible must physically come in contact with the tube bundle. Secondly, the distribution of liquid over the bundle must be as uniform as possible. The variation in refrigerant supply rate from row-to-row can generate significant affects upon the overall average shell-side heat transfer

coefficient. Lateral and vertical tube pitch may have significant influence upon the distribution of refrigerant within the bundle.

Many of the previous film evaporation studies were conducted with only a single-tube in the test section. These studies typically used a perforated pipe or thin slot distributor to deliver the liquid to the heated surface. This project included tube-bundle testing and spray nozzles were used to determine their ability to distribute refrigerant liquid over the entire bundle during the heat transfer testing.

Research Program

The research program whose results are reported within this report was an ASHRAE sponsored research project designated RP-668. The objective of the study was to investigate heat transfer and fluid flow in spray evaporators (i.e. falling-film evaporation), with application to reducing refrigerant inventory. The study included performing experiments on plain, low-finned, and enhanced tubes in both single-tube and tube-bundle arrangements. Spray evaporation data was taken with three different refrigerants, namely, HCFC-123, HCFC-22, and HFC-134a. Data was also taken to evaluate the effects of lubricants (up to 5%) on the film heat transfer process.

Scope

Two different shell-side test facilities were designed and built in support of this research effort. Because the multi-tube test facility was physically much smaller than the bundle test facility, initial trends were investigated on the smaller test rig. This initial work included selecting the nozzles for use on the bundle test facility from the many nozzles types

commercially available. Prior to working with 19.1 mm diameter tubes, single-tube testing was conducted using 12.7 mm diameter, plain surface tubes with both wide-angle, low-pressure drop nozzles and standard-angle, high-pressure drop nozzles. These tests were done at saturation temperatures of -14.0 °C and 2.0 °C with refrigerant HFC-134a. Both of these nozzle types generated a solid circular plume of refrigerant.

Two enhanced condensation, two enhanced evaporation, two low-finned, and plain surface tubes having a 19.1 mm diameter were evaluated on the multi-tube test facility. These experiments were conducted at a saturation temperature of 2.0 °C with HFC-134a to compare the effects of the various surface enhancements upon the film heat transfer performance.

Two different viscosity polyol-ester oils were selected for evaluation on the multi-tube test facility. Tests were conducted with a 160 SUS viscosity oil up to a concentration of 3.0 percent by mass fraction along with a finned tube, an enhanced condensation tube, and a plain surface tube. A 340 SUS lubricant was tested with a finned and an enhanced condensation tube through a lubricant concentration of 5.0 percent.

The bundle test facility was designed and built to conduct tube-bundle tests with refrigerants HFC-134a, HCFC-22, and HCFC-123. Testing on this facility was conducted with the low-pressure drop, wide-angle nozzles which differed only by orifice size from those used during the single-tube testing.

During pure HFC-134a testing, data was taken with enhanced boiling surface tube bundles of two different geometries, namely, a square and triangular pitch geometry. The square pitch geometry was selected as an alternative to the triangular pitch geometry, which was used for the bulk of the tube-bundle experiments. In addition to the enhanced boiling surface, two enhanced condensation surfaces, one finned surface, and a plain surface tube bundle having triangular pitch were tested with pure HCFC-134a at several film-feed supply rates.

The HFC-134a lubricant effects testing was conducted with tube bundles having a triangular pitch. One enhanced boiling surface, one enhanced condensation surface, one finned surface, and a plain surface bundle were tested with HFC-134a and small concentrations of a 340 SUS polyol-ester oil. This testing determined the effects of enhancement upon bundle heat transfer performance with refrigerant/lubricant mixtures. Two film-feed supply rates and lubricant concentrations of 1.0 and 2.5 percent were used in these tests.

Testing of HCFC-22 was conducted with two triangular-pitch tube bundles, one having an enhanced boiling surface and one with a plain surface. The focus of the HCFC-22 work was to provide the necessary data to give indication of the capabilities of this refrigerant relative to HFC-134a in the spray evaporation environment. Only a single film-feed supply rate was used to conduct tests with the pure refrigerant and a lubricant mass fraction of 1 percent. The lubricant used in these tests had a viscosity of 300 SUS.

Testing of HCFC-123 was conducted with three triangular-pitch tube bundles, one having an enhanced boiling surface, one an enhanced condensation surface, and the third having a plain surface. Two film-feed supply rates and pure, 1.0 percent, and 2.5 percent lubricant concentrations were used for these tests. A lubricant having a viscosity of 305 SUS was selected for these tests.

Collector testing was performed in parallel with the heat transfer experiments to calculate the percentage of the refrigerant missing the tube or tube bundle, depending upon the test facility. Information from these collector tests was used to calculate overfeed ratios and Reynolds numbers for the heat transfer tests conducted with all three refrigerants.

Refrigerants of Interest

The three refrigerants used in this study were selected based upon their ability to potentially replace existing CFC refrigerants. Industry has already begun the phase-out of CFC-12, and HFC-134a is currently in the forefront as its replacement for at-least the next several decades. This refrigerant is already being marketed in automobile air conditioning systems by several large American automobile manufacturers and is replacing CFC-12 in the home appliance industry as well. The American Society of Heating Refrigerating and Air-Conditioning Engineers (ASHRAE), has sponsored several research projects over the past several years evaluating its ability as a heat transfer fluid in both flooded type evaporators and direct expansion (DX) type evaporators.

With the phase out of CFC-11, many of the large industrial centrifical chillers have been converted to either HCFC-22 or HCFC-123 depending upon the manufacturer. In parallel with this conversion effort, research has been sponsored by ASHRAE in the past several years evaluating the pool boiling heat transfer performance of refrigerants HCFC-22 and HCFC-123 with finned and enhanced surface tubes typically used in flooded evaporators.

Although HCFC-22 may be phased out early in the next decade, HCFC-123 has shown potential to serve as a long term replacement for CFC-11. High thermodynamic efficiencies are possible with HCFC-123, which offsets it relatively poor heat transfer performance. This refrigerant is used with industrial chillers that are typically equipped with an evaporator that is physically very large. The density of HCFC-123 is 15 to 20 percent higher than that of both HFC-134a and HCFC-22, which increases the hydrostatic head effect upon local saturation temperature within the lower regions of the flooded tube bundle. The problem arises that heat transfer can occur in the wrong direction in the lower rows of a large tube bundle when the compressor approach temperature is minimized. Perhaps current research in alternatives to

the conventional flooded evaporator chiller have potentially the greatest potential for improvement with the low pressure refrigerant, large industrial chillers.

Lubricants of Interest

It was of great interest to use oils that are commonly matched with each respective refrigerant in industrial refrigeration machines. A polyol-ester oil was selected for use with HFC-134a. This oil was known to be miscible throughout the operating conditions used for testing this refrigerant in both the multi-tube and bundle test facilities. For HCFC-22, an alkyl-benzene oil commonly used in industry with this refrigerant was selected. This oil was known to be miscible throughout the entire range of operating conditions used with the bundle test facility during the HCFC-22 tests. A white mineral oil was selected for the HCFC-123 tests. It was verified that this oil was miscible with HCFC-123 at the concentrations evaluated on the bundle test facility.

Solubility data was collected with each of these three refrigerant/lubricant pairs at concentrations of 2.0, 5.0, and 10.0 percent through a temperature range of 0.0 °C to 5.0 °C. This solubility information was used for shell-side heat transfer coefficient calculations on the bundle test facility.

CHAPTER 2. LITERATURE REVIEW

The literature review given in this chapter focuses on previous studies dealing with both film evaporation and film boiling of liquids on plain surfaces and surfaces configured with structures to promote better heat transfer performance. Correlations resulting from these previous studies are presented as well. The main focus of this chapter is to provide a summary of the accomplishments made to date in the area of falling-film evaporation (i.e. spray evaporation) and discuss the fundamentals of the falling-film heat transfer process.

The literature review is divided into four main sections: single-tube heat transfer studies, tube-bundle heat transfer studies, falling-film heat transfer models, and lubricant effects. A significant percentage of the work which has been conducted in previous falling-film evaporation studies has been done with water as the heat transfer fluid. The Ocean Thermal Energy Conversion program contributed a substantial amount of analytical and experimental work done mainly with ammonia as the heat transfer fluid. Falling-film heat transfer studies conducted with chlorofluorocarbon (CFC), hydrofluorocarbon (HFC), and hydrochlorofluorocarbon (HCFC) refrigerants are of more importance to the current work presented herein, but unfortunately this past work is scarce.

Single-Tube Heat Transfer Studies

The falling-film heat transfer phenomena are subdivided into two regimes. Specifically, the heat transfer mode may be convective evaporation only or a combination of evaporation and boiling in which boiling dominates the characteristics of the process. When the wall heat flux is less than the value required to develop nucleate bubbles, only evaporation will be present.

Film Heat Transfer Studies Conducted with Water

Plain surface, single-tube studies are very valuable in determining the effects of saturation temperature, film-feed supply rate, and wall heat flux variation upon the heat transfer performance of a falling film. Parken et al. [3] conducted film heat transfer tests with 25.4 mm and 50.8 mm diameter, plain surface brass tubes using water as the heat transfer fluid. Parken determined that average nonboiling (evaporation) heat transfer coefficients increased with increasing feedwater temperature and flow rate, but remained independent of wall heat flux. In comparison, the same study revealed that the average boiling heat transfer coefficients increased with increasing feedwater temperature and wall heat flux, and increased slightly with increasing flow rate. This work also showed that local nonboiling heat transfer coefficients are highest at the top of the tube and decrease around the circumference of the tube, while local boiling heat transfer coefficients are relatively uniform around the tube.

Film evaporation testing was conducted by Chyu and Bergles [4] with a 25.4 mm diameter plain surface copper tube. As was the case with Parken's results, the average heat transfer coefficient was dependent upon film-feed supply rate only in the nonboiling heat transfer regime. Once nucleate boiling became established at high wall heat fluxes, the heat

transfer coefficient became independent of the Reynolds number. Also, the nonboiling heat transfer coefficient was not significantly influenced by the wall heat flux.

Surface enhancement techniques may be divided into two major categories, the first being convective enhancement, and the second being nucleation enhancement. Some of the convective enhancements that have been evaluated in previous studies are:

- Elliptical diameter
- Longitudinal ribs
- Longitudinal grooves
- Longitudinal or spiral flutes
- Circumferential grooves
- Knurling

A significant amount of research has been conducted with porous metallic-matrix coatings and tunnel-pore surfaces to determine their ability to enhance falling-film heat transfer performance via increased nucleation.

Chyu et al. [5,6,7] conducted several studies evaluating the effects of both convective and boiling enhancement on film heat transfer performance. Porous metallic, tunnel-pore, and "T-Finned" surface copper tubes, nominally 25.4 mm in diameter, were tested in a falling-film environment using water as the heat transfer fluid. During the "T-Finned" surface testing, Chyu et al. noted that the channels carried the liquid flow and the tips of the fins appeared dry at lower flow rates. At higher flow rates, the tips were wetted but dried out at higher heat fluxes. The "T-Finned" surface yielded relatively high heat transfer coefficients in the convective region, and there was no sharp increase in performance at a given wall heat flux indicating an initiation of nucleate boiling. Chyu et al. stated that the large benefit gained by this type of enhancement in pool boiling was not transferable to the falling-film heat transfer environment.

Chyu et al. stated that the falling-film heat transfer performance was dependent upon wall heat flux for boiling enhanced surfaces. Heat transfer coefficients as high as 3.7×10^4 kW/(m²*K) were measured with the tunnel-pore surface. When boiling was dominant, heat transfer was independent of the Reynolds number and changes in feed height.

Chyu et al. noted that the structured surfaces evaluated yield higher heat transfer coefficients in the falling-film evaporation process than the pool boiling mode. The film heat transfer data either merged or showed a tendency to merge with the pool boiling performance as heat flux was increased. The trend indicated is that the heat transfer performance improvement found in film heat transfer decreases at higher heat fluxes.

Both evaporation and boiling tests were conducted by Han and Fletcher [8] with 50.8 mm diameter brass tubes. The effects of both circumferential and longitudinal grooving upon the film heat transfer performance were evaluated and compared to the performance of a plain surface tube. These enhancements generated 50 to 120 % improvement in the nonboiling heat transfer coefficient than those found with the plain surface tube. In the boiling regime, the enhanced surfaces yielded 30 to 75 % improvement in heat transfer performance than the plain surface performance, with the circumferentially grooved surface yielding 15 to 30 % improvement over the longitudinally grooved surface.

Film Heat Transfer Studies Conducted with Refrigerant

A study conducted with vertical plates and refrigerant CFC-11 was conducted by Nakayama et al. [9]. A vertical plate study has a similarity to a single-tube study, where the effective heat transfer length for a single tube is equal to one-half of the circumference. Several enhancements were evaluated in this study including vertical grooving, horizontal grooving, and a porous nucleate boiling surface. The porous surface yielded heat transfer

coefficients near $20 \text{ kW}/(\text{m}^2 \cdot \text{K})$, which were essentially independent of the film-feed supply rate. It was observed that horizontal grooving yielded relatively poor heat transfer performance, which is similar to longitudinal grooving on a horizontal tube.

It has been demonstrated in previous studies conducted with water that film heat transfer performance is capable of yielding much higher heat transfer coefficients than those found in pool boiling. Similarly, Nakayama et al. states that the nucleate boiling heat transfer performance of the porous surface was greater than that found while pool boiling.

Conti [10] reported results generated with 50.8 mm diameter horizontal tubes. Several enhanced surfaces were evaluated in this work including a porous metallic, and two grooved surfaces identified as American Standard threads of 8 and 28 threads per inch. Using anhydrous ammonia as the working fluid, it was found that the porous metallic surface generated heat transfer coefficients 3.0 times that of a plain surface tube of the same nominal diameter. The grooved surfaces yielded heat transfer coefficients 3.5 times that of the plain surface performance based upon nominal area. Conti evaluated a Reynolds number range of 109 to 5440 in this study.

Tube-Bundle Heat Transfer Studies

Lorenz and Yung [11] performed a comparison of single-tube falling-film heat transfer studies with results generated from tube-bundle studies. They determined that caution should be used when making this comparison because at low Reynolds numbers the performance of a single tube varies considerable from that of a tube bundle. This is a result of the bundle depth effects. Comparing their own experimental results from a plain surface tube bundle with single-tube data generated in three previous studies, they determined that the single-tube data

diverged from the bundle data at a nominal Reynolds number of 300. It was determined this divergence was the result of partial dryout within localized regions of the tube bundle at low film-feed supply rates.

The effect of liquid feed rate upon a nonboiling heat transfer process has been studied to a greater depth than the effect of tube spacing between tube rows within a bundle. One such study by Mitrovic [12] evaluated the effects of vertical tube spacing. This study was conducted using 18 mm diameter plain surface tubes and both water and isopropyl alcohol as the heat transfer fluid. Mitrovic found that the influence of vertical tube spacing upon the shell-side heat transfer coefficients depends upon the Reynolds number. At Reynolds numbers less than 80 these effects may be neglected. The results indicated that as the Reynolds numbers increases, the effects of vertical tube spacing increase as well. Mitrovic made the recommendation to utilize tube spacings of about 4 tube diameters in spray coolers.

Several large bundle studies were conducted in the OTEC research effort. One of these tests was presented by Hillis et al. [13] in which ammonia was used as film heat transfer fluid. The heat exchanger was equipped with a triangular-pitch tube bundle consisting of 388 tubes of a 38.1 mm outer diameter. The film side of the tube was enhanced with a porous metallic surface. The findings in this work were consistent with the trends reported in single-tube studies with the porous metallic enhancement. The film heat transfer performance was relatively independent of film-feed supply rate until dryout occurred in the lower rows of the bundle. The minimum feed rates required to wet the entire tube bundle corresponded to bundle overfeed ratios of 1.17 to 1.27, indicating a well designed liquid distribution system. No affect of heat duty (heat flux) upon the shell-side heat transfer performance was reported. The test facility consistently generated shell-side heat transfer coefficients of $26.1 \text{ kW}/(\text{m}^2 \cdot \text{K})$ under normal operating conditions. It was also shown that the heat transfer performance was not a function of inlet temperature. The liquid feed temperature was allowed to decrease 12.0

°C below the saturation temperature in the heat exchanger, and no adverse effects upon the shell-side heat transfer performance were noted.

In addition to the observations made by Hillis et al., Czikk [14] presents results obtained during vapor cross-flow tests conducted as a part of the OTEC research effort. These tests evaluated the effects of vapor shear upon film heat transfer performance, which is an important phenomenon in full-scale tube bundles. This work was done with a porous metallic surface enhancement and ammonia as the heat transfer fluid. Czikk et al. stated that vapor cross flow had no adverse effects upon the heat transfer performance, and at vapor velocities of 1.5 m/s a slight increase in the heat transfer coefficient was noted. This was most likely due to a convective contribution to the heat transfer coefficient in addition to the relatively large nucleate boiling contribution. The liquid deflection from a tube was found to be a function of vapor velocity but not of heat flux.

A film heat transfer study was performed by Danilova et al. [1] with refrigerants CFC-12, CFC-113, and HCFC-22 and plain surface tubes having a diameter of 18 mm. The study included tests done with tube bundles having a vertical spacing to diameter ratio (s/d ratio) of 1.1, 1.3, 1.5, and 2.2 and a variety of row arrangements. It is stated by Danilova et al. that the number of rows had no effect upon the heat transfer rate. Over a heat flux range of 1 kW/m² to 6 kW/m² (the convective evaporation region) the heat transfer coefficients were 2 to 5 times higher than those found in the pool boiling environment.

Danilova et al. also studied the effect of film-feed supply rate upon the heat transfer performance in the film evaporation regime. This effect is divided into three specific regions: the laminar, the transition, and turbulent regimes. A decrease in heat transfer coefficient was noted in the laminar region with an increase in the film-feed supply rate due to increased thermal resistance of a thicker liquid layer. In the transition region heat transfer performance showed relatively little dependence upon the film-feed supply rate, because increased turbulent

fluctuations offset the conduction losses gained from a greater film thickness. In the turbulent region heat transfer performance increased readily with increased film-feed supply rate.

Consistent with studies conducted with water, when boiling dominated the heat transfer process, the heat transfer coefficient became independent of the film-feed supply rate.

Danilova et al. also states that the s/d ratio had no affect upon the heat transfer performance once boiling became dominant.

Falling-Film Heat Transfer Models

Previous heat transfer studies have generated a variety of semi-empirical and empirical models. The models fall into two major groups, those for evaporation (nonboiling) and those for nucleate boiling regimes. Analytical predictions are in the open literature typically for the nonboiling heat transfer regime only. One of the objectives of this project was to determine which of the existing correlations could accurately predict the heat transfer performance with the three refrigerants used in this study. Comparisons are made in following chapters.

Semi-Empirical Models

The number of correlations incorporating analytical techniques are scarce. Two models were developed by Chyu and Bergles [4,15] for saturated nonboiling falling-film evaporation. Both were based upon three defined heat transfer regions: the jet impingement region, the thermally developing region, and the fully developed region. The only difference between the two models was in the fully developed region. The first model used a conduction solution based upon Nusselt's film condensation analysis, while the second used correlations developed

by Chun and Seban [16] for fully developed film evaporation on a vertical tube. Both models take the following form:

$$\bar{h} = \bar{h}_s\left(\frac{\phi_s}{\pi}\right) + \bar{h}_i\left(\frac{\phi_i - \phi_s}{\pi}\right) + \bar{h}_d\left(\frac{\phi_d - \phi_i}{\pi}\right) + \bar{h}_{fd}\left(1 - \frac{\phi_d}{\pi}\right) \quad (2.1)$$

The parameter ϕ_s is the angular position at the end of the stagnation zone, ϕ_i is the angular position the end of the impingement zone, ϕ_d is the angular position at the end of the developing zone. The average heat transfer coefficient (\bar{h}) is comprised of four individual contributions: the heat transfer coefficients in the stagnation region (\bar{h}_s), the heat transfer coefficients in the impingement region (\bar{h}_i), the heat transfer coefficients in the thermally developing region (\bar{h}_d), and the heat transfer coefficients in the fully developed region (\bar{h}_{fd}). Chyu and Bergles conduction model for the fully developed region is defined as follows:

$$\text{Nu}_{fd} = \left(\frac{\bar{h}_{fd} e^{1/4}}{k_f}\right) = \frac{1}{\pi - \phi_d} \int_{\phi_d}^{\pi} \frac{\sin^{1/3}\phi}{A - \frac{4}{3} \int_{\phi_d}^{\phi} \sin^{1/3}\phi' d\phi'} d\phi \quad (2.2)$$

with

$$A = \left[\frac{3\mu_r \Gamma_i^4}{g\rho_f(\rho_f - \rho_g)}\right]^{1/3} \left[\frac{i_{fg}}{Rk_f(T_w - T_s)}\right] \quad (2.3)$$

The main limitation to this model is it is developed for evaporation heat transfer and is not applicable to film boiling.

A combined boiling and evaporation correlation for liquid film heat transfer was developed by Lorenz and Yung [2]. Their model considers both a thermally developing region and a fully developed region similar to that used by Chyu and Bergles.

In the thermally developing region they assume a 1-D transient heat conduction problem where a solid is initially at a uniform temperature and then is subjected to a sudden step increase in temperature at a boundary. The following two equations are used to calculate the average film velocity and the diffusion time respectively.

$$\bar{v} = \frac{\Gamma}{\rho\delta} \quad (2.4)$$

$$t_d = \frac{\delta^2}{4\pi\alpha} \quad (2.5)$$

From Equations 2.4 and 2.5, the thermally developing length is calculated.

$$L_d = \left(\frac{\Gamma^{4/3}}{4\pi\rho\alpha} \right) \left(\frac{3\mu}{g\rho^2} \right)^{1/3} \quad (2.6)$$

Assuming a parabolic velocity distribution and a linear temperature profile the average heat transfer coefficient in the thermal developing region was calculated as:

$$\bar{h}_d = \frac{3}{8} c_p \frac{\Gamma}{L_d} \quad (2.7)$$

In the fully developed region convective heat transfer coefficient (\bar{h}_c) is calculated by applying the laminar and turbulent flow correlations developed by Chun and Seban. These correlations account for only the nonboiling contribution to an average heat transfer coefficient in the fully developed region. The boiling contribution is accounted for by incorporating Rohsenow's nucleate boiling correlation [17,18].

$$\bar{h}_b = \frac{\mu i_{fg}}{C_{sf}^3 \left(\frac{g \sigma}{g \rho} \right)^{1/2}} \left[\frac{c_p}{i_{fg} Pr} \right]^3 \Delta T^2 \quad (2.8)$$

The overall equation for Lorenz and Yung's model is as follows:

$$\bar{h} = \bar{h}_b + \bar{h}_d \frac{L_d}{L} + \bar{h}_c \left[1 - \frac{L_d}{L} \right] \quad (2.9)$$

The first term on the RHS of Equation 2.9 represents boiling over the entire circumference of the tube. The second term represents convection in the developing region, and the last term represents convection in the fully developed region. Unfortunately, use of this model requires knowledge of the fluid-surface factor, which would require gathering a significant amount of pool boiling data so the constant could be statistically determined. A simpler alternative would be to insert experimental nucleate boiling data in place of Equation 2.8 if known.

Empirical Correlations

More common than the semi-empirical falling film correlations are those developed purely empirically. The correlation provided by Chun and Seban [16] for an evaporating liquid film along a vertical wall is subdivided into three regions: laminar, transition and turbulent.

Laminar:

$$\frac{\bar{h}}{k} \left(\frac{v^2}{g} \right)^{1/3} = 1.10 \text{Re}^{-1/3} \quad (2.10)$$

$$\frac{\Gamma}{\mu} \leq 0.61 \left(\frac{\mu^4 g}{\rho \sigma^3} \right)^{-1/11}$$

Wavy-Laminar (Transition):

$$\frac{\bar{h}}{k} \left(\frac{v^2}{g} \right)^{1/3} = 0.822 \text{ Re}^{-0.22} \quad (2.11)$$

$$0.61 \left(\frac{\mu^4 g}{\rho \sigma^3} \right)^{-1/11} < \frac{\Gamma}{\mu} \leq 1450 \text{ Pr}^{-1.06}$$

Turbulent:

$$\frac{\bar{h}}{k} \left(\frac{v^2}{g} \right)^{1/3} = 3.80 \times 10^{-3} \text{ Pr}^{0.65} \text{ Re}^{0.4} \quad (2.12)$$

$$\frac{\Gamma}{\mu} \geq 1450 \text{ Pr}^{-1.06}$$

Chun and Seban's correlation is used to determine \bar{h}_{fd} in Equation 2.1 and \bar{h}_c in Equation 2.9.

The turbulent correlation is widely used throughout many falling-film heat transfer studies, and in simple form it is written as:

$$\frac{\bar{h}_{fd}}{k} \left(\frac{v^2}{g} \right)^{1/3} = a_1 \text{ Pr}^{a_2} \text{ Re}^{a_3} \quad (2.13)$$

Parken et al. in [3] expanded upon this relationship to extend its capabilities to regions dominated by boiling heat transfer. Equation 2.14 shows the modified form of Equation 2.13.

$$\frac{\bar{h}_{fd}}{k} \left(\frac{v^2}{g} \right)^{1/3} = b_1 \text{ Pr}^{b_2} \text{ Re}^{b_3} q^{b_4} \quad (2.14)$$

Table 2.1 summarizes the correlations developed by Parken et al. [3] and Han [8] in which Equations 2.13 and 2.14 are used to fit the falling-film experimental results. Both Parken et al. and Han used water as the heat transfer fluid in these tests.

Owens [19] proposed the following nonboiling correlations from his own experimental data as well as data collected by Conti [10] and Liu [20]. Equation 2.15 applies to the laminar regime while Equation 2.17 applies to the turbulent regime with a transition Reynolds number defined by Equation 2.16. His correlation includes the effects of liquid distributor height above the tube.

$$\text{Laminar:} \quad \text{Nu} = 2.2 (s/d)^{0.1} \text{Re}^{-1/3} \quad (2.15)$$

$$\text{Transition:} \quad \text{Re}_t = 1680 \text{Pr}^{-1.5} \quad (2.16)$$

$$\text{Turbulent:} \quad \text{Nu} = 0.185 (s/d)^{0.1} \text{Pr}^{0.5} \quad (2.17)$$

Mitrovic's study [12] in which the effects of centerline tube distance to tube diameter were investigated with a single column of horizontal tubes is correlated with Equations 2.18 and 2.19. His water data were collected at a wall heat flux of 18.4 kW/m², and Reynolds numbers down to 80.

$$\text{Nu} = 1.75 \times 10^{-2} \text{Re}_L^{0.349} \text{Pr}_L^{0.5} \beta \quad (2.18)$$

$$\beta = \frac{(s/d)^{0.158}}{1 + \exp(-8.0 \times 10^{-3} \text{Re}_L^{1.32})} \quad (2.19)$$

Correlations developed from experimental data taken with refrigerants are fewer than those originating from water studies. The work conducted by Danilova et al. [1] resulted in the development of the following correlations.

Table 2.1: Correlation constants accompanying Equations 2.13 and 2.14

| Heat Transfer Regime | Tube Alloy | Tube Diameter | Surface Enhancement | Constants | Equation | Range of Use |
|----------------------|------------|---------------|--------------------------------|--|----------|---|
| Nonboiling | Brass | 25.4 mm | Plain | $a_1=0.042$ $a_2=0.15$ $a_3=0.53$ | 2.13 | $1000 \leq Re \leq 8000$ $1.3 \leq Pr \leq 3.6$ |
| Nonboiling | Brass | 50.8 mm | Plain | $a_1=0.038$ $a_2=0.15$ $a_3=0.53$ | 2.13 | $1000 \leq Re \leq 8000$ $1.3 \leq Pr \leq 3.6$ |
| Boiling | Brass | 25.4 mm | Plain | $b_1=0.00082$ $b_2=0.10$ $b_3=0.65$ $b_4=0.4$ | 2.14 | $1000 \leq Re \leq 8000$ $1.3 \leq Pr \leq 3.6$ $30 \text{ kW/m}^2 \leq q'' \leq 80 \text{ kW/m}^2$ |
| Boiling | Brass | 50.8 mm | Plain | $b_1=0.00094$ $b_2=0.10$ $b_3=0.65$ $b_4=0.4$ | 2.14 | $1000 \leq Re \leq 8000$ $1.3 \leq Pr \leq 3.6$ $30 \text{ kW/m}^2 \leq q'' \leq 80 \text{ kW/m}^2$ |
| Nonboiling | Brass | 50.8 mm | Plain | $a_1=0.0025$ $a_2=0.20$ $a_3=0.53$ | 2.13 | $770 \leq Re \leq 7000$ $1.3 \leq Pr \leq 3.6$ |
| Nonboiling | Brass | 50.8 mm | Circumferential & Axial Groove | $a_1=0.0028$ $a_2=0.0.50$ $a_3=0.85$ | 2.13 | $770 \leq Re \leq 7000$ $1.3 \leq Pr \leq 3.6$ |
| Boiling | Brass | 50.8 mm | Plain | $b_1=0.0004$ $b_2=0.20$ $b_3=0.65$ $b_4=0.4$ | 2.14 | $770 \leq Re \leq 7000$ $1.3 \leq Pr \leq 3.6$ $30 \text{ kW/m}^2 \leq q'' \leq 80 \text{ kW/m}^2$ |
| Boiling | Brass | 50.8 mm | Axial Groove | $b_1=0.009$ $b_2=0.20$ $b_3=0.65$ $b_4=0.15$ | 2.14 | $770 \leq Re \leq 7000$ $1.3 \leq Pr \leq 3.6$ $30 \text{ kW/m}^2 \leq q'' \leq 80 \text{ kW/m}^2$ |
| Boiling | Brass | 50.8 mm | Circumferential Groove | $b_1=0.0007$ $b_2=0.20$ $b_3=0.65$ $b_4=0.4$ | 2.14 | $1000 \leq Re \leq 8000$ $1.3 \leq Pr \leq 3.6$ $30 \text{ kW/m}^2 \leq q'' \leq 80 \text{ kW/m}^2$ |

$$\text{Nu}_{\text{film}} = 0.03 \text{Re}_{\text{film}}^{0.22} \text{Re}_{*\text{film}}^{0.04} \text{Pr}^{0.32} (s/d)^{0.48} \quad (2.20)$$

$$\text{Nu}_* = 1.32 \times 10^{-3} \text{Re}_*^{0.63} \text{Kp}^{0.72} \text{Pr}^{0.48} \quad (2.21)$$

Equations 2.20 and 2.21 apply to the film-evaporation and film-boiling regimes, respectively. It should be noted that the tube diameter to tube pitch ratio is not included in Equation 2.21, because film-boiling heat transfer performance is independent of this parameter. The dimensionless parameters in Equations 2.20 and 2.21 are defined by the following equations.

$$\text{Nu}_{\text{film}} = \frac{\bar{h}}{k} \left(\frac{v^2}{g} \right)^{1/3} \quad (2.22)$$

$$\text{Re}_{\text{film}} = \frac{4\zeta}{v} \quad (2.23)$$

$$\text{Re}_{*\text{film}} = \frac{q''}{h_{\text{fg}} \rho'' v} \left(\frac{v^2}{g} \right)^{1/3} \quad (2.24)$$

$$\text{Pr} = \frac{v}{\alpha} \quad (2.25)$$

$$\text{Nu}_* = \frac{\bar{h}}{k} \left(\frac{\sigma}{g(\rho - \rho'')} \right)^{1/2} \quad (2.26)$$

$$\text{Re}_* = \frac{q''}{h_{\text{fg}} \rho'' v} \left(\frac{\sigma}{g(\rho - \rho'')} \right)^{1/2} \quad (2.27)$$

$$\text{Kp} = \frac{\rho}{\sigma} \left(\frac{\sigma}{g(\rho - \rho'')} \right)^{1/2} \quad (2.28)$$

The parameter ζ is the irrigation density with units of $\text{m}^3/(\text{m}\cdot\text{s})$, which is similar to the film-feed supply rate having units of $\text{kg}/(\text{m}\cdot\text{s})$.

Parizhskiy et al. [21] conducted a study which focused on correlating boiling heat transfer coefficients for an ammonia film on the inside of vertical steel tubes. Equation 2.29 presents this correlation.

$$\text{Nu} = 0.068 \text{Bo}^{0.44} \text{Kp}^{-0.83} \text{Pr}^{1/3} \quad (2.29)$$

where the boiling number (Bo) is defined in terms of the boiling velocity (ω_b) and the liquid-film velocity (ω_f)

$$\text{Bo} = \frac{\omega_b}{\omega_f} \quad (2.30)$$

$$\omega_b = \frac{q''}{i_{fg}\rho''} \quad (2.31)$$

Lubricant Effects

Chiller systems which operate with fluorinated hydrocarbon refrigerants are equipped with compressors which require lubrication. The lubricants used in these systems are soluble with the refrigerant resulting in the migration of the compressor lubricant throughout the system in the form of a binary mixture. The amount of lubricant circulated throughout the system varies depending upon design. The effects of oil contamination have been investigated in previous pool boiling heat transfer studies. To gain a better understanding of how

lubricants might effect a spray evaporator, conclusions from several of these studies are presented in this report.

A comprehensive literature review was presented by Chaddock [22] in 1976 which focused upon the effects of oil on both pool-boiling heat transfer performance and in-tube heat transfer performance. Chaddock indicated that the heat transfer performance is affected by lubricants mainly due to increases in both surface tension and viscosity. The surface tension directly affects the ease in which vapor nuclei develop. An increased surface tension makes it more difficult for these nuclei to develop which results in resistance to boiling heat transfer. Chaddock also stated that foaming may result at low lubricant concentrations, and this foaming can enhance the bubble nucleation yielding better boiling heat transfer.

Dougherty and Sauer [23] conducted single-tube heat transfer experiments with 15.9 mm and 28.6 mm diameter plain-surface copper tubes using R-11 and R-113. A paraffin base lubricant was tested at concentrations up to 10.0 % by weight. Their results showed that above oil concentrations of 3.0 % the pool-boiling heat transfer performance always decreased, but at concentrations less than 3.0 % sometimes slightly increased.

Sauer et al. [24] conducted single-tube heat transfer experiments with refrigerant R-12 and three paraffin base oils having viscosities of 155, 290, and 515 SUS. The tests showed that lubricant concentrations greater than 7 % always reduced pool boiling heat transfer performance, and concentrations less than 7 % sometimes significantly increased the heat transfer performance. Peak boiling performance occurred with a 3.0 % oil concentration and further increases in concentration yielded a degradation in heat transfer performance.

More pool boiling heat transfer results with R-12 refrigerant/lubricant mixtures are reported by Stephan and Mitrovic [25,26]. The trend shown by Stephan and Mitrovic's data is generally a decrease in heat transfer performance with an increase in lubricant concentration. However, at the highest heat flux investigated (21.75 kW/m²), it was shown that increases in

the heat transfer performance occurred relative to the pure refrigerant results up to concentrations of 6.0 %. Whether foaming enhancement is greater at higher or lower heat fluxes appears to be dependent upon the refrigerant or lubricant used.

Another study conducted by Wanniarachchi et al. [27] with R-114 refrigerant/lubricant mixtures indicated that the maximum enhancement from the lubricant occurred at concentrations of 3 to 6 percent with a wall heat flux of 1 kW/m². At heat fluxes of 5 kW/m² and greater, the effects of the lubricant always decreased heat transfer performance relative to the pure refrigerant results.

A later study conducted by Sauer et al. [28] with R-11 and a naphthene based oil of two different viscosities yielded similar trends to the study with R-12 [24]. The data supported previous studies in that small lubricant concentrations could generate small improvements in the shell-side heat transfer coefficient. Sauer notes that this phenomena is related to foaming which occurs in the upper rows of flooded evaporator tube bundles.

Chongrungleong and Sauer [29] conducted a single-tube experimental study in which correlations were developed to model the pool boiling heat transfer data for refrigerant/oil mixtures. One correlation was developed by the investigators which could predict their data without knowledge of the thermodynamic and transport properties of the mixture. Namely, the correlation was developed considering only the wall heat flux, the lubricant volume fraction (ψ_l), and the saturation pressure from the single-tube heat transfer experimental data. The correlation is shown below.

$$h = 6.17 [q'']^{0.55} [\psi_l]^{3.65} P^{0.24} \quad (2.32)$$

This equation predicts an increase in heat transfer coefficient with an increase in saturation pressure, a decrease in viscosity (i.e. lower lubricant concentration), and an increase in wall

heat flux. One limitation of this correlation is that it does not predict the effects of foaming at low lubricant concentrations.

Other investigations have been conducted in which no enhancement to the heat transfer coefficients were obtained. Webb and McQuade [30] conducted experiments with refrigerants R-11 and R-123 and a mineral oil. Results from this study indicated that enhanced surface tubes suffered greater degradation in heat transfer performance from the effects of the oil than plain-surface tubes. None of the data presented indicated that lubricant effects could generate higher heat transfer performance than that found with the pure refrigerant. Jensen and Jackman [31] came to similar conclusions from experiments conducted with R-113 refrigerant/lubricant mixtures. Jensen and Jackman attributed the decrease in heat transfer performance to increased resistance to diffusion of the more volatile component through an oil rich boundary layer at the vapor-liquid interface of the nucleate bubble.

The phenomenon of lubricant effects upon pool boiling heat transfer performance has not been thoroughly studied, but it is clear that in some cases oil enhanced heat transfer performance. It is known that foaming occurs in the upper rows of a tube bundle in a flooded evaporator [28] because hydrostatic head is minimal at this location. Previous falling-film evaporation studies have been conducted with pure liquids only. If the foaming effect is known to occur with a shallow liquid height, it might be concluded that such enhancement is possible in falling-film heat transfer as well, because the hydrostatic head effects have been eliminated in this process.

CHAPTER 3. MULTI-TUBE TEST FACILITY

The first test facility designed and constructed was the multi-tube test facility. The multi-tube test facility was used to conduct single-tube and multi-tube tests with refrigerant HFC-134a in both spray evaporation and pool-boiling heat transfer modes. Sequential construction of the two test facilities used in project RP-668 was done so learning experiences from the smaller multi-tube test facility could be used for the construction and operation of the larger bundle rig. It is important to note that both test facilities were designed to measure shell-side heat transfer coefficients in conditions that might be found in the evaporator of a spray evaporation chiller. Neither facility was equipped with a refrigerant compressor, which would be found in a real industrial spray chiller system.

Facility Description

The multi-tube test facility has several main parts: the test section, the test-tube(s), the refrigerant flow loop, the spray nozzles, the glycol/water flow loop, and data acquisition equipment. A schematic drawing of the rig is shown in Figure 3.1, and a detailed description is presented below.

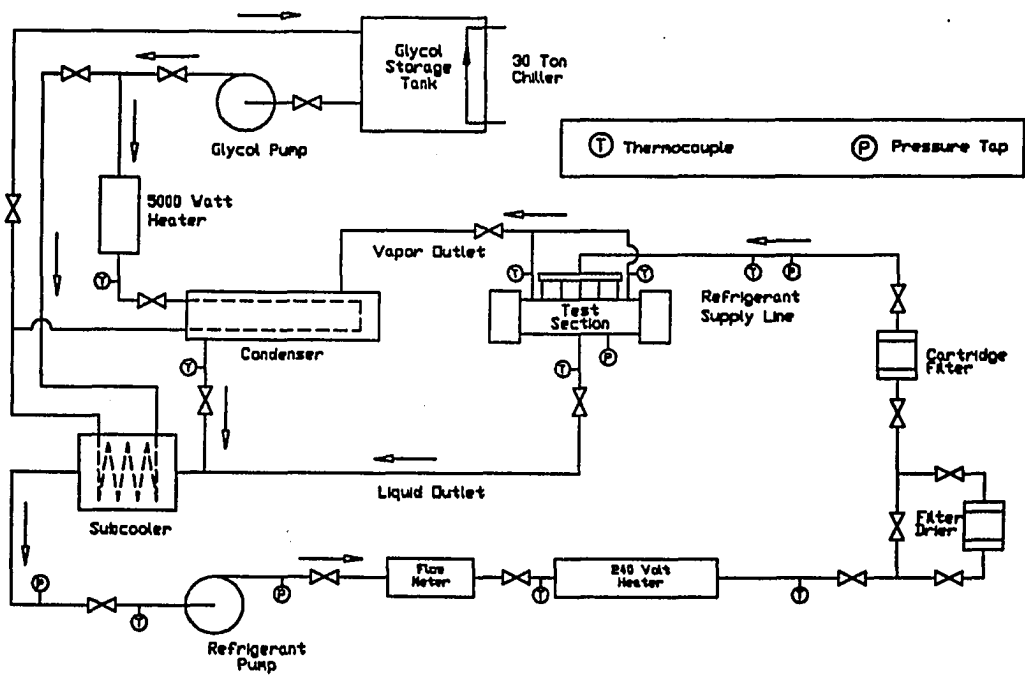


Figure 3.1: Multi-tube test facility schematic

Test Section

The stainless-steel test section is equipped with two glass-view side ports (one per side) and a circular viewport in one end. On the opposite end to the circular view port, a tube sheet is attached which has two threaded ports. The test section is 101.6 mm in diameter and 406.4 mm long. Along the top of the test section are 5 threaded ports with compression fittings and spray nozzles. The nozzle ports are machined with a gap of 76.2 mm separating them. At 45 degrees off top-dead center, along opposite sides, are the two refrigerant vapor outlets. Two liquid outlets lie along bottom dead center of the test section. A compression fitting is attached to a threaded port on the tube sheet which allows insertion of a copper alloy test-tube. The test section is equipped with 2 thermocouples which measure the refrigerant liquid/vapor space temperature. A pressure tap allows saturation pressure to be measured which can then be used to determine saturation temperature.

Copper Test-Tube(s)

Two different diameters were used during the plain surface spray evaporation testing; namely, 12.7 mm and 19.1 mm diameter tubes. The 12.7 mm tubes were equipped with a 572 watt heater and the 19.1 mm tubes used an 860 watt heater. The heaters were sized so that a heat flux of 40 kW/m² could be supplied across the outer surface of the test-tube. Spacers were machined and installed on the cartridge heater to maintain the cartridge heater in a centerline position within the test-tube.

Thermocouples were mounted on the wall of the test-tube through a drilled port, which was filled with a lead-tin solder. The thermal conductivity of the lead-tin solder was determined to be roughly 1/10 of that of copper. The size of the drilled port was kept to the minimum required so that the temperature of the solder bead would be as close to the actual

wall temperature as possible. Thermocouple wires were run through the space between the outer surface of the cartridge heater and the inner surface of the copper tube.

Two different substances were independently evaluated as filler material in the gap located between the cartridge heater and the copper tube. For both the 12.7 mm and 19.1 mm diameter test-tubes this gap was a nominal 1.6 mm in radius. First a fine MgO_2 powder was tried but this provided insufficient thermal conductivity and was cumbersome to work with. Eventually a highly conductive grease was found which worked quite well with the test-tube arrangement used in this study. The thermal grease is a non-hardening type, commonly used with thermocouple installations to reduce thermal contact resistance.

The 12.7 mm plain surface tubes were equipped with 9 thermocouples located in pairs of three (top, side, bottom) at distances of 25.4 mm, 177.8 mm, and 330.2 mm from the free-end of the test-tube. Figure 3.2 shows the location of the thermocouples on the surface of the 19.1 mm diameter tubes. Each tube was instrumented with 9 type-T thermocouples. The thermocouples were installed at distances of 152.4 mm, 177.8 mm, and 203.2 mm from the free-end of the tube. At each of these axial locations, a thermocouple was soldered at top-dead center, bottom dead center and 90° from top dead center along one side only.

Along with the 19.1 mm diameter plain surface tubes, six enhanced and finned surface tubes were tested on the multi-tube rig. Using descriptors proposed by Webb [32], the tubes tested were the W-SE [33], the W-SC [34], the Tu-B [35], the Tu-Cii [36], the W-26 fpi [37], and the W-40 fpi [38]. The W-26 fpi and W-40 fpi tubes are low-finned tubes. The W-SE and Tu-B tubes have a shell-side nucleate boiling enhancement and were developed for pool boiling application. The W-SC and Tu-Cii tubes have an enhanced condensation shell-side surface. All tubes tested had a total length of 470 mm with a 76.2 mm plain end. Other tube specifications are included in Table 3.1. It should be noted that all finned and enhanced tubes are referred to as 19.1 mm tubes which distinguishes them from the smaller 12.7 mm diameter

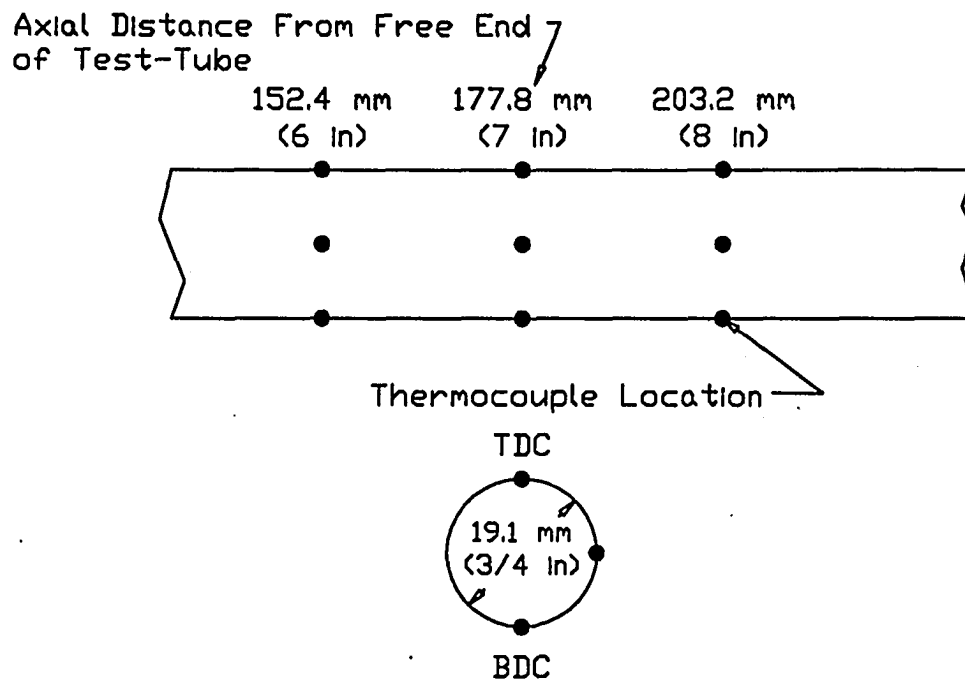


Figure 3.2: Thermocouple location diagram for the 19.1 mm diameter test-tubes

Table 3.1: Geometric specifications for tubes tested on the multi-tube test facility

| tube | fin count fins/m | D_o nominal mm | D_r nominal mm | fin height mm |
|----------|------------------------|------------------------|------------------------|---------------------|
| plain | - | 12.7 | - | - |
| plain | - | 19.1 | - | - |
| W-26 fpi | 1024 | 19.1 | 15.9 | 1.6 |
| W-40 fpi | 1575 | 19.1 | 17.1 | 1.0 |
| W-SC | 1024 | 19.6 | 17.5 | 1.1 |
| W-SE | 1024 | 19.6 | 17.5 | 1.1 |
| Tu-Cii | 1575 | 18.9 | 17.1 | 0.9 |
| Tu-B | 1575 | 18.7 | 17.5 | 0.6 |

tubes. Only plain surface tubes were tested with the 12.7 mm outer diameter. The actual outer diameter over the fins for each tube is presented in Table 3.1.

Refrigerant Flow Loop

The refrigerant flow loop is a closed-circulation loop, and it delivers refrigerant at desired saturation conditions to the test section. Refrigerant is pumped through the closed-flow loop with a triplex diaphragm pump driven by a 3/4 hp shunt wound motor. The principle advantage of the diaphragm pump is that it is self lubricated with an oil sump that is sealed from the refrigerant side of the pump. Therefore, no oil is required in the working fluid for pump lubrication, and pure refrigerant tests may be conducted without excessive pump wear. Refrigerant is pumped through a true-mass flow meter to a 240 volt heater section. This heater raises the liquid temperature back to the test-section saturation temperature. Refrigerant exits from the heater section and flows through a filter/drier, a cartridge filter, and then enters the spray manifold.

The spray manifold that was initially installed and used with the high-pressure drop nozzles had variable head loss within the five branches of the manifold. Refrigerant supply was equalized by using small orifice nozzles that generated sufficient pressure drop to equalize the flow rate to each individual nozzle. When using wide-angle, low-pressure drop nozzles at flow rates in the 3.0 kg/min range (system mass flow rate), the differential pressure across the spray manifold was found to be only 1.7×10^4 Pa (2.5 psi) which was insufficient differential pressure to equalize flow rates across the five nozzles. Therefore, a new spray manifold was constructed having a large internal diameter in its main chamber and five equal-length supply lines from the main chamber to the test section. Tubes were tested with the new manifold arrangement, and it was verified with temperature measurements along the top surface of the copper test-tube that flow was being supplied evenly to each of the five nozzles.

Refrigerant is sprayed into the test section so as to impinge upon the test-tube that is fixed in the center of the test section (radially). The refrigerant that vaporizes on the heated test-tube then flows to the condenser by exiting out either of the two vapor outlets. The refrigerant which does not vaporize, along with the refrigerant droplets that did not impact along the test-tube wall, flows out two liquid outlets located on the bottom of the test section. This test-section liquid return combines with the refrigerant condensed in the condenser, and then flows to the subcooler. The subcooler ensures a multi-phase mixture is supplied to the suction of the diaphragm pump. Figure 3.1 shows the location of temperature and measurement points within the system.

Spray Nozzles

Two types of nozzles, mainly low and high-pressure drop nozzles, were tested. High-pressure drop, solid-cone nozzles were employed with the 12.7 mm diameter test-tubes. The differential pressure across the nozzle manifold was maintained at greater than 8.6×10^5 Pa

(125 psi), and the nozzles were capable of producing a finely atomized cone. Bore sizes of 63.5×10^{-3} mm, 73.7×10^{-2} mm, and 81.3×10^{-2} mm were tested. It was found that the 81.3×10^{-2} mm orifice size yielded the most favorable performance of the three.

The second type of nozzles evaluated were low pressure drop, wide-angle, solid cone nozzles having an orifice diameter of 1.6 mm. These nozzles supplied a much wider droplet pattern of refrigerant along the entire length of the test-tube. Testing was performed with both the 12.7 mm and 19.1 mm diameter tubes using these wide-angle nozzles. With either nozzle type the height of the nozzle over the tube was fixed at 36.5 mm for the 19.1 mm diameter tubes and 39.7 mm for the 12.7 mm diameter tubes.

Glycol/Water Flow Loop

A glycol/water solution is used to cool several components of the test rig via an auxiliary flow loop. The glycol/water mixture is pumped from a 30-ton chiller tank reservoir to the test rig's distribution manifold. Separate throttling valves direct cooling liquid to the subcooler and the condenser. Cooling liquid flowing to the condenser passes through a 5 kW circulation heater. The circulation heater allows condenser supply water to be increased in temperature in order to maintain test-section saturation conditions. This process is controlled by an automatic temperature controller. The water/glycol mixture supplied to the condenser and the subcooler recombines and returns to the 30 ton chiller tank reservoir.

Data Acquisition

Data acquisition is done with a personal computer, a 50-channel scanner, and a multimeter. The controlling program on the personal computer operates the multimeter and scanner. It also displays temperature, pressure, power, and mass flow rate measurements to the CRT and writes the information to a disc file for data reduction. The data acquisition

system monitors two pressure transducers, two watt transducers, a flow meter, and 20 thermocouples.

Experimental Methods

The following is a description of the data taking procedure used with the multi-tube test facility for all results presented in this work. Test-section saturation conditions were maintained by controlling the flow rate and temperature of the glycol/water fluid supplied to the condenser. For the pure HFC-134a testing, the test section was maintained at a saturation temperature of 2.0 °C. However, during the lubricant effects testing with HFC-134a and two polyol-ester oils, all data was collected at a test-section pressure of 314.5 kPa. This pressure corresponds to a saturation temperature of 2.0 °C for pure HFC-134a. Heat flux was varied in increments of approximately 5 kW/m² in an increasing manner between data points. Power to the cartridge heater was controlled with a variac, and the power level was measured with a watt transducer. Each data point was obtained by averaging at least 5 data acquisition scans.

When only a single tube was tested, it was located in the radial center of the test section. Size restrictions within the test section prevented two 19.1 mm diameter tubes from being tested simultaneously. However, limited testing with two tubes was done with the 12.7 mm tubes. When conducting multi-tube tests, the second tube was mounted to the tube sheet directly under and parallel to the upper tube, with a pitch length of 28.6 mm. During these multi-tube tests, heat flux was varied on each tube so that wall heat flux on the upper and lower tubes was nominally the same (± 2 kW/m²) for any given data acquisition scan.

Collector Tests

The majority of the previous single-tube, falling-film evaporation studies have been conducted with a thin-slot or perforated plate distribution system rather than nozzles. These distributors rely upon gravity flow of the liquid and direct all of the circulated refrigerant onto the test-tube surface. This study was conducted with nozzles similar to those which might be used in a large industrial spray evaporation system. Therefore, in single-tube test analysis a portion of the nozzle plume did not come in contact with the tube wall. To determine what percentage of the refrigerant supplied to the test section contacted the tube surface, a series of collector tests was performed with two different size collectors. Specifically, one collector was sized with a width at its top equal to the 19.1 mm tube diameter and a length equal to the heated length of the cartridge heater. The second collector had the same length but its width at the top was only 12.7 mm. Both collectors had increasing diameter with depth so the inclined walls minimized splatter out of the collector, and this also increased the volume of the collector improving the accuracy of the tests. The fraction of liquid hitting the tube surface when a given refrigerant mass flow rate is supplied to the spray manifold is termed the collector test fraction (CTF). The HFC-134a, 2.8 kg/min manifold supply rate corresponds to a film-feed supply rate of 0.066 kg/(s*m) assuming no parasitic pumping losses (i.e. all refrigerant contacts the tube). The collector test fractions are stated below for each diameter tube for the HFC-134a mass flow rate of 2.8 kg/min. It should be noted that this fraction is specific to the geometry and test conditions in this work. Collector testing of the HFC-134a 2.3 kg/min and 3.0 kg/min flow rates was not conducted.

19.1 mm Diameter Tube: CTF = 0.193 (19.3%)

12.7 mm Diameter Tube: CTF = 0.143 (14.3%)

Using the collector test fraction, the effective refrigerant mass flow rate hitting tube surface is

$$\dot{m}_e = (\dot{m}_{spr})(CTF) \quad (3.1)$$

To obtain the effective film supply rate (Γ_e), the following equation is applied:

$$\begin{aligned} \Gamma_e &= (\Gamma_d)(CTF) \\ &= \{[0.066 \text{ kg/(s*m)}](0.193)\} \\ &= 0.013 \text{ kg/(s*m)} \end{aligned} \quad (3.2)$$

Lubricant Addition and Sampling

During the lubricant effects testing on the multi-tube test facility, the desired lubricant concentration was obtained by measuring the mass of refrigerant while charging the system. Knowing the mass of refrigerant in the system, a precise amount of lubricant was injected into the test section with a syringe to obtain the desired mass fraction of lubricant. After each lubricant injection, the system was circulated for a four hour period at a high flow rate to ensure even mixing within the system. Upon completion of data collection with a given lubricant, the test facility was thoroughly distilled and verified clean.

Sampling was conducted on the multi-tube test facility only to verify cleanliness of the system upon completion of distilling a lubricant out of the flow loop. Refrigerant samples of approximately 50 grams were taken out of a charge valve on the discharge line of the refrigerant pump while circulating refrigerant. After applying heat for several hours to the sample allowing the refrigerant to vaporize off, the cylinder weight was measured and

compared to its initial pre-sample weight. No weight gain indicated a pure refrigerant sample was drawn.

CHAPTER 4. TUBE-BUNDLE TEST FACILITY

The tube-bundle test facility was built to simulate the environment found in a real industrial chiller equipped with a spray manifold for refrigerant distribution over the tube bundle. This arrangement allowed for the assessment of bundle depth effects upon spray evaporation heat transfer performance, which is different than the bundle depth effects found in flooded evaporators.

Facility Description

The test facility used in this study is capable of measuring shell-side heat transfer coefficients on tube bundles in either a spray evaporation or pool boiling mode. The test rig has several main parts: a test section, a tube bundle(s), a refrigerant flow loop, the spray nozzles, a glycol/water flow loop, a closed water loop, and the data acquisition equipment. A schematic of the rig is shown in Figure 4.1, and a detailed description is presented below.

Test Section

The stainless-steel test section is equipped with two glass-view side ports (one per side) so visual observations may be made while conducting heat transfer experiments. The test section has a diameter of 203.2 mm and is 660.4 mm long from flange face to flange face.

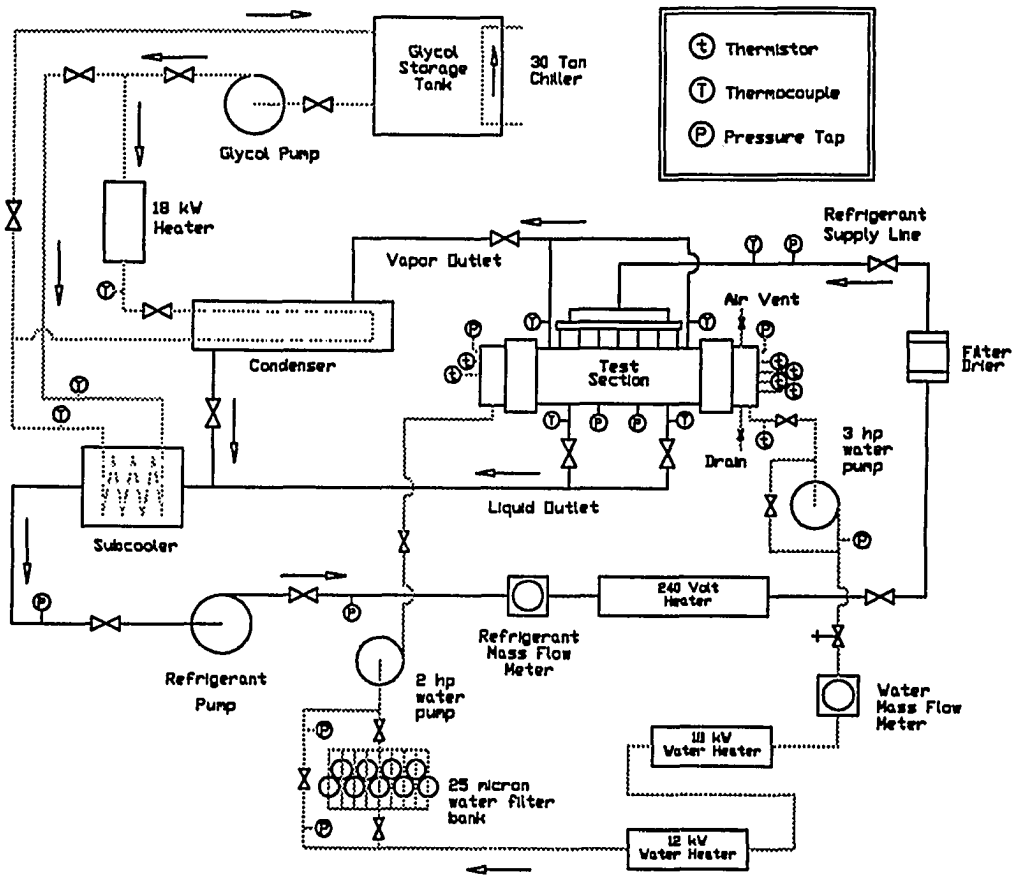


Figure 4.1: Bundle Test Facility Schematic

Along the top of the test section are 7 threaded ports with compression fittings, stainless-steel supply tubes, and spray nozzles. These ports lie along the longitudinal centerline of the test section. The nozzle ports are machined with a gap of 88.9 mm separating them. The middle nozzle port (nozzle number 4) is positioned at the midpoint from one end of the test section to the other. The height of the nozzles may be varied by adjusting the vertical position of the stainless-steel supply tube in the compression fitting. At 45 degrees off top-dead-center, along opposite sides, are the two refrigerant vapor outlets. Two liquid outlets lie along bottom-dead-center of the test section. Two pressure taps allow saturation pressure to be measured which can then be used to determine the saturation temperature.

Tube Bundle(s)

The majority of the tube-bundle work conducted in this study was done with triangular-pitch tube bundles consisting of 4 rows of 5 tubes. The rows are numbered from top to bottom with identifiers of 1,2,3, and 4. Figure 4.2 shows the dimensions of the triangular-pitch tube bundle. Dimensions of the square-pitch tube bundle are shown in Figure 4.3. Dimensions shown in Figures 4.2 and 4.3 are in inches. The length of the tube bundle is 660.4 mm. The tube bundle was constructed by expanding the 19.1 mm diameter copper tubes into 25.4 mm thick, 203.2 mm diameter stainless-steel tube sheets.

It was necessary to inactivate several tubes due to load limitations of the test facility's ultimate heat sink. Plugging the fourth row was considered because this offered the advantage of maintaining symmetry within the bundle. However, the bottom row is important for conducting a performance comparison of alternative nozzle configurations. The bottom row is the first to suffer dryout when the nozzle configuration does not adequately distribute the liquid over the bundle. Therefore, the first tube in each row was plugged removing it from the heat transfer process during the HFC-134a and HCFC-22 testing. The first and last tube

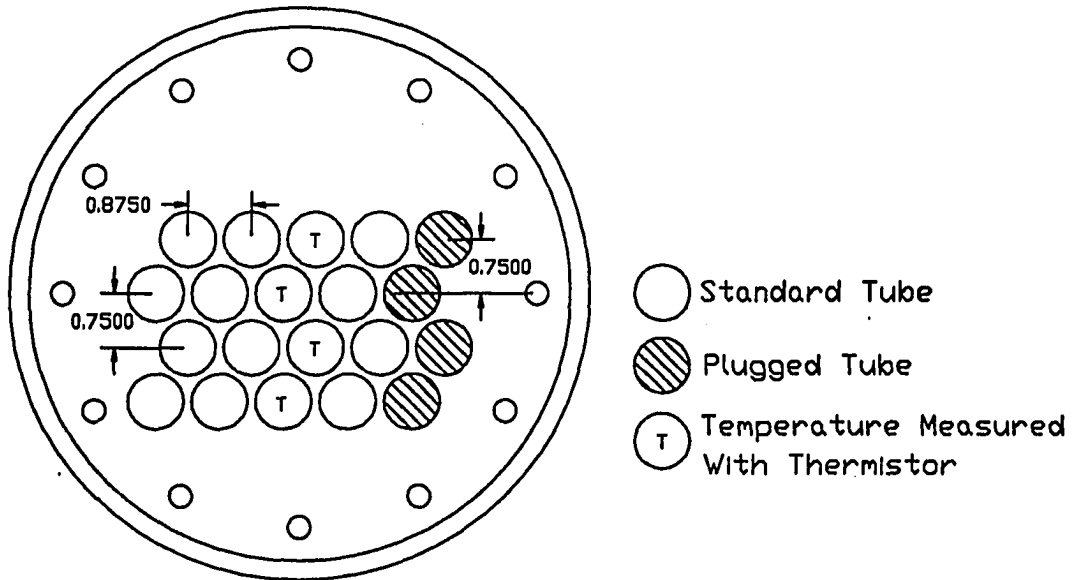


Figure 4.2: Triangular-pitch tube bundle geometry

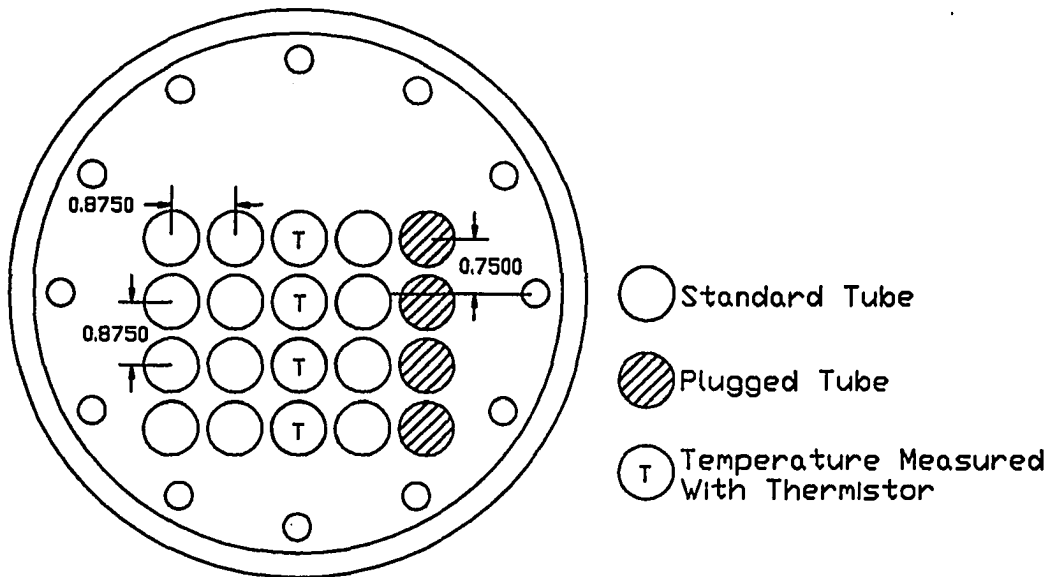


Figure 4.3: Square-pitch tube bundle geometry

in each row was plugged in a similar fashion during the HCFC-123 testing for the same reason.

Five different tube surfaces were used with this test facility. The tubes tested were the W-SC, the Tu-B, the Tu-Cii, the W-40 fpi, and a plain surface [39]. Dimensions for the five tube surfaces used during the tube-bundle testing are given in Table 4.1.

Table 4.1: Geometry specifications for the tubes tested on the bundle test facility

| tube | fin count fins/m | D_o nominal mm | D_i nominal mm | D_r nominal mm | fin height mm |
|----------|------------------------|------------------------|------------------------|------------------------|---------------------|
| plain | - | 18.9 | 16.4 | - | - |
| W-40 fpi | 1575 | 18.7 | 15.7 | 17.1 | 0.9 |
| W-SC | 1024 | 18.9 | 14.2 | 16.8 | 1.1 |
| Tu-Cii | 1575 | 18.9 | 15.5 | 17.1 | 0.9 |
| Tu-B | 1575 | 18.7 | 16.1 | 17.4 | 0.7 |

Refrigerant Flow Loop

The refrigerant flow loop is a closed circulation loop similar in design to the one used on the multi-tube test facility. Two different refrigerant pumps were used on the bundle test facility during different portions of the tube-bundle testing. Refrigerant was pumped with a triplex diaphragm pump driven by a 5.6 kW (7-1/2 hp), 3 phase, 480 volt motor during the HFC-134a and HCFC-22 testing. Speed control was obtained with a 3 phase, 480 volt inverter power supply capable of delivering an output frequency as low as 5 hertz. For the HCFC-123 testing, a centrifical pump was used due to suction-line low-pressure limitations of the triplex diaphragm pump. Like the diaphragm pump, it was powered by the inverter, but a discharge line throttling valve was the primary flow control device.

Refrigerant is pumped through a true-mass flow meter and a 15 kW heater section before entering the spray manifold. The heater section has a 50 micron filter/drier unit at its outlet. The 15 kW heater allows for the liquid temperature to be controlled so that the spray manifold temperature is maintained within 2.0 °C of the saturation temperature in the test section.

The spray manifold used on this facility was designed based upon experiences gained on the multi-tube test facility. The main chamber is sized with a large internal diameter so that head loss is minimized, and 7 equal length nylon tubes branch off from the main chamber to the individual stainless-steel supply tubes. The refrigerant liquid is supplied to both ends of the spray manifold's main chamber to further ensure uniformity in the refrigerant supply to the individual nozzles. A pressure port in the manifold's main chamber allows nozzle differential pressure to be recorded during the experimental tests.

The majority of the refrigerant sprayed into the test section comes in contact with the tube bundle. The refrigerant which misses the tube bundle is referred to as a parasitic pumping loss. Refrigerant vaporizing on the heated copper tubes leaves the test section via two vapor outlets and is supplied to the condenser(s). During the high-pressure refrigerant testing, a single 20-ton condenser was used on this test rig. For the HCFC-123 testing, a second 10-ton condenser was added to increase the condensation UA value relative to that of the single 20-ton condenser. Refrigerant which does not vaporize combines with the liquid droplets which did not contact the tube bundle, and the adjoining liquid stream exits the bottom of the test section via two liquid outlets. Liquid leaving the test section combines with refrigerant condensed in the condenser and is supplied to the refrigerant pump via a subcooler. The subcooler ensures that a single-phase liquid is supplied to the pump minimizing the chance of cavitation developing at any point during a data run.

Spray Nozzles

A wide variety of nozzles are commercially available. The nozzles used on the bundle test facility were solid pattern, circular and square types. These nozzles generate wide-angle refrigerant plumes at nozzle differential pressures as low as 17.2 kPa (2.5 psid). Table 4.2 provides a summary of the nozzle orifice sizes and heights used during this study. The nozzle height is defined as the vertical distance from the horizontal plane intersecting top-dead-center of the top row of tubes to the horizontal plane intersecting the nozzle tips positioned directly above the tube bundle.

A seven digit code was developed to categorize the various nozzle configurations used on the bundle test facility. The first two digits of the code present an orifice size identifier (17, 24, or 30), the third character uses the letter W to refer to wide-angle nozzles, the fourth character uses a letter to identify the nozzle height (H, L, or D), and the last three characters refer to either a circular or square plume (CRC or SQR).

Glycol/Water Flow Loop

The ultimate heat sink for the bundle test facility is the 30 ton chiller in the heat transfer lab at Iowa State University. A centrifugal pump supplies a glycol/water mixture from the chiller to the test facility. The water is supplied via separate globe valves to the subcooler and the condenser(s). The globe valves provide adequate throttling capabilities for system operation. The refrigerant saturation temperature is controlled via an 18 kW circulation heater in the glycol/water supply line to the condenser. This process is regulated by an automatic temperature controller which receives a temperature signal from a thermocouple probe in the glycol/water inlet to the condenser.

Table 4.2: Geometric specifications for the nozzle configurations used on the bundle test facility

| Nozzle Configuration | Orifice Diameter (mm) | Distance Above Bundle (mm) | Spray Pattern | Refrigerant Application |
|----------------------|-----------------------|----------------------------|---------------|-------------------------|
| 17WHCRC | 3.97 | 66.7 | Circular | R-134a |
| 17WLCRC | 3.97 | 41.3 | Circular | R-134a |
| 24WHCRC | 4.76 | 66.7 | Circular | R-134a |
| 24WLCRC | 4.76 | 41.3 | Circular | R-134a |
| 24WHSQR | 4.76 | 66.7 | Square | R-134a |
| 24WLSQR | 4.76 | 41.3 | Square | R-134a |
| 24WDCRC | 4.76 | 44.3 | Circular | R-123 |
| 30WHCRC | 5.56 | 66.7 | Circular | R-134a, R-22 |
| 30WHSQR | 5.56 | 66.7 | Square | R-134a |
| 30WDCRC | 5.56 | 44.3 | Circular | R-123 |

Closed Water Loop

Two centrifugal pumps, one a 2 hp pump, and the second a 3 hp pump, circulate water through the two circulation heaters, a filter bank, and the tube bundle in the test section. The filter bank consists of 9 dual element filters capable of removing particulates of a 25 micron diameter and larger. These filters are used to ensure no particulates foul the heat transfer surface on the inside of the tubes in the bundle. A controller is used to operate the two circulation heaters. The controller can operate with either automatic temperature control or manual percent power control. It was found that the latter provided a much steadier inlet temperature to the tube bundle, therefore it was used throughout this testing. The combined heating capacity of the two circulation heaters is 30 kW. This loop is equipped with a true-mass flow meter so that an accurate mass flow rate could be used for the calculation of the water-side heat transfer coefficients in the tube bundle.

Water temperature is measured at the inlet to the test section by two thermistors in the inlet water header. Row-by-row bundle performance analysis is made possible by 4 thermistor probes which protrude through the outlet water header so the thermistor beads lie approximately 12.7 mm (1/2 inch) into the outlet hole of the third tube in each row. It should be noted that this depth corresponds to one-half of the thickness of the stainless-steel tube sheet. The instrumented tubes are shown in Figures 4.2 and 4.3. Another thermistor monitors the water temperature leaving the outlet water header. This temperature is used to calculate the overall bundle heat transfer coefficient.

Data Acquisition

Data acquisition is done with a personal computer, a 50-channel scanner, and a multimeter. The controlling program on the personal computer operates the multimeter and scanner. It also displays temperature, pressure, power, and mass flow rate measurements to the CRT and writes the information to a disc file for data reduction. The data acquisition system monitors three pressure transducers, two true-mass flow meters, seven thermistors, and ten thermocouples.

Experimental Procedure

The following is a description of the data taking procedure used with the tube-bundle test facility. Data was taken with a decreasing heat flux, similar to the approach used by Webb [32] during a pool boiling study. The lowest heat flux evaluated in the current study was 5 kW/m² on the multi-tube test facility and 19 kW/m² on the tube-bundle test facility.

Hysteresis effects were not observed in the data taken on either test facility because even a heat flux of 5 kW/m^2 is sufficient to develop boiling effects in the heat transfer process.

With refrigerants HFC-134a and HCFC-22, heat transfer coefficients in the condenser were high enough so that only one tube in each row was plugged. Even though an extra 10 tons of condenser capacity were added to the test facility, two tubes in each row were plugged during the HCFC-123 testing to allow saturation temperature/pressure to be maintained within the band of interest. The heat flux range evaluated in each bundle run was the same regardless of the number of active tubes, thus the bundle load required for a given heat flux depended upon the number of active tubes within the bundle. With the 16-tube configuration, the bundle load was varied from 23 kW to 11 kW in increments of 2 kW between data points during each data run. These loads correspond to nominal heat fluxes of 40 kW/m^2 to 19 kW/m^2 , respectively. Bundle load was varied with the 12-tube configuration from 17.25 kW to 8.25 kW in increments of 1.5 kW between data points. These loadings correspond to the same nominal heat flux range used during 16-tube configuration testing.

All pure refrigerant data was taken at a saturation temperature of $2.0 \text{ }^\circ\text{C}$ on the bundle test facility so a comparison could be made of the performance characteristics of the three different refrigerants. During the lubricant effects evaluation testing, the test-section pressure was maintained at the value which corresponded to that of the respective pure refrigerant at a saturation temperature of $2.0 \text{ }^\circ\text{C}$. For each of the three refrigerant/lubricant combinations, the refrigerant/lubricant mixture data was corrected for the effects of solubility on the test-section saturation temperature.

In each experimental run the refrigerant supply rate was held at nominally the same value while heat flux was decreased. This was done to avoid hysteresis effects which could be generated if the film-feed supply rate as well as the heat flux was varied simultaneously

throughout the test. Operating parameter set points and maximum allowable deviations from respective set points are presented below.

| | |
|---|--------------------------------|
| Bundle Load | Desired Value \pm 0.3 kW |
| Refrigerant Mass Flow Rate (diaphragm pump) | Desired Value \pm 2.0 kg/min |
| Refrigerant Mass Flow Rate (centrifical pump) | Desired Value \pm 1.0 kg/min |
| Spray Manifold Temperature | 0.0 °C to 3.0 °C |
| Bundle Δ T (Waterside) | 1.9 °C to 2.1 °C |

A 2.0 °C temperature drop was maintained on the water-side of the tube bundle throughout each data run. Allowing a greater temperature differential across the water-side could create variations in the mode of heat transfer axially along the surface of a tube. With differential temperatures less than 2.0 °C, the uncertainty became unreasonably high. It was verified that 2.0 °C of subcooling in the refrigerant supplied to the spray manifold had no effect upon shell-side heat transfer performance.

Each data point was obtained by averaging 10 data acquisition scans. These ten scans were transferred via a disk file to a spread sheet where the means for each measurement were calculated. This spread sheet also indicated which individual readings were more than 2 standard deviations from a respective parameters' mean. This capability was used to determine the quality of each individual measurement so that a given point could be retaken if needed. Output from the spread sheet was post-processed with a FORTRAN code.

Inside Heat Transfer Coefficient Determination

Prior to conducting shell-side heat transfer testing using log mean temperature difference (LMTD) analysis, the inside heat transfer coefficient must be known. A modified Wilson Plot

analysis was used to determine the inside heat transfer coefficient for the tubes evaluated in this study. This technique is described in detail by Huber et al. [40].

The Seider-Tate correlation is used to describe the water-side flow field.

$$h_i = \text{STC} \frac{k}{D_i} \text{Re}^{0.8} \text{Pr}^{0.33} \left(\frac{\mu_h}{\mu_w} \right)^{0.14} \quad (4.1)$$

It was desired to conduct shell-side heat transfer tests through a Reynolds number range of 7000 to 25000 on the water-side of the tube. It was found that the internal enhancement of only the W-40 fpi and W-SC tubes yielded a linear Seider-Tate coefficient through the low end of this Reynolds number range. The other three tubes, including the plain tube, were equipped with a spring-type turbulator, which maintained turbulent internal heat transfer performance through the entire Reynolds number range evaluated in the Wilson Plot analysis testing. There is a friction fit between the coils of the turbulator and the inner surface of the tube wall which holds it in place as water flows through the tube. Turbulence is maintained by continuously tripping of the boundary layer along the inner wall of the tube. These turbulators are used in several industrial chiller applications [41].

The Seider-Tate coefficient is determined by boiling refrigerant on the shell-side of the tube at a constant saturation temperature and a constant heat flux while varying the inside water mass flow rate through the tube. The data are plotted on x-y coordinates using the following relations.

$$x = \frac{\frac{A_o}{A_i}}{\frac{k}{D_i} \text{Re}^{0.8} \text{Pr}^{0.33} \left(\frac{\mu_h}{\mu_w} \right)^{0.14}} \quad (4.2)$$

$$y = \frac{A_o LMTD}{q} - A_o R_w \quad (4.3)$$

Wilson Plot data for the Tu-B tube is shown in Figure 4.4, and data for the plain tube is shown in Figure 4.5, both having turbulators installed. The Seider-Tate coefficient is defined as the inverse of the slope of the data. Seider-Tate coefficients of 0.066 for the Tu-B and 0.063 for the plain tube were determined in this testing. Seider-Tate coefficients of 0.055 for the W-40 fpi, 0.054 for the W-SC, and 0.065 for the Tu-Cii tubes were determined by testing conducted by Huber et al. [40, 42].

Collector Tests

Collector testing was performed on the bundle test facility with each refrigerant to determine the percentage of refrigerant supplied to the spray manifold contacting the tubes. A collector was constructed of steel with graduated side-glass assemblies on either side for this testing. The dimensions of the collector correspond to the exact dimensions of the triangular-pitch bundle geometry. Attachments can be added to the top of the collector, which allows for collector testing to be conducted for the square-pitch bundle geometry. Results of these collector tests are summarized in Table 4.3. The triangular and square-pitch bundle geometry collector test fractions for the 30WHCRC nozzle configuration at a 45 kg/min refrigerant supply rate were calculated with statistical curve fits of the measurements made at the lower supply rates. The investigators deemed this to be a more accurate approach than using collector test results at this flow rate due to excessive splashing in the collector and the rapid transient time of the test at this high circulation rate.

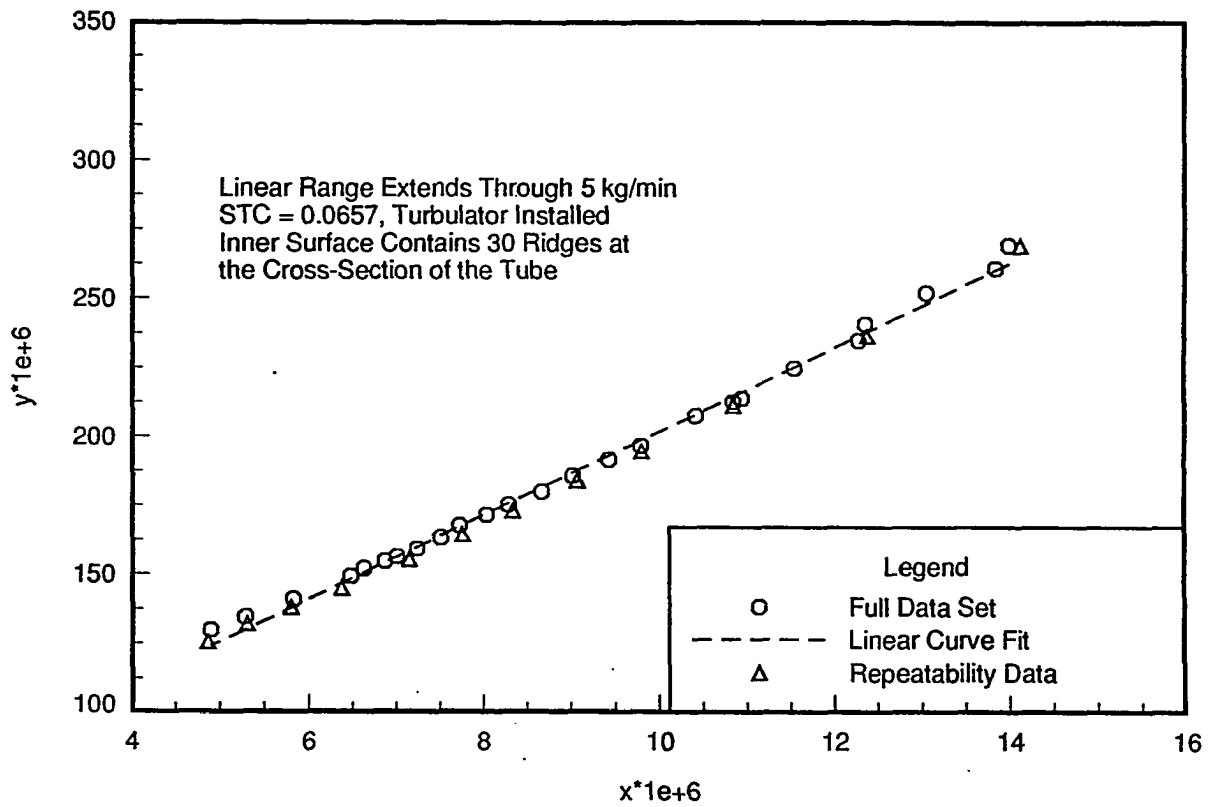


Figure 4.4: Wilson plot data for the Tu-B tube with turbulator installed

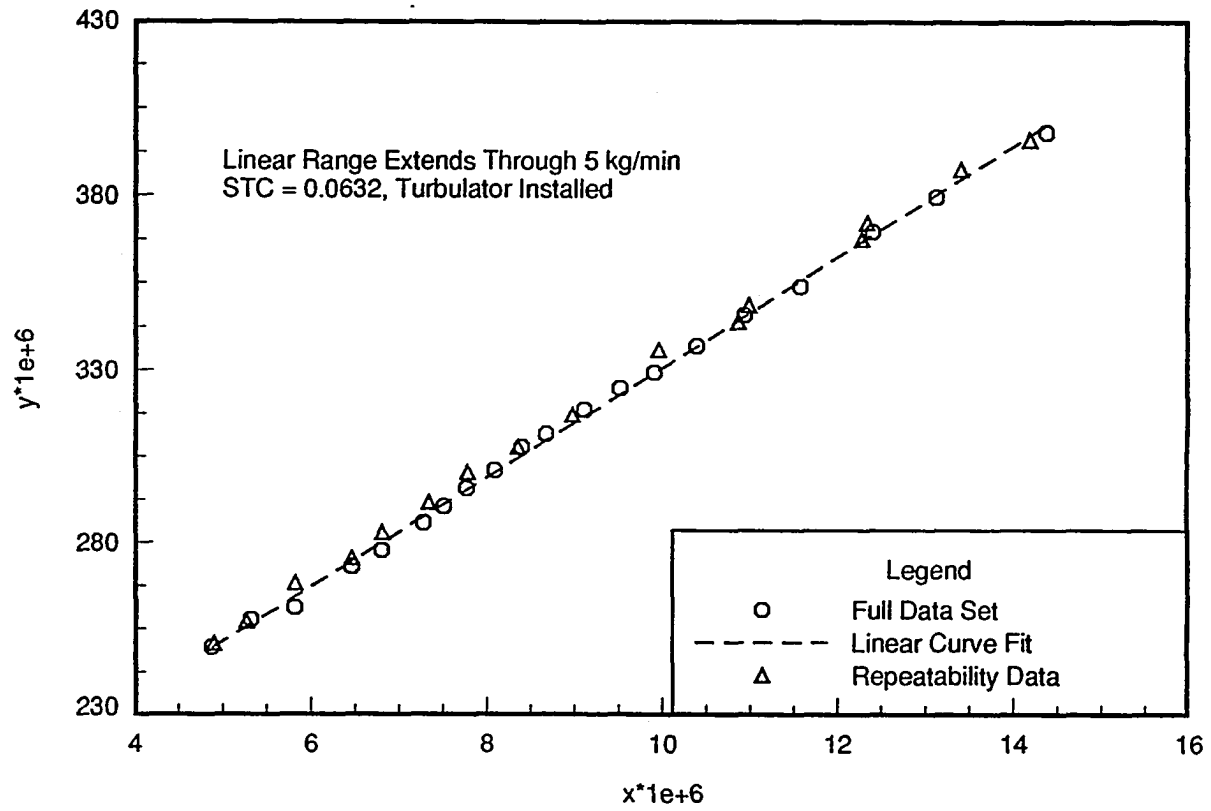


Figure 4.5: Wilson plot data for the plain tube with turbulator installed

Table 4.3: Bundle test facility, collector test results

| Nozzle Configuration | Bundle Pitch Geometry | Refrigerant | Refrigerant System Mass Flow Rate (kg/min) | Collector Test Fraction |
|----------------------|-----------------------|-------------|--|-------------------------|
| 17WLCRC | Triangular | R-134a | 25 | 0.54 |
| 24WLCRC | Triangular | R-134a | 25 | 0.62 |
| 30WHCRC | Triangular | R-134a | 15 | 0.83 |
| 30WHCRC | Triangular | R-134a | 25 | 0.77 |
| 30WHCRC | Triangular | R-134a | 35 | 0.75 |
| 30WHCRC | Square | R-134a | 15 | 0.78 |
| 30WHCRC | Square | R-134a | 35 | 0.70 |
| 30WHCRC | Triangular | R-22 | 15 | 0.80 |
| 24WDCRC | Triangular | R-123 | 25 | 0.64 |
| 24WDCRC | Triangular | R-123 | 35 | 0.54 |
| 30WDCRC | Triangular | R-123 | 25 | 0.79 |
| 30WDCRC | Triangular | R-123 | 35 | 0.69 |

Lubricant Addition and Sampling

Lubricant was injected and sampled at the facility's oil-handling station. The lubricant was injected in a batch process with a double actuating cylinder which required testing to be conducted from progressively lower to higher concentrations. Sampling was conducted with two double actuating cylinders during the HFC-134a lubricant effects phase of the tube-bundle testing. A second method of sampling on the bundle test facility was provided by a stainless-steel sample cell fixed into the refrigerant flow loop in a bypass circuit between the refrigerant spray manifold and the refrigerant pump's suction line. This sample cell was used during the HCFC-22 and HCFC-123 tube-bundle, lubricant effects testing.

The amount of oil injected into the facility was calculated by measuring the density of the oil, and the length of displacement of the piston shaft during the injection. Nitrogen gas

provided the force for injecting the oil into the system. Nitrogen gas was also used while sampling with the double actuating cylinder to apply a back-pressure to the piston, which was bled off slowly allowing the refrigerant/lubricant mixture to enter the sampling piston without flashing into a two-phase mixture. When sampling with the sample cell in the bypass circuit this step was not required.

Samples were drawn off the refrigerant flow loop at a point located physically upstream from the oil injection port. This was advantageous since lubricant drawn out at the sample port in the form of a mixture physically had to circulate through the entire system before arriving at this point. Four hours of mixing were conducted between lubricant injection and performing the sampling procedure.

After the samples were drawn, refrigerant was bled off from the mixture via a throttling valve through a cloth filter which entrapped any lubricant passing through the cylinder or cell's vapor outlet. The remaining lubricant in either the double actuating cylinder or sample cell was evacuated to remove any refrigerant remaining in the oil. Weights were recorded for the clean, full, and evacuated sample assemblies which were used with *ASHRAE Standard 41.4-1984* [43] to calculate the mass fraction of lubricant, with the exception that the sample size is smaller than that stated in the standard. The weights were measured with an electronic scale accurate to ± 0.01 g (2.2×10^{-5} lbm).

CHAPTER 5. DATA ANALYSIS

The analysis of data from both spray evaporation test facilities consisted of a three step process. First, important experimental factors are calculated from the raw experimental data. This step is followed by the calculation of experimental uncertainties. Finally, the results are presented in a manner to emphasize important characteristics and trends. In the following sections these three phases are discussed.

Data Reduction

Both test facilities are similar in design and construction. The primary difference between the two test facilities is the means of measuring shell-side heat transfer coefficients. On the multi-tube test rig the shell-side heat transfer coefficients are measured with wall mounted thermocouples and refrigerant-space temperatures. The larger bundle test facility utilized log mean temperature difference analysis for shell-side heat transfer coefficient determination.

Multi-Tube Test Facility

The parameters of particular interest on the multi-tube test facility during a data run are the test-tube's thermocouple wall temperatures, the test-section refrigerant-space probe temperatures, the test-section refrigerant inlet and outlet-thermocouple probe temperatures, refrigerant mass flow rate, the watt transducer reading, and test-section refrigerant-space pressure.

Heat flux on the surface of the tube is based upon the measured power level of the cartridge heater and a nominal 12.7 mm or 19.1 mm diameter tube surface area. Only the active length of the heater is considered for the heat flux calculation. Each thermocouple on the tube surface is area weighted, and the side thermocouples are superimposed upon the opposite side of the tube. This approach counts each side thermocouple twice, which is accounted for in the uncertainty analysis. The following equation is used to determine the wall heat flux.

$$q'' = \frac{Q_{hr}}{A} \quad (5.1)$$

The parameter Q_{hr} is the power supplied to the cartridge heater, which is measured with a watt transducer. The average shell-side heat transfer coefficient is based upon the following equation,

$$h = \frac{q''}{T_s - T_r} \quad (5.2)$$

where T_s is the area weighted average wall temperature and T_r is the average refrigerant-space temperature measured with thermocouple probes in the test section.

The test-section recirculation ratio is defined as the ratio of the mass flow rate of refrigerant supplied to the test section to the mass flow rate of refrigerant vapor leaving the test section. Because the facility is equipped with only one mass flow meter, this parameter must be calculated from a thermodynamic energy balance across the test section which is shown in Equations 5.3, 5.4, and 5.5. The enthalpies i_{spr} , i_{vap} , i_{liq} are calculated from thermocouple probe temperatures and known saturated liquid and vapor enthalpies.

$$Q_{hr} + (\dot{m}_{spr})(i_{spr}) = x(\dot{m}_{spr})(i_{vap}) + (1-x)(\dot{m}_{spr})(i_{liq}) \quad (5.3)$$

$$\dot{m}_{vap} = (x)(\dot{m}_{spr}) \quad (5.4)$$

$$\dot{m}_{liq} = (1-x)(\dot{m}_{spr}) \quad (5.5)$$

Equation 5.3, 5.4 and 5.5 are solved for the parameter x , which is defined as the fraction of refrigerant supplied to the test section that vaporizes. Equation 5.6 defines the recirculation ratio as the inverse of the parameter x .

$$RCR = \frac{\dot{m}_{spr}}{\dot{m}_{vap}} = \frac{1}{x} \quad (5.6)$$

Since the refrigerant supply rate was held constant during each data run, the film-feed supply rate remained constant while test-section recirculation ratio varied. The tube overfeed ratio may be calculated by multiplying the test-section recirculation ratio by the collector test fraction.

$$OFR = (RCR)(CTF) \quad (5.7)$$

Bundle Test Facility

The measured parameters and data reductions of particular interest during a data run on the bundle test facility are the water energy transfer rate, the water-side inlet and outlet temperatures, the temperature of the refrigerant in the test section, and all of the test-section refrigerant inlet and outlet temperatures. The test-section refrigerant temperature (saturation temperature) is determined from the known relationship between temperature and pressure of the three refrigerants evaluated on this facility and the measured test-section pressure. Thermistors provide water-side inlet and outlet temperatures which are used to calculate the bundle energy transfer rate using Equation 5.8.

$$q_w = \dot{m}_w c_p (T_{w-i} - T_{w-o}) \quad (5.8)$$

The water energy transfer rate is used to calculate the test-section recirculation ratio and the log mean temperature difference (LMTD). Equation 5.9 defines the log mean temperature difference for the test section. Note, both Equations 5.8 and 5.9 can be applied to the overall bundle or each respective row utilizing the individual row outlet temperatures.

$$\text{LMTD} = \frac{T_{w-i} - T_{w-o}}{\ln \left[\frac{T_{w-i} - T_{\text{sat}}}{T_{w-o} - T_{\text{sat}}} \right]} \quad (5.9)$$

Knowing the water-side energy transfer rate and the log mean temperature difference, the overall heat transfer coefficient may be calculated using Equation 5.10.

$$U_o = \frac{q_w}{A_o \text{LMTD}} = \frac{1}{\frac{1}{h_i} \frac{A_o}{A_i} + \frac{A_o \ln \frac{D_o}{D_i}}{2\pi k L} + \frac{1}{h_o}} \quad (5.10)$$

The Nusselt number is calculated with the Seider-Tate correlation [44] using Equation 5.11. Water-side bulk temperature values are used to calculate the Reynolds number, the Prandtl number, and the thermal conductivity.

$$\text{Nu} = \text{STC Re}^{0.8} \text{Pr}^{0.33} \left(\frac{\mu_h}{\mu_w} \right)^{0.14} = \frac{h_i D}{k} \quad (5.11)$$

Rearranging Equation 5.10, the shell-side heat transfer coefficient is defined as follows:

$$h_o = \frac{1}{A_o} \left(\frac{\text{LMTD}}{q_w} - \frac{1}{A_i h_i} - \frac{\ln \frac{D_o}{D_i}}{2\pi k L} \right)^{-1} \quad (5.12)$$

Equations 5.3, 5.4, and 5.5 may be applied to the bundle test facility as well as the multi-tube test rig. When applied to the bundle test facility the cartridge heater power Q_{hr} is replaced with the bundle energy load q_w . The actual bundle overfeed ratio (OFR) is calculated with Equation 5.13.

$$\text{OFR} = (\text{RCR})(\text{CTF})(\text{DF}) \quad (5.13)$$

A dummy factor is included in the equation to account for the plugged tubes in the bundle. This factor is equal to 0.8 for the 16 active tube configuration and 0.6 for the 12 active tube configuration. It should be noted that the tubes were plugged in columns.

Experimental Uncertainty

The uncertainties in the shell-side heat transfer coefficients on both test facilities were determined with propagation-of-error (POE) analysis [45]. In order to determine the experimental uncertainty related to variability in the experimental data, statistical packages are available which predict confidence intervals, confidence bands, and experimental error. These techniques were not used in this study since the independent variable heat flux was not controlled in a random manner on either test facility. However, approximately 20 % of the data runs were randomly selected during each phase of this project and repeated. This repeatability testing verified that the variability in the data from either test facility fell within acceptable limits, typically being on the order of 3 to 6 percent. Overall, the investigators considered the repeatability capabilities of both test rigs very favorable.

Multi-Tube Test Facility

Uncertainty in the shell-side heat transfer coefficients measured on the multi-tube test facility are evaluated with the following equation:

$$\delta h = \left[\left(\frac{\partial h}{\partial Q_{\text{htc}}} \delta(\Delta Q_{\text{htc}}) \right)^2 + \left(\frac{\partial h}{\partial T_s} \delta(\Delta T_s) \right)^2 + \left(\frac{\partial h}{\partial T_r} \delta(\Delta T_r) \right)^2 \right]^{0.5} \quad (5.14)$$

The partial fractions shown in Equation 5.14 are defined as follows:

$$\frac{\partial h}{\partial Q_{\text{htc}}} = \frac{1}{A(T_s - T_r)} \quad (5.15)$$

$$\frac{\partial h}{\partial T_s} = \frac{-Q_{\text{htc}}}{A(T_s - T_r)^2} \quad (5.16)$$

$$\frac{\partial h}{\partial T_r} = \frac{+Q_{hr}}{A(T_s - T_r)^2} \quad (5.17)$$

The parameter $\delta(\Delta Q_{hr})$ is the uncertainty in the cartridge heater power, $\delta(\Delta T_s)$ is the uncertainty in the average surface temperature, and $\delta(\Delta T_r)$ is the uncertainty in the refrigeration temperature. Uncertainty in the cartridge heater power is simply 0.2% of the reading from the watt transducer. The average wall temperature uncertainty is evaluated with Equations 5.18 and 5.19 noting that T_1 through T_9 are test-tube surface temperatures, and T_2 , T_5 and T_8 are the surface temperatures along the side of the test-tube wall.

$$T_s = \frac{T_1 + 2(T_2) + T_3 + T_4 + 2(T_5) + T_6 + T_7 + 2(T_8) + T_9}{12} \quad (5.18)$$

$$\delta(\Delta T_s) = \left\{ 3 \left[\left(\frac{1}{6} (0.2 \text{ }^\circ\text{C}) \right)^2 \right] + 6 \left[\left(\frac{1}{12} (0.2 \text{ }^\circ\text{C}) \right)^2 \right] \right\}^{0.5} \quad (5.19)$$

Test-section refrigerant-space temperature uncertainty is calculated with Equations 5.20 and 5.21. The terms T_{ts-l} and T_{ts-r} are the two test-section temperatures measured with thermocouple probes.

$$T_r = \frac{T_{ts-l} + T_{ts-r}}{2} \quad (5.20)$$

$$\delta(\Delta T_r) = \left[2 \left(\frac{1}{2} [0.2 \text{ }^\circ\text{C}] \right)^2 \right]^{0.5} \quad (5.21)$$

Table 5.1 contains the propagation-of-error uncertainty for the 19.1 mm diameter plain, finned, and enhanced surface results taken with pure HFC-134a.

Table 5.1: Multi-tube test facility shell-side heat transfer coefficient experimental uncertainty

| Surface Geometry | Uncertainty at 10 kW/m ² (percent) | Uncertainty at 40 kW/m ² (percent) |
|------------------|---|---|
| W-SC | ± 15.3 | ± 4.3 |
| W-SE | ± 12.5 | ± 2.9 |
| Tu-B | ± 13.3 | ± 1.9 |
| Tu-Cii | ± 13.3 | ± 3.1 |
| W-26 fpi | ± 12.6 | ± 3.1 |
| W-40 fpi | ± 10.7 | ± 2.1 |
| Plain | ± 4.1 | ± 1.0 |

In the higher heat flux range, the uncertainty of the heat transfer coefficient decreases because the magnitude of wall superheat increases. A summary of the accuracy for the instrumentation on the multi-tube facility is shown below.

| | |
|-----------------|---------------------|
| T/C Temperature | ± 0.20 °C |
| Watt Transducer | ± 0.20 % of Reading |
| Mass Flow Meter | ± 0.20 % |
| T/S Pressure | ± 0.11 % |

Bundle Test Facility

Shell-side heat transfer coefficient uncertainty for the bundle test facility is defined by the following equation:

$$\delta h_o = \left[\left(\frac{\partial h_o}{\partial \dot{m}_w} \delta(\Delta \dot{m}_w) \right)^2 + \left(\frac{\partial h_o}{\partial h_i} \delta(\Delta h_i) \right)^2 + \left(\frac{\partial h_o}{\partial c_p} \delta(\Delta c_p) \right)^2 + \left(\frac{\partial h_o}{\partial T_{sat}} \delta(\Delta T_{sat}) \right)^2 + \left(\frac{\partial h_o}{\partial T_{w-o}} \delta(\Delta T_{w-o}) \right)^2 + \left(\frac{\partial h_o}{\partial T_{w-i}} \delta(\Delta T_{w-i}) \right)^2 \right]^{0.5} \quad (5.22)$$

The parameter $\delta(\Delta\dot{m}_w)$ is the uncertainty of the water mass flow rate, $\delta(\Delta h_i)$ is the uncertainty in the inside heat transfer coefficients, and $\delta(\Delta c_p)$ is the uncertainty of the specific heat calculated from the bulk temperature on the water-side of the tube bundle. Uncertainty in the temperature measurements are represented by $\delta(\Delta T_{sat})$ for the saturation temperature, $\delta(\Delta T_{w-o})$ for the bundle water outlet temperatures, and $\delta(\Delta T_{w-i})$ for the bundle water inlet temperature. The partial fractions shown in Equation 5.22 are defined by the following equations.

$$X = -1 \left[\frac{A_o}{\dot{m}_w c_p \ln \left[\frac{T_{w-i} - T_{sat}}{T_{w-o} - T_{sat}} \right]} - \frac{A_o}{A_i h_i} - \frac{A_o \ln \frac{D_o}{D_i}}{2\pi k L} \right]^{-2} \quad (5.23)$$

$$\frac{\partial h_o}{\partial \dot{m}_w} = X \left[\frac{-A_o}{\dot{m}_w^2 c_p \ln \left[\frac{T_{w-i} - T_{sat}}{T_{w-o} - T_{sat}} \right]} \right] \quad (5.24)$$

$$\frac{\partial h_o}{\partial h_i} = X \left[\frac{A_o}{h_i^2 A_i} \right] \quad (5.25)$$

$$\frac{\partial h_o}{\partial c_p} = X \left[\frac{-A_o}{\dot{m}_w c_p^2 \ln \left[\frac{T_{w-i} - T_{sat}}{T_{w-o} - T_{sat}} \right]} \right] \quad (5.26)$$

$$\frac{\partial h_o}{\partial T_{sat}} = X \frac{-A_o}{\dot{m}_w c_p} \frac{1}{\left(\ln \left[\frac{T_{w-i} - T_{sat}}{T_{w-o} - T_{sat}} \right] \right)^2} \left(\frac{T_{w-i} - T_{sat}}{T_{w-o} - T_{sat}} \right) \left[\frac{T_{w-i} - T_{sat}}{(T_{w-o} - T_{sat})^2} - \frac{1}{T_{w-o} - T_{sat}} \right] \quad (5.27)$$

$$\frac{\partial h_o}{\partial T_{w-o}} = X \frac{A_o}{\dot{m}_w c_p} \frac{1}{\left(\ln \left[\frac{T_{w-i} - T_{sat}}{T_{w-o} - T_{sat}} \right] \right)^2} \left(\frac{T_{w-i} - T_{sat}}{T_{w-o} - T_{sat}} \right) \left[\frac{T_{w-i} - T_{sat}}{(T_{w-o} - T_{sat})^2} \right] \quad (5.28)$$

$$\frac{\partial h_o}{\partial T_{w-i}} = X \frac{-A_o}{\dot{m}_w c_p} \frac{1}{\left(\ln \left[\frac{T_{w-i} - T_{sat}}{T_{w-o} - T_{sat}} \right] \right)^2} \left(\frac{T_{w-i} - T_{sat}}{T_{w-o} - T_{sat}} \right) \left[\frac{1}{T_{w-o} - T_{sat}} \right] \quad (5.29)$$

Uncertainties of the shell-side heat transfer coefficients for all of the tube-bundle data reported herein were calculated while reducing the data with a FORTRAN post-processor in parallel with data reduction. Table 5.2 summarizes the shell-side heat transfer coefficient propagation-of-error uncertainties from the pure HFC-134a bundle work.

Table 5.2: Pure HFC-134 testing shell-side heat transfer coefficient uncertainty, bundle test facility

| Tube Bundle | M.F.R. (kg/min) | 11 kW Bundle Load (percent) | 23 kW Bundle Load (percent) |
|----------------------------|--------------------|-----------------------------------|-----------------------------------|
| Plain | 15 | 3.8 | 3.4 |
| | 35 | 4.6 | 3.7 |
| W-40 fpi | 15 | 8.6 | 11.3 |
| | 45 | 9.4 | 10.7 |
| W-SC | 15 | 10.5 | 14.7 |
| | 45 | 11.1 | 14.6 |
| Tu-Cii | 15 | 22.6 | 39.9 |
| | 45 | 26.8 | 35.5 |
| Tu-B (triangular pitch) | 15 | 10.8 | 14.7 |
| | 45 | 11.2 | 15.8 |

Note, the uncertainty for the Tu-Cii surface is considerably larger than that found with the other tubes. The greater the performance of a given tube surface, the higher the uncertainty in the shell-side heat transfer coefficient. The Tu-Cii surface results should be viewed considering the degree of uncertainty in the reported data. Table 5.3 summarizes the shell-side heat transfer coefficient propagation-of-error uncertainties from the HFC-134a and HCFC-22 lubricant effects testing. The Tu-B bundle performed very well in the lower heat flux range

Table 5.3: HFC-134a and HCFC-22 lubricant effects testing shell-side heat transfer coefficient uncertainty, bundle test facility

| Tube Bundle | Refrigerant | M.F.R. (kg/min) | % Oil | 11 kW Bundle Load (percent) | 23 kW Bundle Load (percent) |
|-------------|-------------|--------------------|-------|-----------------------------------|-----------------------------------|
| Plain | R-134a | 15 | 2.5 | 9.7 | 6.7 |
| Plain | R-134a | 35 | 2.5 | 10.6 | 7.5 |
| W-40 fpi | R-134a | 15 | 2.5 | 13.9 | 17.3 |
| W-40 fpi | R-134a | 35 | 2.5 | 14.7 | 22.5 |
| W-SC | R-134a | 15 | 2.5 | 18.3 | 13.5 |
| W-SC | R-134a | 35 | 2.5 | 19.8 | 18.3 |
| Tu-B | R-134a | 15 | 2.5 | 41.0 | 13.7 |
| Tu-B | R-134a | 35 | 2.5 | 45.7 | 18.8 |
| Plain | R-22 | 15 | 1.0 | 8.2 | 6.0 |
| Tu-B | R-22 | 15 | 1.0 | 44.6 | 15.0 |

Table 5.4: HCFC-123 lubricant effects testing shell-side heat transfer coefficient uncertainty, bundle test facility

| Tube Bundle | M.F.R. (kg/min) | % Oil | 8.25 kW Bundle Load (percent) | 17.25 kW Bundle Load (percent) |
|-------------|--------------------|-------|-------------------------------------|--------------------------------------|
| Plain | 25 | 0.0 | 9.1 | 6.1 |
| | 25 | 2.5 | 10.6 | 5.6 |
| | 35 | 0.0 | 9.2 | 6.2 |
| | 35 | 2.5 | 11.0 | 5.6 |
| Tu-Cii | 25 | 0.0 | 25.5 | 8.4 |
| | 25 | 2.5 | 28.6 | 9.5 |
| | 35 | 0.0 | 19.6 | 8.9 |
| | 35 | 2.5 | 32.3 | 10.3 |
| Tu-B | 25 | 0.0 | 44.9 | 22.4 |
| | 25 | 2.5 | 36.5 | 15.7 |
| | 35 | 0.0 | 46.0 | 23.4 |
| | 35 | 2.5 | 38.9 | 17.0 |

with small concentrations of lubricant. This yielded fairly high uncertainty in the shell-side heat transfer coefficients for the Tu-B bundle. Table 5.4 presents propagation-of-error from the HCFC-123 testing done with the 30WDCRC nozzle configuration. As was the case in the high-pressure refrigerant lubricant effects testing, the highest shell-side heat transfer coefficient uncertainties occurred with the Tu-B bundle. It should be noted that the variability in the lubricant effects repeatability data was in the 3 to 6 percent range. A summary of the accuracy for the instrumentation on the bundle facility is shown below.

| | |
|----------------------------------|---------------|
| Thermocouple Temperatures | ± 0.20 °C |
| Thermistor Temperatures | ± 0.05 °C |
| Water-Side Mass Flow Meter | ± 0.40 % |
| Refrigerant-Side Mass Flow Meter | ± 1.20 % |
| Test-Section Pressure (R-134a) | ± 0.17 % |
| Test-Section Pressure (R-22) | ± 0.32 % |
| Test-Section Pressure (R-123) | ± 0.72 % |

Data Analysis

The experimental heat transfer coefficients are analyzed and presented several different ways to help identify specific trends. This study focused on the effects of heat flux, surface enhancement, and lubricant concentration upon shell-side heat transfer coefficients. The effect of heat flux is shown by plotting the data on axes of heat transfer coefficient and heat flux.

To quantify the degree of heat transfer improvement gained by a type of surface enhancement, the surface enhancement factor (SEF) is defined.

$$SEF = \frac{h_{o-es}}{h_{o-ps}} \quad (5.30)$$

This is the ratio of the bundle shell-side heat transfer coefficient measured with a finned or enhanced surface tube bundle to that found with the plain surface bundle tested at the same operating conditions. This parameter demonstrates how a given type of shell-side enhancement performs relative to that of a plain surface tube in the same environment through the heat flux range evaluated in this study.

The lubricant enhancement factor (LEF) is defined as the shell-side heat transfer coefficient obtained during refrigerant/lubricant mixture testing to the shell-side heat transfer coefficient measured with the same tube or bundle at a 0.0 % lubricant concentration. This parameter is shown in the following equation.

$$\text{LEF} = \frac{h_{o-l}}{h_{o-p}} \quad (5.31)$$

The lubricant enhancement factors indicate the affect of an oil upon heat transfer performance for a given tube surface.

On the bundle test facility row-by-row heat transfer coefficients are measured as well as the overall bundle heat transfer coefficients during each data run. The row-to-row heat transfer performance is of great interest for the interpretation of the experimental results since dryout in the lower rows of a tube bundle lower the overall heat transfer performance for the bundle. The row performance factor (RPF) is used to facilitate the comparison of row-to-row performance profiles from data runs conducted with different lubricant concentrations, surface enhancements, and refrigerants. The row performance factor is defined by the following equation:

$$\text{RPF} = \frac{h_{o-r}}{h_{o-b}} \quad (5.32)$$

The row performance factor is an indicator of the ability of a given row to carry an equal portion of the bundle load. An ideal spray evaporator nozzle configuration might be thought of as one in which each row is carrying an equal percentage of the bundle load, or the row performance factor for each row is approaching one.

CHAPTER 6. SOLUBILITY ANALYSIS

Refrigerant is circulated through industrial refrigeration and air conditioning machines by a compressor. The compressor requires lubrication which results in a binary mixture of oil and refrigerant circulating throughout the system. Oil tends to concentrate in the evaporator since refrigerant exits this heat exchanger as a vapor. The amount of lubricant circulating through the system as well as the amount allowed to build up in the evaporator varies from one unit to the next. One of the primary objectives of this study was to investigate the effects of small concentrations of oil on falling-film heat transfer performance.

Webb [30] discussed the two conventional techniques for gathering refrigerant/lubricant mixture data in a pool boiling environment. The two alternatives are taking the data at a constant temperature or a constant pressure. These same techniques are applicable to the spray evaporation heat transfer environment. Previous pool boiling studies have been conducted with both methods indicating that a clear convention has not yet been established. Because the pressure transducers on either test facility take a measurement which is essentially an average pressure throughout a the test section, localized variation in the oil concentration is accounted for. Therefore, the investigators arbitrarily selected the constant pressure technique for use in this study.

The multi-tube test facility used a saturation temperature which was measured directly with thermocouple probes for data analysis with Equation 5.2. These probe temperatures

always agreed to within 0.1 °C of each other indicating that the refrigerant-space temperature was essentially isothermal. The refrigerant-space temperature was compared with the saturation temperature and the difference was verified to be no more than 0.1 °C throughout the pure refrigerant testing. For refrigerant/lubricant mixture work, constant pressure data were taken at the pressure corresponding to that of the pure refrigerant. Due to solubility effects, the refrigerant-space temperature actually increased with no change in pressure as lubricant concentration was increased. Since the refrigerant-space temperature was directly measured, the solubility effects were taken into account inherently.

Temperature measurements were not made in the bundle test facility's test-section liquid/vapor space. Due to the complex geometry of the tube bundle and the test section the investigators were concerned that this approach would likely introduce error into the measurements. Alternatively, the pressure was measured in the test section and from the known temperature/pressure relationships of the refrigerants the saturation temperature was determined for use in the log mean temperature difference calculation. Solubility data was collected for the three refrigerant/lubricant pairs to account for the effect of oil upon saturation temperature.

Solubility Test Facility

The test facility used to obtain solubility data in this study was designed to measure solubility and miscibility characteristics of refrigerant/lubricant mixtures and has been described in previous studies by Eckels et al. [46] and Kang et al. [47]. Each test cell consisted of a double-port, seal-cap type liquid indicator, which is essentially a 31.8 mm pipe cross with sight windows screwed into opposite ports. Complete visibility of the

refrigerant/lubricant mixture is allowed for by the side ports. A refrigerant charge valve and a pressure transducer are attached to the two remaining ports for refrigerant addition into the cell and for monitoring cell pressure. The same pressure transducer was used throughout the testing of each individual refrigerant to eliminate transducer bias from the solubility data. However, three different pressure transducers were used for the separate refrigerants allowing an appropriate range to be matched with each refrigerant.

Cell temperature was controlled by placing them in a portable constant temperature bath capable of operating in a temperature range of $-20.0\text{ }^{\circ}\text{C}$ to $+50.0\text{ }^{\circ}\text{C}$. The precise temperature of the bath was measured with a high precision mercury thermometer calibrated to the $\pm 0.05\text{ }^{\circ}\text{C}$.

Experimental Procedure

Charging the lubricant into each cell was done with a syringe through one of the window spaces. After adding lubricant, the window assembly was replaced and the cell was leak tested. After verifying that the cell was sealed, a vacuum was drawn on the oil in the cell for four hours. This step in the procedure removed dissolved moisture and air from the oil.

Upon completion of the vacuum, refrigerant was added to the test cell from a refrigerant canister with a three-way valve assembly which allowed for evacuation of the lines and connections. The cells were weighed on an electronic scale accurate to the ± 0.01 gram before and after the addition of the lubricant and refrigerant. The vapor space filled approximately 15 % of the cell's volume after charging refrigerant and lubricant.

Data was taken with each cell through a temperature range of $0.0\text{ }^{\circ}\text{C}$ to $5.0\text{ }^{\circ}\text{C}$ in increments of $1.0\text{ }^{\circ}\text{C}$. Lubricant concentrations of 0 %, 2 %, 5 %, and 10 % by mass fraction

were evaluated. Following the establishment of equilibrium conditions at each data point, the cell pressure was recorded. With each refrigerant/lubricant combination, repeatability data was taken at the 0 % and 5 % concentrations.

Solubility Data

Solubility data is presented for the three refrigerant/lubricant mixtures in Figures 6.1, 6.2, and 6.3. Because limited temperature and lubricant concentration ranges were evaluated, correlations such as that used by Eckels et al. [46] were not used for data reduction in this study. Rather, 3-degree polynomial curve fits of the form shown in Equation 6.1 were developed with a statistical software package for each concentration with all three refrigerants. The independent variable x is pressure with units of kPa and the saturation temperature has units of degrees Celsius.

$$T_{\text{sat}}[\% \text{ oil}] = a_1 + a_2(x) + a_3(x)^2 + a_4(x)^3 \quad (6.1)$$

The constants a_1 , a_2 , a_3 , and a_4 for each refrigerant/lubricant concentration equation are shown in Table 6.1. From these equations the saturation temperature may be solved for at the desired saturation pressure for each of the lubricant concentrations. The effects of lubricant concentrations of 0 %, 2 %, 5 %, and 10 % upon saturation temperature are shown in Table 6.2.

The information presented in Table 6.2 was statistically curve fit and used by the FORTRAN post-processor to correct the saturation temperature in the log mean temperature difference calculations while reducing the results from the bundle test facility. Since lubricant concentrations up to only 2.5 % were evaluated on the bundle test facility, the data in Table

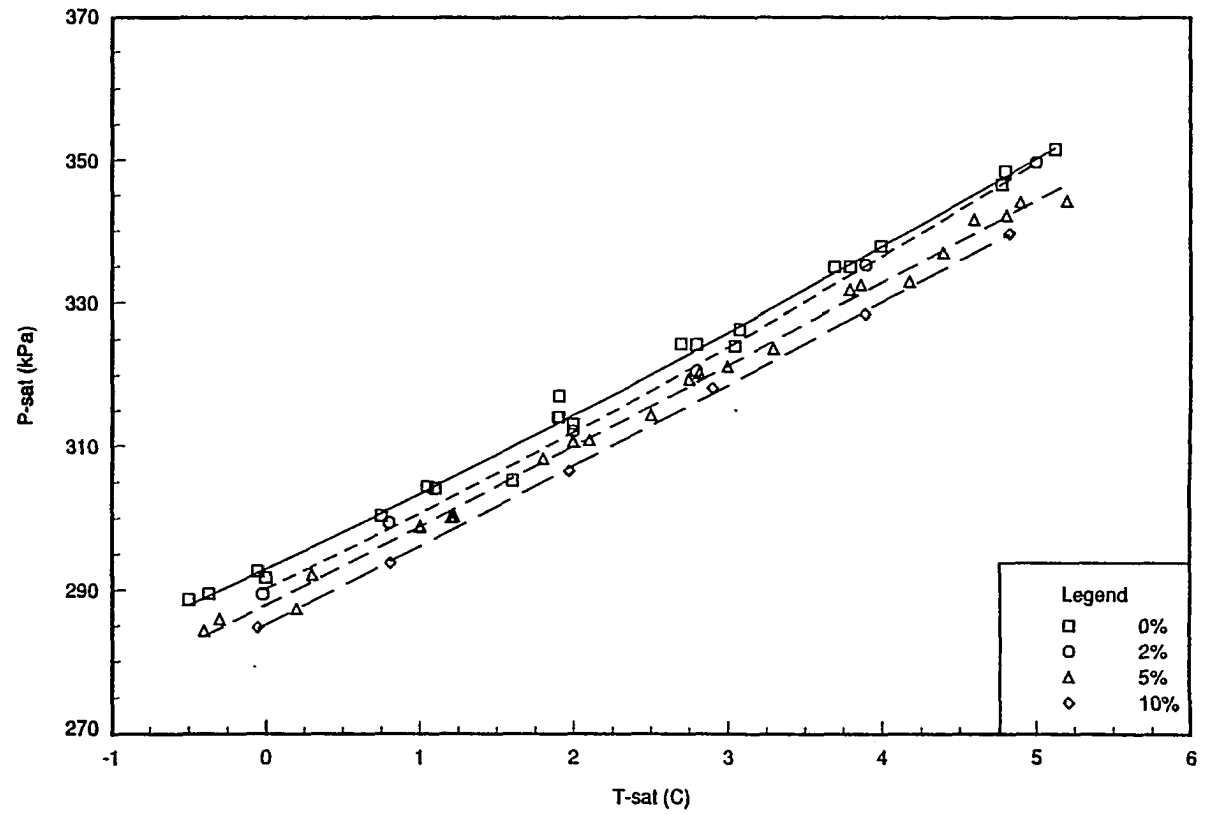


Figure 6.1: HFC-134a/polyol ester oil solubility data

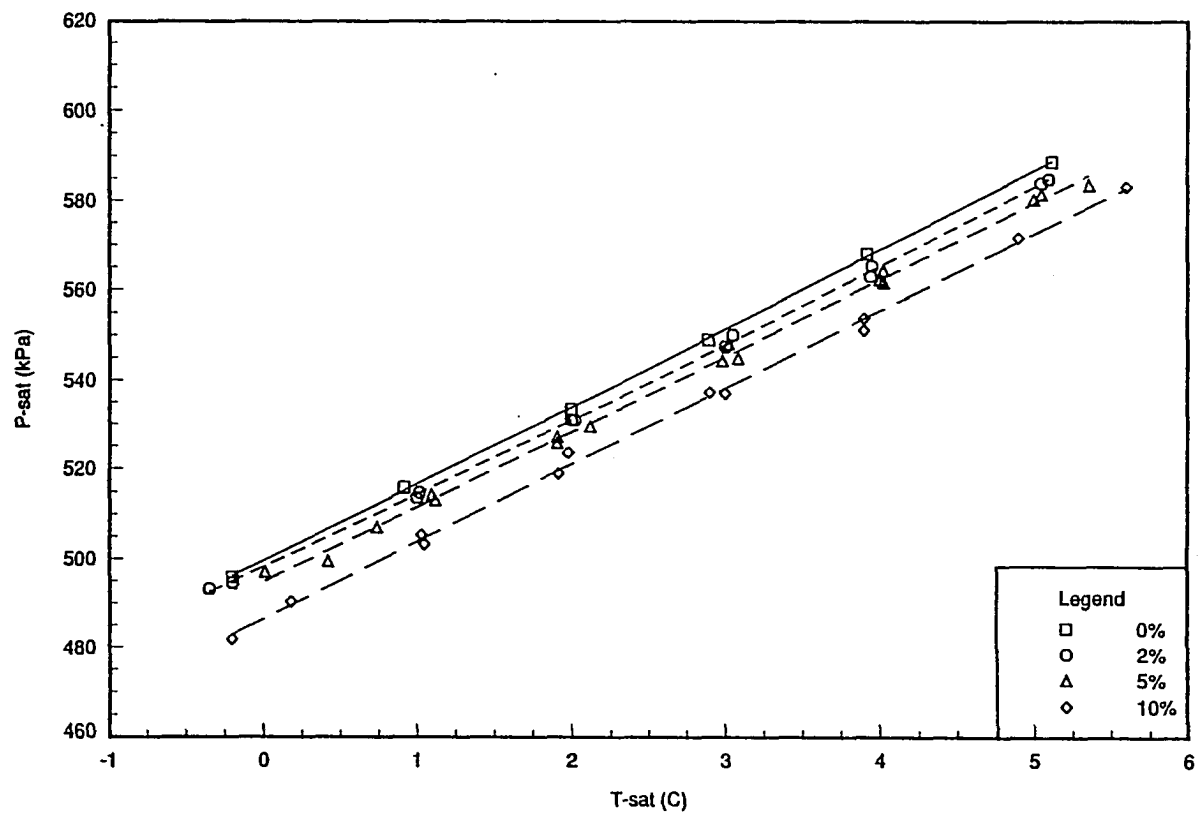


Figure 6.2: HCFC-22/alkyl-benzene oil solubility data

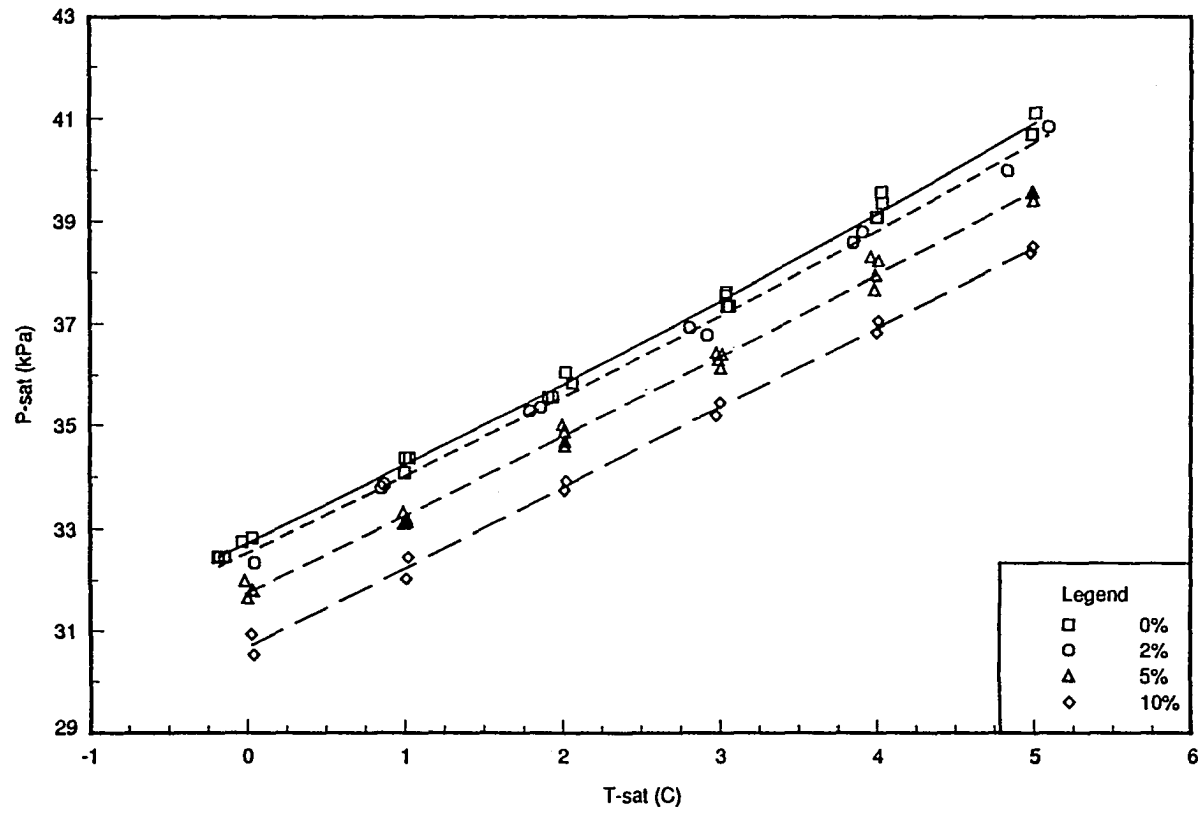


Figure 6.3: HCFC-123/naphthenic mineral oil solubility data

6.2 shows that the error incurred from neglecting the effects of solubility upon the saturation temperature would have introduced only slight error into the shell-side heat transfer coefficient calculations. Nevertheless, this error has been removed from the results taken on the bundle facility by conducting this solubility study.

Table 6.1: Solubility data correlation constants accompanying Equation 6.1

| Refrigerant | Lubricant Concentration (percent) | Polynomial Constants | | | |
|-------------|-----------------------------------|----------------------|-----------|-----------|-----------|
| | | a_1 | a_2 | a_3 | a_4 |
| HFC-134a | 0 | -6.07E+01 | +3.67E-01 | -7.16E-04 | +5.81E-07 |
| | 2 | -7.48E+01 | +4.98E-01 | -1.10E-03 | +9.49E-07 |
| | 5 | -3.13E+01 | +1.29E-01 | -8.43E-05 | +4.17E-08 |
| | 10 | -3.14E+01 | +1.32E-01 | -9.21E-05 | +4.71E-08 |
| HCFC-22 | 0 | -3.30E+01 | +7.42E-02 | -1.84E-05 | +4.32E-09 |
| | 2 | -5.03E+01 | +1.53E-01 | -1.32E-04 | +5.50E-08 |
| | 5 | -3.47E+01 | +8.17E-02 | -2.70E-05 | +7.42E-08 |
| | 10 | -2.58E+01 | +4.72E-02 | +1.46E-05 | -5.47E-09 |
| HCFC-123 | 0 | -8.62E+01 | +5.76E+00 | -1.32E-01 | +1.12E-03 |
| | 2 | +2.72E+01 | -3.57E+00 | +1.23E-01 | -1.19E-03 |
| | 5 | -1.26E+02 | +9.43E+00 | -2.42E-01 | +2.21E-03 |
| | 10 | +9.61E+00 | -1.87E+00 | +7.15E-02 | -6.77E-04 |

Table 6.2: Lubricant effects upon saturation temperature for each refrigerant

| Lubricant Concentration (percent) | Saturation Temperature (°C) | | |
|-----------------------------------|---|--|--|
| | HFC-134a $P_{sat} = 314.5 \text{ kPa}$ | HCFC-22 $P_{sat} = 533.3 \text{ kPa}$ | HCFC-123 $P_{sat} = 35.7 \text{ kPa}$ |
| 0 | 2.00 | 2.00 | 2.00 |
| 2 | 2.21 | 2.14 | 2.13 |
| 5 | 2.39 | 2.29 | 2.64 |
| 10 | 2.63 | 2.71 | 3.27 |

CHAPTER 7. MULTI-TUBE TEST FACILITY PLAIN-SURFACE RESULTS

Pure HFC-134a testing was conducted on the multi-tube test facility with plain surface tubes of two different diameters in an effort to determine the effects of tube diameter, film-feed supply rate, and wall heat flux upon film heat transfer performance. Pool-boiling data was also taken for comparison of film evaporation to pool boiling heat transfer performance with the plain surface tubes.

The data was collected at a fixed film-feed supply rate while heat flux was varied throughout each data run. The film-feed supply rates corresponding to the 12.7 mm and 19.1 mm diameter tubes are 9.34×10^{-3} kg/(s*m) and 1.26×10^{-2} kg/(s*m), respectively at the 2.8 kg/min refrigerant supply rate. The larger diameter tube has a greater film feed supply rate because of the larger collector test fraction as presented in Chapter 3. The 19.1 mm diameter, plain surface experimental data are given in Appendix A in Tables A.1 and A.6.

Multi-Tube Test Facility Accuracy

In this initial testing on the multi-tube test facility it was desired to perform experiments specifically for the purpose of validating the accuracy of the wall mounted thermocouples on

the test-tubes. This step was taken to verify that the method of mounting the thermocouples to the tube wall did not introduce error into the temperature measurements. Calibration of the wall mounted thermocouples was possible in a constant temperature bath. However, calibration of these thermocouples did not ensure accurate measurements while a heat flux was put across the solder bead mounting the thermocouple to the tube wall.

Both pool-boiling and single-phase free convection experiments were conducted with plain-surface tubes. Figure 7.1 compares the data from a single-phase convection test for a 19.1 mm diameter tube with a heat transfer correlation suggested by Churchill and Chu [44] for a long horizontal cylinder. The single-phase testing was halted at a heat flux of 0.7 kW/m² because above this power level nucleate bubbles were seen developing on the bottom section of the tube in the region of thermocouple installations. As can be seen in Figure 7.1, the agreement is fairly good with a maximum deviation from the correlation of approximately 25 percent in the middle of the heat flux range tested. Minimum deviation, which occurred at the lowest heat flux evaluated, is less than 5 percent.

Figure 7.2 shows flooded evaporator data taken at 5 °C compared to a boiling correlation presented by Stephan and Abdelsalam [48] and data taken by Webb [32] at 4.4 °C. The data agrees well within the stated accuracy of the Stephan-Abdelsalam correlation, which is 22.3 percent. The maximum deviation from the correlation of 19 percent occurred at a 40 kW/m² heat flux. The maximum deviation from Webb's data occurs at this heat flux as well and it is 9 percent. In the lower heat flux range the deviation from the Stephan-Abdelsalam correlation and Webb's data is well under 5 percent. It was concluded from this testing that both the overall quality of the thermocouple mounting procedure and temperature measurements taken with the thermocouples were favorable while a heat flux was applied across the tube wall.

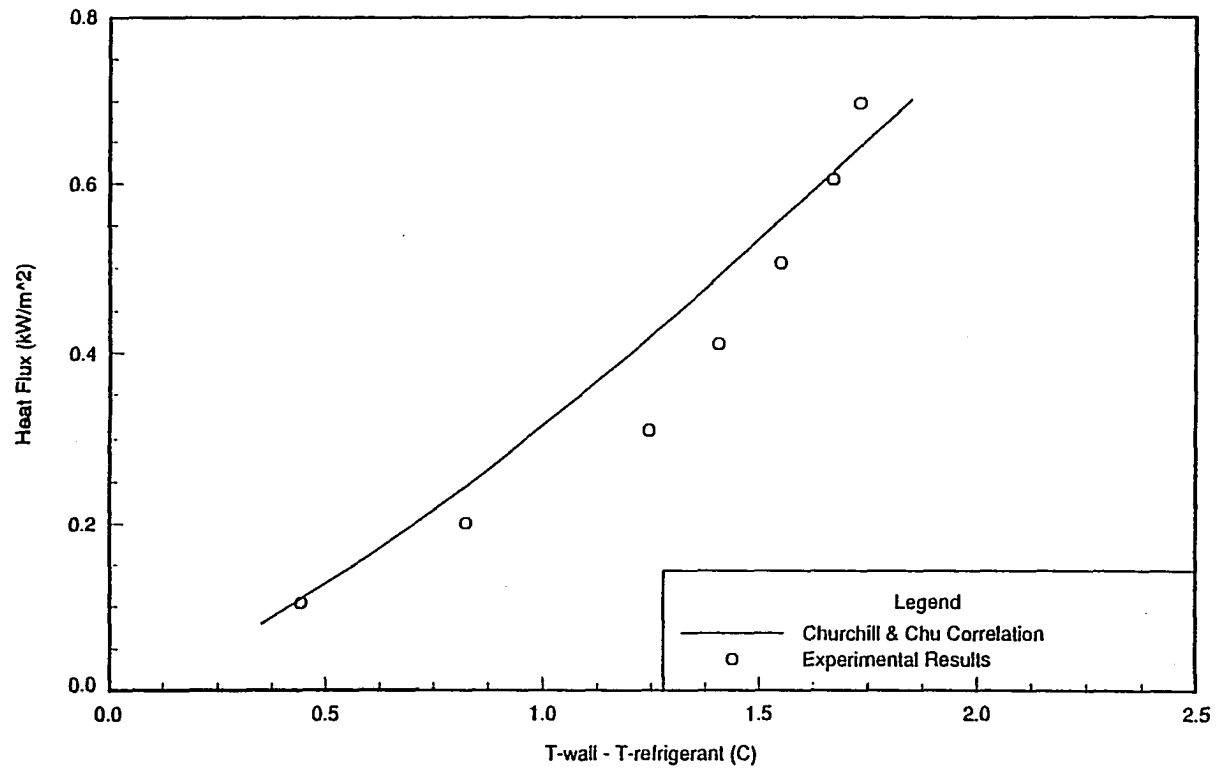


Figure 7.1: Heat flux vs. excess temperature (external free convection, flooded evaporator; $T_{\text{sat}} = 2.0 \text{ }^\circ\text{C}$, tube diameter = 19.1 mm)

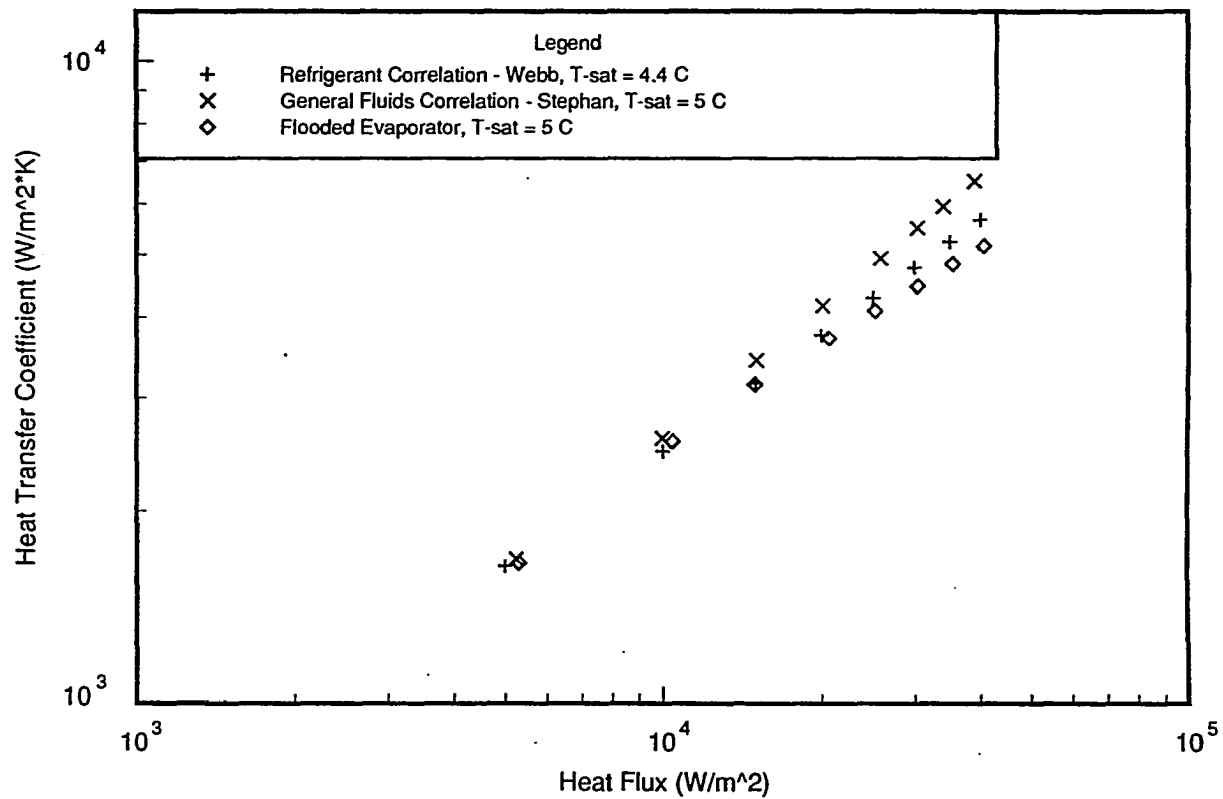


Figure 7.2: Heat transfer coefficient vs. heat flux (flooded evaporator, tube diameter = 19.1 mm)

Heat Transfer Results

Spray evaporation heat transfer results are presented for HFC-134a and plain surface tubes of 12.7 mm and 19.1 mm diameter in Figures 7.3 through 7.7. Average wall heat transfer coefficients are presented based upon a 12.7 mm or 19.1 mm tube diameter.

12.7 mm Diameter Plain Surface Test-Tube Results Wide-Angle, Low-Pressure Drop Nozzles

Unlike the 19.1 mm diameter, the smaller 12.7 mm diameter allowed tubes to be tested in either a single-tube or double-tube arrangement. For the double-tube tests, the first tube was mounted along the radial centerline of the test section and the second tube was located directly below it, with a centerline-to-centerline distance of 28.6 mm between the test-tubes. Figure 7.3 presents single-tube heat transfer data at three different spray manifold mass flow rates, and Figure 7.4 shows the same refrigerant supply rates for two-tube operation.

Figure 7.3 shows that the heat transfer performance is dependent upon heat flux throughout the entire range tested. This indicates that boiling is present in the heat transfer process. The measured heat transfer performance consisted of both evaporative and boiling heat transfer contributions which varied in magnitude depending upon test conditions. The heat transfer performance is dependent upon refrigerant supply rate after dryout begins to occur. It can be seen in Figure 7.3 that heat transfer performance begins to level off at the 25 kW/m² data point. At this wall heat flux when the refrigerant supply rate was increased by approximately 20 % from 2.3 kg/min to 2.8 kg/min mass flow rates, the average heat transfer coefficient increased by 12 percent. Heat transfer performance is only weakly dependent upon flow rate in the lower heat flux range. These data taken before the occurrence of dryout are consistent with film boiling heat transfer results presented by Parken et al. [3]. Parken states

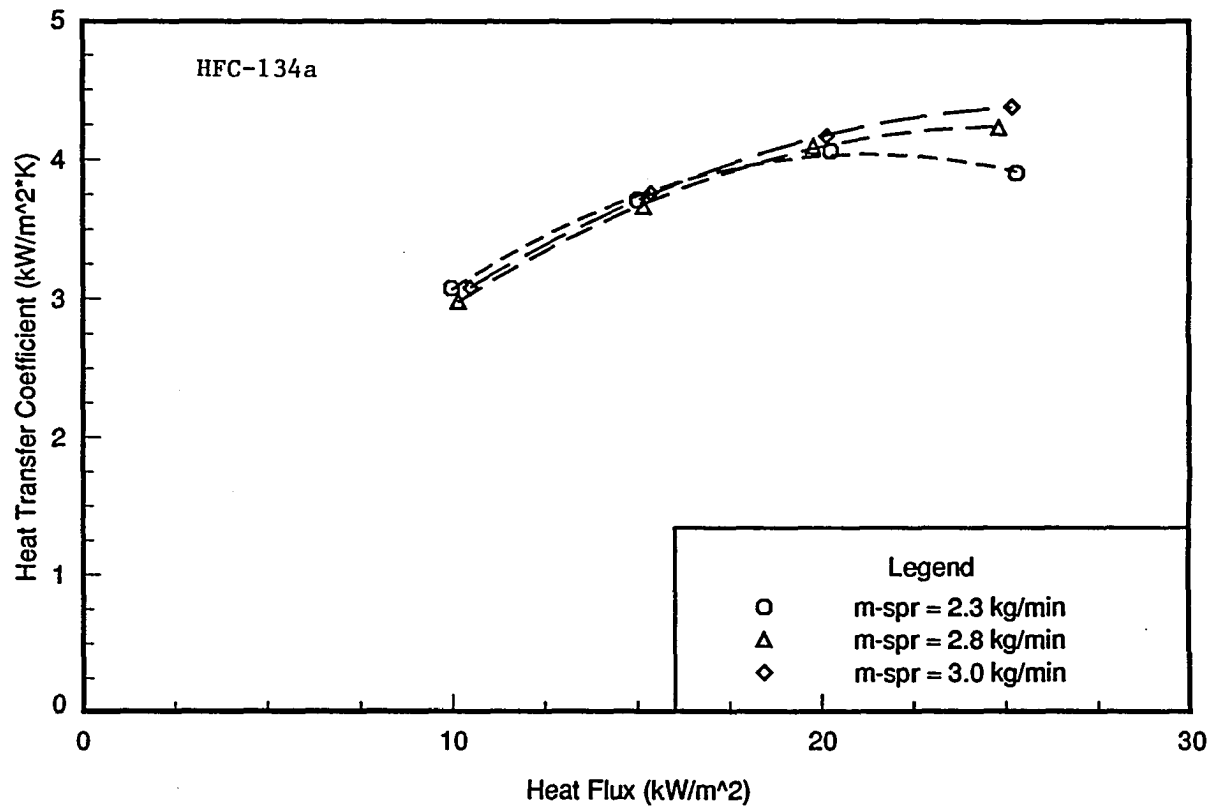


Figure 7.3: Heat transfer coefficient vs. heat flux, single-tube test ($T_{\text{sat}} = 2.0 \text{ }^\circ\text{C}$; tube diameter = 12.7 mm)

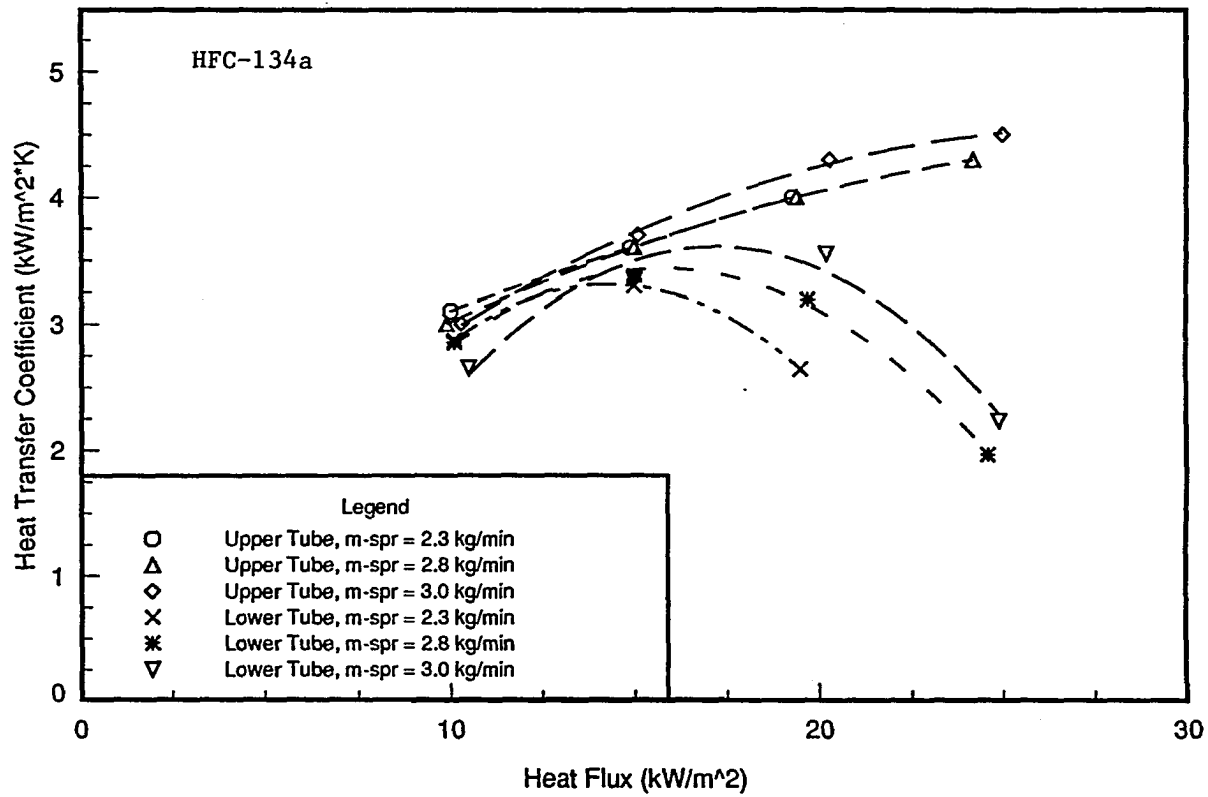


Figure 7.4: Heat transfer coefficient vs. heat flux, multi-tube test ($T_{\text{sat}} = 2.0 \text{ }^\circ\text{C}$; tube diameter = 12.7 mm)

that boiling heat transfer coefficients vary with heat flux, but are only weakly dependent upon film-feed supply rate.

Figure 7.4 shows that for the double-tube arrangement, a refrigerant supply rate of 3.0 kg/min is insufficient to adequately wet the lower tube. Heat transfer performance drops dramatically as heat flux is increased on the lower tube. Dry spots could not be seen on the tube's surface, but the surface temperature measurements indicated dryout was present.

Data taken with the 12.7 mm tube at a spray manifold mass flow rate of 2.8 kg/min are also plotted in Figure 7.5. The average heat transfer coefficient is approximately 5-10% higher for the smaller 12.7 mm diameter tube than the 19.1 mm diameter tube in the heat flux range tested. This is because the convective heat transfer coefficient is highest at top-dead-center and decreases circumferentially downward along the tube wall. Therefore, the longer the flow distance, the lower the evaporative heat transfer coefficient will be.

19.1 mm Plain Surface Test-Tube Results Wide-Angle, Low-Pressure Drop Nozzles

The 19.1 mm diameter plain surface tube was tested up to a heat flux of 40 kW/m². Figure 7.5 shows that the heat transfer performance for the spray evaporation test drops below the pool boiling curve at approximately 22.5 kW/m². The heat transfer coefficient improves with heat flux up to 25 kW/m² and then drops with further increases in the wall heat flux. This behavior is different than most existing film heat transfer data taken with water and ammonia, which could be expected since the thermodynamic and transport properties of HFC-134a are significantly different than water or ammonia. More importantly, the effective refrigerant supply rate being evaluated in this test yields liquid film-feed supply rates lower than those used in the plain-surface falling-film evaporation testing done by Chyu et al. [5, 6, 7] and Parken et al. [3].

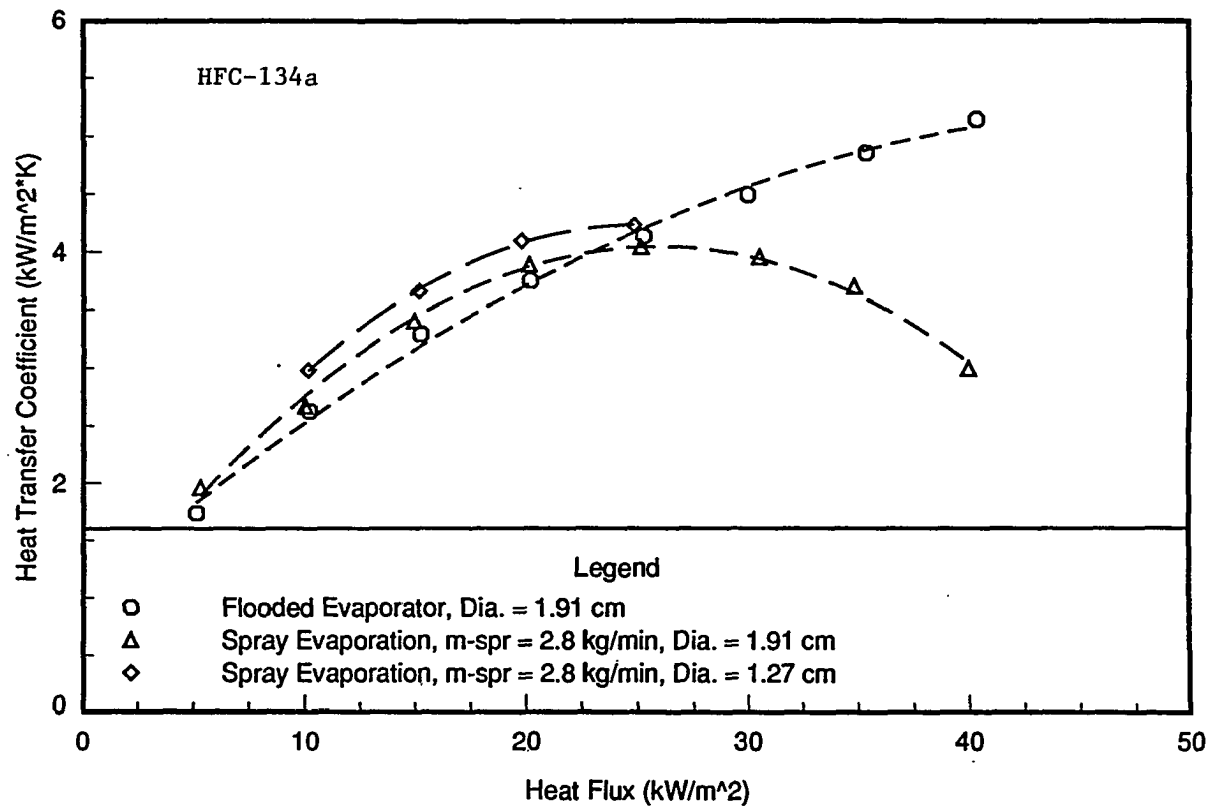


Figure 7.5: Heat transfer coefficient vs. heat flux ($T_{\text{sat}} = 2.0 \text{ }^\circ\text{C}$)

After the heat transfer coefficient reached its maximum value as heat flux was increased, a strong dependence on refrigerant supply rate was noted and dryout effects became dominant. Figure 7.6 shows a large increase in heat transfer performance with increased refrigerant supply rate. The average heat transfer coefficient increased by 25% at the 40 kW/m² data point when the spray manifold mass flow rate was raised to 3.9 kg/min from 2.8 kg/min.

12.7 mm Diameter Plain Surface Test-Tube Results High-Pressure Drop Nozzles

A limited amount of testing was conducted with high-pressure drop 73.66x10⁻² mm bore nozzles, with the results being shown in Figure 7.7. The heat transfer performance with the high-pressure drop nozzles surpasses the pool-boiling data through the heat flux range tested. The local heat transfer coefficient in the region of the nozzle plume drops below the average heat transfer coefficient for the same surface in a pool-boiling environment at heat fluxes greater than 30 kW/m². Comparing the data presented in Figure 7.7 to the wide-angle nozzle results in Figure 7.5, the high-pressure drop nozzles have potential for better heat transfer performance than low-pressure drop nozzles considering spray evaporation heat transfer improves with increasing saturation temperature. This is similar to the effects of saturation temperature on pool boiling heat transfer performance.

Conclusions

This study shows that the refrigerant supply rate affects spray evaporation heat transfer performance significantly after dryout effects become dominant. A dependence upon the wall

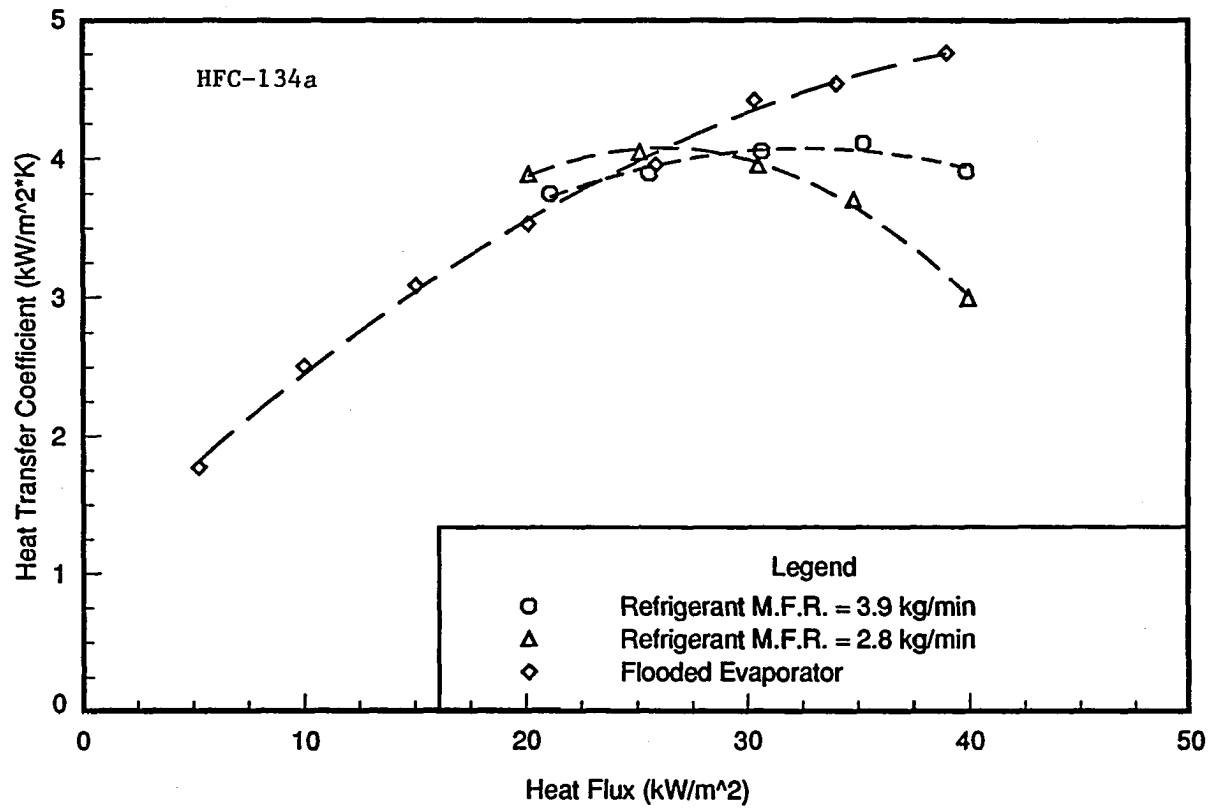


Figure 7.6: Heat transfer coefficient vs. heat flux ($T_{\text{sat}} = 2.0 \text{ }^\circ\text{C}$; tube diameter = 19.1 mm)

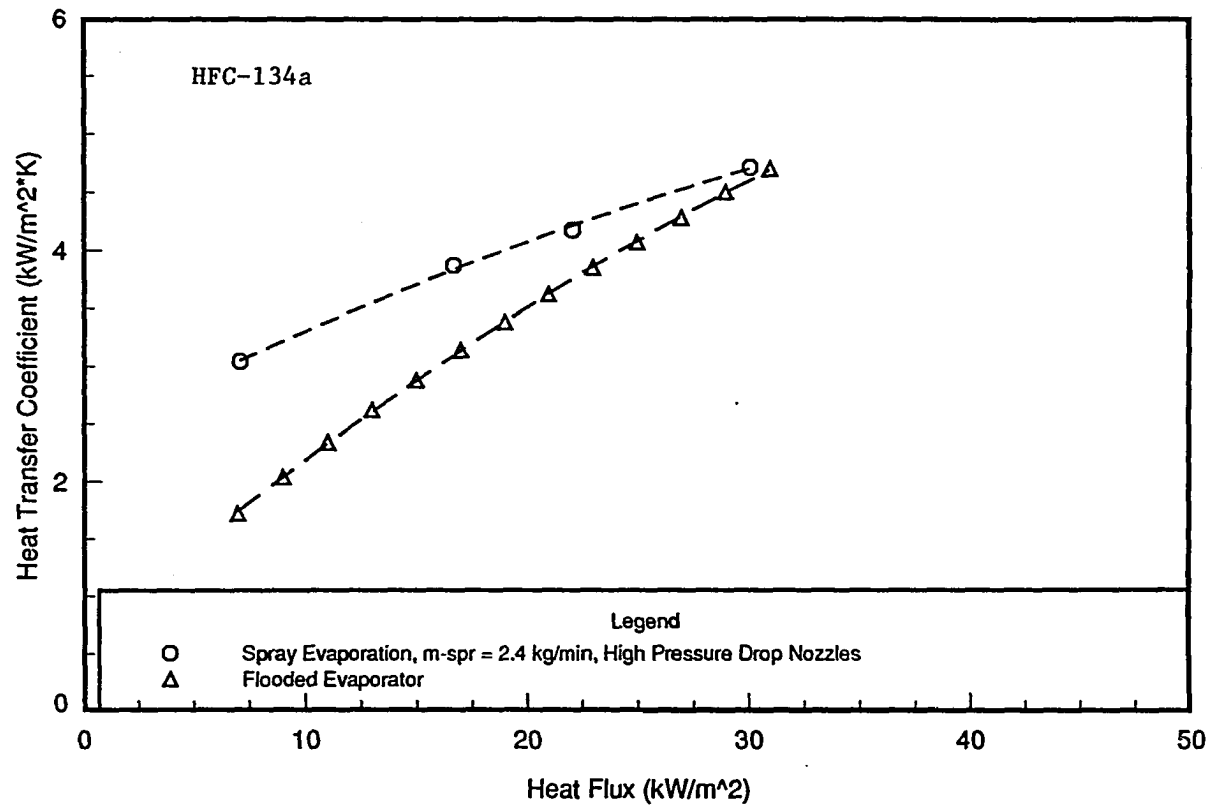


Figure 7.7: Heat transfer coefficient vs. heat flux ($T_{\text{sat}} = -14.0\text{ }^{\circ}\text{C}$; tube diameter = 12.7 mm)

heat flux, at least for the film-feed supply rates evaluated in this study, was also observed. A summary of the plain-surface results follows.

1. The 12.7 mm diameter tube yields 5-10 % higher heat transfer coefficients than the 19.1 mm tube.
2. Boiling heat transfer performance is only weakly dependent upon liquid supply rate until dryout occurs.
3. High-pressure drop nozzles yield good heat transfer performance. However, the high-pressure drop nozzles require greater pumping horsepower and more nozzles to wet a given bundle cross-sectional area than the low-pressure drop nozzles. Also, the benefit gained by increased droplet velocity on the top row of a tube bundle may not be significant considering industrial chiller bundles have several rows of tubes.

CHAPTER 8. MULTI-TUBE TEST FACILITY SURFACE ENHANCEMENT AND OIL EFFECTS

Spray evaporation tests were conducted with 19.1 mm diameter tubes and HFC-134a in order to evaluate the average wall heat transfer coefficients for six different enhanced and finned tube surfaces. The dimensions of the tubes are listed in Table 3.1. Because the spray evaporation phenomenon is so different from pool boiling, both condensation-type and evaporation-type enhanced surfaces were evaluated. All data are presented at a saturation temperature of 2.0 °C, which falls within the operating temperature range of industrial pool-boiling evaporators. The operational set-points and the maximum allowable deviation from these set-points used on the multi-tube test facility during this testing are presented in Table 8.1. A fixed film-feed supply rate was used while heat flux was varied during this testing resulting in variation of the tube overfeed ratio throughout the data run. Tube overfeed ratios are presented in Table 8.2 for the various wall heat fluxes.

Experiments were also conducted to evaluate the effects of small concentrations of a lubricant upon heat transfer performance in the single-tube environment. A polyol-ester oil of two different viscosities was used for this testing. A 160 SUS oil, at concentrations of 1.0, 2.0, and 3.0 percent, was evaluated with plain, W-40 fpi, and Tu-Cii tubes. A 340 SUS oil was evaluated at concentrations of 0.0, 0.5, 1.0, 3.0, and 5.0 percent with the W-40 fpi and Tu-Cii tubes. The experimental data are given in Appendix A in Tables A.2 through A.27.

Table 8.1: Multi-tube test facility operating parameters

| Parameter | Control Band |
|----------------------------|---|
| Saturation Pressure | 314.5 kPa \pm 2.2 kPa |
| Wall Heat Flux | Desired Value \pm 0.2 kW/m ² |
| Refrigerant Mass Flow Rate | 2.8 kg/min \pm 0.2 kg/min |
| Spray Manifold Temperature | 1.0 °C to 2.5 °C |

Table 8.2: Test-section recirculation ratios and tube overfeed ratios

| Nominal Wall Heat Flux (kW/m ²) | Test-Section Recirculation Ratio | Tube Overfeed Ratio [(RCR)(CTF)] |
|---|----------------------------------|----------------------------------|
| 5 | 77.2 | 14.9 |
| 10 | 43.1 | 8.3 |
| 15 | 31.2 | 6.0 |
| 20 | 24.0 | 4.6 |
| 25 | 18.9 | 3.6 |
| 30 | 16.0 | 3.1 |
| 35 | 13.8 | 2.7 |
| 40 | 12.2 | 2.4 |

Heat Transfer Results

Heat transfer coefficients are presented for pure HFC-134a and mixtures of HFC-134a and a polyol-ester oil of two different viscosities. The pure refrigerant work was conducted at a constant saturation temperature of 2.0 °C, and the lubricant effects testing was conducted at a constant saturation pressure of 314.5 kPa, which corresponds to 2.0 °C for pure HFC-134a.

The average wall heat transfer coefficients are based upon a nominal 19.1 mm tube diameter for all tubes tested.

Surface Geometry Comparison Pure Refrigerant Testing

Figure 8.1 shows the relative performance of the four enhanced surfaces relative to a plain-surface tube. Two condensation surfaces, the W-SC and Tu-Cii surfaces, performed the best of the four. Figure 8.2 shows the performance of the two finned surfaces relative to a plain surface. Both the W-26 fpi tube and the W-40 fpi tube performed very similarly, with the W-26 fpi surface yielding slightly higher heat transfer coefficients. A comparison of all of the tubes shows that the enhanced surfaces yield up to 20 % improvement in heat transfer performance compared to the finned tubes. As expected, all six modified surfaces yielded significantly higher heat transfer performance compared to a plain surface in the same environment. Surface enhancement factors for this pure refrigerant testing are presented in Figure 8.3.

The heat transfer coefficient showed varying degrees of dependence on heat flux or wall superheat depending upon the surface geometry. Evaporation heat transfer is independent of wall heat flux. Figure 8.1 shows that the W-SC surface results are very weakly dependent on the wall heat flux in these test conditions. In this case evaporation is making a strong contribution to the average heat transfer coefficient. Nucleate boiling was observed near bottom-dead-center of the tubes where the liquid layer was thickest. Most likely, both evaporation and boiling occurred simultaneously along different circumferential positions of the tubes.

Chyu [4] presents models for film thickness in the thermal developing and fully developed regions on the surface of a horizontal tube. The film thickness varies with film-feed

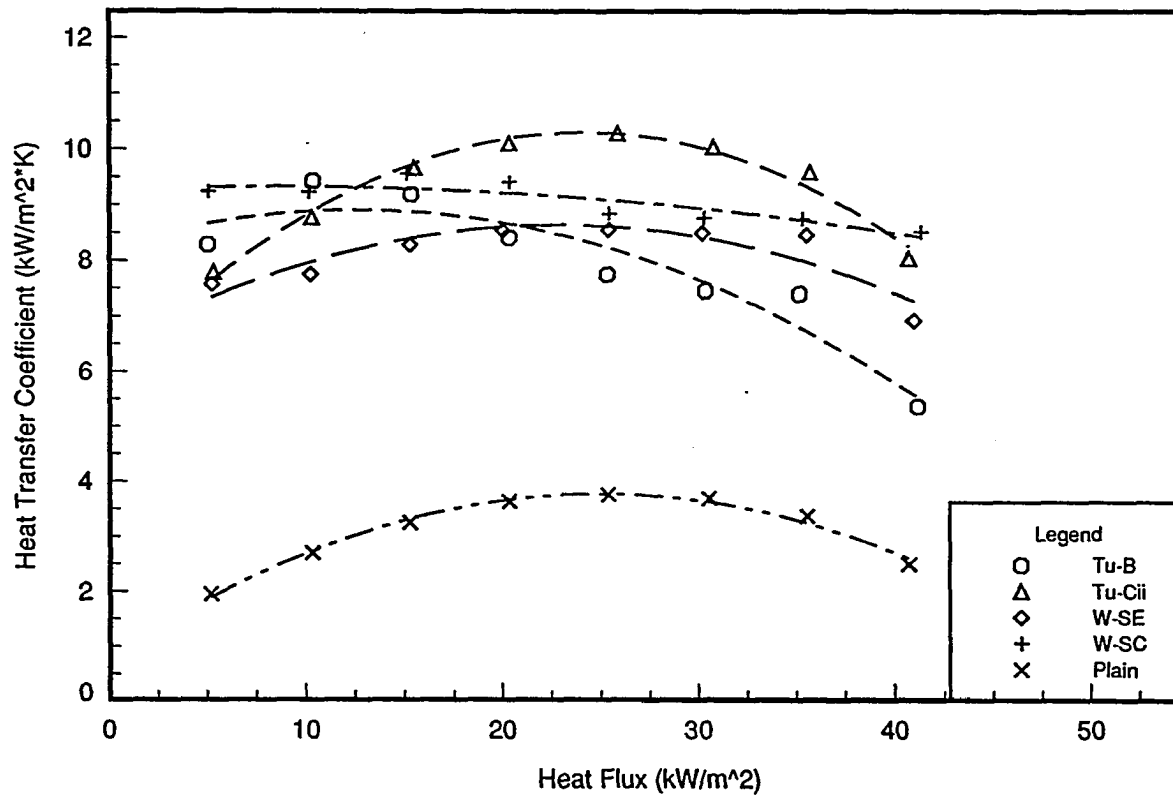


Figure 8.1: Heat transfer coefficient vs. heat flux ($T_{sat} = 2.0\text{ }^{\circ}\text{C}$; pure HFC-134a, enhanced surface results)

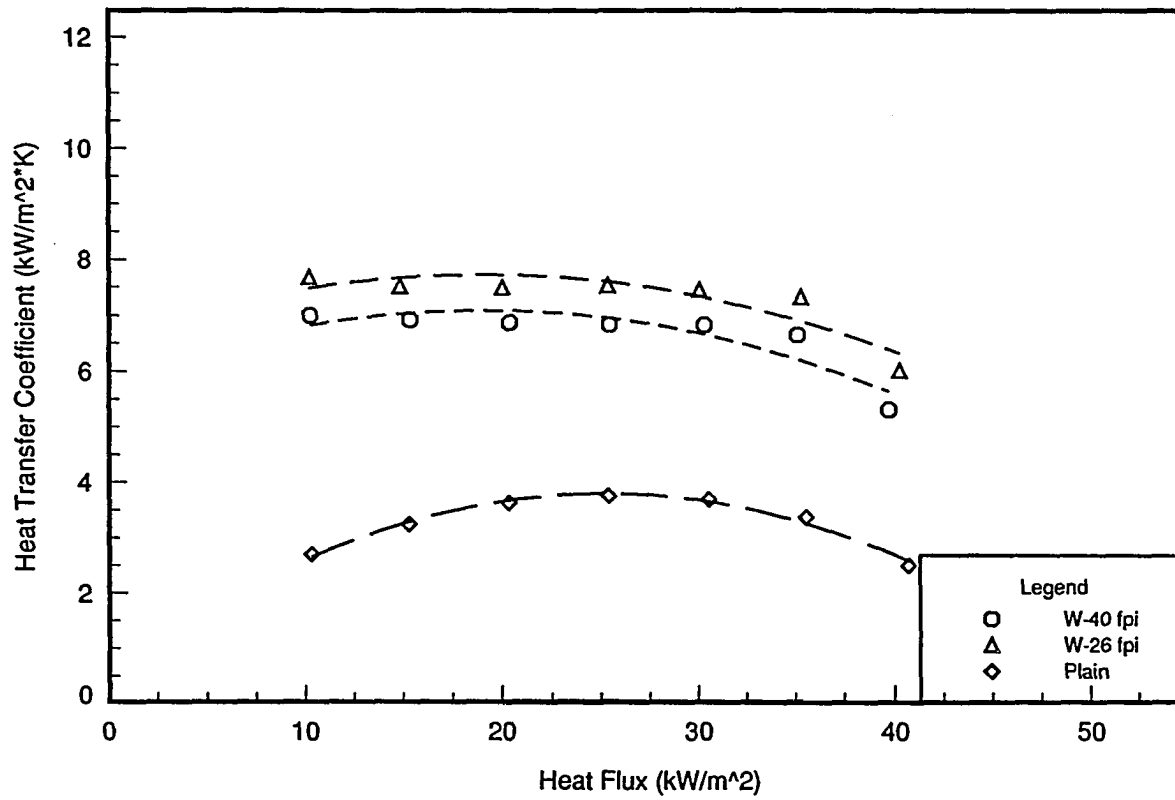


Figure 8.2: Heat transfer coefficient vs. heat flux ($T_{\text{sat}} = 2.0 \text{ }^\circ\text{C}$; pure HFC-134a, low-finned surface results)

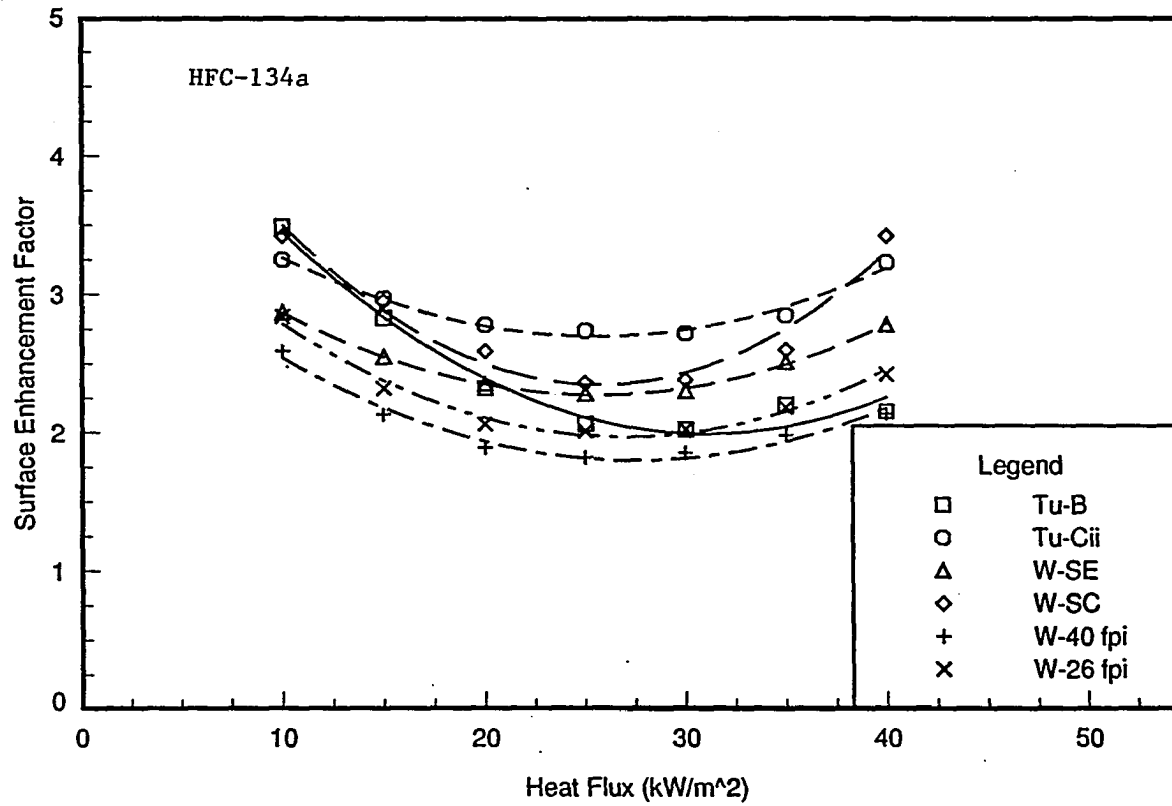


Figure 8.3: Surface enhancement factor vs. heat flux
 ($T_{\text{sat}} = 2.0 \text{ }^\circ\text{C}$; pure HFC-134a)

supply rate to the 1/3 power, and the radial length of the boundary layer is defined by the thickness of the liquid film. Because of a thicker thermal boundary layer in the pool-boiling mode, nucleate bubbles are capable of being generated at lower heat fluxes than the falling-film/spray evaporation mode. During this testing, insufficient liquid film thickness may be the reason the nucleation sites were prevented from becoming fully activated. Heat transfer performance increased with increasing wall heat flux, reached a maximum, and then declined with further increases in heat flux. The decline in heat transfer performance is most likely due to partial dryout of the tube surface.

It is interesting that the enhanced condensation surfaces (W-SC, Tu-Cii) performed better than the enhanced boiling surfaces (W-SE, Tu-B), shown in Figure 8.1. The spray evaporation environment created by low-pressure drop, wide-angle nozzles may be similar to the environment found in the lower tube rows of a commercial chiller condenser. At least when evaporation is the dominant mode of heat transfer, as was the case with this testing, condensation surfaces perform very well in the spray evaporation environment.

Lubricant Effects Testing

Figures 8.4, 8.6, and 8.8 show results from refrigerant/oil mixtures with the 160 SUS oil and the plain, W-40 fpi, and Tu-Cii tubes. Concentrations of 1.0, 2.0, and 3.0 percent were evaluated with this oil. The corresponding lubricant enhancement factors for each tube are presented in Figures 8.5, 8.7, and 8.9. At the 5 kW/m² heat flux, the highest heat transfer coefficients occurred with the 3.0 percent concentration with the three surfaces tested. Relative to pure refrigerant performance, at this concentration and heat flux, the heat transfer coefficient of the plain tube improved 111 percent while the heat transfer coefficient of Tu-Cii tube increased by 30 percent. At the 40 kW/m² heat flux, the highest heat transfer performance occurred with the 2.0 percent concentration for all three surfaces tested.

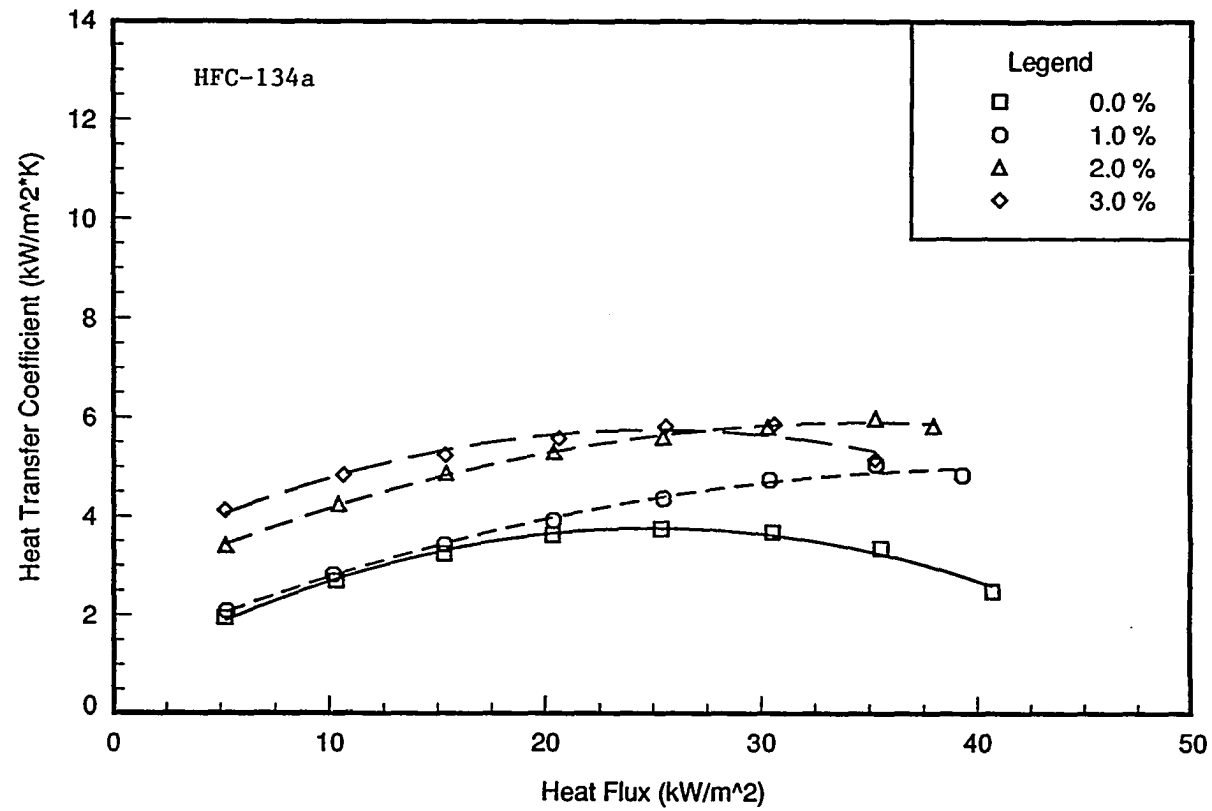


Figure 8.4: Heat transfer coefficient vs. heat flux ($P_{sat} = 314.5$ kPa; 160 SUS oil, plain tube)

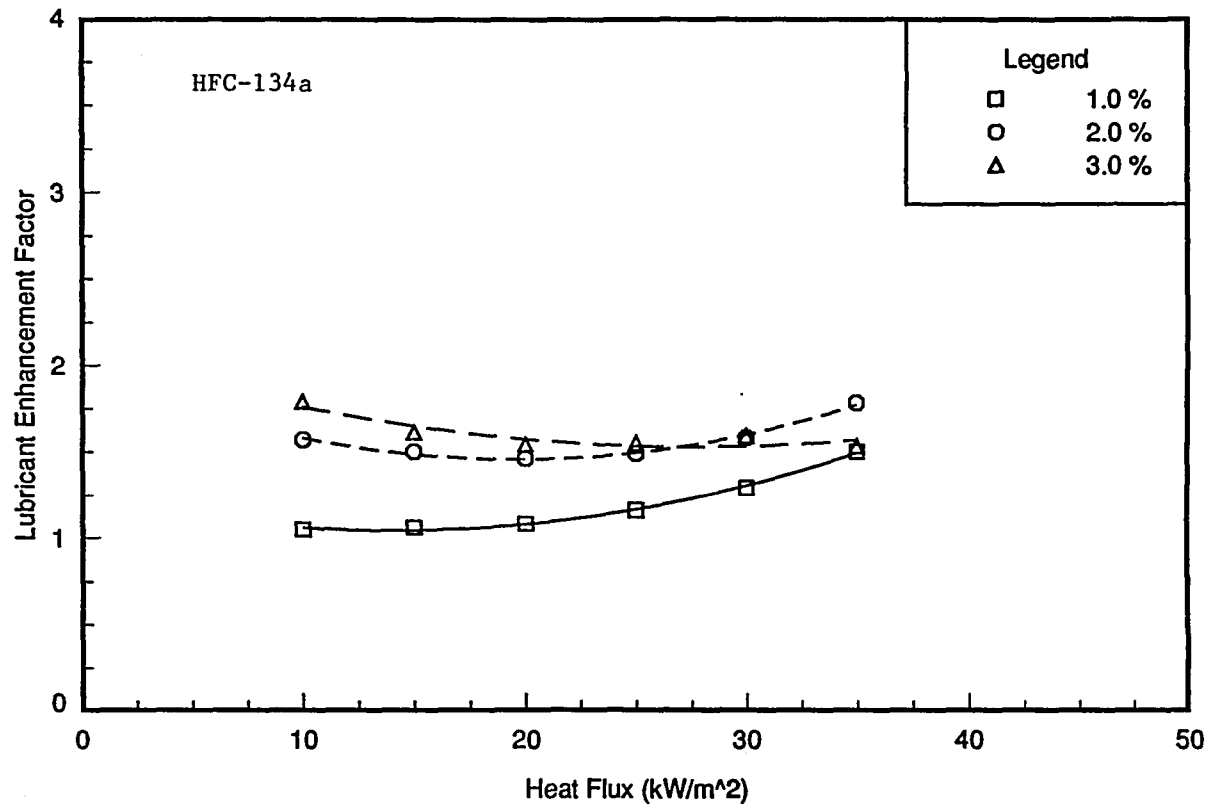


Figure 8.5: Lubricant enhancement factor vs. heat flux
 ($P_{\text{sat}} = 314.5 \text{ kPa}$; 160 SUS oil, plain tube)

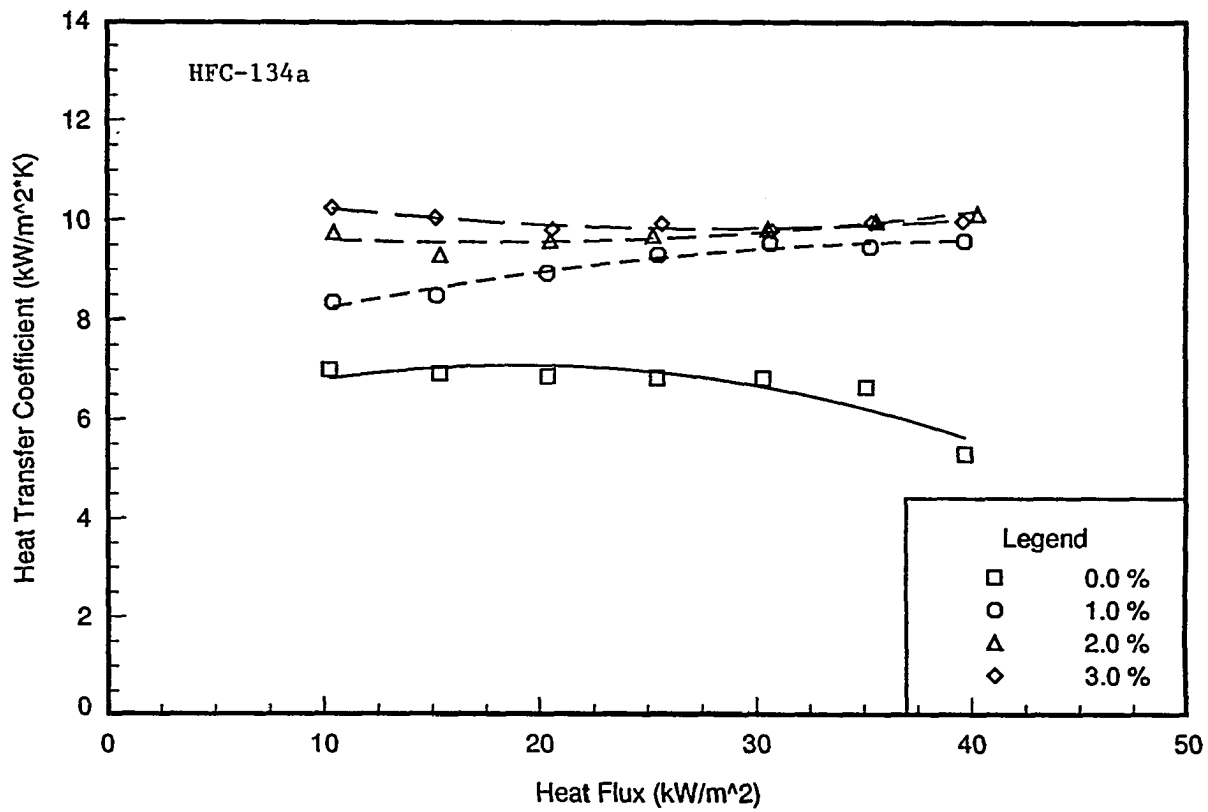


Figure 8.6: Heat transfer coefficient vs. heat flux ($P_{sat} = 314.5$ kPa; 160 SUS oil, W-40 fpi tube)

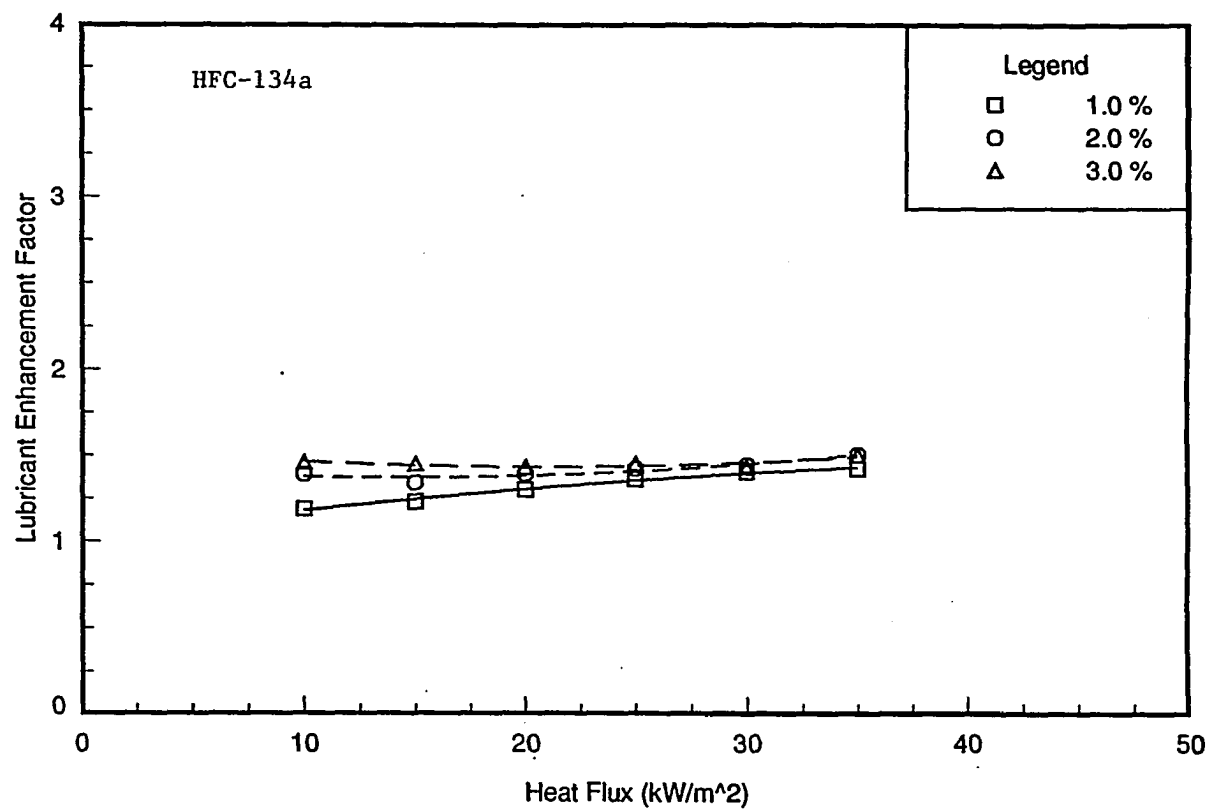


Figure 8.7: Lubricant enhancement factor vs. heat flux ($P_{sat} = 314.5$ kPa; 160 SUS oil, W-40 fpi tube)

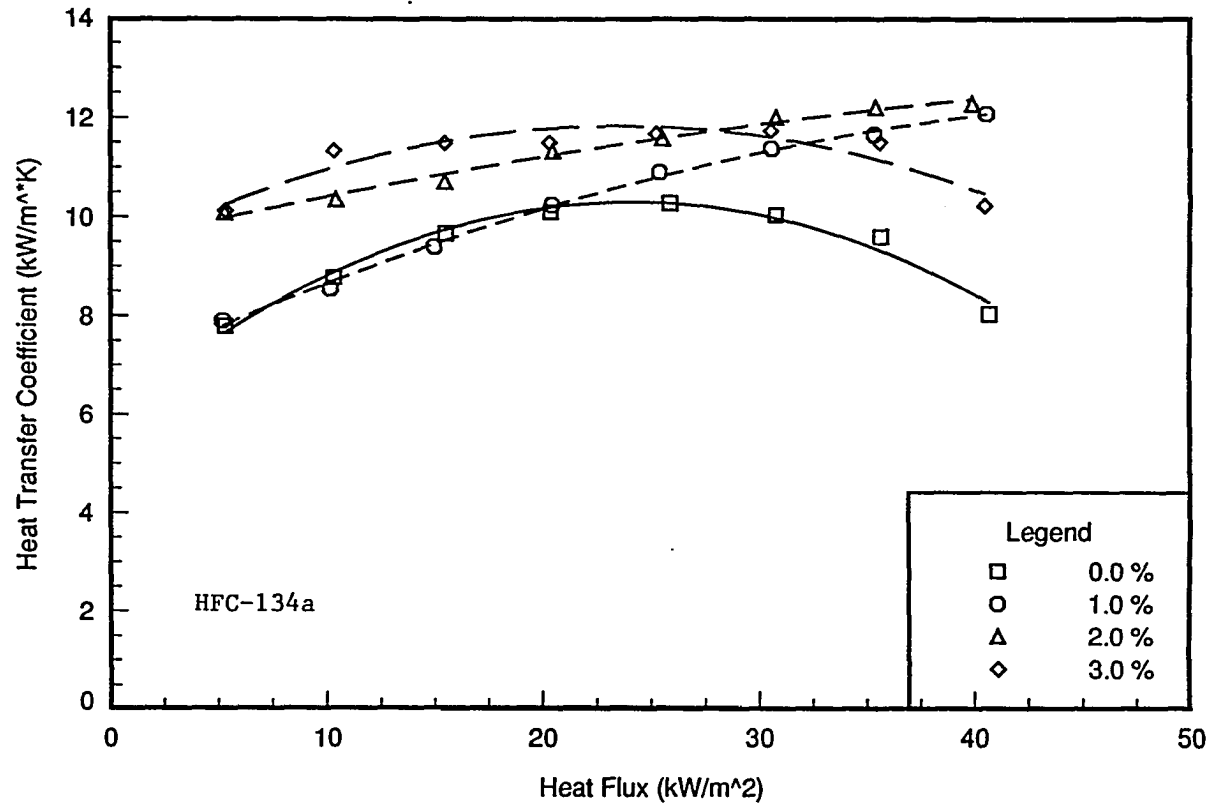


Figure 8.8: Heat transfer coefficient vs. heat flux ($P_{sat} = 314.5$ kPa; 160 SUS oil, Tu-Cii tube)

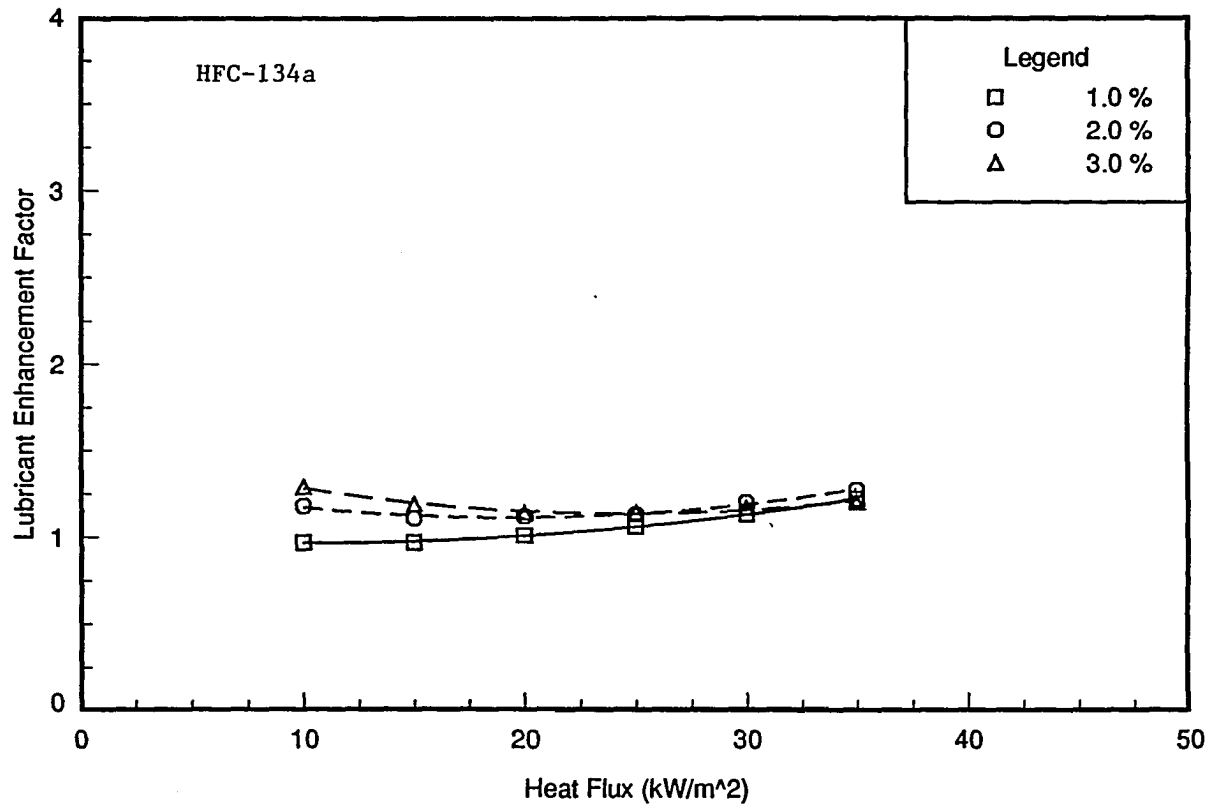


Figure 8.9: Lubricant enhancement factor vs. heat flux ($P_{sat} = 314.5$ kPa; 160 SUS oil, Tu-Cii tube)

The decrease in the tube overfeed ratio, which occurs as the wall heat flux is increased from 5 kW/m² to 40 kW/m², might be the reason the highest heat transfer performance shifts from the 3.0 percent concentration to the 2.0 percent concentration. Possibly, a higher mixture viscosity causes film breakdown to occur at the 40 kW/m² wall heat flux which reduces the heat transfer coefficient.

Figures 8.10 and 8.12 show refrigerant/lubricant mixture results with the 340 SUS oil and the W-40 fpi and Tu-Cii tubes. Lubricant concentrations of 0.5, 1.0, 3.0, and 5.0 percent were evaluated with the 340 SUS lubricant. Figures 8.11 and 8.13 present the corresponding lubricant enhancement factors for each tube. With both of these surfaces, the highest heat transfer coefficients occurred with the 3.0 percent concentration through most of the heat flux range tested. At the 40 kW/m² heat flux, the 1.0 percent concentration yielded the highest heat transfer coefficients. This is a similar trend to that observed with the 160 SUS lubricant.

Conclusions

Results of the spray evaporation testing with six different enhanced and finned tube surfaces are summarized below. The effective film-feed supply rate was 0.013 kg/(s*m) and the tube overfeed ratio varied from 14.9 to 2.4 for the pure refrigerant testing depending upon the wall heat flux.

1. The W-SC and Tu-Cii surfaces, designed originally for use in condensers, perform similarly and they yielded the highest heat transfer performance in the spray evaporation environment. Both surfaces produce heat transfer coefficients nearly

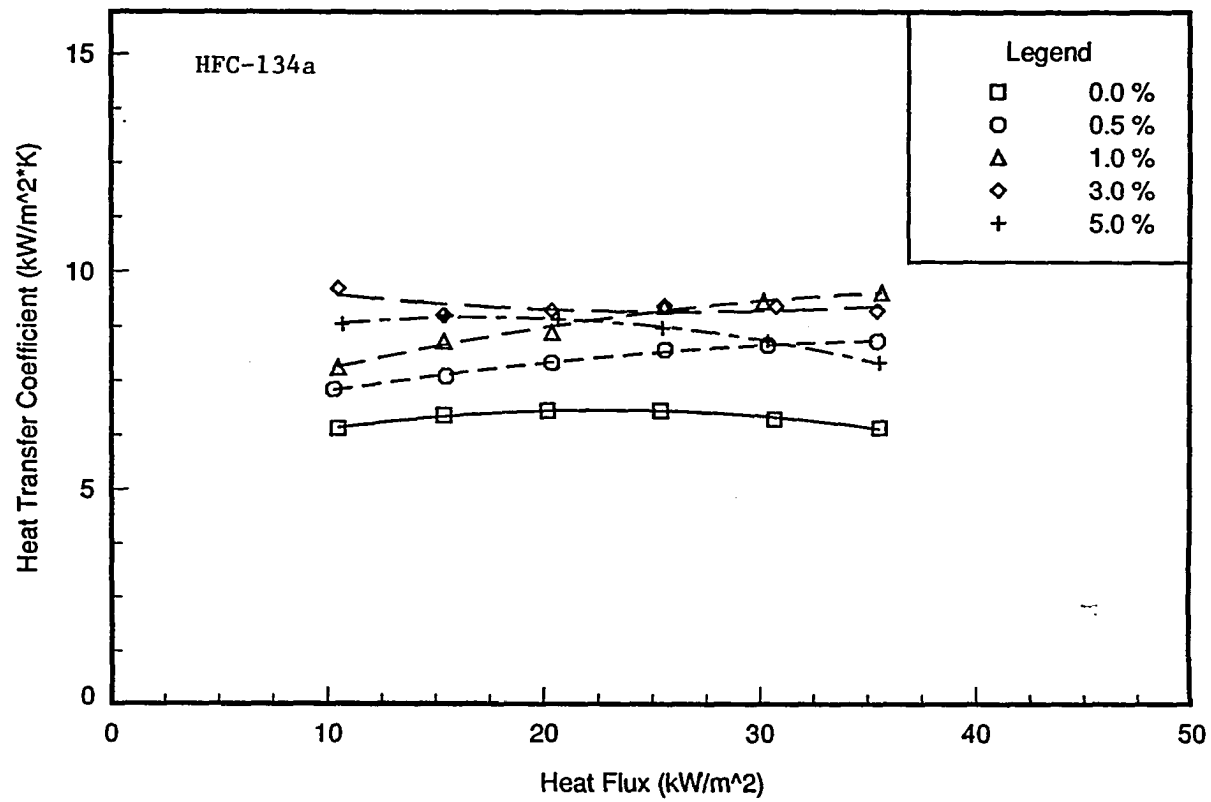


Figure 8.10: Heat transfer coefficient vs. heat flux ($P_{\text{sat}} = 314.5 \text{ kPa}$; 340 SUS oil, W-40 fpi tube)

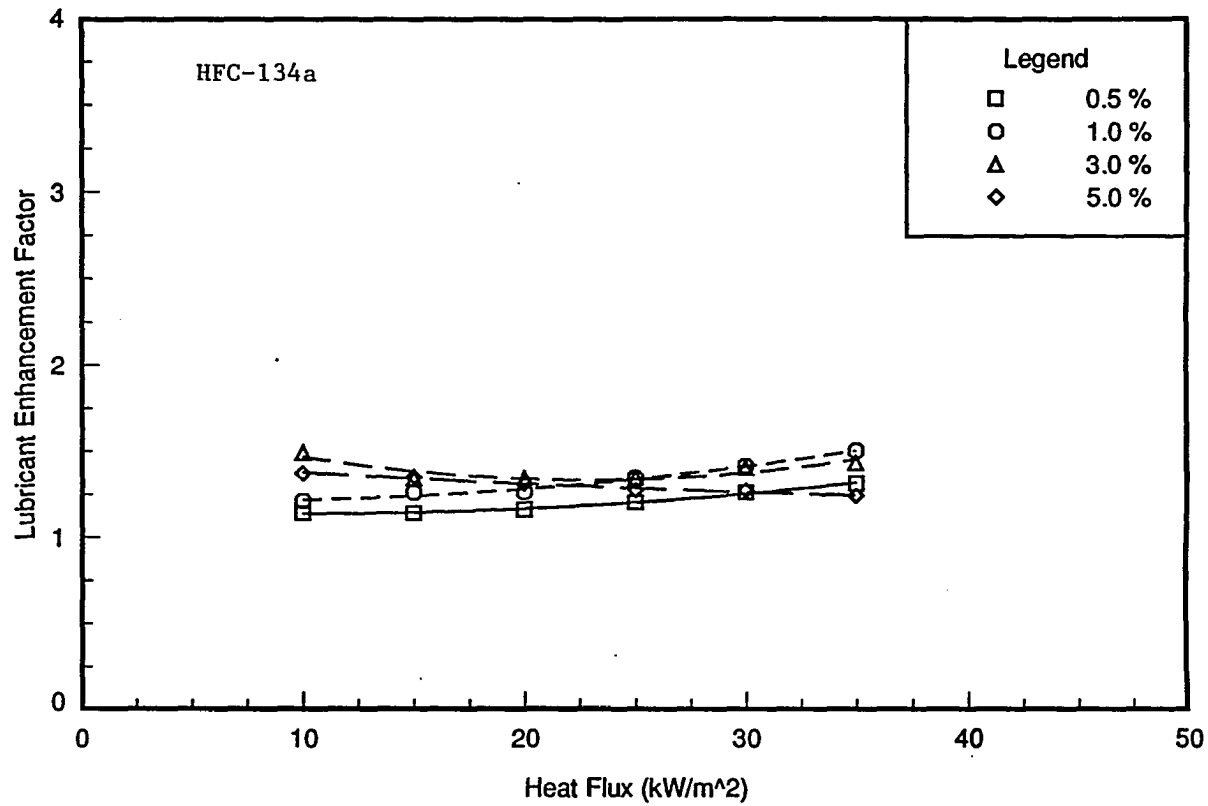


Figure 8.11: Lubricant enhancement factor vs. heat flux ($P_{\text{sat}} = 314.5 \text{ kPa}$; 340 SUS oil, W-40 fpi tube)

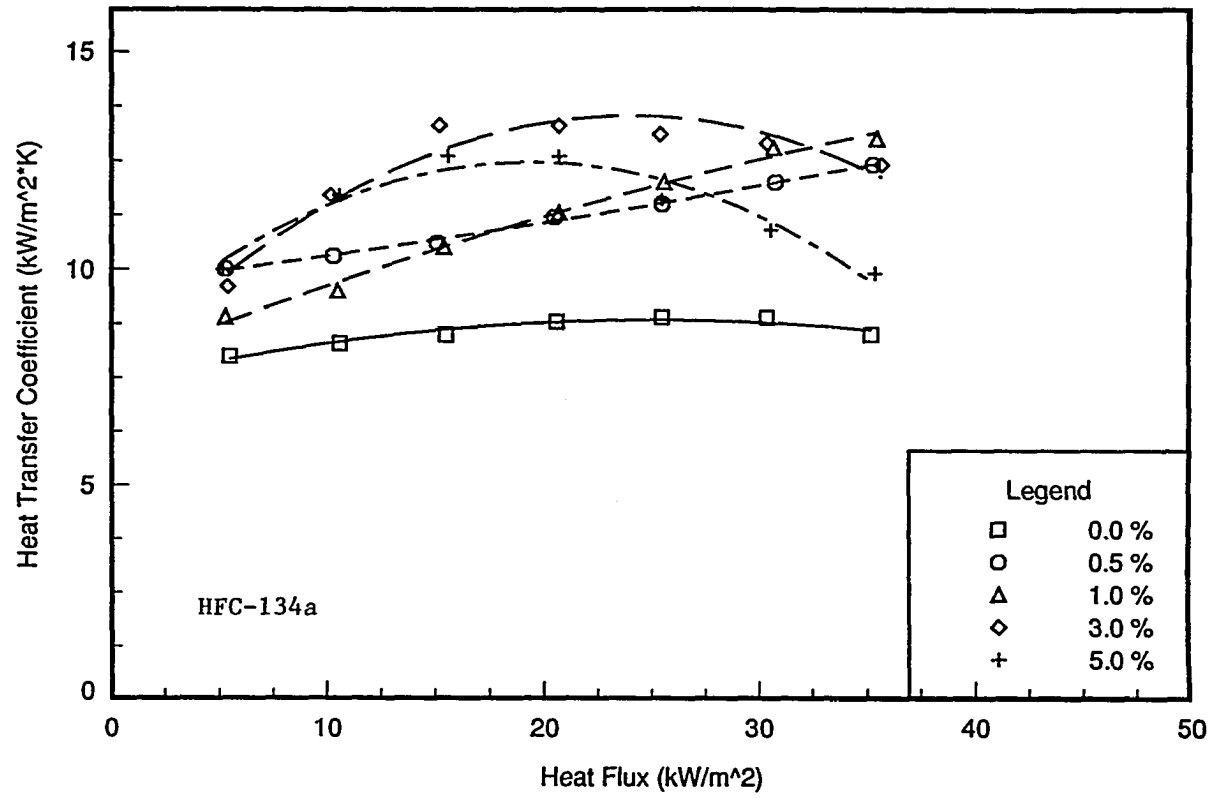


Figure 8.12: Heat transfer coefficient vs. heat flux ($P_{sat} = 314.5$ kPa; 340 SUS oil, Tu-Cii tube)

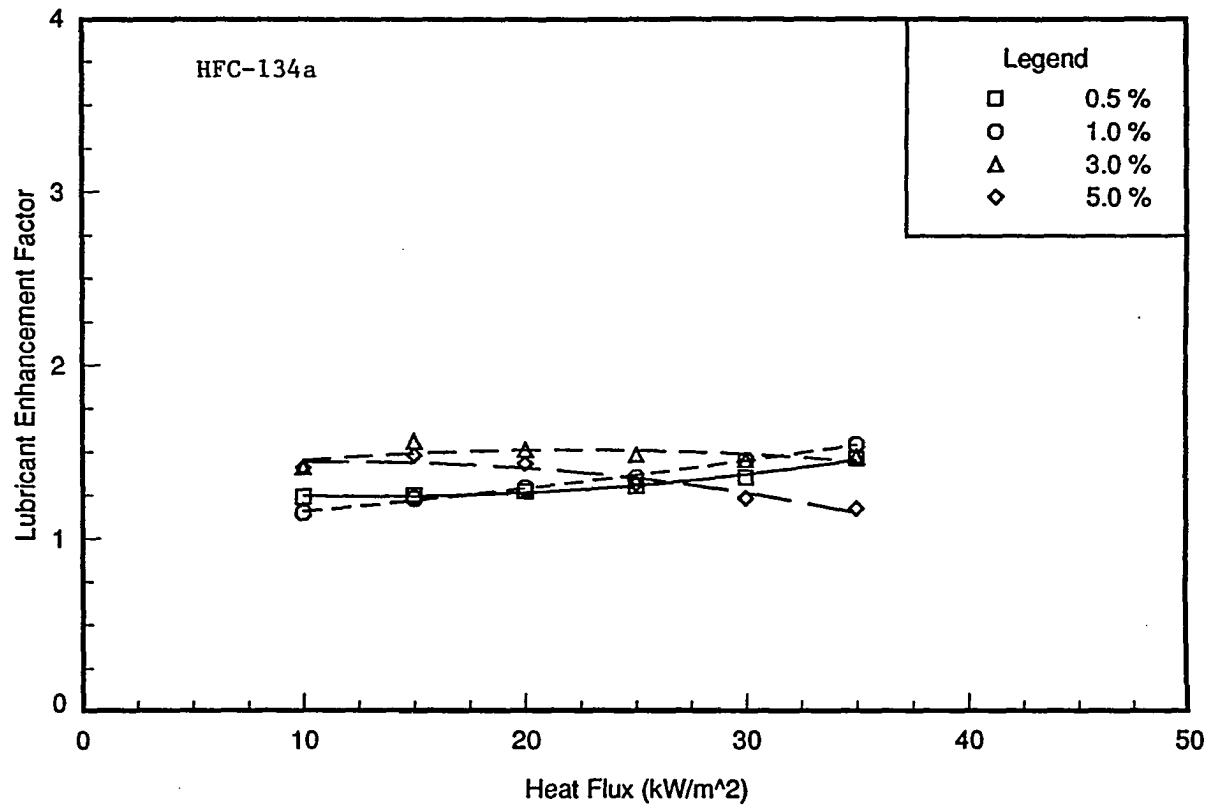


Figure 8.13: Lubricant enhancement factor vs. heat flux ($P_{sat} = 314.5$ kPa; 340 SUS oil, Tu-Cii tube)

three times as great as the plain-surface tube at the same test conditions, and 1.5 times that of a plain-surface in a pool-boiling environment.

2. The pool-boiling enhanced convective surfaces, namely the Tu-B and W-SE, performed poorer than both the W-SC and Tu-Cii surfaces.
3. For finned surface tubes, the W-26 fpi surface appears to perform slightly better than the W-40 fpi surface.
4. Small concentrations of a lubricant can substantially increase heat transfer performance if foaming occurs on the tubes' surface. Heat transfer performance enhancement with refrigerant/lubricant mixtures relative to pure refrigerant results occurred through a concentration of 3.0% with the 160 SUS oil and through 5.0% with the 340 SUS oil, which was the highest concentration evaluated with each oil viscosity. This enhancement occurred with all surfaces tested.

CHAPTER 9. BUNDLE TEST FACILITY NOZZLE CONFIGURATION GEOMETRY EFFECTS

Heat transfer performance of the W-40 fpi, triangular-pitch tube bundle was investigated in a spray evaporation environment with HFC-134a. Geometric specifications for the W-40 fpi tube used with the bundle test facility are listed in Table 4.1. Two different nozzle spray patterns (circular and square) were evaluated at two different nozzle heights and several film-feed supply rates. The geometric specifications of the individual nozzle configurations used in this testing are listed in Table 4.2. Collector testing was conducted in parallel with the heat transfer analysis experiments to determine the amount of refrigerant contacting the top row of the tube bundle for the different nozzle configurations. Collector test results are presented in Table 4.3.

A flooded evaporator test was performed so the spray evaporation results could be compared to that measured during pool boiling. All tube-bundle work included row-by-row heat transfer coefficient measurements as well as the overall bundle heat transfer coefficient measurements. The experimental data are presented in Appendix B in Tables B.3, B.4, B.6, and B.23 to B.31.

The operational set-points and maximum deviation from these set-points used during this testing are presented in Table 9.1. A fixed film-feed supply rate was used in each run

resulting in variation of the overfeed ratio with bundle load. Overfeed ratios and corresponding bundle loads are shown in Table 9.2 for the tests conducted with a known collector test fraction. The heat flux values listed in Table 9.2 are based upon the outer surface area of the W-40 fpi tube bundle.

Table 9.1: Bundle test facility operating parameters, nozzle configuration geometry effects testing

| Parameter | Control Band |
|----------------------------|----------------------------|
| Saturation Temperature | 2.0 °C ± 0.05 °C |
| Bundle Load | Desired Value ± 0.3 kW |
| Refrigerant Mass Flow Rate | Desired Value ± 2.0 kg/min |
| Spray Manifold Temperature | 0.0 °C to 3.0 °C |
| Bundle ΔT (Waterside) | 1.9 °C to 2.1 °C |

Table 9.2: Bundle overfeed ratios for the tests conducted with known collector test fractions, nozzle configuration geometry effects testing

| Bundle Load (kW) | Heat Flux (kW/m ²) | Overfeed ratios corresponding to the following mass flow rates and nozzle configurations | | | |
|---------------------|-----------------------------------|--|-----------|-----------|-----------|
| | | 17WLCRC | 24WLCRC | 30WHCRC | 30WHCRC |
| | | 25 kg/min | 25 kg/min | 25 kg/min | 45 kg/min |
| 11.0 | 19.2 | 3.2 | 3.7 | 4.6 | 7.9 |
| 13.0 | 22.7 | 2.7 | 3.1 | 3.9 | 6.6 |
| 15.0 | 26.2 | 2.4 | 2.7 | 3.4 | 5.8 |
| 17.0 | 29.7 | 2.1 | 2.4 | 3.0 | 5.1 |
| 19.0 | 33.2 | 1.9 | 2.1 | 2.7 | 4.5 |
| 21.0 | 36.7 | 1.7 | 1.9 | 2.4 | 4.1 |
| 23.0 | 40.2 | 1.5 | 1.8 | 2.2 | 3.8 |

Heat Transfer Results

The results that follow focus on showing the relative performance of the different nozzle configurations on shell-side heat transfer performance with a W-40 fpi, triangular-pitch tube bundle in a spray evaporation environment. Shell-side heat transfer coefficients presented are based upon the outer diameter over the enhancement, not the actual surface area of the low-finned structure. Data were taken at a saturation temperature of 2.0 °C which falls within the operating temperature range of most industrial flooded-evaporator units.

Nozzle Configuration Performance Comparison

Figure 9.1 presents the bundle heat transfer coefficients from tests conducted with eight different nozzle configurations. Bundle heat transfer performance showed dependence on nozzle orifice size. This dependence is directly related to the amount of refrigerant contacting the top row of the bundle. Referring to Table 4.3, it was found that the 24WLCRC configuration directed 8 % more refrigerant liquid at the top row of the tube bundle than the 17WLCRC configuration. The 30WHCRC configuration supplied 15 % more liquid to the tube bundle than the 24WLCRC configuration at a system mass flow rate of 25 kg/min. Collector tests were not performed for the 24WHCRC or 17WHCRC configurations, but it can be interpreted from the data shown in Figure 9.1 that the additional 25.4 mm in nozzle height over the bundle had minimal effect upon shell-side heat transfer performance.

A wide variety of nozzles are commercially available. Two types of interest are the solid conical plume and the solid square plume generating nozzles. Solid, implies that the liquid is distributed throughout the plume, and not just around the outer perimeter. Figure 9.2 compares the 30WHSQR (square plume) and the 30WHCRC (circular plume) nozzle configurations. The 30WHSQR configuration clearly yields better bundle heat transfer

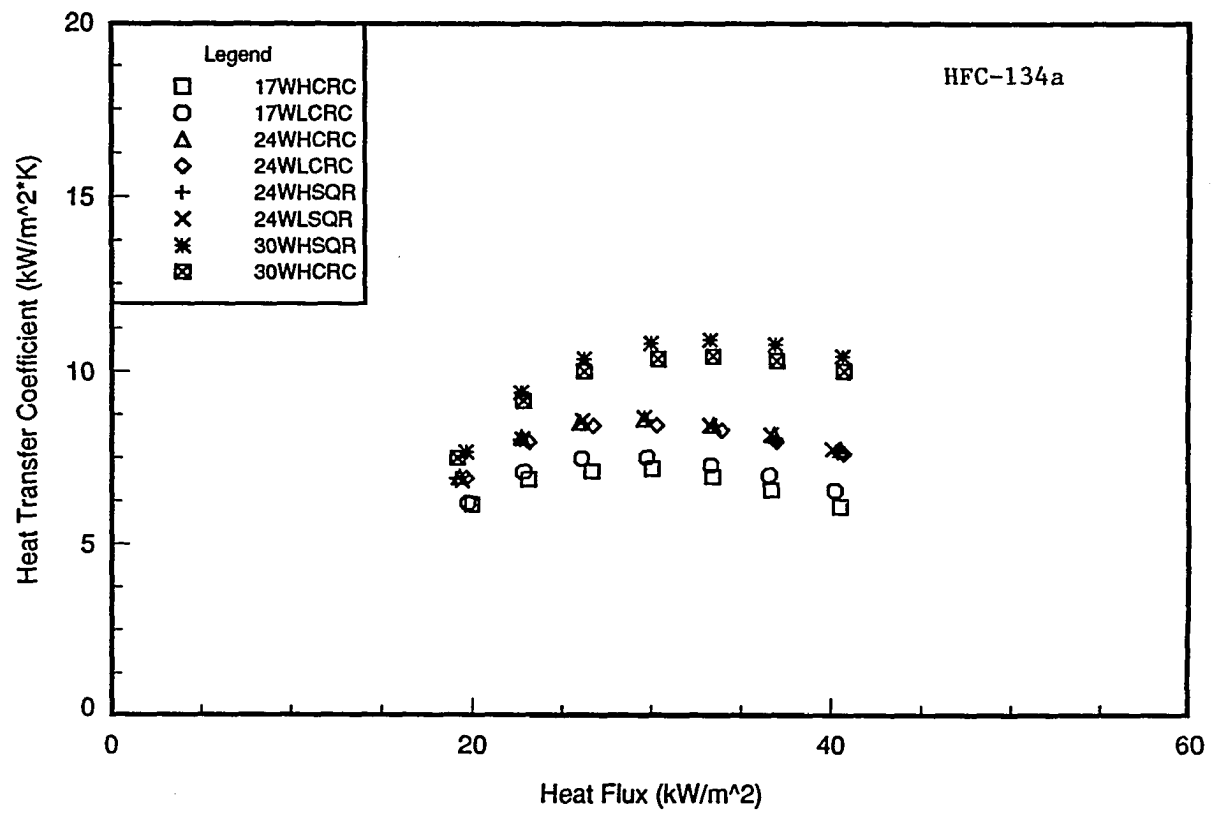


Figure 9.1: Heat transfer coefficient vs. heat flux ($T_{sat} = 2.0\text{ }^{\circ}\text{C}$; M.F.R. = 25 kg/min)

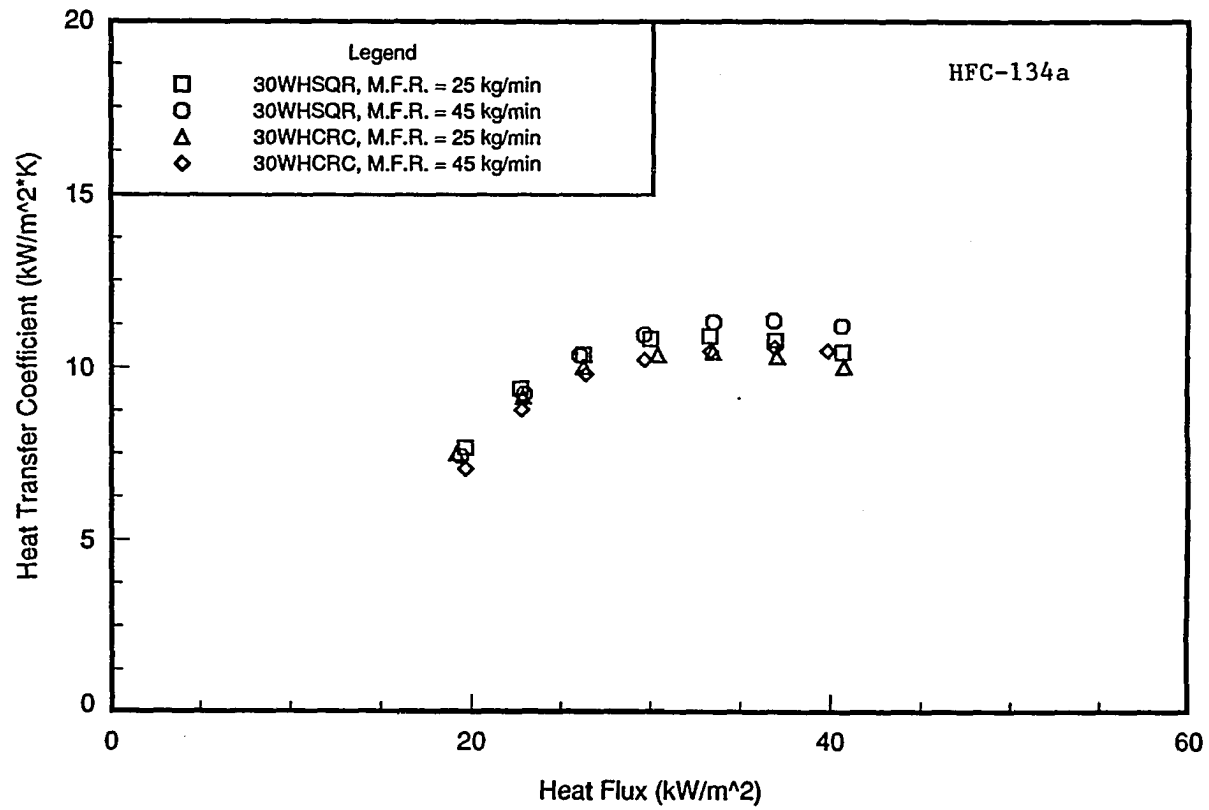


Figure 9.2: Heat transfer coefficient vs. heat flux ($T_{\text{sat}} = 2.0 \text{ }^\circ\text{C}$; square and circular nozzle plume comparison)

performance than the 30WHCRC configuration at both mass flow rates evaluated. The collector tests used on this facility could determine the amount of refrigerant missing the bundle, but not the axial or lateral variation in mass flux seen by the top row of the tube bundle. However, considering only the geometry of the nozzle plumes, square plume nozzles at an optimum height will direct a higher percentage of the refrigerant to the tube bundle. Data taken with the 24WHCRC, 24WLCRC, 24WHSQR, and 24WLSQR configurations show little dependence upon either nozzle height or plume geometry with this orifice size.

Row-by-Row Analysis

Figures 9.3 through 9.7 show row performance factor (RPF) variation with row depth for the triangular-pitch, W-40 fpi bundle. An ideal spray evaporator nozzle configuration might be thought of as one in which each row is carrying an equal percentage of the bundle load, or the row performance factor for each row is approaching one. Possibly, limitations resulting from a given type of shell-side surface enhancement used in a spray evaporator tube bundle might cause a well designed nozzle distribution system to fall short of this goal.

Figure 9.3 shows one example where the row performance is far from equal in each row. Figures 9.3, 9.4, and 9.5 indicate better heat transfer performance on rows 1 and 3 than rows 2 and 4. This is at-least partly due to the effects of a triangular pitch upon the bundle heat transfer performance. Row 1 receives the fully developed spray plumes and row 3 lies directly below row 1. The tubes in row 2 are supplied liquid refrigerant primarily from drip-off from row 1, because the gap between the tubes in each row is only a nominal 3.2 mm in width.

This 'saw toothed effect' in the row performance factors appears to diminish as the local film-feed supply rate is increased. Figures 9.6 and 9.7 show row performance factors for the 30WHCRC nozzle configuration with system mass flow rates of 25 kg/min and 45 kg/min. At

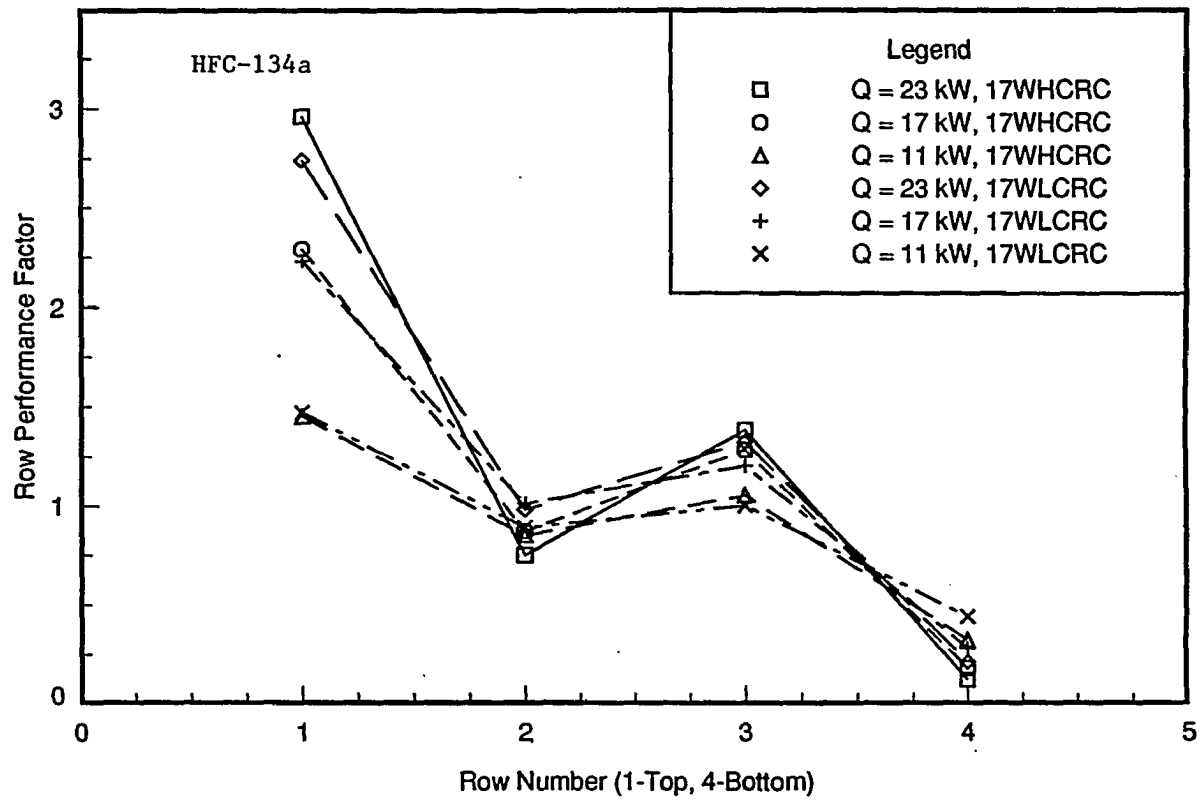


Figure 9.3: Row performance factor variation with row depth ($T_{sat} = 2.0\text{ }^{\circ}\text{C}$; M.F.R. = 25 kg/min, 17WHCRC & 17WLCRC configurations)

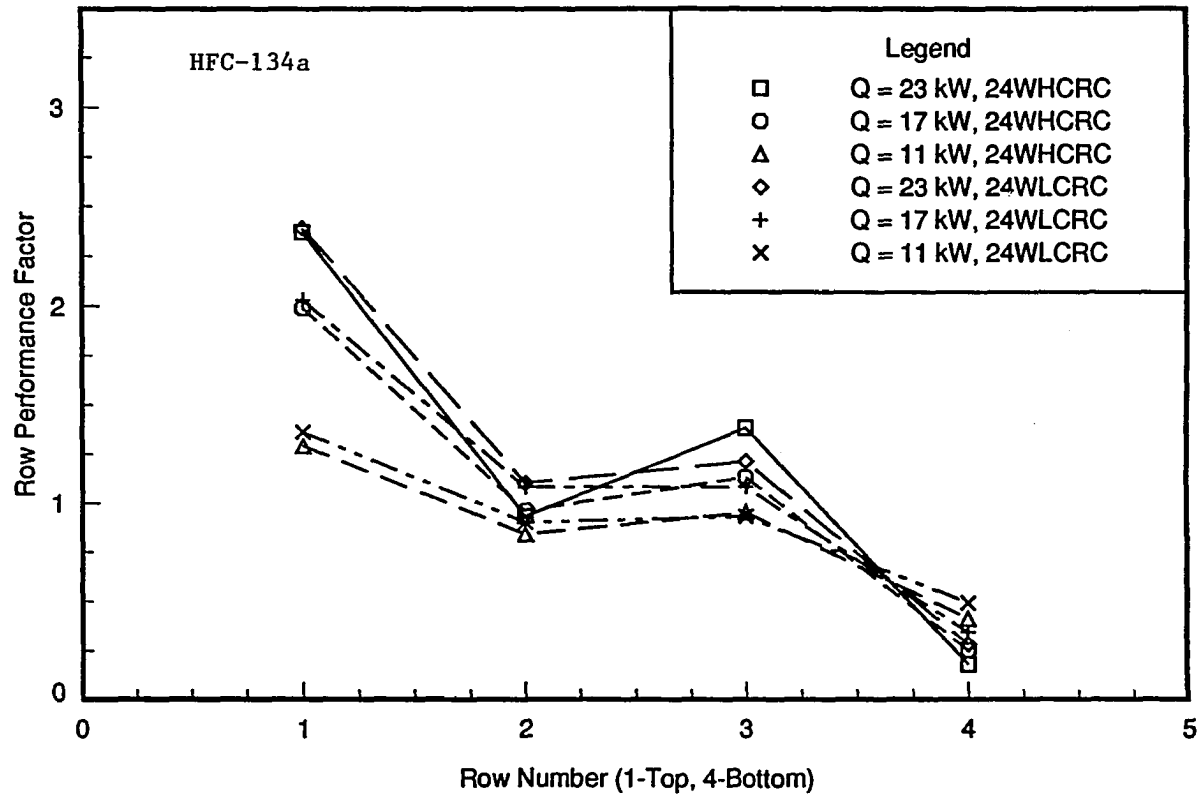


Figure 9.4: Row performance factor variation with row depth ($T_{\text{sat}} = 2.0 \text{ }^\circ\text{C}$; M.F.R. = 25 kg/min, 24WHCRC & 24WLCRC configurations)

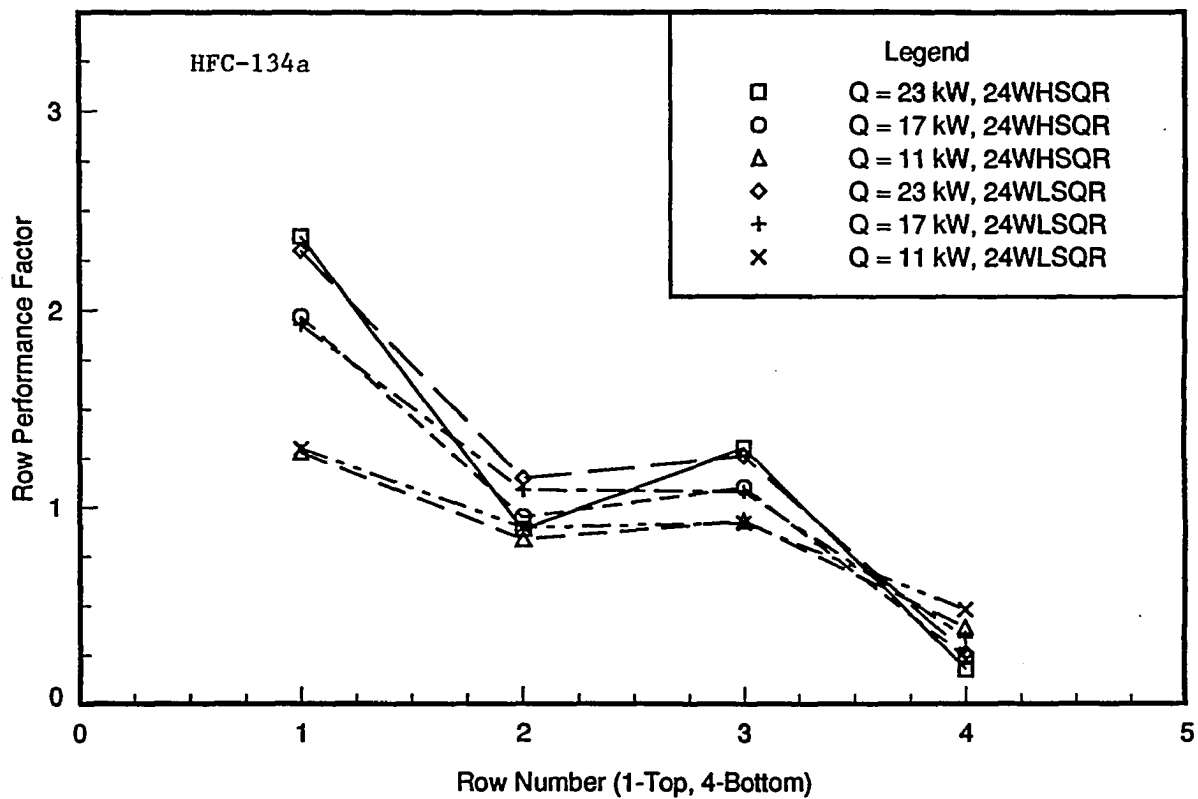


Figure 9.5: Row performance factor variation with row depth ($T_{sat} = 2.0\text{ }^{\circ}\text{C}$; M.F.R. = 25 kg/min, 24WHSQR & 24WLSQR configurations)

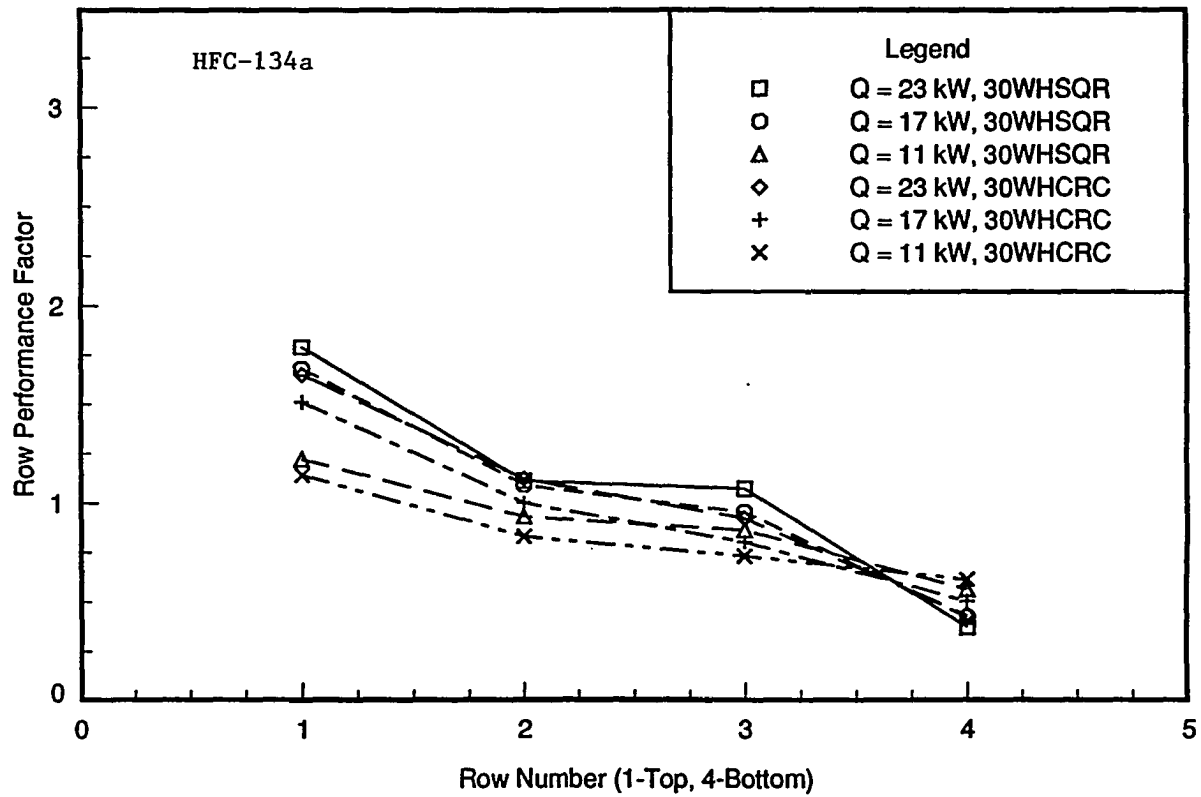


Figure 9.6: Row performance factor variation with row depth ($T_{\text{sat}} = 2.0 \text{ }^\circ\text{C}$; M.F.R. = 25 kg/min, 30WHSQR & 30WHCRC configurations)

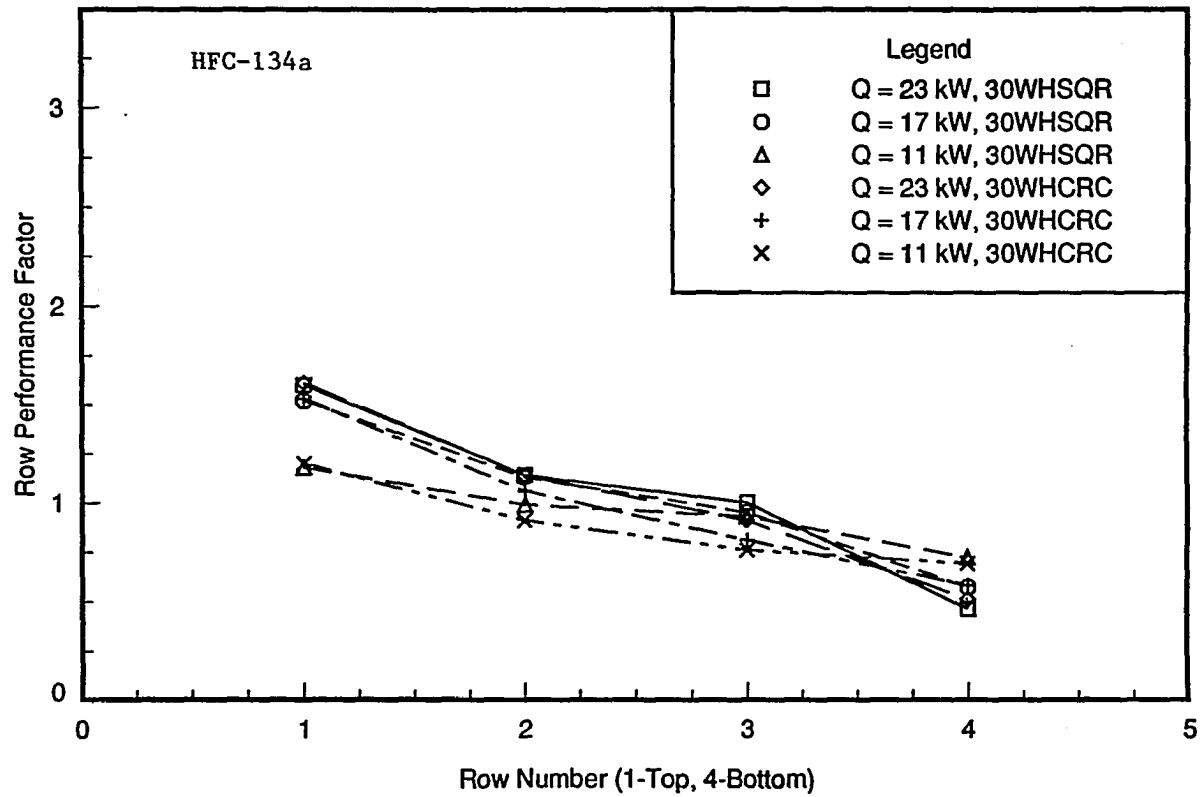


Figure 9.7: Row performance factor variation with row depth ($T_{sat} = 2.0 \text{ }^\circ\text{C}$; M.F.R. = 45 kg/min, 30WHSQR & 30WHCRC configurations)

the bundle load of 11 kW the row performance factors are approaching unity with both nozzle configurations.

Top and bottom row heat transfer coefficients from tests done with the 17WLCRC, 24WLCRC, and 30WHCRC nozzle configurations are shown in Table 9.3. The heat transfer performance of the top row is strongly dependent upon wall heat flux, while showing only little dependence upon film-feed supply rate, indicating that boiling is present in the liquid film. The dependence of the heat transfer coefficient on heat flux is greater here than that found in low-finned, single-tube results presented previously in Chapter 8.

Table 9.3: Top and bottom row shell-side heat transfer coefficients from the 17WLCRC, 24WLCRC, and 30WHCRC nozzle configurations

| Nominal Bundle Load (kW) | Shell-side heat transfer coefficients $\left(\frac{\text{kW}}{\text{m}^2 \cdot \text{K}}\right)$ | | | | | |
|---------------------------------------|---|----------|----------|----------|----------|----------|
| | 17WLCRC | | 24WLCRC | | 30WHCRC | |
| | Row 1 | Row 4 | Row 1 | Row 4 | Row 1 | Row 4 |
| 23 | 1.82E+01 | 1.38E+00 | 1.85E+01 | 2.13E+00 | 1.68E+01 | 4.34E+00 |
| 21 | 1.83E+01 | 1.57E+00 | 1.87E+01 | 2.36E+00 | 1.69E+01 | 4.69E+00 |
| 19 | 1.80E+01 | 1.82E+00 | 1.88E+01 | 2.60E+00 | 1.67E+01 | 4.92E+00 |
| 17 | 1.71E+01 | 2.08E+00 | 1.75E+01 | 2.87E+00 | 1.59E+01 | 5.17E+00 |
| 15 | 1.53E+01 | 2.40E+00 | 1.59E+01 | 3.18E+00 | 1.42E+01 | 5.29E+00 |
| 13 | 1.27E+01 | 2.64E+00 | 1.31E+01 | 3.38E+00 | 1.20E+01 | 5.18E+00 |
| 11 | 9.19E+00 | 2.74E+00 | 9.54E+00 | 3.39E+00 | 8.66E+00 | 4.61E+00 |

The effective film-feed supply rate used in the single-tube testing was $0.013 \text{ kg}/(\text{s}\cdot\text{m})$. The film-feed supply rate seen by the top row of the tube bundle may be calculated by using the collector test fraction results and assuming equal mass flux distribution across the length and width of the bundle. For example, using this assumption the film-feed supply rate for the top row with the 24WLCRC nozzle configuration at the $25 \text{ kg}/\text{min}$ refrigerant supply rate is $0.084 \text{ kg}/(\text{s}\cdot\text{m})$. It is possible that the larger film-feed supply rate and film layer thickness enhanced the nucleate boiling contribution to the shell-side heat transfer coefficient. Visual inspections revealed nucleate bubbles in the thick liquid layer on the bottom portion of the tubes in all 4 rows. Also, the performance in the top row may be enhanced by vapor rising from the lower rows, thus increasing convective evaporation. Possibly the results are influenced by both effects.

The dependence of the heat transfer coefficient upon heat flux in the lower rows of the tube bundle should be scrutinized carefully since these rows are not fully wetted. The low-finned, shell-side enhancement commonly used in industry and used in this study appears to be a very poor surface for spray evaporation. Table 9.3 clearly shows the magnitude of dryout in the lower rows of the bundle. Finned tube heat transfer performance is resistant to inundation effects in a condensation environment at-least partly because liquid is prevented from moving axially along the surface of the tube. For similar reasons, the surface of the finned tube becomes prone to dryout in the spray evaporation environment. The regions of a tube bundle underfed by the nozzle bank suffer dryout in the lower rows.

Pool-Boiling Comparison

To conduct pool-boiling testing the refrigerant charge of the system was increased so that at-least 25.4 mm of liquid covered the top row throughout the data run. Figure 9.8

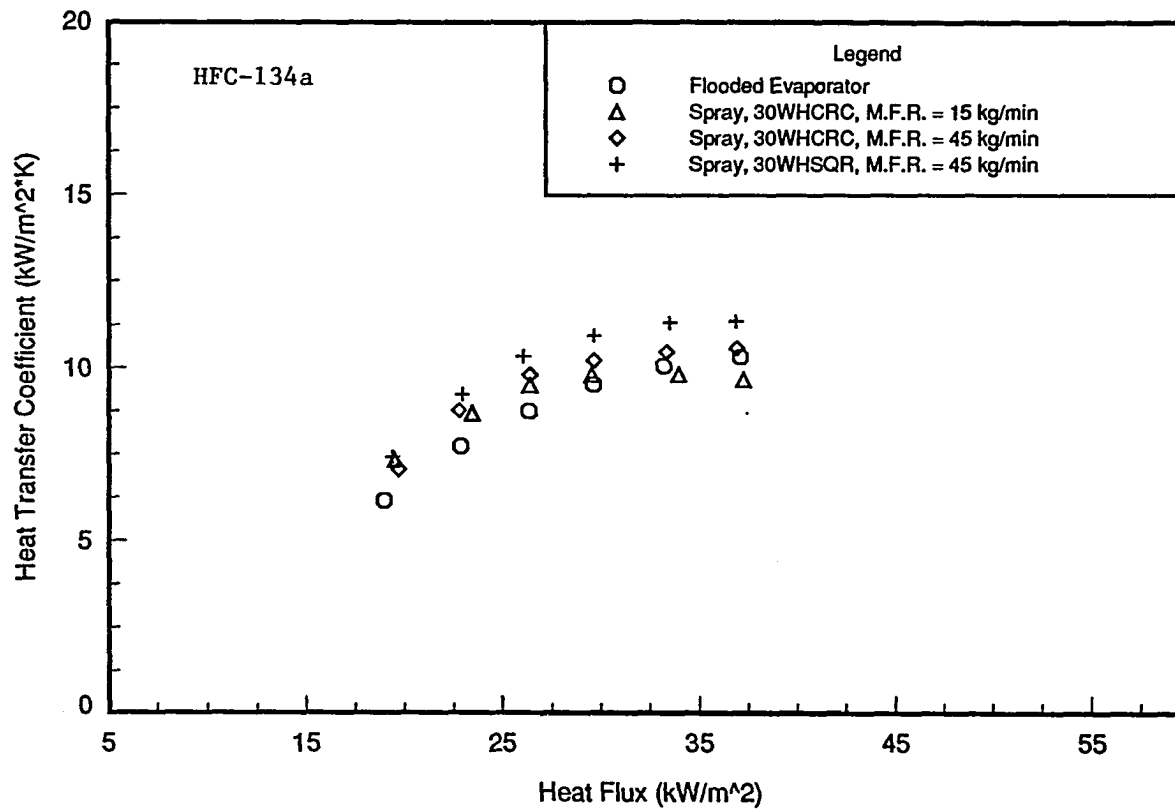


Figure 9.8: Heat transfer coefficient vs. heat flux ($T_{\text{sat}} = 2.0 \text{ }^\circ\text{C}$; pool boiling comparison)

compares the pool-boiling data with results from several spray evaporation tests. The 30WHSQR and the 30WHCRC nozzle configurations with a 45 kg/min system mass flow rate generated better heat transfer performance than that found in the flooded evaporator testing. The test conducted with the 30WHCRC configuration and a 15 kg/min system mass flow rate yielded better heat transfer performance at lower heat fluxes and poorer performance at higher heat fluxes than that found in the flooded evaporator.

Conclusions

Results from pure HFC-134a testing with the W-40 fpi, triangular-pitch tube bundle in the spray evaporation environment are summarized below. Eight different nozzle configurations were used to evaluate the effects of spray pattern geometry, nozzle orifice size, and nozzle height on shell-side heat transfer performance.

1. Heat transfer performance of the low-finned, triangular-pitch tube bundle showed dependence on the bundle overfeed ratio, which in this facility is largely a function of the orifice size of the nozzles in use.
2. At the highest film-feed supply rate evaluated, both the solid circular plume and the solid square plume nozzles generated higher heat transfer coefficients than those found in pool-boiling testing throughout the heat flux range tested. At the lowest heat flux evaluated the spray evaporation performance was 15 to 20 percent higher than that found in pool boiling.

3. The solid square plume nozzles generated heat transfer coefficients 4 to 10 percent higher than those found with solid circular plume nozzles at the same nozzle height with several supply rate/nozzle configuration combinations.
4. The low-finned, triangular-pitch bundle was very prone to dryout in its lower rows. This is likely due to a restriction to axial liquid movement along the surface of the tube. Areas underfed by the nozzles remain liquid deprived.

CHAPTER 10. BUNDLE TEST FACILITY SURFACE ENHANCEMENT, BUNDLE GEOMETRY, AND SUPPLY RATE EFFECTS

Testing was conducted with HFC-134a to evaluate the effects of film-feed supply rate, surface enhancement, and bundle geometry upon shell-side heat transfer performance in a spray evaporation environment. The Tu-Cii, Tu-B, W-SC, W-40 fpi, and plain-surface tubes were tested with the triangular-pitch bundle geometry. The Tu-B tube was also tested with the square-pitch bundle geometry so a performance comparison could be made between the square and triangular-pitch tube arrangements. The plain surface was evaluated in parallel with the finned and enhanced surfaces to determine the degree of improvement obtained with the different surface enhancements. The 30WHCRC nozzle configuration was used for all testing presented in this chapter. A flooded evaporator test was conducted with the triangular-pitch, Tu-B tube bundle so a comparison could be made with the spray evaporation results. It should be noted that the Tu-B surface is an enhanced boiling surface designed specifically for pool boiling use in a flooded evaporator. Dimensions for all tubes evaluated are listed in Table 4.1 while the experimental data are presented in Appendix B in Tables B.1 to B.22 and B.32.

The operational set-points used during this testing along with maximum deviation from these set-points are presented in Table 10.1. A fixed film-feed supply rate was used in this

testing resulting in the variations of overfeed ratio with bundle load. The overfeed ratios and corresponding bundle loads are shown in Table 10.2. The overfeed ratios at each bundle load are slightly lower with the square-pitch geometry, because the square-pitch geometry presents a narrower cross-sectional area to the nozzle plumes than the triangular-pitch geometry.

Collector test results are presented for each of the bundle geometries in Table 4.3.

Table 10.1: Bundle test facility operating parameters, HFC-134a testing

| Parameter | Control Band |
|-------------------------------|----------------------------|
| Saturation Temperature | 2.0 °C ± 0.05 °C |
| Bundle Load | Desired Value ± 0.3 kW |
| Refrigerant Mass Flow Rate | Desired Value ± 2.0 kg/min |
| Spray Manifold Temperature | 0.0 °C to 3.0 °C |
| Bundle ΔT (Waterside) | 1.9 °C to 2.1 °C |

Heat Transfer Results

Experimental spray evaporation data are presented for pure HFC-134a. The effects of surface enhancement, bundle geometry, and film-feed supply rate upon spray evaporation heat transfer performance were evaluated. Shell-side heat transfer coefficients presented are based on the nominal cylindrical area over the surface enhancement or finned structure, not the actual surface area of the tube. All data were taken at 2.0 °C, which is in the temperature range of interest for large industrial chillers.

Table 10.2: Bundle overfeed ratios for the triangular and square-pitch bundle geometries and the 30WHCRC nozzle configuration, HFC-134a testing

| Bundle Geometry | Bundle Load (kW) | Overfeed Ratio at the Four System Mass Flow Rates | | | |
|------------------|---------------------|---|----------------|----------------|----------------|
| | | 15 (kg/min) | 25 (kg/min) | 35 (kg/min) | 45 (kg/min) |
| Triangular Pitch | 11.0 | 3.0 | 4.6 | 6.3 | 7.9 |
| | 13.0 | 2.5 | 3.9 | 5.3 | 6.6 |
| | 15.0 | 2.2 | 3.4 | 4.6 | 5.8 |
| | 17.0 | 1.9 | 3.0 | 4.1 | 5.1 |
| | 19.0 | 1.7 | 2.7 | 3.6 | 4.5 |
| | 21.0 | 1.6 | 2.4 | 3.3 | 4.1 |
| | 23.0 | 1.4 | 2.2 | 3.0 | 3.8 |
| Square Pitch | 11.0 | 2.8 | 4.3 | 5.9 | 7.3 |
| | 13.0 | 2.4 | 3.6 | 5.0 | 6.2 |
| | 15.0 | 2.1 | 3.2 | 4.3 | 5.4 |
| | 17.0 | 1.8 | 2.8 | 3.8 | 4.7 |
| | 19.0 | 1.6 | 2.5 | 3.4 | 4.2 |
| | 21.0 | 1.5 | 2.3 | 3.1 | 3.8 |
| | 23.0 | 1.3 | 2.1 | 2.8 | 3.5 |

Surface Enhancement Effects

Testing was conducted at refrigerant supply rates of 15 kg/min through 45 kg/min with the W-40 fpi, W-SC, Tu-Cij, and the Tu-B, triangular-pitch tube bundles. Figures 10.1 to 10.4 present the bundle shell-side heat transfer coefficients measured during these tests. Data collected with the plain-tube bundle at flow rates of 15 kg/min and 35 kg/min are also shown for comparison with the modified surface results. Table 10.3 presents the surface enhancement factors for these results at the 15 kg/min and 35 kg/min refrigerant supply rates.

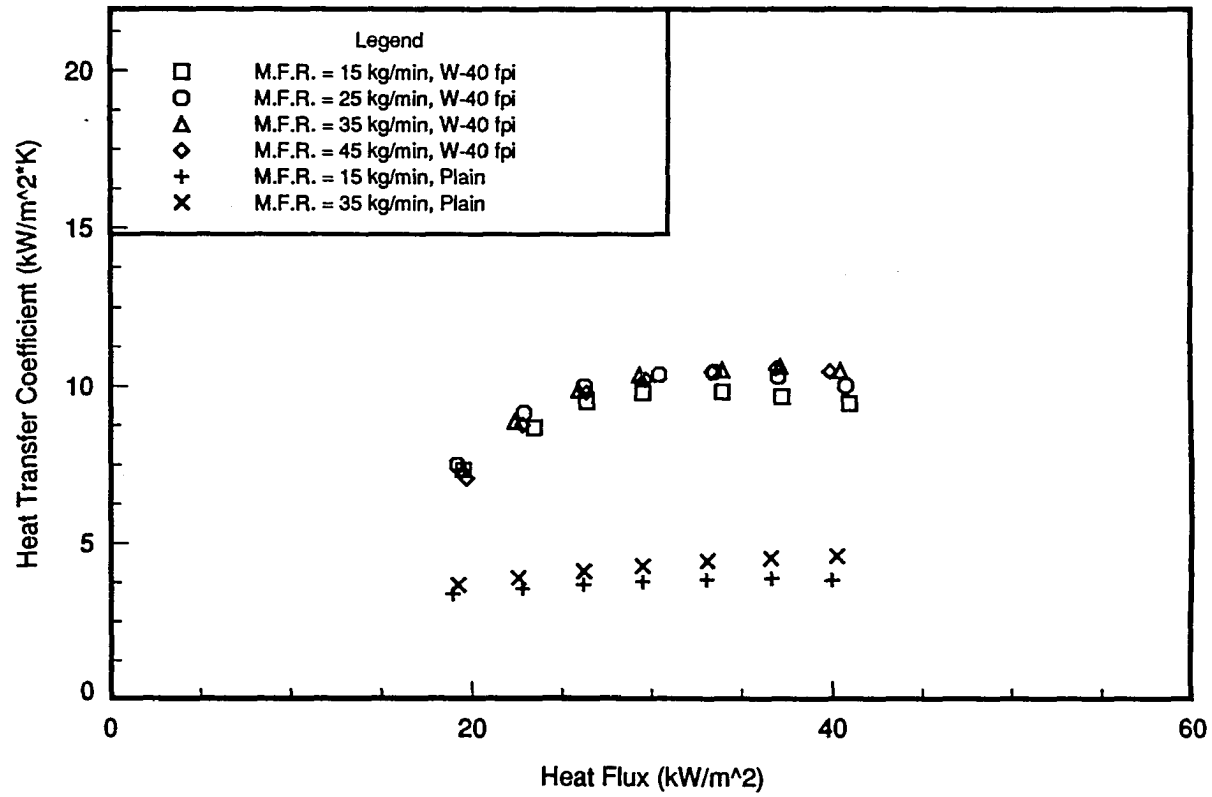


Figure 10.1: Heat transfer coefficient vs. heat flux ($T_{sat} = 2.0$ °C; W-40 fpi and plain surface, triangular-pitch bundles)

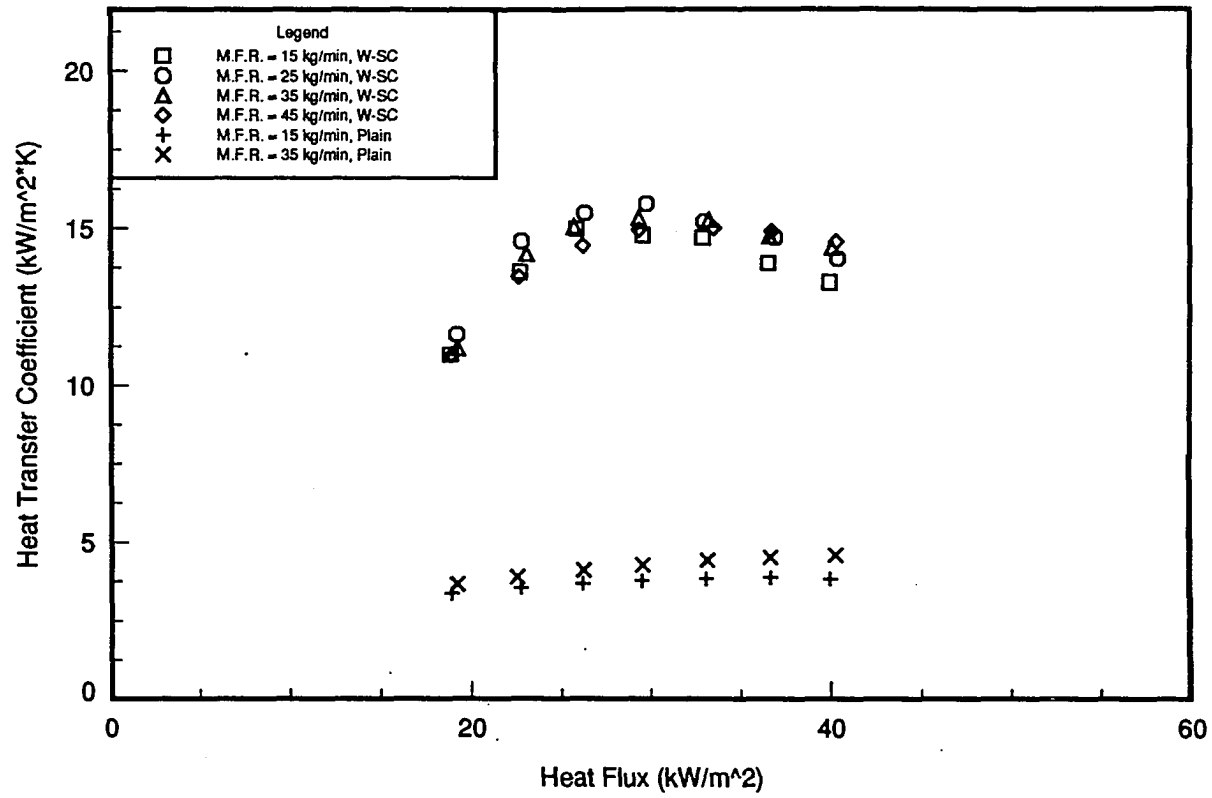


Figure 10.2: Heat transfer coefficient vs. heat flux ($T_{sat} = 2.0$ °C; W-SC and plain surface, triangular-pitch bundles)

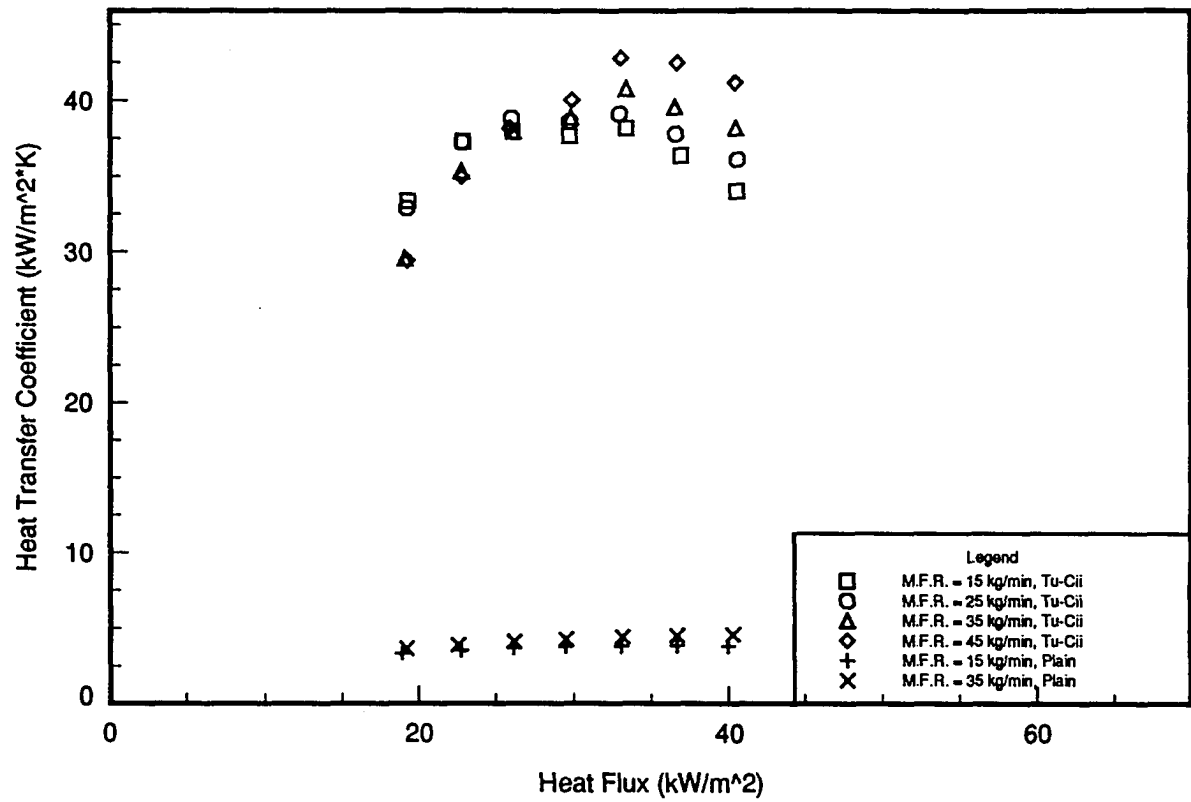


Figure 10.3: Heat transfer coefficient vs. heat flux ($T_{sat} = 2.0\text{ }^{\circ}\text{C}$; Tu-Cii and plain surface, triangular-pitch bundles)

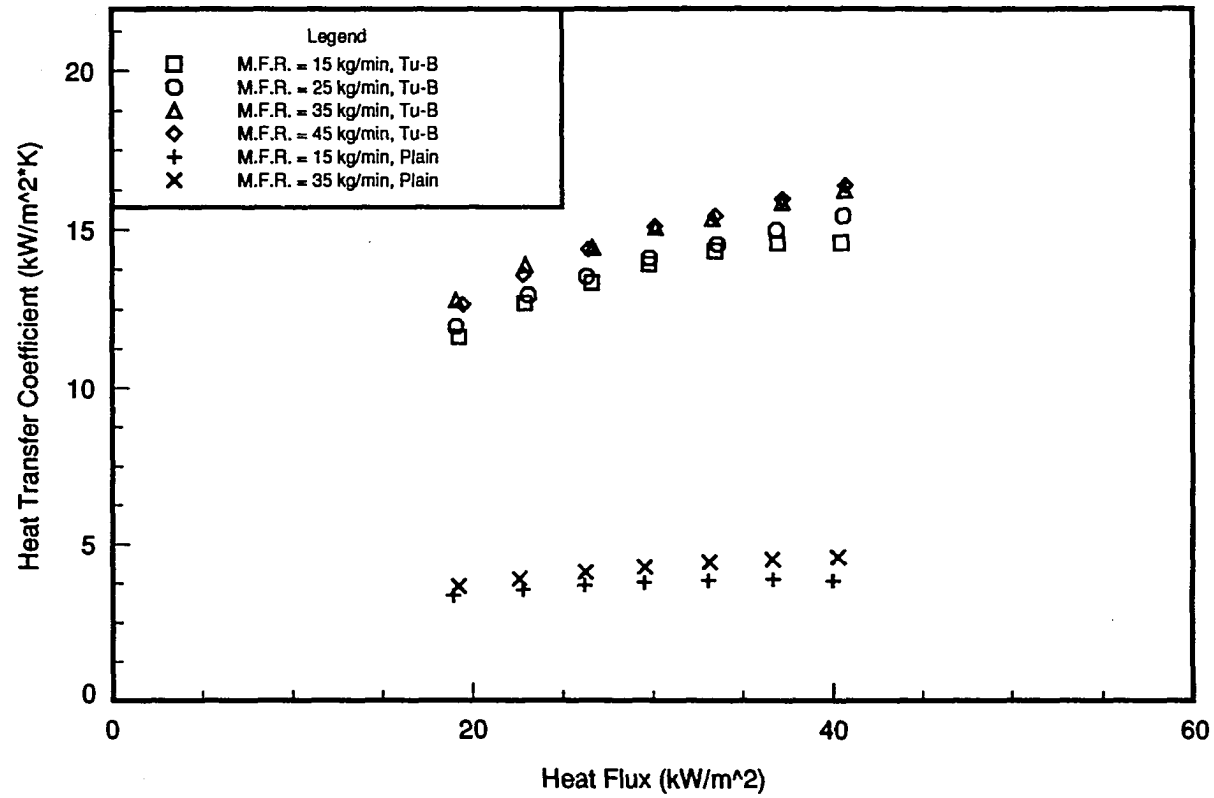


Figure 10.4: Heat transfer coefficient vs. heat flux ($T_{\text{sat}} = 2.0 \text{ }^\circ\text{C}$; Tu-B and plain surface, triangular-pitch bundles)

Table 10.3: Surface enhancement factors for the triangular-pitch geometry tests, HFC-134a results

| Bundle Load (kW) | M.F.R. = 15 kg/min | | | | M.F.R. = 35 kg/min | | | |
|------------------|--------------------|------|--------|------|--------------------|------|--------|------|
| | W-40 fpi | W-SC | Tu-Cii | Tu-B | W-40 fpi | W-SC | Tu-Cii | Tu-B |
| 23 | 2.47 | 3.47 | 8.88 | 3.81 | 2.29 | 3.14 | 8.34 | 3.54 |
| 21 | 2.50 | 3.59 | 9.40 | 3.76 | 2.35 | 3.27 | 8.77 | 3.52 |
| 19 | 2.55 | 3.83 | 9.94 | 3.73 | 2.37 | 3.45 | 9.20 | 3.47 |
| 17 | 2.59 | 3.92 | 9.97 | 3.68 | 2.42 | 3.58 | 9.08 | 3.52 |
| 15 | 2.57 | 4.05 | 10.26 | 3.60 | 2.40 | 3.67 | 9.24 | 3.51 |
| 13 | 2.44 | 3.82 | 10.48 | 3.57 | 2.27 | 3.64 | 9.06 | 3.56 |
| 11 | 2.18 | 3.26 | 9.89 | 3.45 | 2.00 | 3.05 | 8.05 | 3.49 |

The Tu-Cii bundle yielded the highest shell-side heat transfer coefficients at both flow rates for the entire heat flux range evaluated. The surface enhancement factors vary from 8 to 10.5 for this surface. The Tu-B and W-SC surfaces yield similar results with surface enhancement factors ranging from 3 to 4. As expected, the W-40 fpi bundle yielded surface enhancement factors less than any of the enhanced surfaces tested in this study.

Bundle Geometry Effects

Figure 10.5 shows results obtained with the triangular-pitch and square-pitch, Tu-B bundles. The triangular-pitch geometry yielded a greater heat transfer performance at high heat fluxes and a lower heat transfer performance at low heat fluxes compared to the square-pitch geometry. Figure 10.5 also shows that the square-pitch geometry generates a film heat transfer performance that is less dependent upon heat flux than the triangular-pitch geometry. Results from both bundle geometries indicate that the heat transfer performance is moderately dependent upon the refrigerant supply rate, but this dependence is greater with the triangular-pitch geometry. Considering the 40 kW/m² heat flux, the bundle heat transfer coefficient

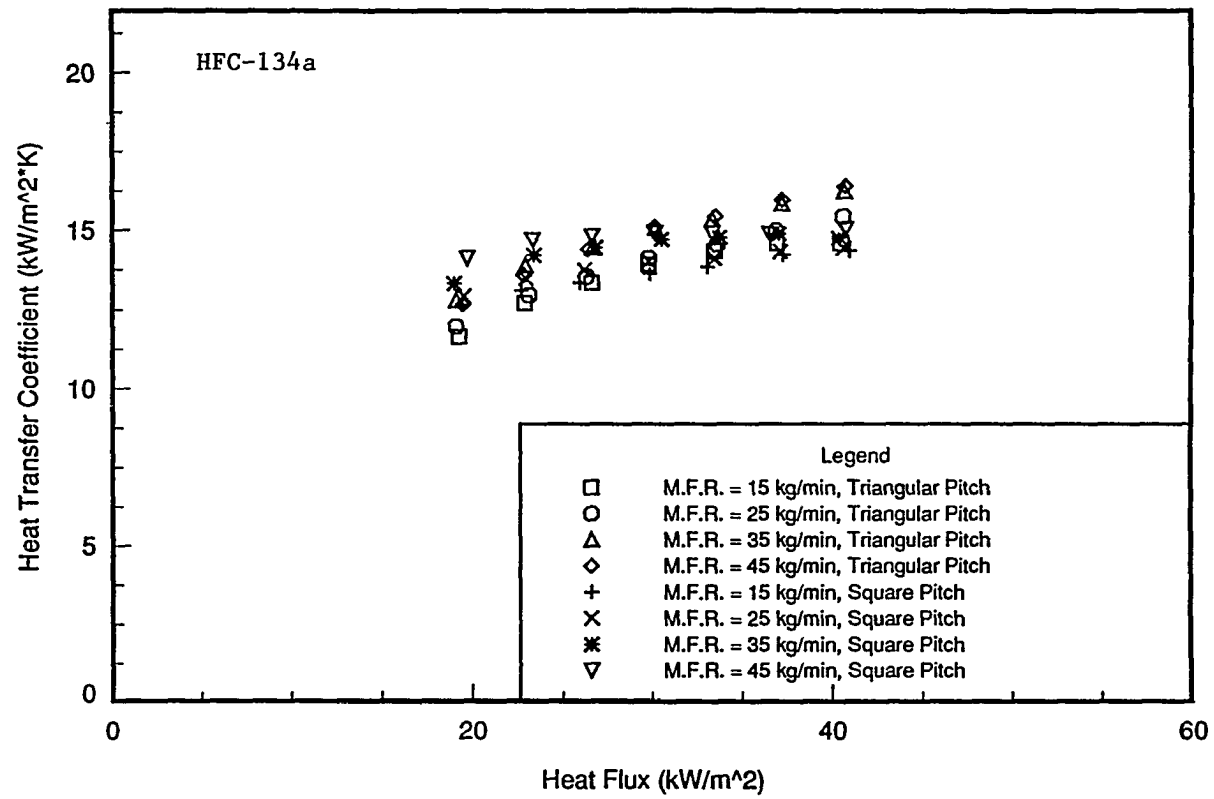


Figure 10.5: Heat transfer coefficient vs. heat flux ($T_{\text{sat}} = 2.0 \text{ }^\circ\text{C}$;
Tu-B, triangular and square-pitch bundles

increased by 12.3 percent from the lowest flow rate to the highest flow rate for the triangular-pitch geometry, and only 4.9 percent for the square-pitch geometry.

Film-Feed Supply Rate Effects

All five triangular-pitch bundles experienced a moderate dependence on film-feed supply rate. At a wall heat flux of 40 kW/m^2 , the variation in the shell-side heat transfer coefficient from the lowest to the highest film-feed supply rate is no more than 13 % for the W-40 fpi, W-SC, and Tu-B, triangular-pitch bundles. At this same heat flux, the variation in the shell-side heat transfer coefficient from the lowest to highest flow rate with the Tu-Cii bundle is 18 %. Considering the bundle overfeed ratio is 1.4 at the 15 kg/min supply rate and 3.8 at the 45 kg/min supply rate, a larger increase in the bundle shell-side heat transfer coefficient might be expected. This is especially true for the W-40 fpi and W-SC surface bundles since the lower rows of these bundles suffered dryout to a greater degree than the other surfaces tested.

Some evidence exists that increased heat transfer performance does not always occur with increased film-feed supply rate. At the 23 kW bundle load, heat transfer improves with increased refrigerant supply rates through the range tested. Therefore, it can be concluded that further increases in heat transfer performance at this bundle loading might be obtained with higher refrigerant supply rates. At the lower bundle loadings, the shell-side heat transfer coefficient is greater at the 25 kg/min supply rate than the 45 kg/min supply rate with the Tu-Cii, W-40 fpi, and Tu-B, triangular-pitch bundles. This performance characteristic might be a result of increased thermal conduction resistance due to thicker films on the tubes at higher refrigerant supply rates. Single-tube film evaporation tests conducted in previous studies indicated that decreased heat transfer performance occurred with increased in film-feed supply rate only in the laminar regime [1], not the transition or turbulent regimes. It is possible that some regions of the bundle have film-feed supply rates low enough so that laminar flow does

exist locally. Single-tube studies have also shown that film heat transfer in the boiling regime is very weakly dependent upon film-feed supply rate, and increased film-feed supply rate results in slightly better film heat transfer performance [3]. It is likely that the divergence in the tube-bundle data from these single-tube performance trends results from the complex geometry used in the bundle test facility relative to a single-tube environment.

Condensation Surface Performance Comparison with Single-Tube Results

Single-tube tests with both the W-SC and Tu-Cii surfaces were conducted and are presented in Chapter 8. These tests indicated that these two enhanced condensation surfaces provided similar film heat transfer performance with the Tu-Cii tube being slightly superior. In this study, the Tu-Cii surface generated nearly 100 percent greater heat transfer performance compared to the W-SC surface. The overfeed ratios evaluated on the bundle test facility were 6.3 to 3.0 at the 35 kg/min supply rate and 3.0 to 1.4 at the 15 kg/min supply rate depending upon bundle load. For the same heat flux range, the corresponding overfeed ratios used in the single-tube testing were 4.6 to 2.4. Therefore, the differences in the heat transfer performance measured for the single-tube testing and the bundle testing are not likely due to differences in refrigerant supply rates. The W-SC tube performance is severely reduced in the bundle environment due to the similarities of the "Y-finned" surface to a low-finned structure. This performance limitation is shown by row performance factor (RPF) profiles.

Row-by-Row Analysis

Row performance factors are shown in Table 10.4 for the triangular-pitch bundle results at refrigerant supply rates of 15 kg/min and 45 kg/min. It should be noted that the row performance factor is normalized with respect to the overall bundle heat transfer coefficient

for a given surface and operating condition. This normalization enables row performance profiles to be readily compared regardless of the surface/operating condition combination.

The row performance factors in Table 10.4 show that a large variation occurs from rows 1 to 4 for the W-40 fpi and W-SC bundles. A "saw-toothed" effect is also evident in the W-SC results where a "saw-toothed" effect describes a row performance profile when the shell-side heat transfer coefficient is greater in rows 1 and 3 than rows 2 and 4. With both of these bundles, there is a 25 to 35 percent decrease in heat transfer performance from rows 1 to 2. It can be concluded that these two surfaces are very effective when fully wetted for film heat transfer use. However, a severe decrease in performance with row depth occurs due to dryout. These two bundles experienced dryout in the lower rows at refrigerant supply rates that sufficiently wetted the Tu-B, Tu-Cii, and plain-surface bundles. Dryout is occurring with these two surfaces because they have a shell-side, low-finned enhancement, and this type of enhancement restricts axial film movement along the surface of the tube. Results from this study regarding the feed distribution over low-finned tubes are consistent with those reported by Zeng et al. [49].

The Tu-Cii bundle consistently yielded its highest row performance factors in row 2. All other bundles had better heat transfer performance in row 1 than rows 2, 3, and 4. A higher row performance factor in row 1 would be expected since row 1 is directly impacted by the refrigerant spray from the nozzles. This surface is designed to move liquid freely in both the circumferential and axial directions. A possible explanation is that the second row receives liquid drip-off more evenly distributed than that delivered by the spray assembly to the top row.

Both the Tu-Cii and Tu-B bundles have a slight increase in the row performance factor from row 3 to 4 in several cases. This trend is similar to the increase in shell-side heat transfer performance on the lowest row in condensation bundle heat transfer that has been observed in

the past [40, 42]. This might be a result of the bottom row having the thinnest film of any row within the bundle, yet still being fully wetted.

Tests were also performed with a square-pitch, Tu-B bundle at refrigerant supply rates of 15 kg/min through 45 kg/min. Table 10.5 shows the row performance factors resulting from these tests. The square-pitch, Tu-B bundle's top row yields the highest heat transfer coefficient as was the case with the triangular-pitch, Tu-B bundle. The variation between the row performance factors in rows 2, 3, and 4 is slightly less than that found with the triangular-pitch bundle, but both may be described as low relative to all other enhanced surfaces tested.

Table 10.4: Row performance factor variation with row depth, triangular-pitch geometry, HFC-134a results

| Surface | Row | M.F.R. = 15 kg/min at the following bundle loadings | | | M.F.R. = 45 kg/min at the following bundle loadings | | |
|----------|-----|---|-------|-------|---|-------|-------|
| | | 23 kW | 17 kW | 11 kW | 23 kW | 17 kW | 11 kW |
| W-40 fpi | 1 | 1.66 | 1.46 | 1.16 | 1.61 | 1.53 | 1.20 |
| | 2 | 1.23 | 1.09 | 0.94 | 1.14 | 1.06 | 0.91 |
| | 3 | 0.95 | 0.82 | 0.75 | 0.91 | 0.81 | 0.76 |
| | 4 | 0.50 | 0.58 | 0.65 | 0.51 | 0.58 | 0.69 |
| W-SC | 1 | 1.49 | 1.35 | 1.09 | 1.30 | 1.27 | 1.09 |
| | 2 | 1.03 | 0.89 | 0.73 | 0.93 | 0.84 | 0.72 |
| | 3 | 0.88 | 0.95 | 0.98 | 0.90 | 0.97 | 1.14 |
| | 4 | 0.33 | 0.40 | 0.53 | 0.34 | 0.38 | 0.55 |
| Tu-Cii | 1 | 1.02 | 0.91 | 0.84 | 0.85 | 0.82 | 0.87 |
| | 2 | 1.43 | 1.32 | 1.19 | 1.26 | 1.27 | 1.14 |
| | 3 | 0.99 | 0.81 | 0.69 | 0.89 | 0.74 | 0.64 |
| | 4 | 0.65 | 0.71 | 0.70 | 0.78 | 0.80 | 0.77 |
| Tu-B | 1 | 1.21 | 1.14 | 1.10 | 1.23 | 1.22 | 1.22 |
| | 2 | 1.04 | 0.98 | 1.01 | 1.03 | 1.03 | 1.06 |
| | 3 | 0.96 | 0.91 | 0.85 | 0.82 | 0.80 | 0.76 |
| | 4 | 0.96 | 1.07 | 1.08 | 0.91 | 0.92 | 0.91 |

Table 10.5: Row performance factor variation with row depth, square-pitch geometry, HFC-134a results

| Surface | Row | M.F.R. = 15 kg/min at the following bundle loadings | | | M.F.R. = 45 kg/min at the following bundle loadings | | |
|---------|-----|---|-------|-------|---|-------|-------|
| | | 23 kW | 17 kW | 11 kW | 23 kW | 17 kW | 11 kW |
| Tu-B | 1 | 1.14 | 1.17 | 1.28 | 1.01 | 1.15 | 1.40 |
| | 2 | 1.07 | 1.05 | 1.05 | 0.90 | 0.87 | 0.84 |
| | 3 | 1.09 | 1.07 | 0.95 | 1.00 | 0.91 | 0.78 |
| | 4 | 0.96 | 0.97 | 0.98 | 0.95 | 0.91 | 0.86 |

Pool-Boiling Comparison

Since enhanced nucleate boiling tubes (i.e. Tu-B) are commonly used in industrial chillers, it was important to determine if spray evaporation heat transfer performance could at least match that of the nucleate boiling surface in the pool-boiling environment. Figure 10.6 compares HFC-134a spray evaporation results taken on bundles assembled with the two enhanced condensation surfaces with pool boiling data taken with the Tu-B bundle. Also shown in Figure 10.6, are pool-boiling data gathered by Webb and Pais [50] at a saturation temperature of 4.4 °C. The Tu-Cii film heat transfer results are approximately 100 % greater than both the Tu-B, pool-boiling results and the data taken by Webb and Pais.

Because the shell-side heat transfer coefficients for the Tu-Cii tube have 20 to 40 percent uncertainty, the data is also presented in Figure 10.7 on axes of heat flux and LMTD. This is a useful comparison between the Tu-B and the Tu-Cii tubes since their Seider-Tate coefficients are 0.066 and 0.065, respectively. At a heat flux of 37 kW/m², the LMTD is 17 percent lower for the Tu-Cii tube at a refrigerant supply rate of 45 kg/min than the LMTD for the Tu-B bundle in the pool boiling mode. At a heat flux of 19 kW/m² the difference is 8

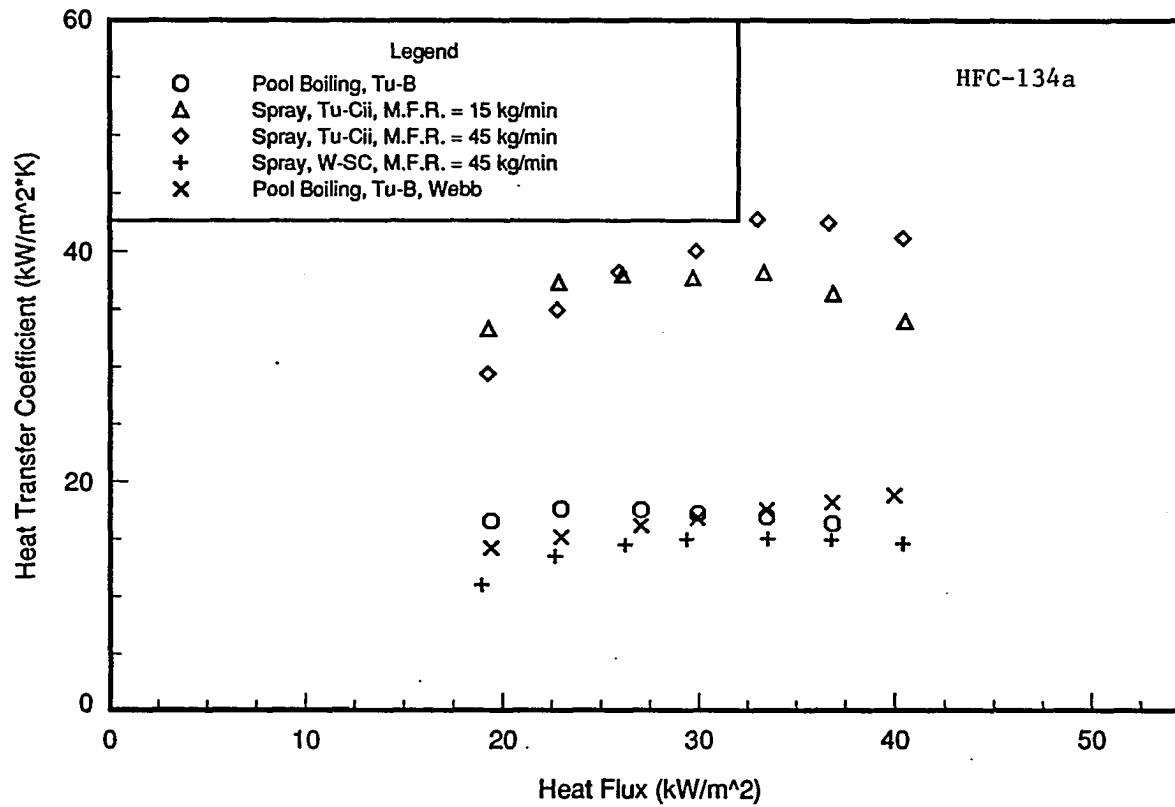


Figure 10.6: Heat transfer coefficient vs. heat flux ($T_{\text{sat}} = 2.0 \text{ }^\circ\text{C}$; pool boiling comparison, triangular-pitch geometry)

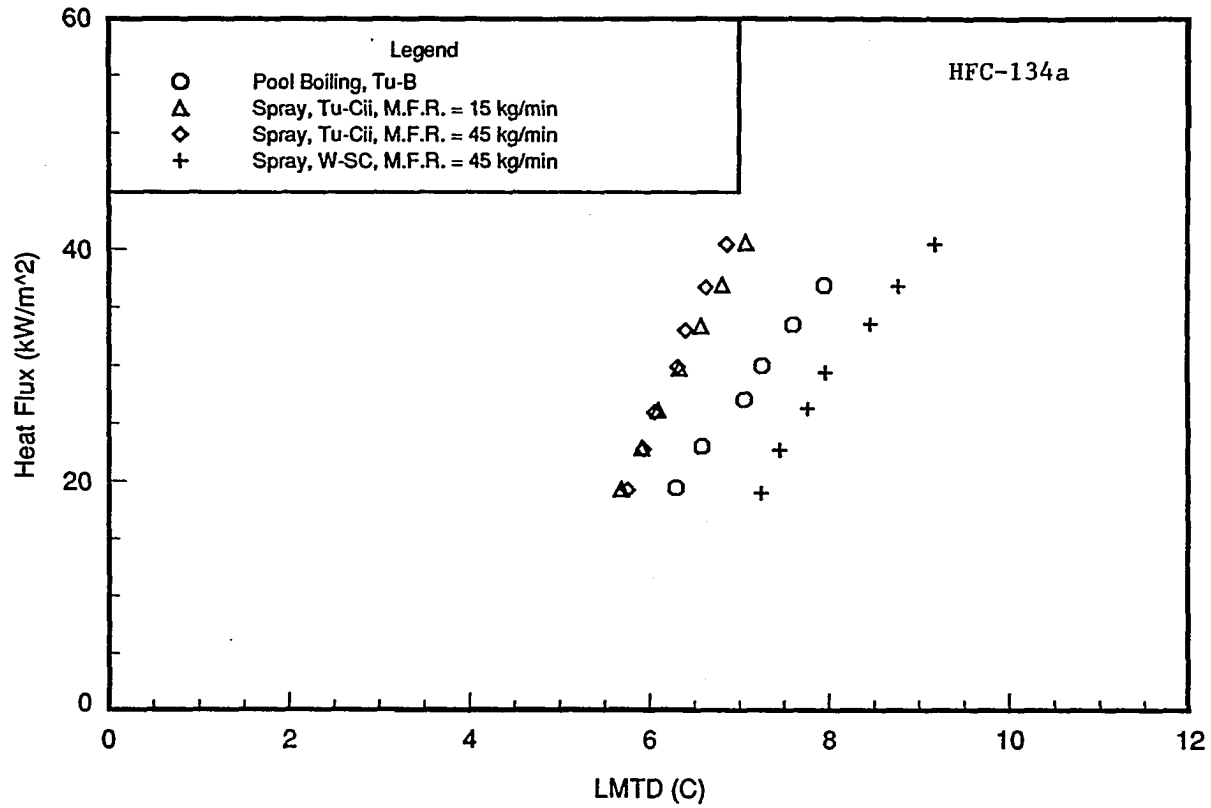


Figure 10.7: Heat flux vs. LMTD ($T_{sat} = 2.0\text{ }^{\circ}\text{C}$; pool boiling comparison, triangular-pitch geometry)

percent. The spray evaporation performance of the Tu-Cii surface is clearly better than that of the Tu-B bundle in a pool boiling environment.

Conclusions

Film heat transfer performance testing was conducted with tube bundles consisting of two enhanced condensation tubes, one enhanced boiling tube, one low-finned tube, and a plain-surface tube in a triangular-pitch tube configuration with pure HFC-134a at a saturation temperature of 2.0 °C. A square-pitch bundle geometry was tested with the enhanced boiling surface tube so a comparison could be made between triangular and square-pitch tube arrangements. A summary of the results obtained in this study are listed below.

1. Spray evaporation heat transfer coefficients for all tubes showed a moderate dependence on film-feed supply rate which increased at the higher heat fluxes. The dependence of the heat transfer performance on film-feed supply rate for the triangular-pitch, Tu-B bundle was twice as great as that measured for the square-pitch, Tu-B bundle in the upper heat flux range evaluated.
2. The shell-side heat transfer coefficients showed dependence on wall heat flux indicating boiling was present in the heat transfer process for all surfaces tested in this study. Bubbles were only clearly visible in the thick liquid layer at the lowest portion of the tube's circumference in each row. Considering the Tu-B, square and triangular-pitch bundle results, the dependence of the shell-side heat transfer coefficient on wall heat flux is 5 percent greater with a triangular-pitch alignment than a square-pitch alignment.

3. Tube bundles having a low-finned or "Y-finned" surface enhancement suffer dryout in their lower rows at flow rates which do not produce this effect in tube bundles without this type of enhancement including plain surface bundles. This dryout occurs because a finned structure on the shell-side of the tube restricts axial-film movement. Axial regions of a bundle which were underfed by the spray manifold can not receive liquid which is overfed at other axial positions.
4. Although previous single-tube tests have indicated that both the Tu-Cii and the W-SC surfaces perform similarly in spray evaporation heat transfer, heat transfer coefficients measured with the W-SC surface fall short of those measured with the Tu-Cii surface by 50 percent in the bundle environment.
5. Spray evaporation heat transfer performance for the Tu-Cii bundle is 100 percent greater than the nucleate boiling performance of the Tu-B bundle in a pool-boiling environment.

CHAPTER 11. BUNDLE TEST FACILITY HFC-134a AND HCFC-22 RESULTS INCLUDING LUBRICANT EFFECTS

This chapter focuses on evaluating the effects of small concentrations of refrigerant oil upon shell-side heat transfer performance in a spray evaporation environment. Tests were conducted with HFC-134a and bundles made up of plain, W-40 fpi, W-SC, and Tu-B tubes, in a triangular-pitch configuration. Geometric specifications for these tubes were listed previously in Table 4.1. A 340 SUS polyol-ester (POE) oil was used for the HFC-134a lubricant effects testing since this lubricant is being integrated into industry for use with this refrigerant. Data are presented at oil concentrations of 1.0 and 2.5 percent by mass fraction. Data was collected at two refrigerant supply rates so the effects of film-feed supply rate could be evaluated. Testing was also conducted with HCFC-22 and the enhanced boiling and plain surface bundles. Only a single refrigerant supply rate and a single lubricant concentration were evaluated with R-22. A 300 SUS alkyl-benzene oil was used for the R-22 mixture tests. The experimental data from the HFC-134a lubricant effects testing are presented in Appendix B in Tables B.33 to B.48. Data from pure refrigerant and lubricant effects testing conducted with HCFC-22 are presented in Appendix C in Tables C.1 to C.4.

The operational set-points used during this testing along with the maximum deviation from these set-points are presented in Table 11.1. The 30WHCRC nozzle configuration was used for both the HFC-134a and HCFC-22 lubricant effects testing. Data was collected at a fixed film-feed supply rate resulting in variation of the overfeed ratio with bundle load. Overfeed ratios are summarized in Table 11.2.

Table 11.1: Bundle test facility operating parameters, HFC-134a and HCFC-22 lubricant effects testing

| Parameter | Control Band |
|-------------------------------|--------------------------------|
| Saturation Pressure (R-134a) | 314.5 kPa \pm 0.6 kPa |
| Saturation Pressure (R-22) | 531.3 kPa \pm 0.8 kPa |
| Bundle Load | Desired Value \pm 0.3 kW |
| Refrigerant Mass Flow Rate | Desired Value \pm 2.0 kg/min |
| Spray Manifold Temperature | 0.0 °C to 3.0 °C |
| Bundle Δ T (Waterside) | 1.9 °C to 2.1 °C |

Table 11.2: Bundle overfeed ratios for the 30WHCRC nozzle configuration with refrigerants HFC-134a and HCFC-22

| Bundle Load (kW) | OFR R-134a | | OFR R-22 |
|---------------------|----------------|----------------|----------------|
| | 15 (kg/min) | 35 (kg/min) | 15 (kg/min) |
| 11.0 | 2.98 | 6.27 | 2.98 |
| 13.0 | 2.52 | 5.31 | 2.52 |
| 15.0 | 2.18 | 4.60 | 2.19 |
| 17.0 | 1.93 | 4.06 | 1.93 |
| 19.0 | 1.72 | 3.63 | 1.73 |
| 21.0 | 1.56 | 3.29 | 1.56 |
| 23.0 | 1.42 | 3.00 | 1.43 |

Heat Transfer Results

Experimental data are presented for HFC-134a and HCFC-22 refrigerant/lubricant mixtures to evaluate the effects of small concentrations of oil, surface enhancement, and film-feed supply rate upon spray evaporation heat transfer performance with triangular-pitch tube bundles. Data were taken at a constant pressure equal to the saturation pressure corresponding to a saturation temperature of 2.0 °C for the respective pure refrigerants. The shell-side heat transfer coefficients presented are based upon the nominal cylindrical area over the surface enhancement or finned structure, not the actual surface area of the tube.

HFC-134a Lubricant Effects Results Bundle Performance Comparison

Figures 11.1 through 11.4 show results obtained during testing conducted with HFC-134a and the polyol-ester oil at concentrations of 1.0 % and 2.5 %. Heat transfer performance improved with lubricant addition up to the 2.5 % concentration. This enhancement is attributed to foaming in the refrigerant film layer flowing over the tubes within the bundle. Foaming was observed during the 1.0 % testing and became even more pronounced at the 2.5 % concentration. A small amount of foam was observed in the plume emitted from the nozzles as well as in the liquid pool below the tube bundle which received drip-off and the portion of the refrigerant sprayed into the test section missing the tube bundle. The amount of foam or bubbles seen in the nozzle plume or in the pool below the bundle was several orders of magnitude less than that observed on the tube bundle. This indicates that the heat transfer surface generated foam in the liquid layer flowing over it. Foaming was also observed during single-tube testing presented in Chapter 8 with HFC-134a using the same polyol-ester oil. In the single-tube work the amount of foam increased with lubricant concentration through 5.0 %.

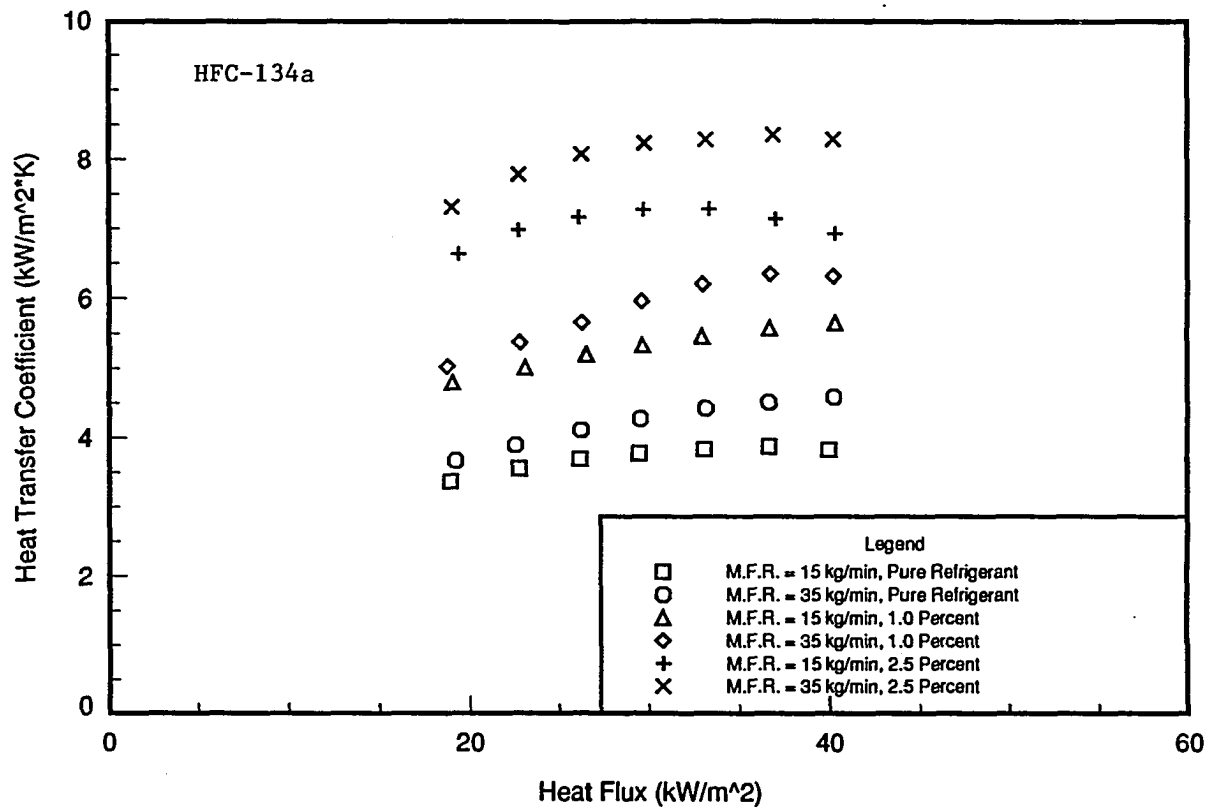


Figure 11.1: Heat transfer coefficient vs. heat flux ($P_{\text{sat}} = 314.5 \text{ kPa}$; oil effects testing, plain surface bundle)

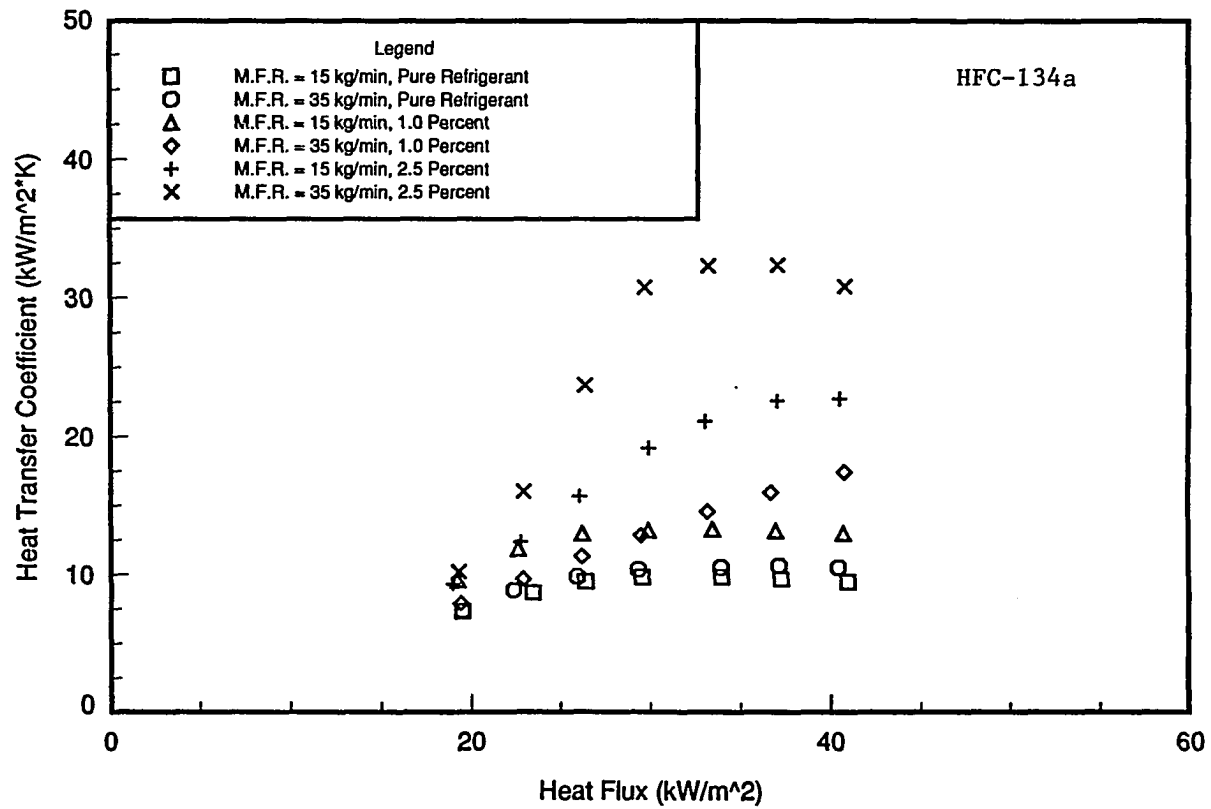


Figure 11.2: Heat transfer coefficient vs. heat flux ($P_{sat} = 314.5$ kPa; oil effects testing, W-40 fpi bundle)

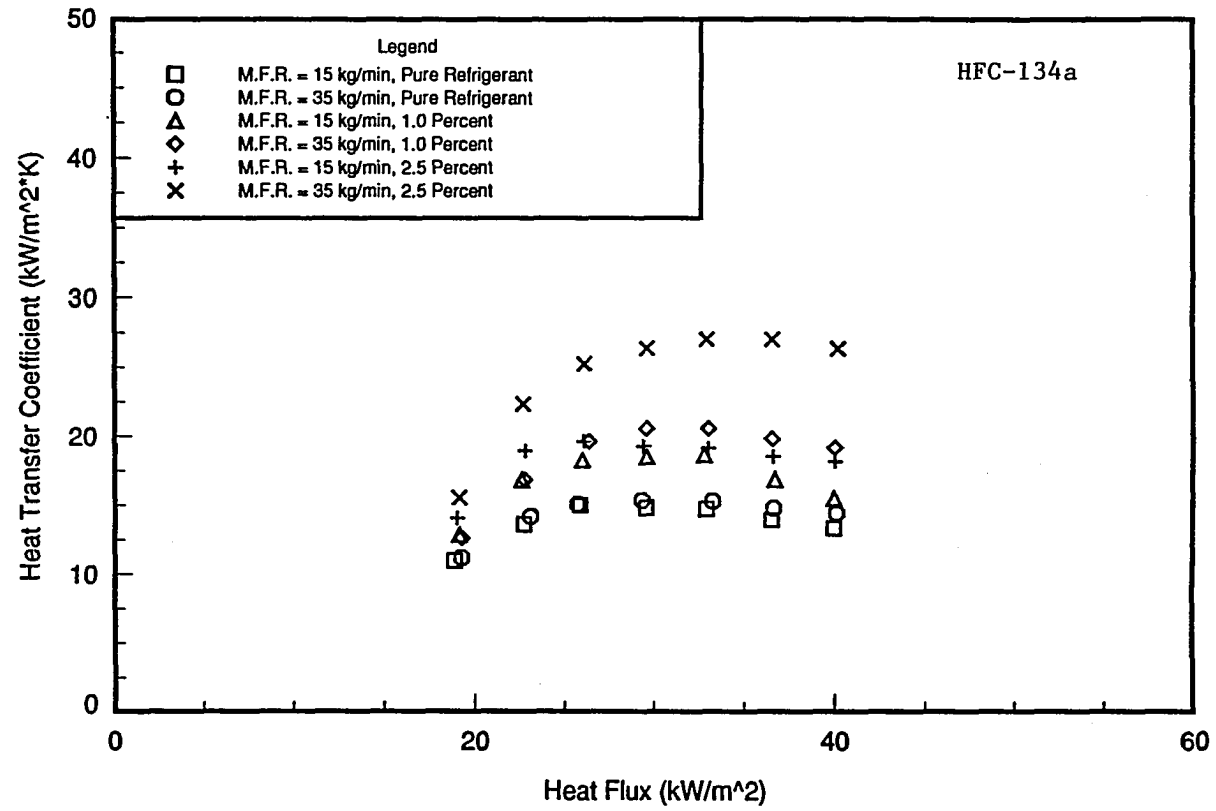


Figure 11.3: Heat transfer coefficient vs. heat flux ($P_{\text{sat}} = 314.5 \text{ kPa}$; oil effects testing, W-SC bundle)

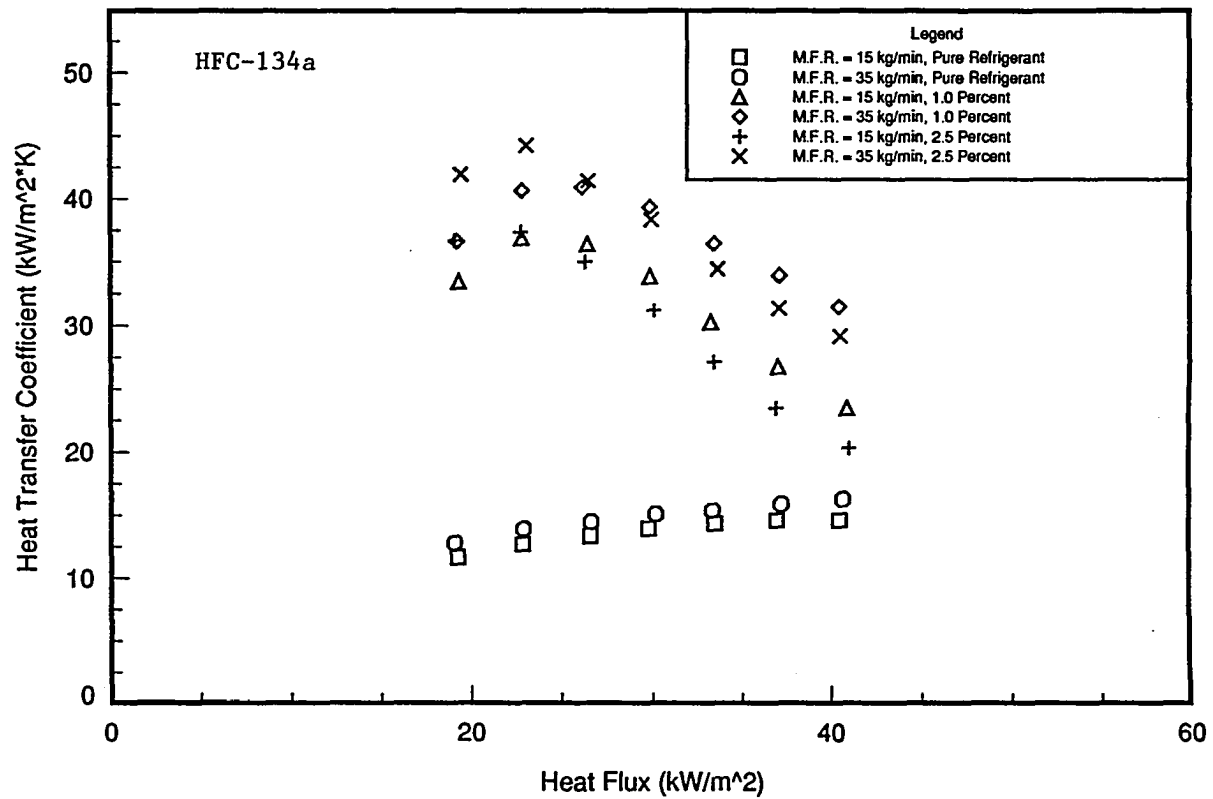


Figure 11.4: Heat transfer coefficient vs. heat flux ($P_{sat} = 314.5$ kPa; oil effects testing, Tu-B bundle)

Figures 11.5 and 11.6 show the surface enhancement factors for the W-40 fpi, Tu-B, and W-SC tube bundles at the 15 kg/min and 35 kg/min refrigerant/lubricant mixture supply rates. The surface enhancement factors with the W-40 fpi and W-SC bundles range from 1 to 4 depending upon the bundle load. These two bundles generated surface enhancement factors similar in magnitude, because the W-SC surface enhancement is like that of a low-finned structure with the exception of "Y-tips" on the fins. The Tu-B bundle at a 1.0% lubricant concentration yielded the largest surface enhancement factors, which were at a maximum at the 13 kW bundle load and decreased through the 23 kW bundle load.

Figures 11.7 and 11.8 present the lubricant enhancement factors. These enhancement factors indicate the affect of lubricant upon heat transfer performance for a given tube surface. The W-SC bundle's lubricant enhancement factors at the 15 kg/min refrigerant supply rate and the Tu-B bundle's lubricant enhancement factors at both refrigerant supply rates show little dependence upon lubricant concentration. The lubricant enhancement factors for the plain surface and W-40 fpi bundles were 20% and 80% higher at the 2.5% concentration than the 1.0% concentration, respectively at a nominal heat flux of 40 kW/m².

From visual observations, it was determined that foaming was more pronounced at high bundle loads than at low bundle loads. In addition, heat transfer performances for the W-40 fpi bundle were more improved at the higher loads relative to its performance at low bundle loads. At a nominal heat flux of 40 kW/m², the heat transfer coefficient for the W-40 fpi bundle was 200% higher at the 35 kg/min, 2.5% concentration test conditions than the 35 kg/min, 0.0% concentration test conditions. In comparison, the heat transfer coefficient at a nominal heat flux of 19 kW/m² for the W-40 fpi bundle was 42% higher at the 35 kg/min, 2.5% concentration test condition than the 35 kg/min, 0.0% concentration test condition. This trend might be due to the fact that more foam was generated at these higher bundle loads. It is likely that the foam improved heat transfer with this bundle through the wetting of

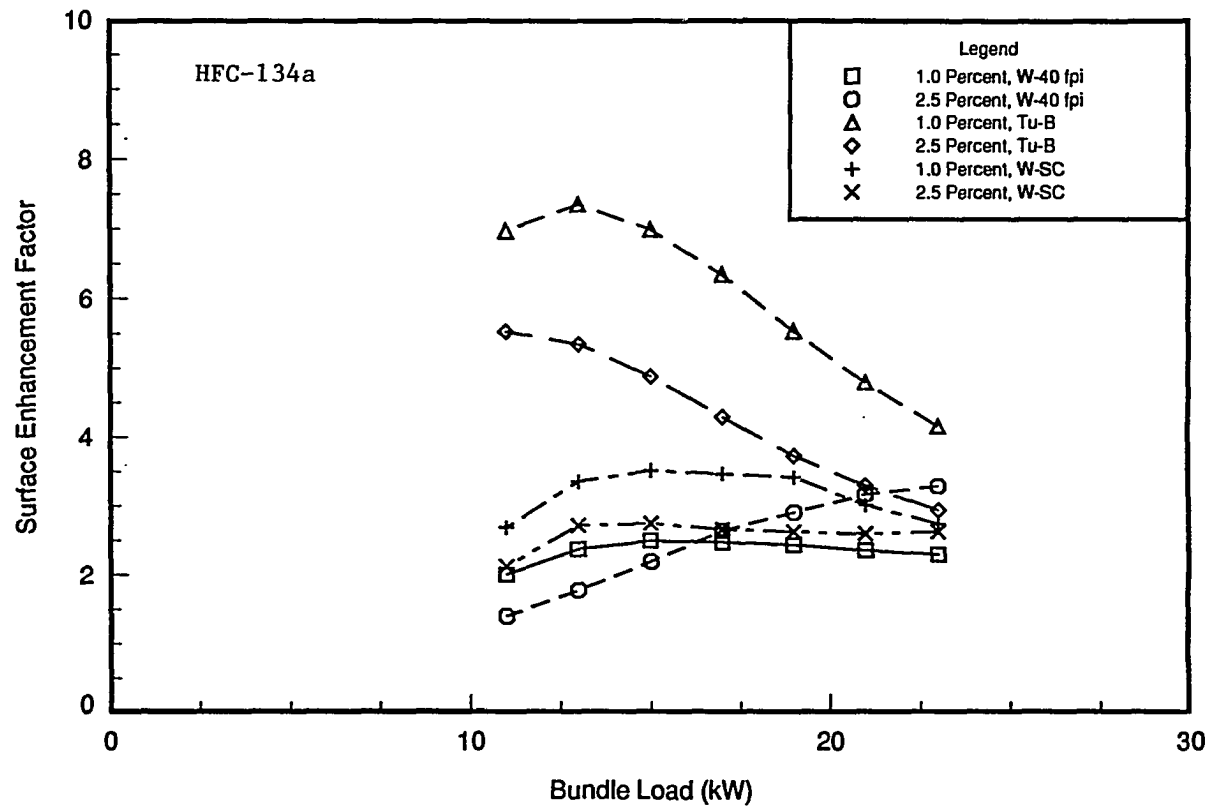


Figure 11.5: Surface enhancement factor vs. bundle load ($P_{sat} = 314.5$ kPa; oil effects testing, M.F.R. = 15 kg/min)

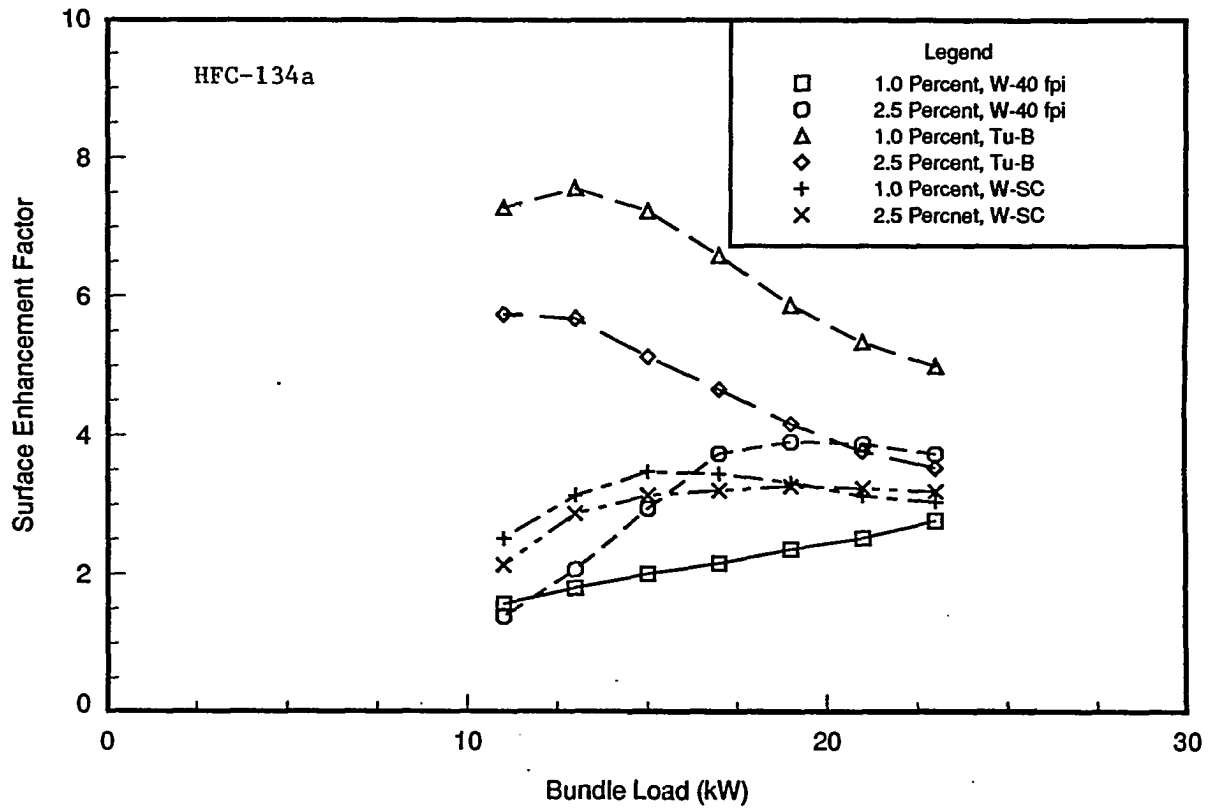


Figure 11.6: Surface enhancement factor vs. bundle load ($P_{sat} = 314.5$ kPa; oil effects testing, M.F.R. = 35 kg/min)

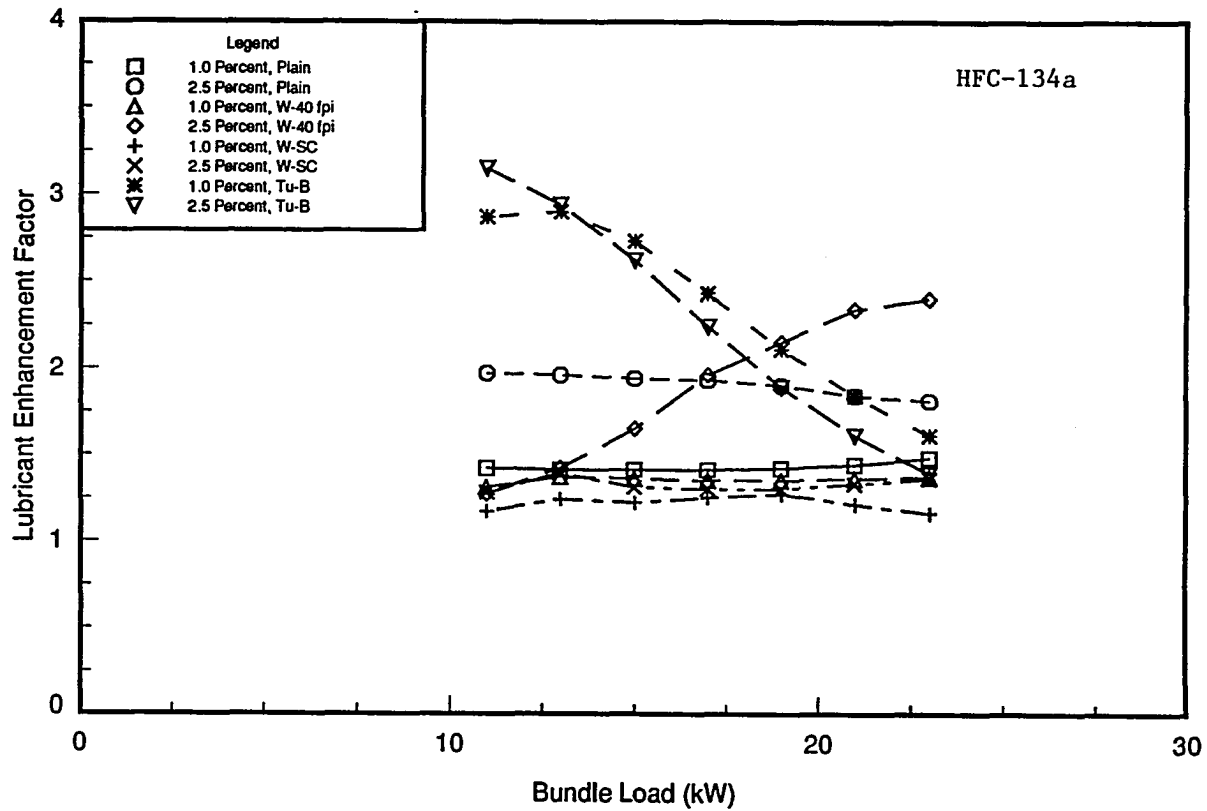


Figure 11.7: Lubricant enhancement factor vs. bundle load ($P_{\text{sat}} = 314.5 \text{ kPa}$; oil effects testing, M.F.R. = 15 kg/min)

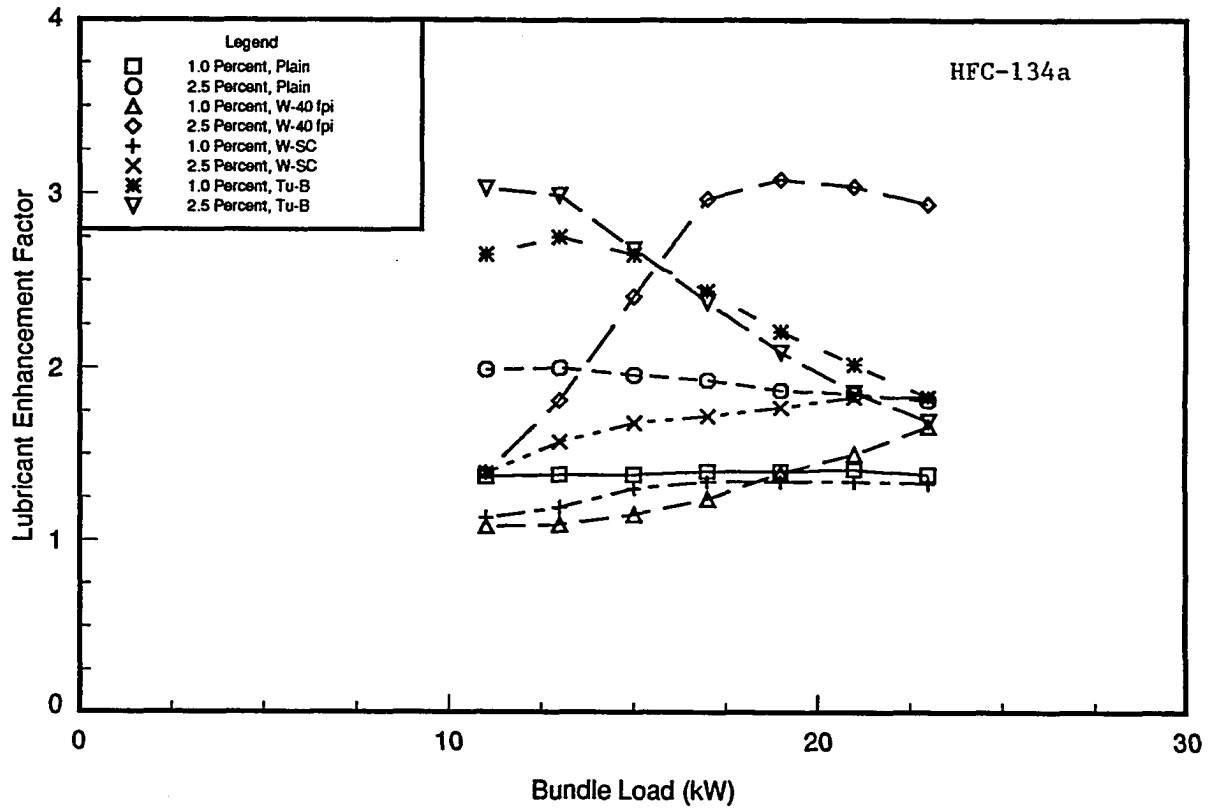


Figure 11.8: Lubricant enhancement factor vs. bundle load ($P_{sat} = 314.5$ kPa; oil effects testing, M.F.R. = 35 kg/min)

a greater percentage of the shell-side area of the tube bundle. The lubricant enhancement factors for the W-SC bundle indicate that this bundle received less benefit from the foaming relative to the W-40 fpi bundle. It might be concluded the "Y-tips" on the fins of the W-SC tube, which partially enclose the gap between any two adjacent fins, prevented the foam from wetting the interior cavities on the tube wall.

The lubricant effects with the Tu-B bundle are opposite of that seen with the other tubes. The lubricant enhancement factors for the Tu-B bundle approached a value of 3 at the 11 kW and 13 kW bundle loads and decreased 50 % through the upper heat-flux range. It should be noted that Figure 10.4 shows that this bundle produced heat transfer performance which was directly proportional to heat flux in the pure refrigerant testing. With the addition of oil, the heat transfer performance of the Tu-B bundle has become inversely proportional to heat flux.

HFC-134a Lubricant Effects Results Row-by-Row Analysis

Row performance factors are presented in Tables 11.3 and 11.4. One of the effects of lubricant concentrations of 1.0 and 2.5 percent upon the heat transfer performance with the plain tube bundle is less variance in the shell-side heat transfer coefficient from row-to-row. Referring to the 15 kg/min supply rate, the row performance factors at the 23 kW bundle load in the pure refrigerant test show a significant decrease in performance from the top to the bottom row. The bottom-row coefficient is only 63 % of that on the top row. With a concentration of 2.5 % lubricant, this ratio improved to 92 %. This trend is also shown by the row performance factors of the W-40 fpi bundle.

The W-SC bundle has a reduced heat transfer coefficient in the lower rows. Even at the higher bundle loads, where foaming improved heat transfer performance in the lower rows of

Table 11.3: Row performance factor variation with row depth, HFC-134a lubricant effects results, 15 kg/min refrigerant supply rate

| Surface | Row | 0.0 % Oil | | 1.0 % Oil | | 2.5 % Oil | |
|----------|-----|-----------|-------|-----------|-------|-----------|-------|
| | | 23 kW | 11 kW | 23 kW | 11 kW | 23 kW | 11 kW |
| Plain | 1 | 1.31 | 1.01 | 0.95 | 0.81 | 1.05 | 0.84 |
| | 2 | 1.23 | 1.00 | 1.03 | 0.97 | 1.11 | 1.00 |
| | 3 | 0.95 | 0.94 | 0.92 | 0.89 | 1.05 | 0.96 |
| | 4 | 0.82 | 0.83 | 0.96 | 0.90 | 0.97 | 0.83 |
| W-40 fpi | 1 | 1.66 | 1.16 | 1.78 | 1.08 | 1.27 | 1.23 |
| | 2 | 1.23 | 0.94 | 1.19 | 0.81 | 0.98 | 0.93 |
| | 3 | 0.95 | 0.75 | 0.55 | 0.66 | 0.71 | 0.48 |
| | 4 | 0.50 | 0.65 | 0.24 | 0.75 | 0.92 | 0.60 |
| W-SC | 1 | 1.49 | 1.09 | 1.54 | 1.15 | 1.49 | 1.10 |
| | 2 | 1.03 | 0.73 | 1.15 | 0.75 | 1.03 | 0.69 |
| | 3 | 0.88 | 0.98 | 0.79 | 1.17 | 1.08 | 1.35 |
| | 4 | 0.33 | 0.53 | 0.30 | 0.59 | 0.28 | 0.46 |
| Tu-B | 1 | 1.21 | 1.10 | 1.11 | 0.59 | 1.38 | 0.59 |
| | 2 | 1.04 | 1.01 | 1.08 | 0.76 | 1.35 | 0.77 |
| | 3 | 0.96 | 0.85 | 0.92 | 0.57 | 0.91 | 0.58 |
| | 4 | 0.96 | 1.08 | 0.80 | 1.36 | 0.57 | 1.53 |

the W-40 fpi bundle, little improvement can be seen in the performance of the bottom row for the W-SC bundle. At the 15 kg/min refrigerant supply rate and the 2.5 % concentration, the row performance factor on the bottom row actually decreased by 15 % at the maximum bundle load and 13 % at the lowest bundle load in comparison with the pure refrigerant results.

The row-to-row performance profile for the Tu-B bundle at the 23 kW bundle load in comparison with the 11 kW bundle load shows opposite performance trends with row depth. At the 1.0 % oil concentration with the 23 kW bundle load and the 15 kg/min refrigerant supply rate, there is a 28 % decrease in heat transfer performance from the top to the bottom row. However, at the lowest bundle loading and 1.0 % oil concentration, the row

performance factors more than double from rows 1 to 4. The row performance factors for the Tu-B bundle also increase with row depth at the 2.5 % oil concentration, 11 kW bundle load test conditions for both refrigerant supply rates evaluated.

In the lubricant effects testing, the Tu-B bundle generated larger heat transfer coefficients at low bundle loads compared to high bundle loads. This trend could indicate dryout occurring at the higher loads. If this is the case, it should be noted that this tube bundle did not experience significant dryout in the pure refrigerant testing. Therefore, if dryout is prevalent in the lubricant effects testing with the Tu-B bundle, it must be the oil itself creating the dryout condition.

Table 11.4: Row performance factor variation with row depth, HFC-134a lubricant effects results, 35 kg/min refrigerant supply rate

| Surface | Row | 0.0 % Oil | | 1.0 % Oil | | 2.5 % Oil | |
|----------|-----|-----------|-------|-----------|-------|-----------|-------|
| | | 23 kW | 11 kW | 23 kW | 11 kW | 23 kW | 11 kW |
| Plain | 1 | 1.09 | 0.99 | 0.82 | 0.80 | 0.84 | 0.75 |
| | 2 | 1.03 | 0.93 | 0.86 | 0.92 | 0.91 | 0.92 |
| | 3 | 0.93 | 0.88 | 0.94 | 0.88 | 1.01 | 0.94 |
| | 4 | 0.83 | 0.85 | 0.91 | 0.91 | 0.97 | 0.83 |
| W-40 fpi | 1 | 1.63 | 1.22 | 1.41 | 1.35 | 0.93 | 1.13 |
| | 2 | 1.14 | 0.90 | 0.94 | 1.05 | 0.70 | 0.87 |
| | 3 | 0.93 | 0.77 | 0.59 | 0.57 | 0.60 | 0.34 |
| | 4 | 0.48 | 0.66 | 0.37 | 0.87 | 0.87 | 0.44 |
| W-SC | 1 | 1.35 | 1.09 | 1.15 | 1.11 | 1.02 | 0.98 |
| | 2 | 0.92 | 0.71 | 0.87 | 0.74 | 0.72 | 0.62 |
| | 3 | 0.92 | 1.08 | 0.69 | 1.22 | 0.86 | 1.40 |
| | 4 | 0.32 | 0.51 | 0.34 | 0.58 | 0.49 | 0.57 |
| Tu-B | 1 | 1.25 | 1.18 | 0.91 | 0.58 | 1.04 | 0.60 |
| | 2 | 1.05 | 1.08 | 0.85 | 0.72 | 0.92 | 0.75 |
| | 3 | 0.85 | 0.77 | 0.71 | 0.52 | 0.76 | 0.50 |
| | 4 | 0.90 | 0.95 | 0.97 | 1.31 | 0.75 | 1.25 |

HCFC-22 Lubricant Effects Results Bundle Performance Comparison

Results from the HCFC-22 testing done with the plain and Tu-B bundles in a triangular-pitch configuration are shown in Figures 11.9 and 11.10. Refrigerant HFC-134a, 15 kg/min results are also shown in these two figures for comparison. The pure refrigerant heat transfer coefficients measured with both tube bundles are greater with HCFC-22 than HFC-134a. A 1.0 % lubricant concentration of the alkyl-benzene oil with HCFC-22 yielded less improvement to shell-side heat transfer than a 1.0 % concentration of the polyol-ester oil with HFC-134a relative to the pure refrigerant testing. The Tu-B bundle heat transfer coefficient is greatest at the 13 kW bundle load and decreases with increased bundle load through the range evaluated. This trend is similar to the HFC-134a results. Better performance from the HFC-134a refrigerant/mixture testing might be due to the higher viscosity of the POE oil. The study conducted by Sauer et al. [24] indicated heat transfer performance was effected by lubricant concentration and viscosity. Sauer stated that higher lubricant viscosities yielded larger heat transfer coefficients than those found with lower viscosity lubricants. More data is needed to support this hypothesis.

Figure 11.11 shows the lubricant enhancement factors obtained from the HCFC-22 testing. The HCFC-22 lubricant enhancement factors for the plain bundle are 20 to 40 percent lower than those obtained with the 1.0 % HFC-134a mixture testing. With the Tu-B bundle at the 11 kW bundle loading, the lubricant enhancement factor for HFC-134a and the polyol-ester oil is over 100.0 percent greater than that of the 1.0 % mixture of alkyl-benzene oil and HCFC-22. The performance difference between the two refrigerant/lubricant combinations with the Tu-B bundle decreases with increasing bundle load.

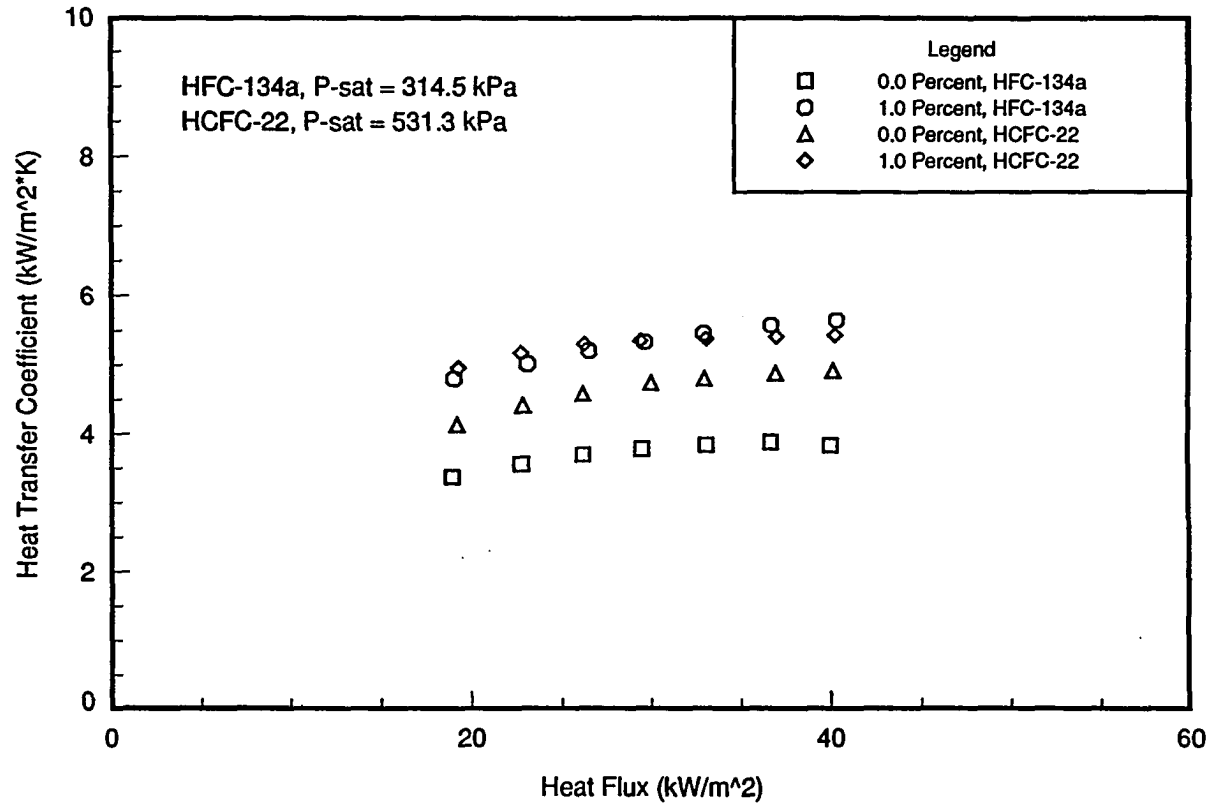


Figure 11.9: Heat transfer coefficient vs. heat flux (plain surface bundle, HCFC-22 and HFC-134a results, M.F.R. = 15 kg/min)

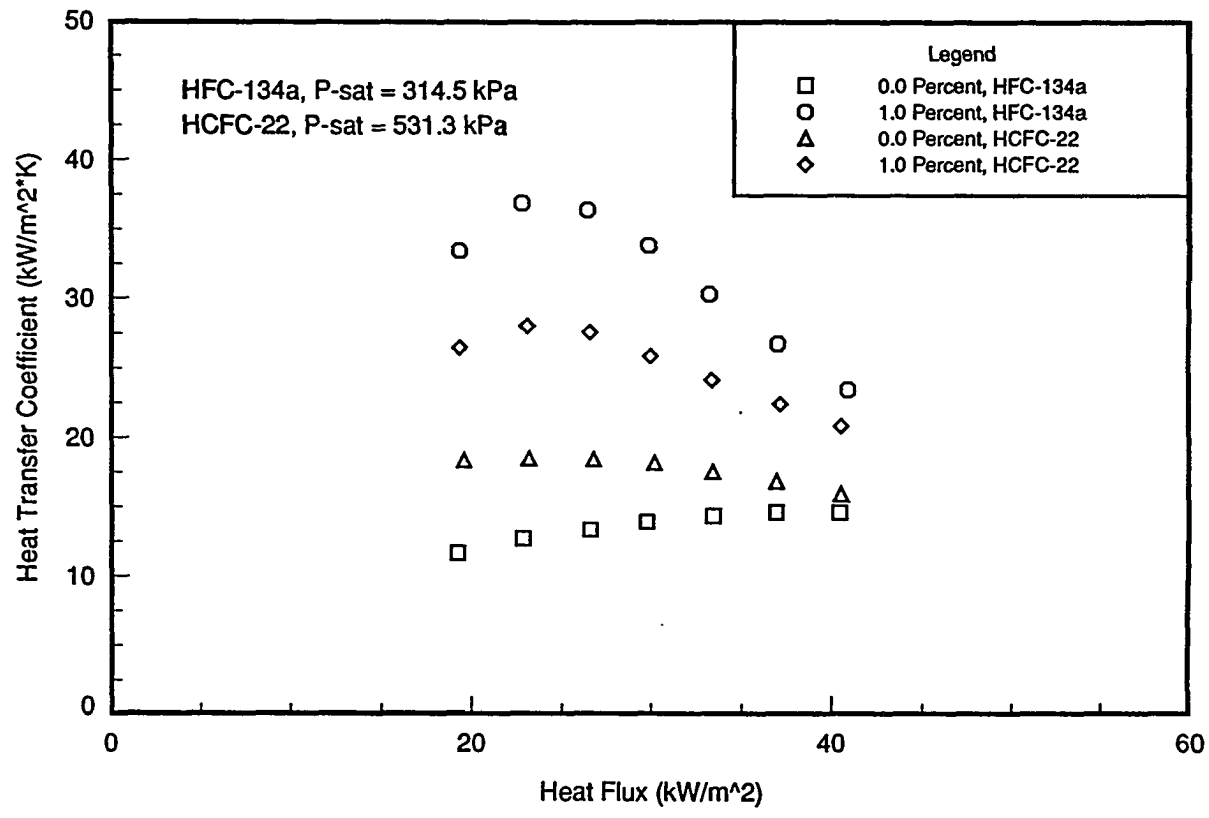


Figure 11.10: Heat transfer coefficient vs. heat flux (Tu-B bundle, HCFC-22 and HFC-134a results, M.F.R. = 15 kg/min)

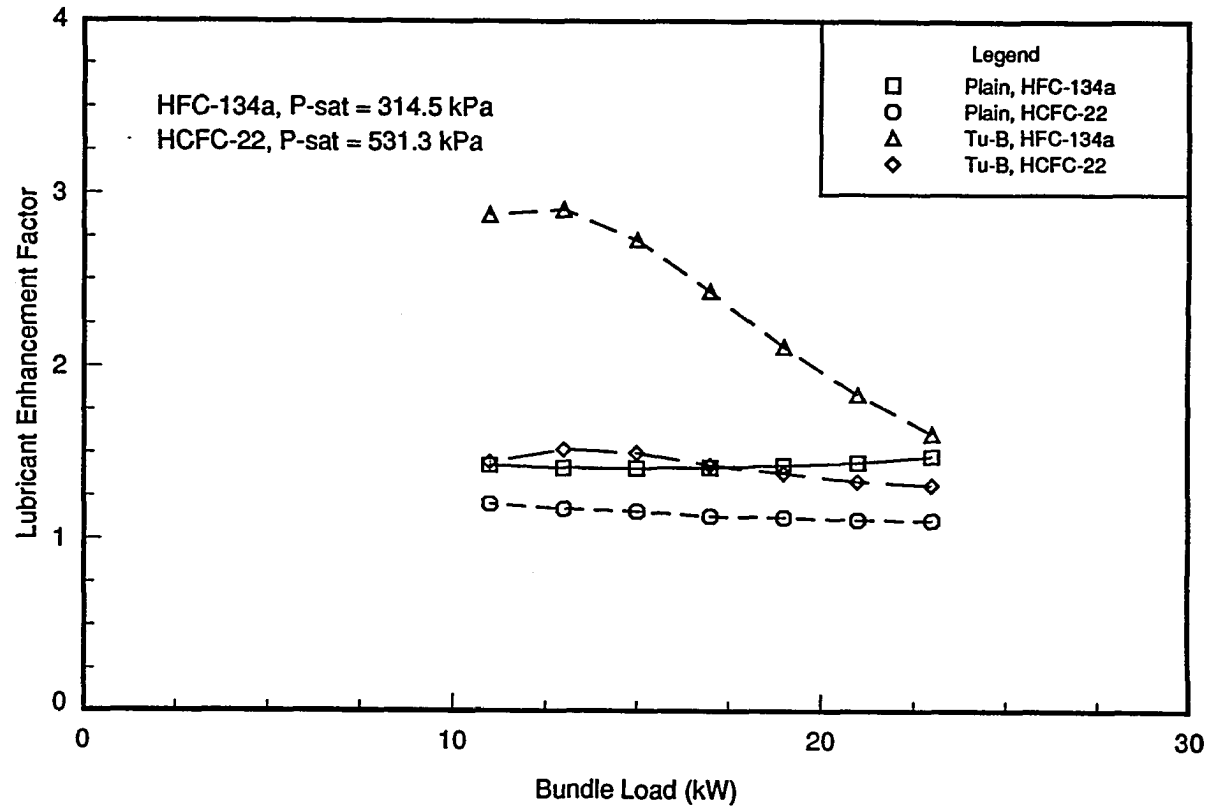


Figure 11.11: Lubricant enhancement factor vs. bundle load (HCFC-22 and HFC-134a results, M.F.R. = 15 kg/min)

Table 11.5: Row performance factor variation with row depth, HCFC-22 lubricant effects results, 15 kg/min refrigerant supply rate

| Surface | Oil | 0.0 % Oil | | 1.0 % Oil | |
|---------|-----|-----------|-------|-----------|-------|
| | | 23 kW | 11 kW | 23 kW | 11 kW |
| Plain | 1 | 1.17 | 0.87 | 1.15 | 0.85 |
| | 2 | 1.02 | 0.87 | 1.04 | 0.90 |
| | 3 | 1.07 | 0.91 | 0.78 | 0.87 |
| | 4 | 0.81 | 0.99 | 0.80 | 0.85 |
| Tu-B | 1 | 1.27 | 0.86 | 0.96 | 0.64 |
| | 2 | 1.11 | 0.93 | 0.99 | 0.78 |
| | 3 | 0.79 | 0.66 | 0.93 | 0.63 |
| | 4 | 0.75 | 0.99 | 0.88 | 1.45 |

HCFC-22 Lubricant Effects Results Row-by-Row Analysis

Row performance factors for the HCFC-22 testing are shown in Table 11.5. These row-by-row profiles are similar to those measured during the HFC-134a testing. The row-to-row performance for the plain bundle shows a variance from the top to bottom row of less than about 30% at the highest heat flux and less than 13% at the lowest heat flux in both the 0.0% and 1.0% tests. At low bundle loads the heat transfer performance for the Tu-B bundle improved significantly from the top to bottom row, which was also seen in the HFC-134a testing.

Conclusions

Film heat transfer performance testing was conducted with tube bundles consisting of an enhanced condensation tube, an enhanced boiling tube, a low-finned tube, and a plain-surface

tube in a triangular-pitch configuration with refrigerant/lubricant mixtures of HFC-134a and a polyol-ester oil. Lubricant concentrations of 1.0 %, and 2.5 % were evaluated at a saturation pressure of 314.5 kPa. Testing was also conducted with the enhanced boiling and plain-surface tube bundles and refrigerant/lubricant mixtures of HCFC-22 and an alkyl-benzene oil at concentrations of 0.0 % and 1.0 %. A summary of the results obtained from this study are listed below.

1. Heat transfer coefficients showed dependence on both the bundle overfeed ratio and lubricant concentration. Heat transfer performance improved with higher lubricant concentration and increased refrigerant supply rate. Increases in heat transfer performance near 100 % were noted for the Tu-B bundle at a heat flux of 23 kW/m² and the W-40 fpi bundle at a heat flux of 40 kW/m² with the 2.5 % oil concentration in comparison with pure HFC-134a, 35 kg/min results.
2. Foaming was observed during both the HFC-134a/polyol-ester oil and HCFC-22/alkyl-benzene oil tests. This foaming increased heat transfer coefficients for all surfaces evaluated. It was visually observed that the amount of foam being generated on the tube bundle was greater at high heat flux (i.e. wall temperature) than low heat flux. Foaming increases the convective component of the overall heat transfer coefficient as well as wets surface area that might otherwise remain dry in the lower rows of a tube bundle.
3. Tubes having a low-finned or modified-fin type of enhancement (i.e. W-40 fpi, W-SC) receive a 50 % to 100 % increase in heat transfer performance at high heat fluxes from foam wetting regions in the lower rows of the bundle that would otherwise remain dry if foaming was absent from the process.

4. The heat transfer coefficients improved with increasing heat flux with the plain, W-40 fpi, and W-SC tube bundles. Although behaving similarly during the pure refrigerant testing with HFC-134a, the effect of the lubricant resulted in heat transfer performance of the Tu-B bundle decreasing up to 50 % through the heat flux range evaluated. Pure HCFC-22, Tu-B bundle testing did show a marginal decrease in the heat transfer coefficient with increased heat flux, which was also the case with HCFC-22 refrigerant/lubricant mixture testing.
5. Heat transfer coefficients measured during pure HCFC-22 testing were greater than those found in pure HFC-134a testing. However, the lubricant enhancement factor for the Tu-B bundle at a heat flux of 23 kW/m² was nearly 100 % greater with the 1.0 % HFC-134a/polyol-ester oil mixture than the 1.0 % HCFC-22/alkylbenzene oil mixture. At this point it is unclear whether this phenomenon is due to the difference in lubricant viscosities or other thermodynamic and transport properties of the refrigerant/lubricant mixtures.

CHAPTER 12. BUNDLE TEST FACILITY HCFC-123 RESULTS INCLUDING LUBRICANT EFFECTS

Shell-side heat transfer coefficients during spray evaporation were measured for HCFC-123. The Tu-Cii, Tu-B, and plain-surface tubes were evaluated in triangular-pitch bundles with this low-pressure refrigerant. Geometric specifications for these tubes are listed in Table 4.1. The plain-surface bundle was tested so that the effects of tube surface enhancement could be interpreted from the data. Lubricant effects evaluation testing was conducted for a 305 SUS naphthenic mineral oil at concentrations of 1.1 % and 2.5 % oil by mass fraction. This mineral oil is one commonly used in industry with HCFC-123. Experimental data for both the pure refrigerant and the refrigerant/lubricant mixtures are presented in Appendix D in Tables D.1 to D.19.

Several runs were conducted with the 24WDCRC nozzle configuration, but the majority of the results presented in this chapter were taken with the 30WDCRC configuration. The geometric specifications for both nozzle configurations are listed in Table 4.2. Collector testing was performed in parallel with the heat transfer analysis experiments to determine the percentage of refrigerant supplied to the distribution manifold that actually contacted the tube bundle. Collector test results are presented in Table 4.3.

Low-pressure refrigerants like HCFC-123 typically yield heat transfer coefficients significantly less than would be expected with a high-pressure refrigerant in the same

application. Decreased heat transfer performance in the 20-ton condenser on the bundle test facility made it significantly more difficult to operate at a saturation temperature of 2.0 °C. To decrease the load on the condenser, the fifth tube in each row of the tube bundle was plugged. This action reduced the bundle to 12 active tubes of the 20 available, with the first and fifth tube in each row plugged. In addition to this bundle modification, it was also necessary to add a 10-ton condenser to the bundle test facility. This condenser was piped in parallel on the refrigerant side and in series on the glycol/water mixture side to the existing 20 ton condenser. This combination of reducing the surface area of the bundle to 12 tubes and increasing the condensation UA value of the bundle test facility allowed the work to be conducted at a saturation pressure of 35.7 kPa, for comparison with the high-pressure refrigerants. This pressure corresponds to a saturation temperature of 2.0 °C for pure HCFC-123.

It was desired to continue taking 7 data points in each test run, which corresponded to the nominal bundle heat fluxes of the 7 points taken during the 16-tube, high-pressure refrigerant testing. Instead of taking data through a bundle-load range of 23 kW to 11 kW, a range of 17.25 kW to 8.25 kW was used with HCFC-123. This corresponds to a nominal heat flux range of 40 kW/m² to 19 kW/m².

The operational set-points used during this testing along with maximum deviation from these set-points are presented in Table 12.1. The data were collected at a fixed film-feed supply rate resulting in variations of the overfeed ratio with bundle load. The overfeed ratios for combinations of the two nozzle configurations and refrigerant flow rates used in this testing are presented in Table 12.2.

Table 12.1: Bundle test facility operating parameters, HCFC-123 testing

| Parameter | Control Band |
|-------------------------------|--------------------------------|
| Saturation Pressure | 35.7 kPa \pm 0.08 kPa |
| Bundle Load | Desired Value \pm 0.3 kW |
| Refrigerant Mass Flow Rate | Desired Value \pm 1.0 kg/min |
| Spray Manifold Temperature | 0.0 °C to 3.0 °C |
| Bundle Δ T (Waterside) | 1.9 °C to 2.1 °C |

Table 12.2: Bundle overfeed ratios for the 24WDCRC and 30WDCRC nozzle configurations, HCFC-123 testing

| Bundle Load (kW) | OFR 24WDCRC | | OFR 30WDCRC | |
|---------------------|----------------|----------------|----------------|----------------|
| | 25 (kg/min) | 35 (kg/min) | 25 (kg/min) | 35 (kg/min) |
| 8.25 | 3.5 | 4.1 | 4.3 | 5.3 |
| 9.75 | 3.0 | 3.5 | 3.7 | 4.5 |
| 11.25 | 2.6 | 3.0 | 3.2 | 3.9 |
| 12.75 | 2.3 | 2.7 | 2.8 | 3.4 |
| 14.25 | 2.0 | 2.4 | 2.5 | 3.1 |
| 15.75 | 1.8 | 2.2 | 2.3 | 2.8 |
| 17.25 | 1.7 | 2.0 | 2.1 | 2.5 |

Heat Transfer Results

Spray evaporation heat transfer data are presented here for HCFC-123 as a function of film-feed supply rate, surface enhancement, and oil concentration. All data were taken at a constant saturation pressure of 35.7 kPa in the test section, which corresponds to a saturation temperature of 2.0 °C for the pure refrigerant. The shell-side heat transfer coefficients are

based upon the nominal cylindrical area over the surface enhancement, not the actual surface area of the enhanced and finned tubes.

Nozzle Configuration Performance Comparison

Refrigerant mass flow rates of 25 kg/min and 35 kg/min were selected for the HCFC-123 testing to cover approximately the low to mid-range of film-feed supply rates used previously for the HFC-134a testing. A teflon lined, magnetic drive, centrifugal pump was installed in the refrigerant flow loop due to low-pressure limitations of the triplex diaphragm pump. This pump was sized to supply up to 45 kg/min of HCFC-123 at the desired test conditions. The 35 kg/min flow rate was used for the upper limit rather than the 45 kg/min flow rate to add a margin of safety in regards to cavitation prevention during the lubricant effects testing.

A series of experimental data runs were conducted with the 24WDCRC and 30WDCRC nozzle configurations using bundles made of Tu-Cii and plain-surface tubes in an effort to determine the sensitivity of the bundle heat transfer performance to refrigerant distribution. Results from these tests are presented in Figure 12.1. Similar testing was done previously with HFC-134a to optimize refrigerant distribution in the test section prior to conducting full scale HFC-134a testing on the bundle test facility.

The shell-side heat transfer coefficients for the plain surface bundle are approximately one-half in magnitude of those measured with HFC-134a. Also, the variation in the heat transfer coefficients for the plain bundle with film-feed supply rate are less than that found during the HFC-134a testing. In single-tube, evaporation testing conducted by Danilova et al. [1], it was shown that in the transition region between the laminar and turbulent flow regimes, heat transfer performance was virtually independent of film-feed supply rate. Reynolds numbers shown in Appendix D from these pure HCFC-123 tests fall in the transition regime.

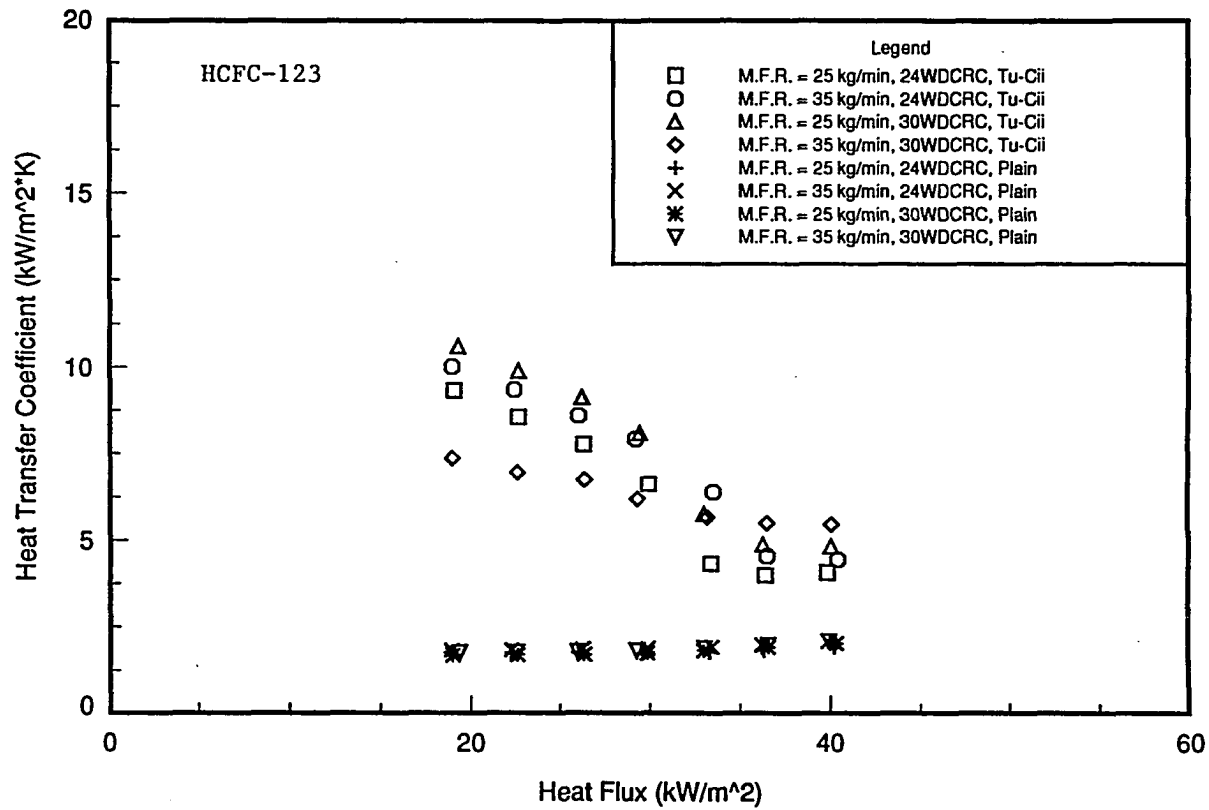


Figure 12.1: Heat transfer coefficient vs. heat flux ($P_{\text{sat}} = 35.7 \text{ kPa}$; 24WDCRC & 30WDCRC configurations).

The film-evaporation study conducted by Danilova et al. also showed that when boiling became dominant, the coefficients were independent of the film-feed supply rate. However, the study conducted by Parken et al. [3] indicated a marginal dependence existed, with heat transfer performance improving slightly with film-feed supply rate. It is important to note that the experiments done by Danilova et al. were conducted with hydrocarbon type refrigerants, while Parken et al. used water. Referring to Tables D.1 through D.4 in Appendix D, a 25 to 35 percent decrease in the heat transfer coefficient of the top row for a heat flux decrease of 40 kW/m² to 19 kW/m² indicates that boiling was at-least partially contributing to the heat transfer performance of the plain-surface bundle with HCFC-123.

One observation that can be made from the data presented in Figure 12.1 is that the shell-side heat transfer coefficient of the Tu-Cii bundle is dependent on wall heat flux. Specifically, the shell-side heat transfer coefficient drops through the full heat flux range evaluated. However, the top row shell-side heat transfer coefficients of the Tu-Cii bundle are less dependent on heat flux than any refrigerant/surface combination evaluated on the bundle test facility. It is unclear why the low heat flux performance of the Tu-Cii bundle at the 35 kg/min refrigerant supply rate with the 30WDCRC nozzle configuration is significantly less than the measured performance for the three other flow rate/nozzle configuration combinations used with HCFC-123.

Bundle Performance Comparison

Shell-side heat transfer coefficients measured during lubricant effects testing with triangular-pitch tube bundles made with plain-surface, Tu-Cii, and Tu-B tubes are presented in Figures 12.2, 12.3, and 12.4. It can be seen in these figures, that the three bundles behaved differently from each other in these refrigerant/lubricant mixture tests. The Tu-B bundle exhibited the best overall performance, through an oil concentration of 2.5 %. The

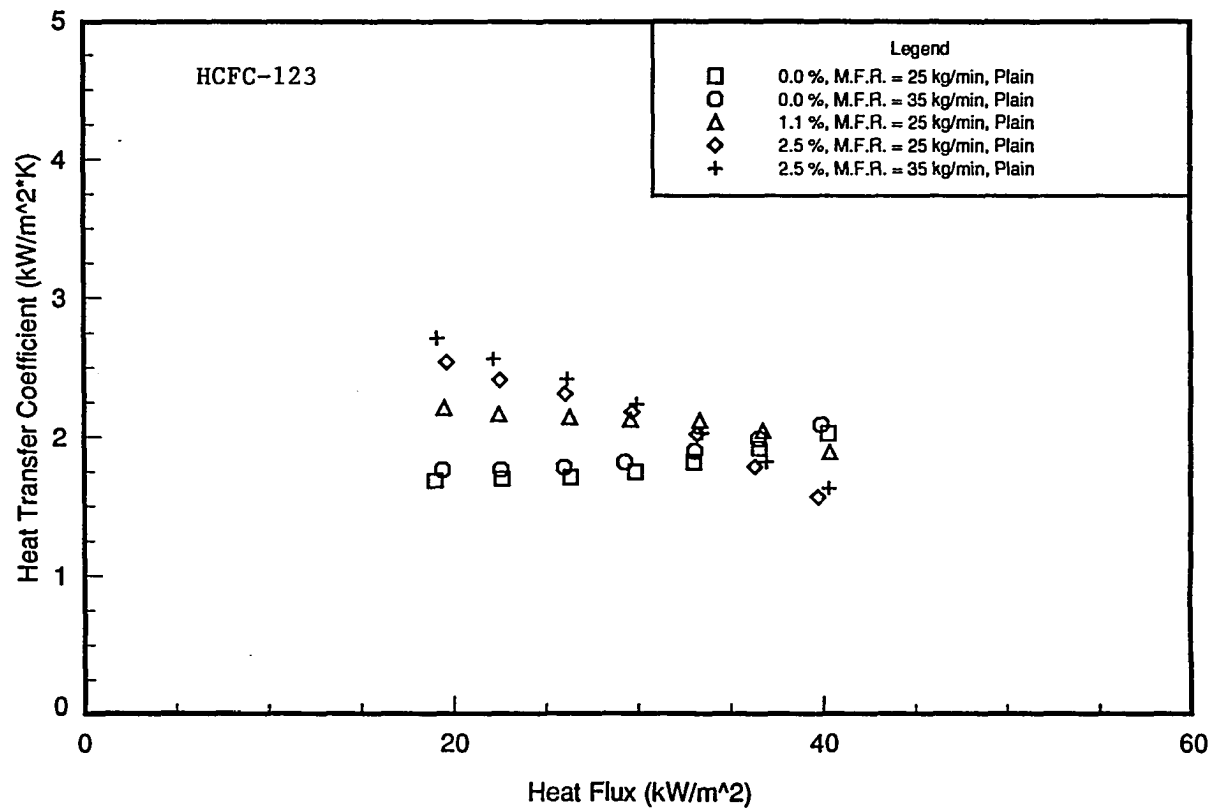


Figure 12.2: Heat transfer coefficient vs. heat flux ($P_{sat} = 35.7$ kPa; lubricant effects testing, plain surface bundle)

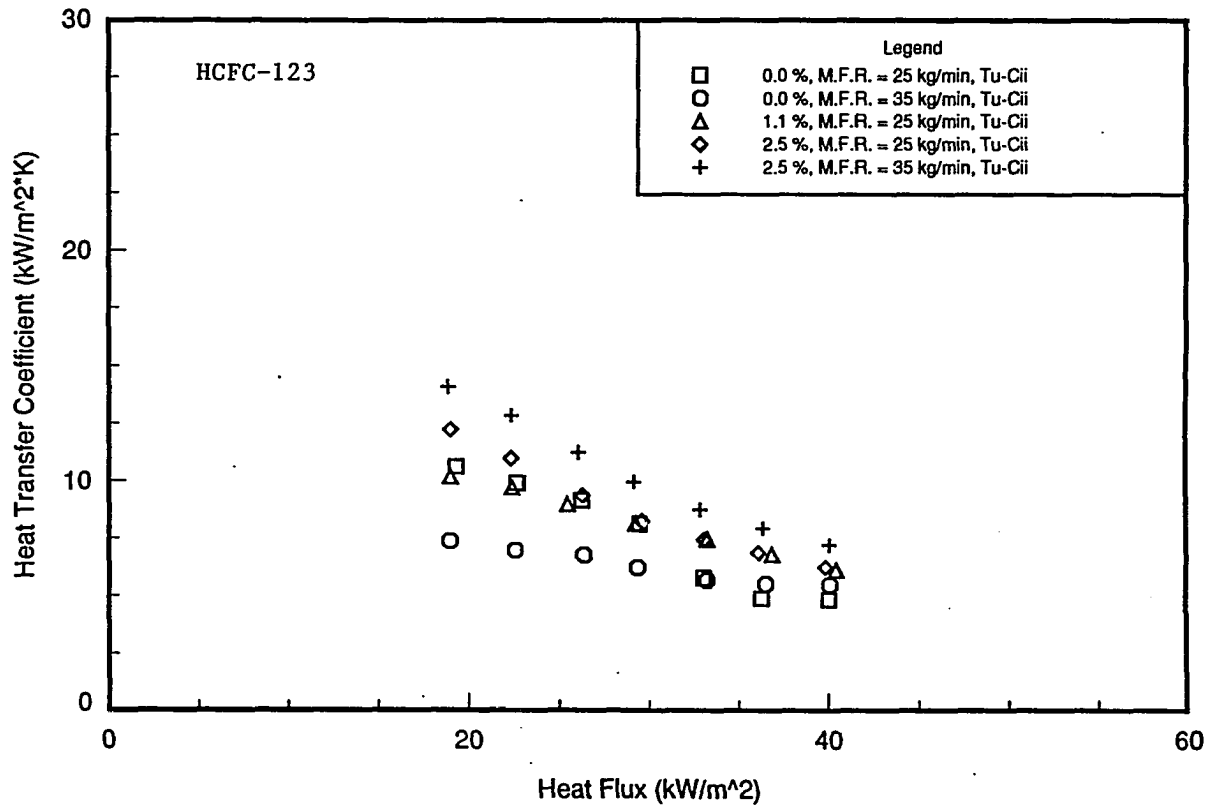


Figure 12.3: Heat transfer coefficient vs. heat flux ($P_{\text{sat}} = 35.7 \text{ kPa}$; lubricant effects testing, Tu-Cii bundle)

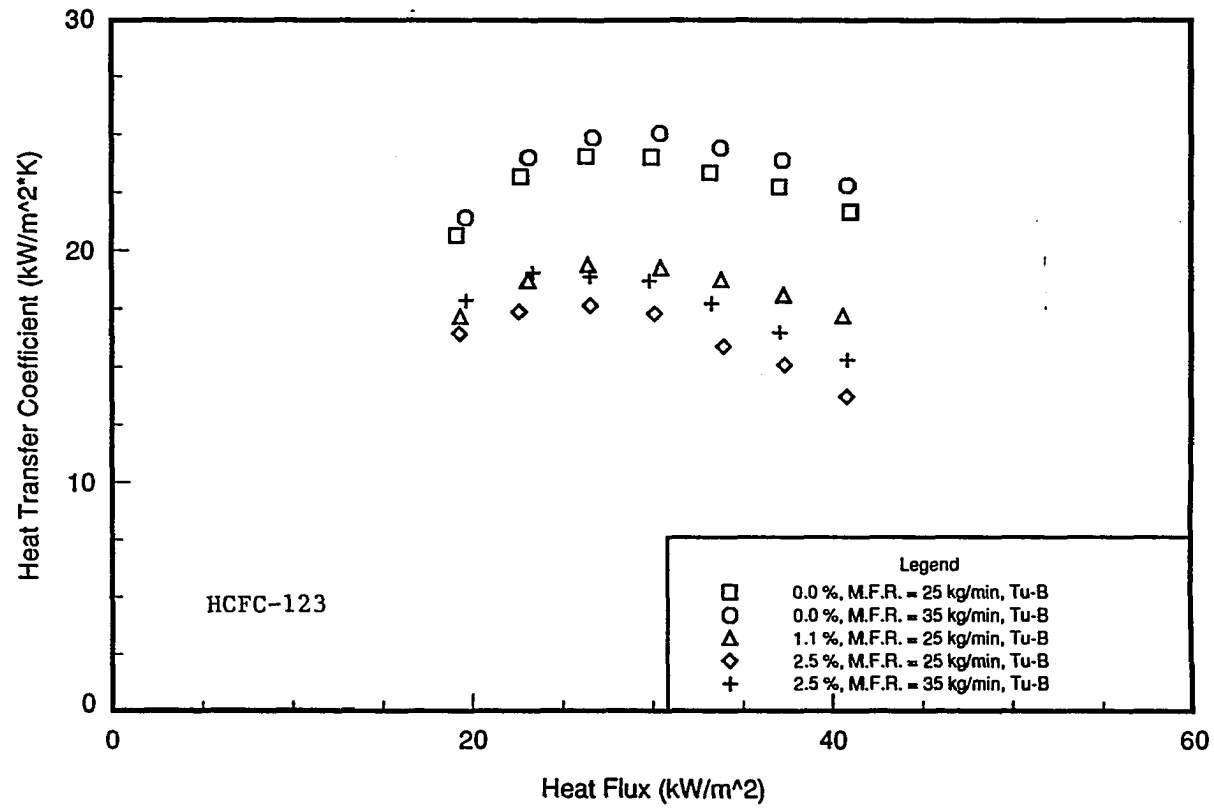


Figure 12.4: Heat transfer coefficient vs. heat flux ($P_{\text{sat}} = 35.7$ kPa; lubricant effects testing, Tu-B bundle)

30WDCRC nozzle configuration was used throughout the lubricant effects testing with HCFC-123.

Considerable foaming was observed during the lubricant effects testing with the plain-surface bundle, but it would be described as less than that seen with this bundle during the HFC-134a/POE oil testing at similar concentrations. Virtually no foam was generated on the surface of the Tu-Cii or Tu-B bundles. Both of these bundles performed better than the plain surface bundle, thus had lower tube wall temperatures. It can probably be concluded that relatively high wall temperatures are required to generate this foaming effect with the naphthenic mineral oil. It was noted previously in the HFC-134a lubricant effects testing that more foam was generated at higher tube wall temperatures as well.

Plain-surface bundle results are presented in Figure 12.2. These results show that the heat transfer coefficients were more dependent upon lubricant concentration than film-feed supply rate. Very little variance in heat transfer coefficients existed between the 25 kg/min and the 35 kg/min refrigerant supply rate results at either the 0.0 % or 2.5 % concentrations. Compared to pure refrigerant performance, small concentrations of mineral oil caused the heat transfer performance to be greater at low heat flux and poorer at high heat flux.

As was the case in the nozzle configuration comparison testing, Figure 12.3 shows that the Tu-Cii bundle experienced a large reduction in heat transfer performance with increased heat flux in all lubricant effects tests conducted with this bundle. There was a slight improvement in bundle heat transfer performance at the 2.5 % oil concentration with the refrigerant supply rate of 35 kg/min, but these data show a large reduction in the heat transfer coefficients in the upper heat flux range.

The 25 kg/min HCFC-123 supply rate for the 30WDCRC nozzle configuration corresponds to an overfeed ratio range of 2.1 to 4.3. Triangular-pitch bundle testing for pure HFC-134a was conducted at a 15 kg/min refrigerant supply rate which yielded an overfeed

ratio range of 1.4 to 3.0. The heat transfer performance of the Tu-Cii bundle with HFC-134a yielded good overall heat transfer performance compared to the that found in the HCFC-123 testing. One possible reason the performance difference exists between HCFC-123 and HFC-134a is because the surface tension of HCFC-123 is approximately 60 % greater than that of HFC-134a in this temperature range. Also, the viscosity of HCFC-123 is over 100 % greater than that of HFC-134a. Although there are conflicting results from previous pool boiling studies regarding the effects of viscosity upon shell-side heat transfer performance, the higher surface tension would definitely result in poorer performance because the development of vapor embryos would be suppressed.

The Tu-B bundle yielded significantly better heat transfer performance during pure HCFC-123 testing than expected with performance being 70 % greater than the HFC-134a case. The shell-side heat transfer coefficients for the Tu-B bundle increased with heat flux until the performance peaked near a heat flux of 30 kW/m² and then declined up through the maximum heat flux evaluated. The performance decline from 30 kW/m² to 40 kW/m² is likely due to film breakdown in the lower rows of the bundle.

Figure 12.4 shows that the naphthenic mineral oil mixed with HCFC-123 decreased heat transfer performance of the Tu-B bundle in all cases compared to the pure refrigerant results. At a nominal heat flux of 40 kW/m², with a refrigerant supply rate of 35 kg/min and a lubricant concentration of 2.5 %, the shell-side heat transfer coefficient decreased by 33 % relative to the pure refrigerant results. During the HFC-134a testing, lubricant concentrations of a polyol-ester oil up to 2.5 % yielded increased heat transfer performance relative to pure refrigerant results with this bundle.

The Tu-B bundle yielded the highest heat transfer coefficients during the HCFC-123 testing. Recall that the Tu-Cii bundle performed the best of all surfaces evaluated with HFC-134a. Figures 12.5 and 12.6 present surface enhancement factors for the Tu-Cii and Tu-B

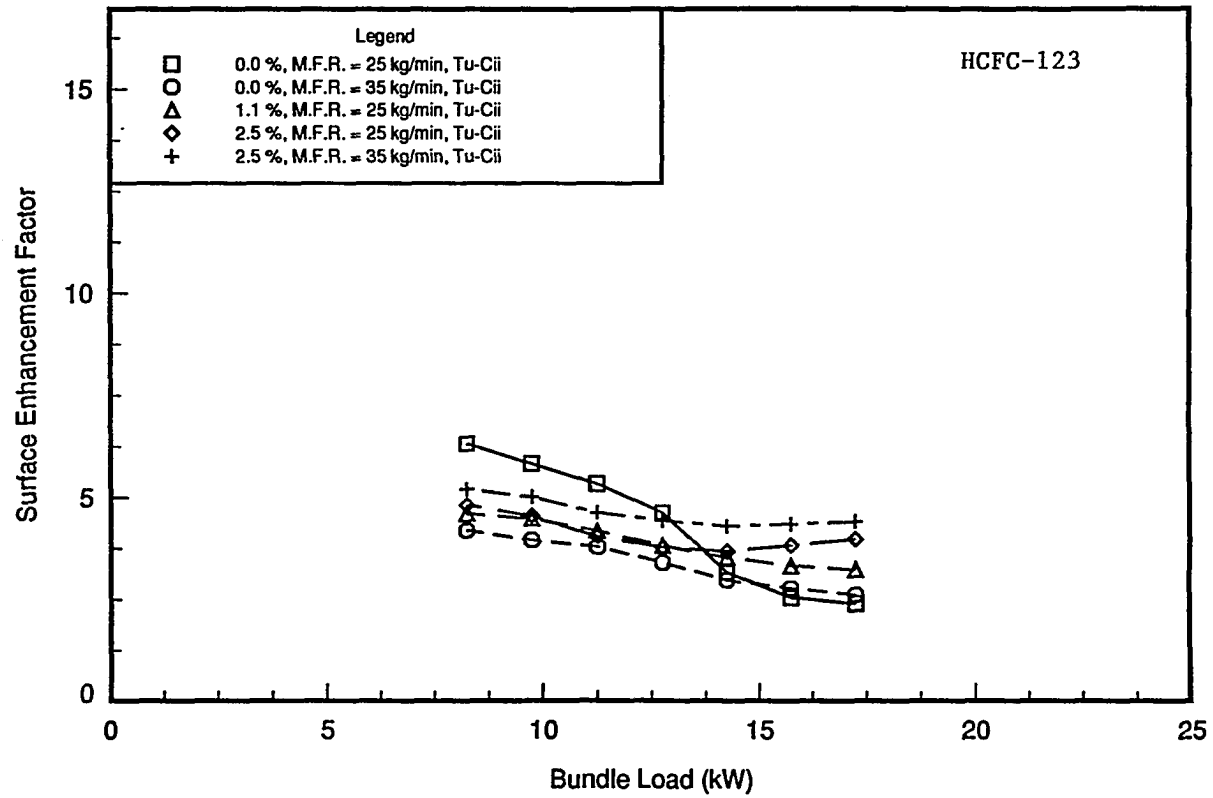


Figure 12.5: Surface enhancement factor vs. bundle load ($P_{\text{sat}} = 35.7 \text{ kPa}$; lubricant effects testing, Tu-Cii bundle)

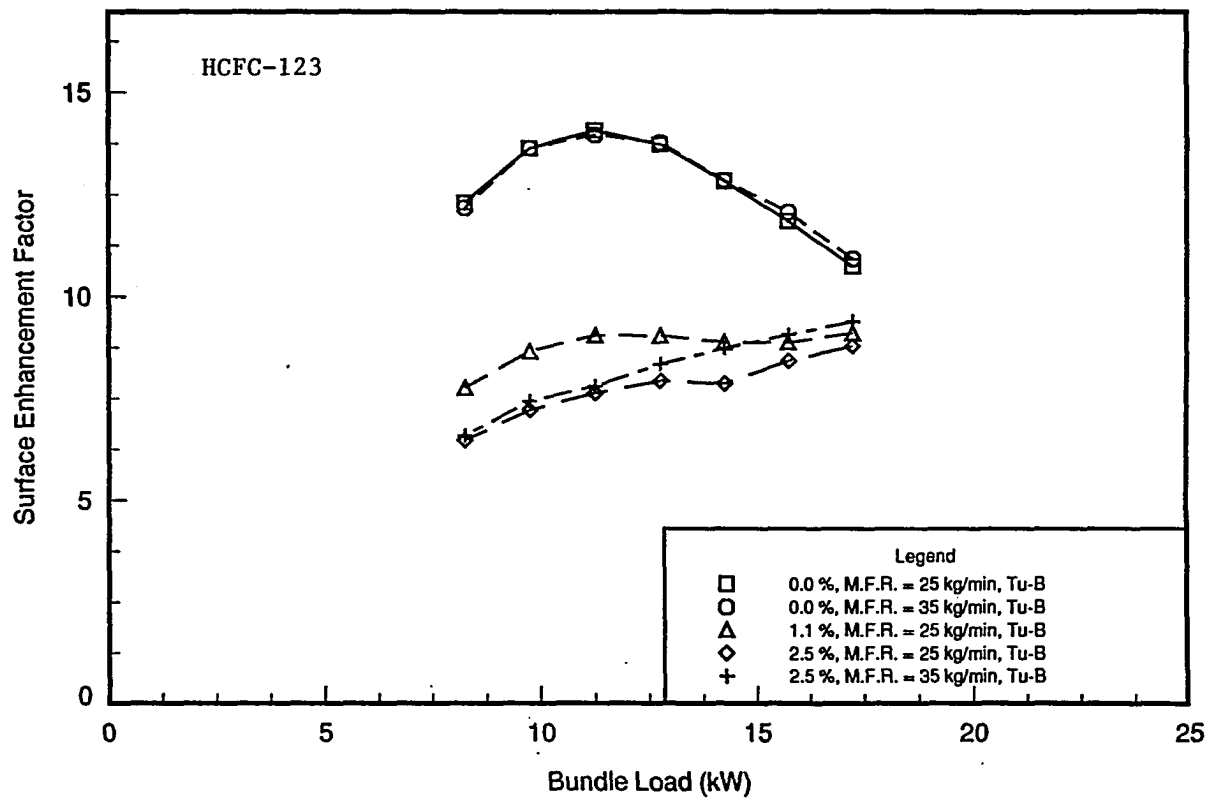


Figure 12.6: Surface enhancement factor vs. bundle load ($P_{sat} = 35.7$ kPa; lubricant effects testing, Tu-B bundle)

bundles. Figure 12.6 demonstrates the outstanding performance of the Tu-B surface. The surface enhancement factors from the pure refrigerant testing with the Tu-B bundle are all over 10 through the entire heat flux range evaluated. The majority of the work conducted with the Tu-Cii bundle yielded surface enhancement factors in the 2.5 to 5.0 range.

Lubricant enhancement factors from this testing are presented in Figures 12.7, 12.8, and 12.9. The plain-surface bundle yielded lubricant enhancement factors that peak near 1.5 then drop with increased bundle load down to the 0.7 to 0.8 range. The 2.5 % concentration results show that flow rate effects are negligible with the plain surface. With the Tu-Cii bundle, the lubricant enhancement factors show significant dependence on lubricant concentration and relatively little dependence on flow rate. The Tu-B bundle generated lubricant enhancement factors which show a slight decrease in performance at higher lubricant concentrations in the upper heat flux range, but were less than unity in all cases.

HCFC-123 Row-by-Row Analysis

Row performance factors are presented in Tables 12.3 and 12.4 for all of the runs conducted during the HCFC-123 lubricant effects testing. The row performance factors for the pure refrigerant tests done with both the plain and Tu-B bundles show that heat transfer performance degrades slightly with row depth. This decrease in the shell-side heat transfer coefficient is less than 30 % from the top to bottom row, with both bundles at the 17.25 kW bundle load. At the lowest bundle load (8.25 kW), the heat transfer performance of the Tu-B bundle improves with row depth. This is the only bundle that exhibits this performance trend.

The reduced performance of the Tu-Cii bundle at high loads is readily shown by its row performance factor profile with row depth. Heat transfer performance on the top row is over 10 times that measured on the bottom row for the 17.25 kW, 25 kg/min pure refrigerant flow

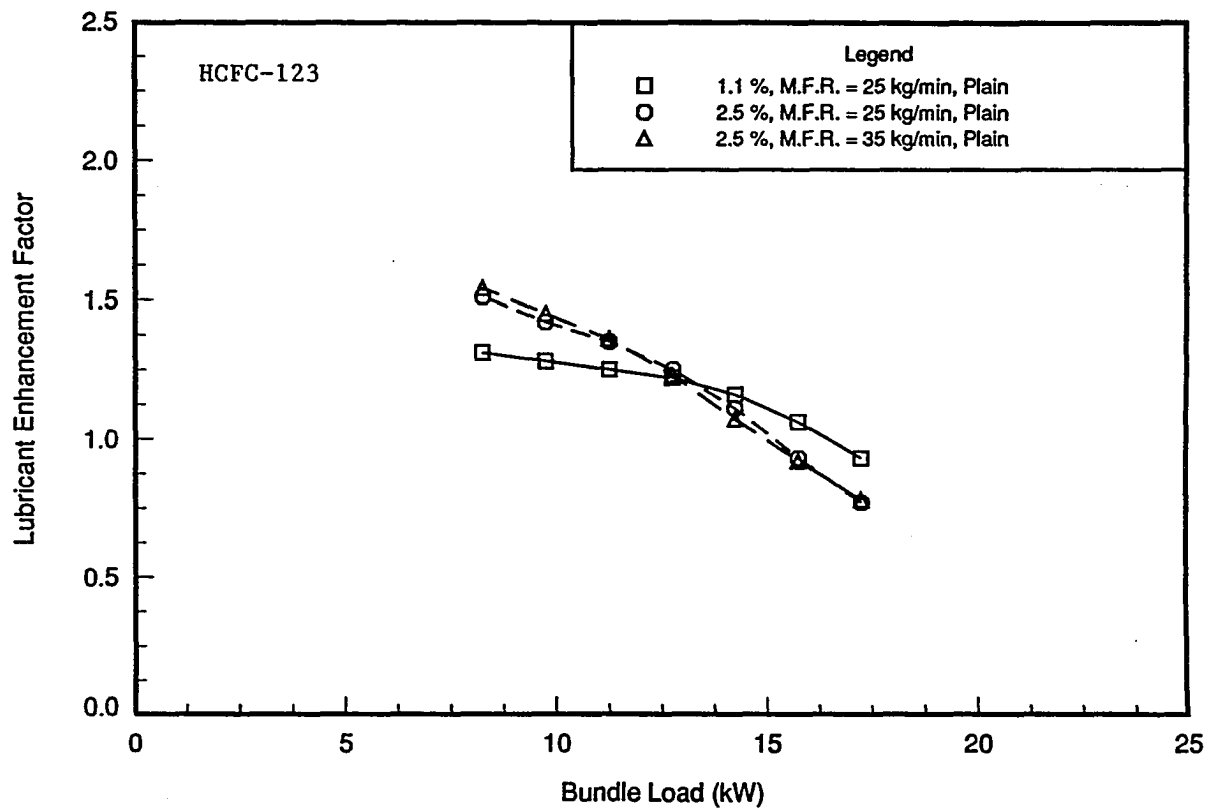


Figure 12.7: Lubricant enhancement factor vs. bundle load
 ($P_{\text{sat}} = 35.7 \text{ kPa}$; plain surface bundle)

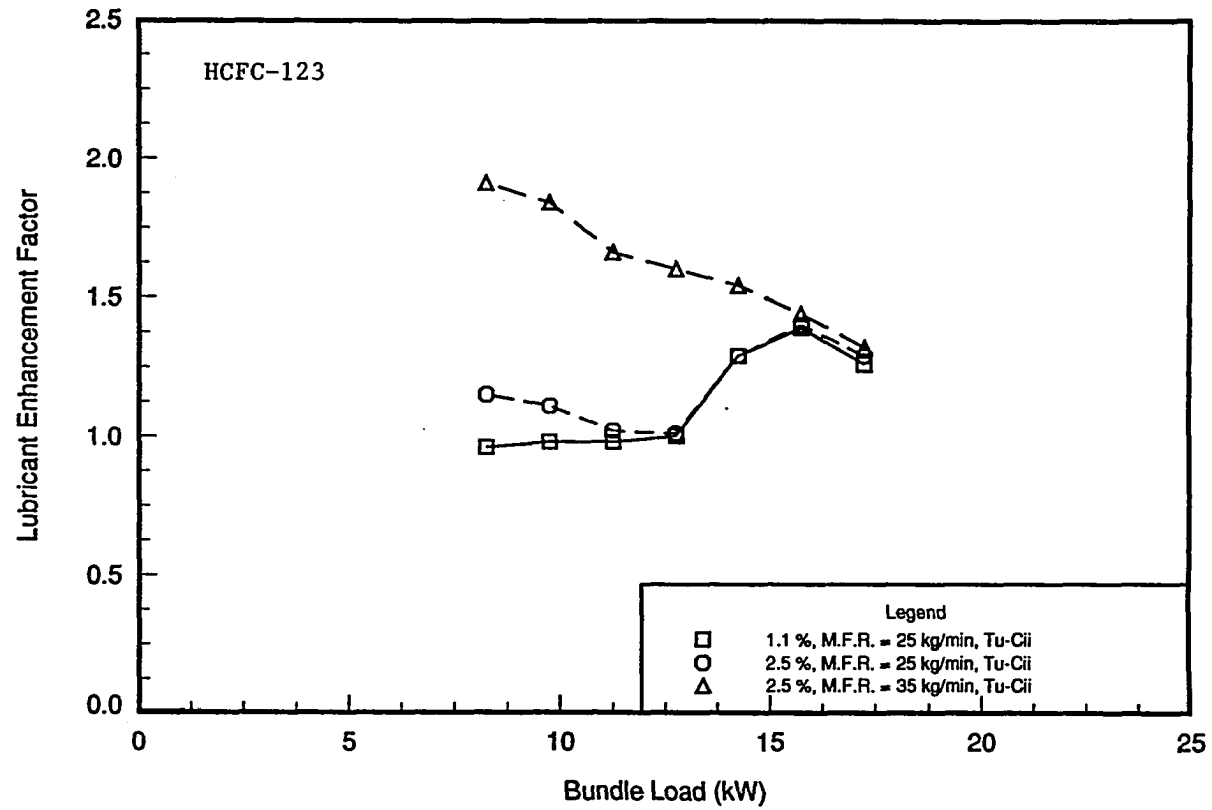


Figure 12.8: Lubricant enhancement factor vs. bundle load
 ($P_{\text{sat}} = 35.7 \text{ kPa}$; Tu-Cii bundle)

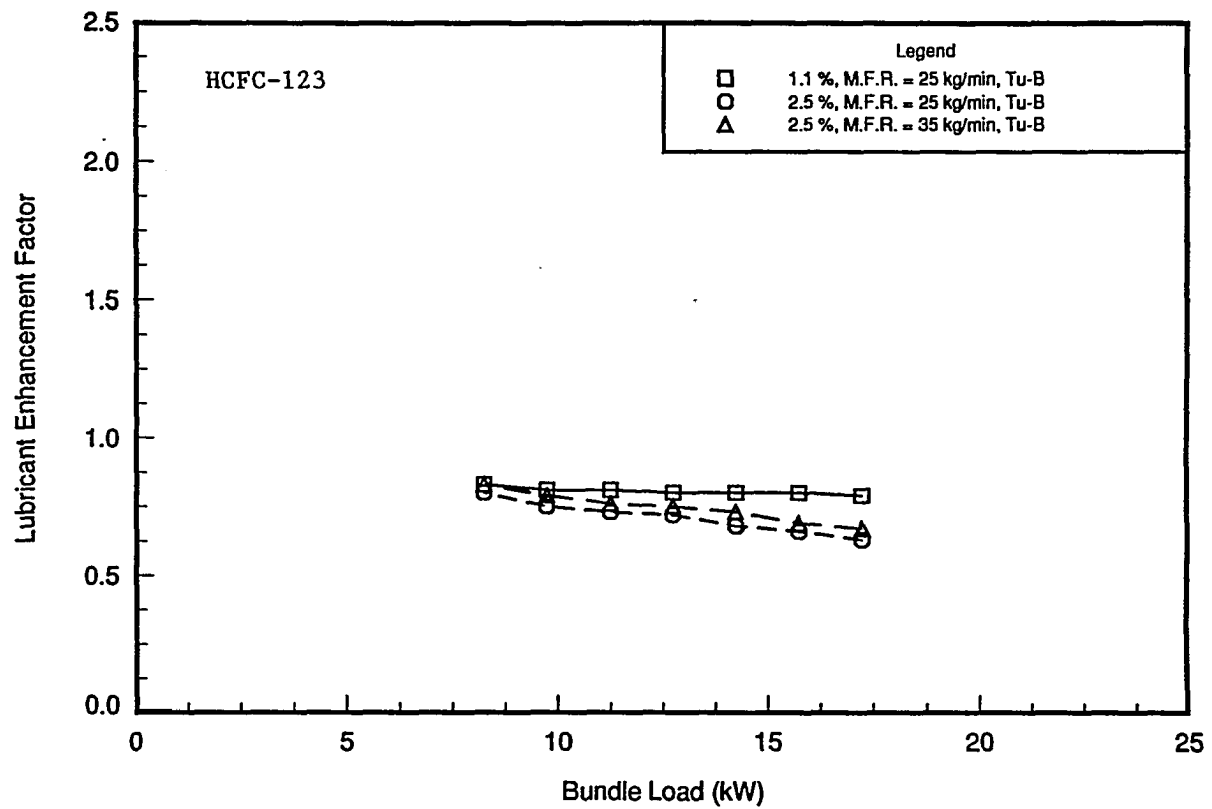


Figure 12.9: Lubricant enhancement factor vs. bundle load
 ($P_{sat} = 35.7$ kPa; Tu-B bundle)

Table 12.3: Row performance factor variation with row depth, pure HCFC-123 results

| Surface | Row | M.F.R. = 25 kg/min | | M.F.R. = 35 kg/min | |
|---------|-----|--------------------|-----------|--------------------|-----------|
| | | 0.0 % | | 0.0 % | |
| | | 17.25 (kW) | 8.25 (kW) | 17.25 (kW) | 8.25 (kW) |
| Plain | 1 | 1.11 | 1.01 | 1.13 | 1.12 |
| | 2 | 0.98 | 0.87 | 0.92 | 0.86 |
| | 3 | 0.97 | 0.87 | 0.93 | 0.84 |
| | 4 | 0.79 | 0.89 | 0.83 | 0.85 |
| Tu-Cii | 1 | 2.27 | 1.07 | 2.02 | 1.44 |
| | 2 | 2.22 | 0.96 | 2.07 | 1.43 |
| | 3 | 0.45 | 0.72 | 0.72 | 0.68 |
| | 4 | 0.21 | 0.82 | 0.38 | 0.96 |
| Tu-B | 1 | 1.24 | 0.89 | 1.23 | 0.90 |
| | 2 | 1.36 | 1.06 | 1.33 | 1.05 |
| | 3 | 0.80 | 0.73 | 0.78 | 0.72 |
| | 4 | 0.90 | 1.25 | 0.90 | 1.22 |

Table 12.4: Row performance factor variation with row depth, HCFC-123 lubricant effects results

| Surface | Row | M.F.R. = 25 kg/min | | M.F.R. = 25 kg/min | | M.F.R. = 35 kg/min | |
|---------|-----|--------------------|-----------|--------------------|-----------|--------------------|-----------|
| | | 1.1 % | | 2.5 % | | 2.5 % | |
| | | 17.25 (kW) | 8.25 (kW) | 17.25 (kW) | 8.25 (kW) | 17.25 (kW) | 8.25 (kW) |
| Plain | 1 | 1.29 | 1.06 | 1.50 | 1.10 | 1.60 | 1.19 |
| | 2 | 1.03 | 0.89 | 1.15 | 0.92 | 1.10 | 0.95 |
| | 3 | 1.00 | 0.87 | 0.91 | 0.84 | 0.86 | 0.80 |
| | 4 | 0.66 | 0.80 | 0.58 | 0.76 | 0.59 | 0.74 |
| Tu-Cii | 1 | 1.64 | 1.11 | 1.48 | 1.05 | 1.49 | 1.04 |
| | 2 | 1.51 | 0.81 | 1.47 | 0.91 | 1.38 | 1.04 |
| | 3 | 0.79 | 0.67 | 0.88 | 0.89 | 0.96 | 0.89 |
| | 4 | 0.53 | 1.00 | 0.69 | 1.02 | 0.81 | 0.97 |
| Tu-B | 1 | 1.11 | 0.93 | 1.39 | 0.91 | 1.33 | 0.91 |
| | 2 | 1.08 | 0.80 | 1.43 | 1.03 | 1.34 | 1.01 |
| | 3 | 0.80 | 0.74 | 0.78 | 0.74 | 0.75 | 0.72 |
| | 4 | 0.91 | 1.14 | 0.92 | 1.16 | 0.92 | 1.16 |

rate test condition. It should be noted that for the 8.25 kW, 2.5 % oil concentration test condition, the 35 kg/min supply rate yields a heat transfer coefficient for the Tu-Cii bundle in the spray evaporation environment that is 20 % lower than that measured on the Tu-B bundle. This clearly demonstrates that the Tu-B surface is better matched for HCFC-123 use than the Tu-Cii surface.

The Tu-B bundle yielded the best heat transfer performance with HCFC-123, but a decrease in performance at high heat fluxes indicates that film breakdown may be present on the lower rows of the bundle. The film-feed supply rates used in this testing are documented in Appendix D. At the 35 kg/min refrigerant supply rate, with a bundle load of 17.25 kW and a 2.5 % oil concentration, there is a 31 % decrease in performance from the top to the bottom row with this bundle. The overfeed ratio at the 35 kg/min refrigerant supply rate is 2.5. Testing is required at higher refrigerant supply rates to better determine a recommended overfeed ratio range for use with this surface.

Conclusions

Spray evaporation performance testing was conducted for HCFC-123 with triangular-pitch tube bundles made from an enhanced boiling tube, an enhanced condensation tube, and a plain-surface tube. The lubricant effects testing consisted of a matrix of 15 runs including refrigerant supply rates of 25 kg/min and 35 kg/min and lubricant concentrations of 1.1 % and 2.5 %. A summary of the results obtained during this testing are listed below.

1. Overfeed ratios greater than 2.5 are should be used with HCFC-123. The investigators would recommend at-least an overfeed ratio of 5 to prevent film break down in the lower rows of the bundle.
2. The Tu-B bundle yielded the best heat transfer performance during the HCFC-123 testing. This is in contrast to the HFC-134a testing, which showed the Tu-Cii bundle to be better.
3. Significant foaming occurred during the plain-surface bundle testing, but very little was observed in the enhanced bundle testing. In addition, there is less tendency for foam to generate on a heated surface with HCFC-123 and a mineral oil than HFC-134a and a polyol-ester oil.
4. Oil concentrations of 1.1 % and 2.5 % decreased the heat transfer performance of the Tu-B bundle through the entire heat flux range evaluated. Small concentrations of oil improved the heat transfer performance of the plain-surface bundle in the lower heat flux range. The Tu-Cii bundle showed significant improvement in heat transfer performance only at the 2.5 % concentration with a 35 kg/min refrigerant supply rate. It should be noted that the heat transfer performance increased with small concentrations of oil up to 2.5 % during the HFC-134a testing with the plain-surface and Tu-B bundles.

CHAPTER 13. DESIGN CORRELATION COMPARISON

Film-evaporation and film-boiling correlations were presented in Chapter 2. This chapter presents the results of using some of these correlations to predict data taken on the bundle test facility. Because heat transfer coefficients have been dependent on heat flux with both test facilities in test conditions where dryout conditions were not present, it is likely that boiling was participating in the heat transfer process. Results from the film-evaporation, hydrocarbon refrigerant study conducted by Danilova et al. [1] indicated that the heat flux range used on the bundle test facility is higher than that required to generate boiling effects in the heat transfer process. However, a significant amount of nucleate bubble generation was only observed during the lubricant effects testing with refrigerants HFC-134a and HCFC-22. Small bubbles were seen in the thick liquid layer at the bottom-dead-center of the tubes, but no bubbles were observed on the top or sides of the tubes. This was true for all finned and enhanced surfaces evaluated. It should be noted that fewer bubbles were seen during the lubricant effects testing of HCFC-123 than the other two refrigerants.

Two possible reasons for the heat transfer coefficient dependency upon heat flux are boiling at the bottom-dead-center of the tube and the effects of dryout. Another possibility is that bubbles were generated throughout the film layer, however, they were too small to be readily detectable through the view-port assemblies of the test section. Although the

investigators believe this to be unlikely, the hypothesis should be further investigated with enhanced optical techniques prior to being ruled out.

Correlation Comparison

The existing correlations can be divided into two groups, namely, boiling and nonboiling. These correlations were developed in a variety of studies which were conducted with both horizontal and vertical surfaces (plates, tubes, etc.). As discussed in Chapter 2, the majority of the correlation development work which incorporated analytical techniques into the solution focused on the nonboiling regime. Less analytical film boiling work has been done, most likely due to the complex nature of the process.

HFC-134a Results Comparison

Lorenz and Yung [11] stated that comparisons between tube-bundle and single-tube results could be made at Reynolds numbers high enough to ensure full wetting of the tubes in the lower rows of the bundle. A recommendation of a Reynolds number greater than 300 for this comparison was made from results generated during horizontal, plain-surface tube tests with ammonia. The Reynolds number for which single-tube and tube-bundle results may be compared will unlikely be the same for different tube surfaces, tube diameters, and liquids. To date, insufficient heat transfer testing has been conducted over a wide Reynolds number range with the three refrigerants used in this study to make a conclusive recommendation. An assumption will be made that for single-tube/tube-bundle comparisons to be accurate, a Reynolds number of 300 applies to hydrocarbon type refrigerants as well. If film breakdown does exist in the lower rows of the tube bundle in a given operating condition, it would be

expected that the bundle heat transfer coefficient would be less than that predicted by a single-tube correlation.

Figures 13.1 and 13.2 present four different nonboiling and one boiling film-wise heat transfer correlations developed in previous studies of water. These correlations are presented in Chapter 2 by Equations 2.12 (Chun & Seban), 2.17 (Owens), 2.18 (Mitrovic), 2.13 (Parken et al., nonboiling), and 2.14 (Parken et al., boiling). Plain-surface bundle heat transfer coefficients, all taken with a Reynolds number greater than 300 on the bottom row, are also shown in the figures for comparison.

Lorenz and Yung [2] presented a combined boiling and evaporation model (shown in Equations 2.4 to 2.9) that is unique from the other correlations presented in Chapter 2. This model superimposed the separate boiling and nonboiling contributions which predicted a band which set upper and lower limits for the bundle heat transfer coefficients. This approach requires a good understanding of both the boiling and evaporation mechanisms. Although the investigators believe this to be an interesting approach for the prediction of spray-evaporation and film-boiling data, the technique requires knowledge of a fluid-surface factor to model the boiling contribution to the shell-side heat transfer coefficient. Pure-refrigerant pool-boiling data have been presented by Webb and Pais [32] which might be used to develop these factors for the surfaces evaluated in both the pool boiling study and this current spray-evaporation project. This is currently left for future work. Since the best performing bundle during the high-pressure refrigerant testing was a condensation surface, no previous pool boiling data are available.

A comparison is made in Figures 13.1 and 13.2 between correlation predictions and data from the bundle test facility. Many of these correlations are based on the evaporation of water. This comparison shows that these nonboiling correlations do not accurately predict the experimental data which is for a hydrocarbon refrigerant. The nonboiling correlation

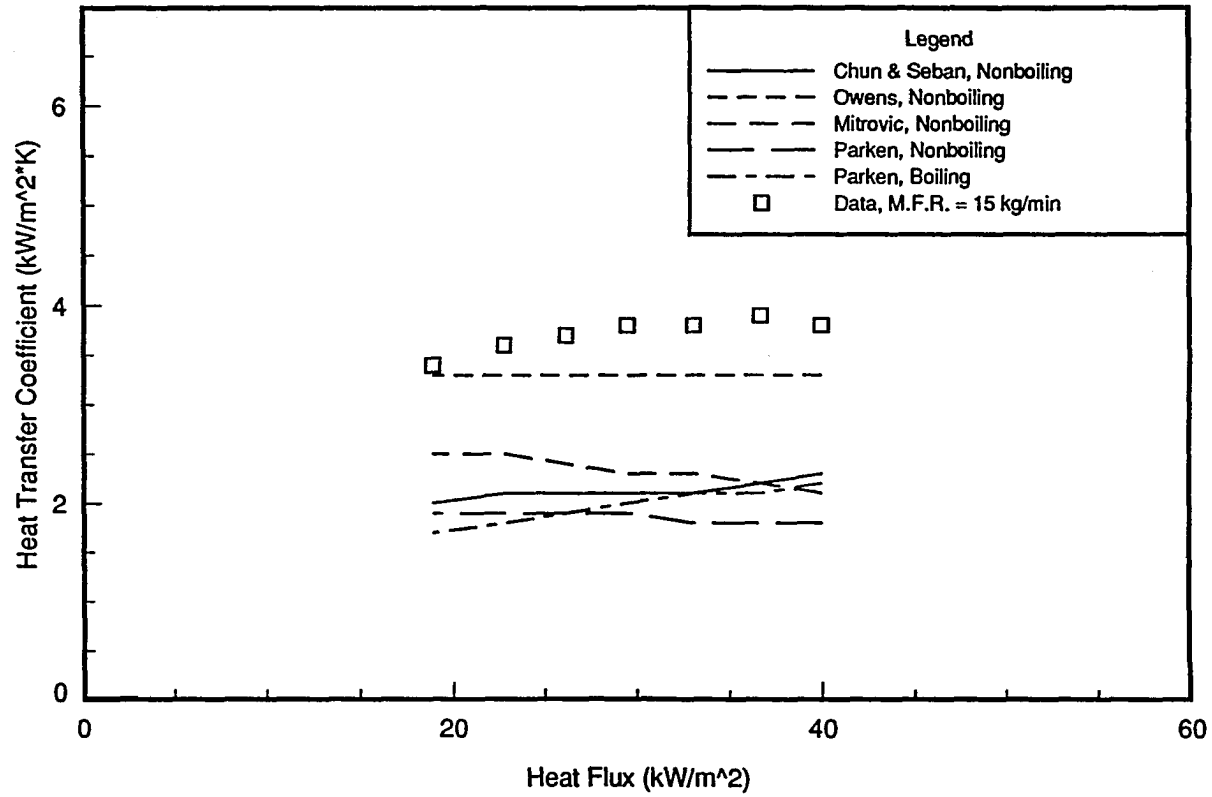


Figure 13.1: Heat transfer coefficient vs. heat flux ($P_{\text{sat}} = 314.5 \text{ kPa}$; plain-surface bundle data, HFC-134a, M.F.R. = 15 kg/min)

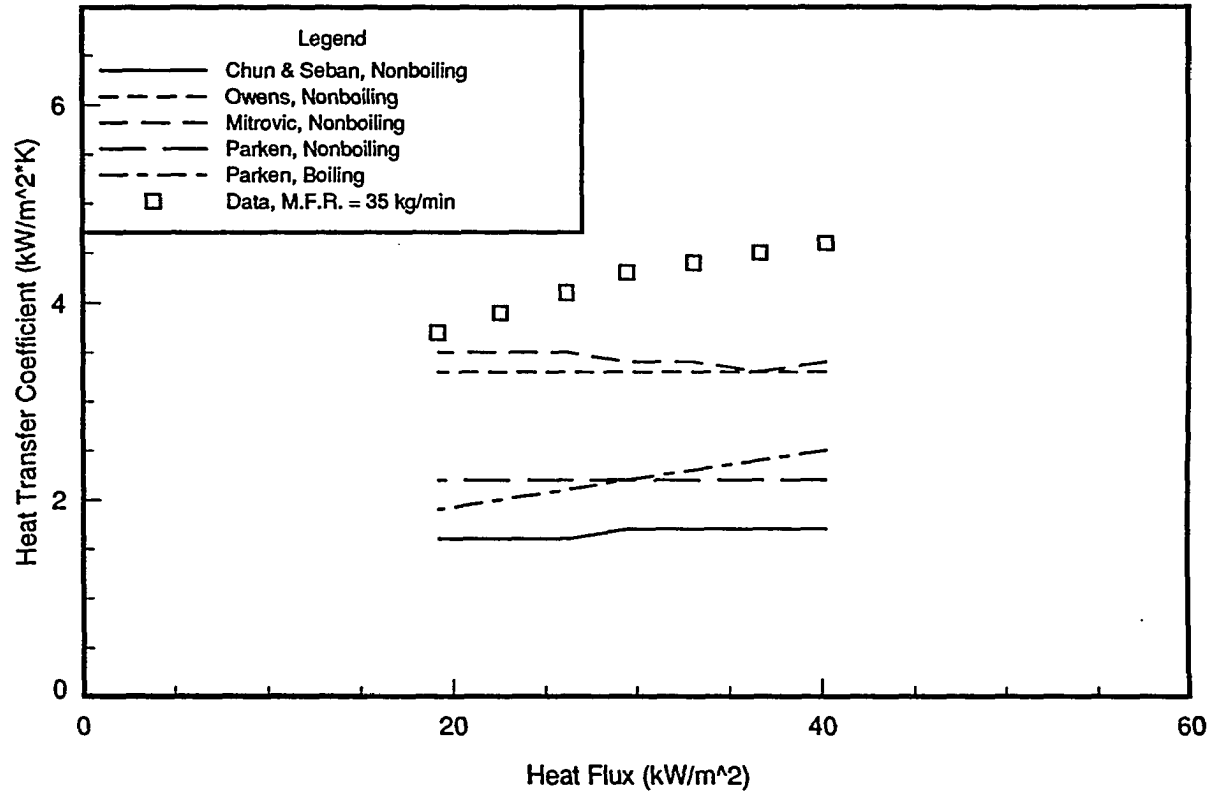


Figure 13.2: Heat transfer coefficient vs. heat flux ($P_{\text{sat}} = 314.5 \text{ kPa}$; plain-surface bundle data, HFC-134a, M.F.R. = 35 kg/min)

presented by Owens [19] shows the best agreement to the data collected at a 15 kg/min refrigerant supply rate, while the nonboiling correlation presented by Mitrovic [12] shows the best agreement with the 35 kg/min supply-rate data. The correlations presented in Figures 13.1 and 13.2 were calculated using the Reynolds and Prandtl numbers given in Appendix B in Table B.1 and B.2. Lorenz and Yung [11] recommended the use of the Reynolds number and Prandtl number as calculated for the bottom row to represent the overall tube-bundle heat transfer performance.

A boiling correlation developed by Parken et al. [3] from 25.4 mm diameter horizontal-tube testing with water as the heat transfer fluid is shown in Figures 13.1 and 13.2 as well. This correlation underpredicts the plain-bundle heat transfer performance by 50 percent. The investigators believe this demonstrates that the correlations developed in water studies can not be readily applied to refrigerant studies because of differences in fluid properties. The overall trends are likely to be similar, but the constants in the individual correlation equations need to be statistically re-evaluated for use with hydrocarbon refrigerants.

One study conducted by Danilova et al. [1] with CFC-type hydrocarbon refrigerants yielded horizontal, plain-surface tube correlations for use in both the boiling and nonboiling regimes. These two correlations are shown in Figure 13.3 with plain-surface, tube-bundle data collected at refrigerant supply rates of 15 kg/min and 35 kg/min with the 30WHCRC nozzle configuration. These correlations are shown in Chapter 2 in Equations 2.20 and 2.21. It should be noted that the effects of refrigerant supply rate (i.e. film-feed supply rate) are not taken into account in the boiling correlation, thus this correlation is applicable to the results collected at either flow rate. At a heat flux of 19 kW/m², the correlation predicts the high and low flow-rate data within 22 and 15 percent, respectively. At a heat flux of 40 kW/m² the agreement is 2 and 24 percent for the high and low flow-rate data. As can be seen in the

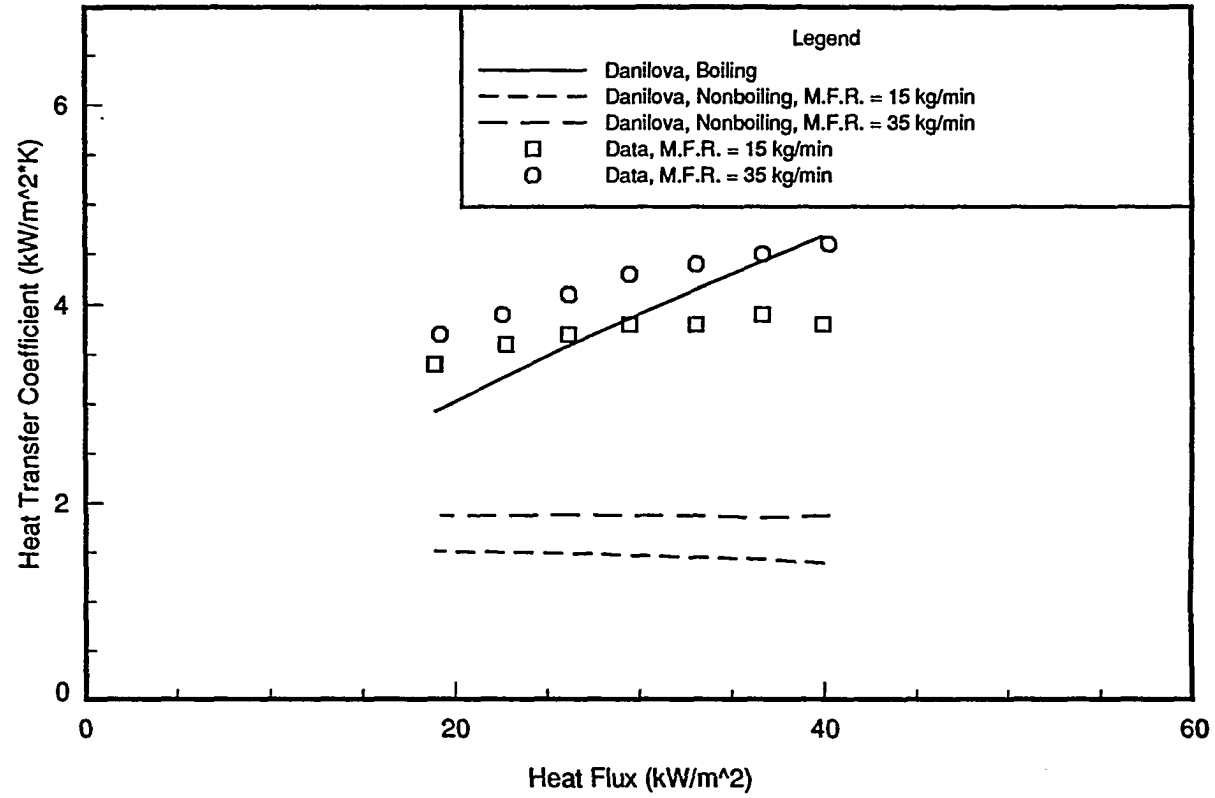


Figure 13.3: Heat transfer coefficient vs. heat flux ($P_{\text{sat}} = 314.5 \text{ kPa}$; plain-surface bundle data, HFC-134a)

figure, the correlation predicts more of a dependence upon heat flux than that shown by the data.

HCFC-123 Results Comparison

Refrigerant HCFC-123 data taken with the 30WDCRC nozzle configuration at a refrigerant mass flow rate (M.F.R.) of 35 kg/min are presented in Figure 13.4 along with predictions from the boiling and nonboiling correlations presented in the study conducted by Danilova et al. [1] with CFC-type refrigerants. The agreement between the experimental data taken with HCFC-123 and that predicted by the boiling correlation is much worse than the prediction of the boiling correlation for the HFC-134a data. The deviation from the correlation is 31 percent at a heat flux of 40 kW/m² and 80 percent at 19 kW/m². It is possible that the correlation is better suited for high-pressure refrigerant applications, however CFC-113 data was also included along with CFC-12 and HCFC-22 data in the development of this correlation.

It should be noted that the lack of dependence on heat flux shown by the bundle heat transfer coefficient in the lower half of the range evaluated is much less than that experienced by the individual rows. Because performance increased in the lower rows and decreased in the upper rows with decreasing bundle load throughout the data run, the dependency of the bundle heat transfer coefficient on heat flux was weak in the lower heat flux range.

Conclusions

A comparison was made between data collected with the triangular-pitch, plain-surface tube bundle and predictions made from existing correlations developed in previous film-

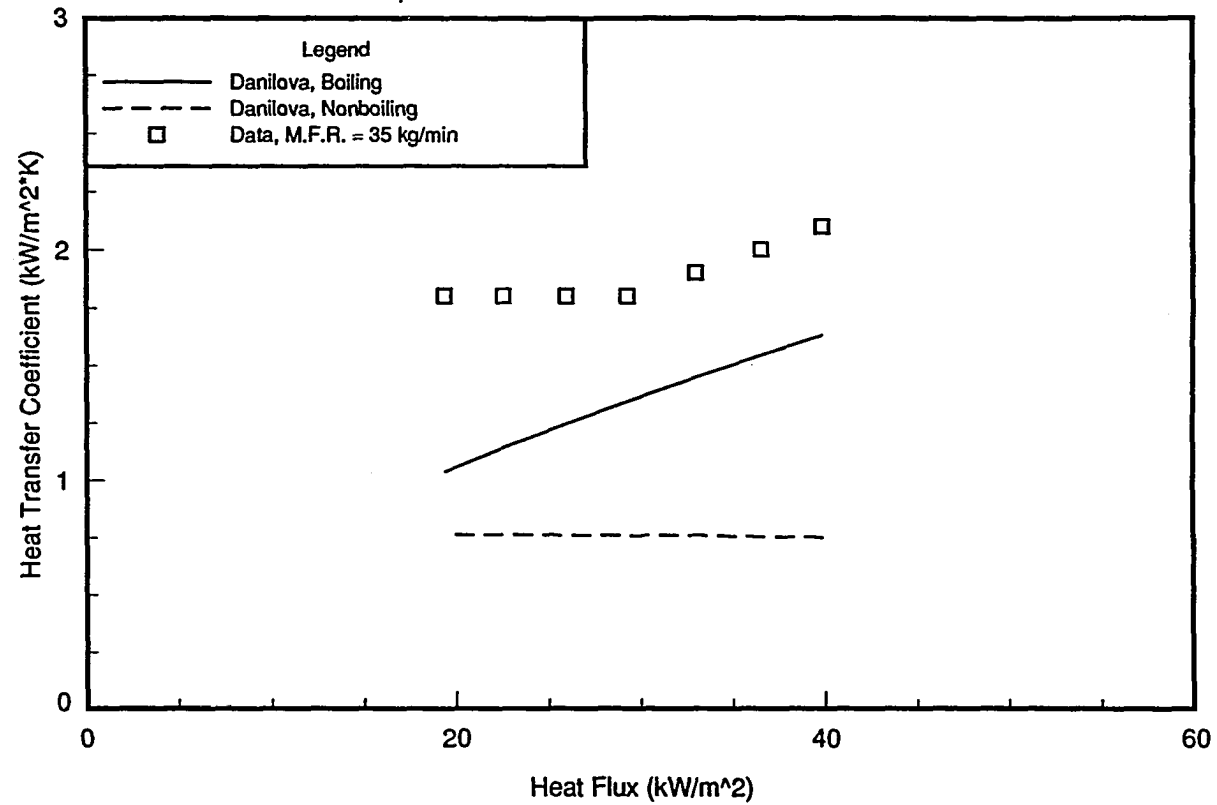


Figure 13.4: Heat transfer coefficient vs. heat flux ($P_{\text{sat}} = 35.7 \text{ kPa}$; plain-surface bundle data, HCFC-123)

evaporation and film-boiling studies. Due to a lack of property information for the refrigerant/lubricant mixtures used in this study, it was not possible to compare lubricant effects data with any existing correlations.

1. Boiling contributes to the heat transfer coefficients measured in this study in the heat flux range of 19 kW/m² to 40 kW/m².
2. Correlations developed in studies of water and non-hydrocarbon type refrigerants do not accurately predict the heat transfer performance of hydrocarbons.
3. The film-boiling correlation presented by Danilova et al., which was developed from single-tube and tube-bundle results, predicted pure HFC-134a heat transfer performance within a maximum deviation of 25 percent. It is thought by the investigators that this film-boiling correlation to be the best in existence to date for use with hydrocarbon refrigerants.

CHAPTER 14. CONCLUSIONS AND RECOMMENDATIONS

Conclusions

The main objective of this research program was to measure the shell-side heat transfer performance of refrigerants HFC-134a, HCFC-22, and HCFC-123 in a spray evaporation environment. The majority of this work was conducted on a facility which simulated an actual tube-bundle environment that might be found in an industrial refrigeration unit. In addition, this work also addressed issues such as refrigerant distribution in the test section and the effects of small concentrations of oil upon heat transfer performance.

Multi-Tube Test Facility

Refrigerant HFC-134a was evaluated on the multi-tube test facility predominantly with single-tube arrangements. Testing on this facility included the evaluation of two different viscosities of a polyol-ester oil, namely, 160 SUS and 340 SUS. Two enhanced condensation tubes, two enhanced boiling tubes, two finned tubes, and a plain-surface tube were evaluated in this phase of the research program.

It was found that the two enhanced condensation surfaces performed best in the spray evaporation environment. The two surfaces yielded heat transfer coefficients three times as great as a plain-surface tube in the same spray environment and nearly one and a half times the

heat transfer performance of a plain surface tube in a pool boiling environment. The 1024 fins/m surface yielded heat transfer coefficients 5 % to 10 % better than that found with a 1575 fins/m surface, and both tubes performed nearly twice as great as the plain-surface tube in the same test conditions. The effects of diameter were evaluated with plain surface tubes, and it was found that a 12.7 mm tube diameter generated heat transfer coefficients up to 10 % higher than those measured with a 19.1 mm diameter tube.

Limited testing was done with high-pressure drop nozzles on the multi-tube test facility in addition to the low-pressure drop, wide-angle nozzles, which were used in the majority of the work on the multi-tube test facility and all of the work on the bundle-test facility. The high-pressure drop nozzles generated a finely atomized refrigerant spray pattern that yielded good heat transfer performance in the proximity of the refrigerant plume. However, these nozzles generated a much narrower pattern of refrigerant than that produced with the wide-angle, low-pressure drop nozzles.

Small concentrations of a the 160 SUS lubricant increased heat transfer up to 50 % with the W-40 fpi and Tu-Cii tubes, and 75 % with the plain-surface tube. The 340 SUS lubricant yielded increases to the heat transfer coefficient up to 50 % with the W-40 fpi and Tu-Cii tubes as well. This increase in performance was a result of foaming which readily occurred with small concentrations of the polyol-ester oil and HFC-134a. This foaming phenomenon is known to occur in the upper rows of tube bundles in a pool-boiling environment as well. Both environments have little hydrostatic head which deters heat transfer performance, and it appears that the absence of this hydrostatic head allows foaming to occur. Foaming increased heat transfer performance at low heat fluxes where the overfeed ratio was as high as 15, and also at the higher heat fluxes with corresponding overfeed ratios as low as 2.4.

Both viscosities of oil yielded similar effects for the W-40 fpi tube, while the 340 SUS oil seemed to generate performance 10 % to 20 % greater than that found with the 160 SUS

oil for the Tu-Cii tube. The 160 SUS oil was tested up to a 3.0 % concentration by mass fraction, and the 340 SUS oil was tested up to a 5.0 % concentration. Shell-side heat transfer performance remained greater than that found in pure refrigerant testing through the highest concentration evaluated with either viscosity oil.

Tube-Bundle Test Facility

The work conducted on this facility consisted of pure refrigerant and refrigerant/lubricant mixture testing of HFC-134a, HCFC-22 and HCFC-123. A polyol-ester oil was used with HFC-134a for the evaluation of the effects of oil upon heat transfer performance. An alkyl-benzene oil was selected for use with HCFC-22, and a naphthenic mineral oil was used with HCFC-123.

HFC-134a Results Film-feed supply rate effects testing was conducted with HFC-134a at a saturation temperature of 2.0 °C with tube bundles made of two enhanced condensation tubes, one enhanced boiling tube, one low-finned tube, and a plain surface tube in a triangular-pitch configuration. A square-pitch tube bundle was also tested with the enhanced boiling tube so a comparison could be made between the triangular-pitch and square-pitch tube alignments. These tests revealed that spray evaporation heat transfer performance showed dependence on film-feed supply rate for all surfaces and both geometries evaluated. The heat transfer performance dependence on film-feed supply rate was found to be twice as great for the triangular-pitch than the square-pitch alignment.

The shell-side heat transfer coefficients for all surfaces evaluated during the film-feed supply rate effects testing showed dependence on wall heat flux indicating boiling was present in the film. The dependence of the heat transfer coefficient on wall heat flux was 5 % greater with the triangular-pitch than the square-pitch alignment.

The Tu-Cii bundle yielded the highest heat transfer coefficients during the pure HFC-134a testing. The heat transfer coefficients for the W-SC bundle were only 50 % of those measured with the Tu-Cii bundle. It should be noted that in the single-tube testing these two surfaces performed similarly, yielding heat transfer coefficients within 10 to 15 percent of each other. The difference in performance between the tube-bundle and single-tube environments is most likely due to the "Y-finned" structure on the shell-side of the W-SC tube. Like the W-40 fpi tube, this type of enhancement restricts axial film movement.

A pool-boiling test was conducted with the Tu-B bundle so a comparison could be made with the spray evaporation performance of all surfaces evaluated. It was found that the pool-boiling performance of the Tu-B bundle was 50 % lower than the spray evaporation performance of the Tu-Cii bundle. Pool-boiling tests were also conducted with the W-40 fpi bundle. It was found the W-40 fpi bundle generated better shell-side heat transfer coefficients in the spray evaporation environment than those measured during pool boiling. At a heat flux of 19 kW/m², the spray evaporation performance was a full 15 % to 20 % higher than that found in the pool-boiling environment.

The HFC-134a lubricant effects testing was conducted with tube bundles made of an enhanced condensation tube, an enhanced boiling tube, a low-finned tube, and a plain-surface tube in a triangular-pitch configurations. Foaming was observed during this testing which increased the heat transfer coefficients for all surfaces tested, up to oil concentrations of 2.5 percent. Increases in heat transfer performance near 100 % were noted for the Tu-B bundle at a heat flux of 23 kW/m² and the W-40 fpi bundle at a heat flux of 40 kW/m² for the 2.5 % oil concentration.

The foaming phenomenon present in the lubricant effects testing was found to reduce dryout experienced in the lower rows of the W-40 fpi and W-SC tube bundles. These two bundles received a 50 % to 100 % percent increase in heat transfer performance at a heat flux

of 40 kW/m² in comparison with pure refrigerant results. It is likely that the foam generated on the upper rows flows downward through the bundle wetting surface area that would otherwise remain dry.

HCFC-22 Results Film heat transfer performance testing was conducted for HCFC-22 with the plain-surface and Tu-B, triangular-pitch tube bundles. A single oil concentration of 1.0 % was evaluated at a single film-feed supply rate, for a comparison with pure HCFC-22 results.

Heat transfer coefficients measured during pure HCFC-22 testing were greater than those found in pure HFC-134a testing. However, the lubricant enhancement factor for the Tu-B bundle at a heat flux of 23 kW/m² was nearly 100 % greater with the 1.0 % HFC-134a/polyol-ester oil mixture than the 1.0 % HCFC-22/alkyl-benzene oil mixture. It is unclear whether this performance difference exists as a result of a difference of viscosities or other thermodynamic and transport properties.

HCFC-123 Results Film heat transfer performance testing was conducted for HCFC-123 with triangular-pitch tube bundles made from an enhanced boiling tube, an enhanced condensation tube, and a plain surface tube. Lubricant effects testing was conducted at refrigerant supply rates of 25 kg/min and 35 kg/min and oil concentrations of 1.1 % and 2.5 %.

Heat Transfer performance was found to be approximately 50 % lower with the plain-surface tube bundle in the HCFC-123 testing than that found with HFC-134a. The Tu-B bundle performed the best with HCFC-123 of the three surfaces evaluated. It should be noted that the Tu-Cii bundle performed better with HFC-134a, but with HCFC-123 the reverse was true.

Although the lowest refrigerant supply rate used with HCFC-123 provided overfeed ratios greater than those used in the HFC-134a testing, dryout was experienced with this refrigerant. It is likely that the dryout is a result of the higher viscosity of HCFC-123 in comparison with HFC-134a. In the temperature range used in this study, the viscosity of HCFC-123 is twice that of either HFC-134a or HCFC-22.

Oil concentrations of 1.1 % and 2.5 % were found to decrease heat transfer performance for the Tu-B bundle through the entire heat flux range evaluated. Heat transfer performance was reduced up to 33 % at the 2.5 % oil concentration with the Tu-B bundle in comparison with pure refrigerant results. Small concentrations of oil improved the heat transfer performance nearly 50 % for the plain-surface and Tu-Cii bundles in the lower heat flux range. However, in the upper heat flux range the heat transfer performance for the plain-surface bundle was found to be up to 25 % less than that found in the pure refrigerant testing.

Correlation Comparison A comparison was made of the data taken on the bundle test facility with existing correlations. It was concluded that correlations which were developed in studies conducted with fluids other than non-hydrocarbon refrigerants should not be used to predict the performance of hydrocarbons. One study conducted by Danilova et al. [1] with CFC and HCFC refrigerants generated both boiling and nonboiling correlations. The boiling correlation predicted HFC-134a plain-surface bundle data within 25 %. This correlation is believed to be the best in existence to date for use with hydrocarbon refrigerants.

Recommendations

Several important areas for future research have evolved during this project. Research is needed in all aspects of film-wise heat transfer with small concentrations of oil due to the lack of existing information in this area. The following recommendations for future research focus on developing a better understanding of the spray evaporation heat transfer process.

1. Conducting bundle heat transfer analysis at overfeed ratios higher than those used in this study to determine what overfeed ratios are required to completely eliminate film breakdown in the lower bundle rows.
2. Evaluate important thermodynamic and transport properties of refrigerant/oil mixtures. Without this information it is not possible to nondimensionalize the models which predict spray evaporation heat transfer performance.
3. Further single-tube work is required over a wider Reynolds number range and a variety of saturation temperatures to better develop design correlations. It is not recommended to use a spray distribution system for single-tube work, because a significant percentage of the liquid supplied to the test section does not contact the surface of the tube. A thin-slot or perforated tube distributor will adequately simulate the drip-off received in a tube bundle.
4. The Tu-B tube performed the best with HCFC-123 while the Tu-Cii tube performed the best with HFC-134a. More research should be conducted evaluating the effects of various surface micro-structures on heat transfer

performance. Since the tubes evaluated in this study are commercially available condensation and pool-boiling surfaces, it is likely that further improvements could be made by optimizing a surface for the spray-evaporation environment.

5. The majority of the existing pool-boiling studies focus on the macroscopic effects of oil rather than the microstructure of a two-phase, binary-mixture heat transfer mechanism. This is most likely so because foaming only occurs in the uppermost rows of a tube bundle. Therefore, this information is of less importance in pool-boiling than spray evaporation heat transfer analysis. A better understanding of the foaming phenomenon and its effects upon the heat transfer process will greatly benefit the development of spray evaporation chillers.

BIBLIOGRAPHY

- [1] Danilova, B.G., V.G. Burkin, and V.A. Dyundin. "Heat transfer spray-type refrigerator evaporators." *Heat Transfer-Soviet Research* 8, no. 6 (1976): 105-113.
- [2] Lorenz, J.J. and D. Yung. "A note on combined boiling and evaporation of liquid films on horizontal tubes." *ASME Journal of Heat Transfer* 101 (1979): 178-180.
- [3] Parken, W.H., L.S. Fletcher, V. Sernas, and J.C. Han. "Heat transfer through falling film evaporation and boiling on horizontal tubes." *ASME Journal of Heat Transfer* 112 (1990): 744-750.
- [4] Chyu, M.C. and A.E. Bergles. "An analytical and experimental study of falling-film evaporation on a horizontal tube." *ASME Journal of Heat Transfer* 109 (1987): 983-990.
- [5] Chyu, M.C. and A.E. Bergles. "Horizontal-tube falling-film evaporation with structured surfaces." *ASME Journal of Heat Transfer* 111 (1989): 518-524.
- [6] Chyu, M.C. and A.E. Bergles. "Enhancement of horizontal tube spray film evaporators by structured surfaces." Paper presented at the 23rd National Heat Transfer Conference, Denver, Colorado, August, 1985.
- [7] Chyu, M.C., A.E. Bergles, and F. Mayinger. "Enhancement of horizontal tube spray film evaporators." *Heat Transfer 1982, Proceedings of the 7th International Heat Transfer Conference* 6 (1982): 275-280.
- [8] Han, J. and L.S. Fletcher. "Falling film evaporation and boiling in circumferential and axial grooves on horizontal tubes." *Industrial & Engineering Chemistry Process Design and Development* 24, no. 3 (1985): 570-575.

- [9] Nakayama, W., T. Daikoku, and T. Nakajima. "Enhancement of boiling and evaporation on structured surfaces with gravity driven film of R-11." *Heat Transfer 1982, Proceedings of the 7th International Heat Transfer Conference 4* (1982): 409-414.
- [10] Conti, R.J. "Experimental investigation of horizontal-tube ammonia film evaporators with small temperature differentials." *Proceedings of the Fifth Ocean Thermal Energy Conversion Conference 6* (1978): 161-180.
- [11] Lorenz, J.J. and D. Yung. "Film breakdown and bundle-depth effects in horizontal-tube, falling-film evaporators." *ASME Journal of Heat Transfer* 104 (1982): 569-571.
- [12] Mitrovic, J. "Influence of tube spacing and flow rate on heat transfer from a horizontal tube to a falling liquid film." *Proceedings of the 8th International Heat Transfer Conference 4* (1986): 1949-1956.
- [13] Hillis, D.L., J.J. Lorenz, D.T. Yung, and N.F. Sather. "OTEC performance tests of the Union Carbide sprayed-bundle evaporator." Department of Energy Report ANL/OTEC-PS-3, May, 1979.
- [14] Czikk, A.M., H.D. Fricke, E.N. Ganic, and B.I. Sharma. "Fluid dynamic and heat transfer studies of OTEC heat exchangers." *Proceedings of the Fifth Ocean Thermal Energy Conversion Conference 6* (1978): 181-236.
- [15] Chyu, M.C. and A.E. Bergles. "Falling film evaporation on a horizontal tube." Paper presented at the 23rd National Heat Transfer Conference, Denver, Colorado, 1985.
- [16] Chun, K.R. and R.A. Seban. "Performance prediction of falling-film evaporators." *ASME Journal of Heat Transfer* (1972): 432-436.
- [17] Rohsenow, W.M. "A method of correlating heat transfer data for surface boiling of liquids." *Transactions of the ASME* 74, no. 6 (1952).
- [18] Rohsenow, W.M. "Discussion on the Rohsenow pool boiling correlation." *ASME Journal of Heat Transfer* 94 (1971).
- [19] Owens, W.L. "Correlation of thin film evaporation heat transfer coefficients for horizontal tubes." ASME Paper 78-WA/HT-67, 1978.
- [20] Liu, P.J. "The evaporating falling film on horizontal tubes." Ph.D. diss., University of Wisconsin, Madison, Wisconsin, 1975.

- [21] Parizhskiy, O.V., V.P. Chepurnenko, L.F. Lagota, and L.F. Taranets. "Study of boiling heat transfer with a falling film of refrigerant." *Heat Transfer-Soviet Research* 4, no. 4 (1972): 43-47.
- [22] Chaddock, J.B. "Influence of oil on refrigerant evaporator performance." *ASHRAE Transactions* 82 (1976).
- [23] Dougherty, R.L. and H.J. Sauer. "Nucleate pool boiling of refrigerant-oil mixtures from tube." *ASHRAE Transactions* 80 (1975).
- [24] Sauer, H.J., R.K. Gibson, and S. Chongrungreong. "Influence of oil on the nucleate boiling performance of refrigerants." Paper presented at the 6th International Heat Transfer Conference, Toronto, Ontario, 1978.
- [25] Stephan, K. and J. Mitrovic. "Heat transfer in natural convective boiling of refrigerants and refrigerant-oil mixtures in bundles of T-shaped finned tubes." *Advances in Enhanced Heat Transfer* 18 (1981): 131-146.
- [26] Stephan, K. and J. Mitrovic. "Heat transfer in natural convective boiling of refrigerant-oil mixtures." *Proceedings of the Seventh International Heat Transfer Conference* 4 (1982): 73-87.
- [27] Wanniarachchi, A.S., P.J. Marto, and J.T. Reilly. "The effect of oil contamination on the nucleate pool-boiling performance of R-114 from a porous-coated surface." *ASHRAE Transactions* 92 (1986).
- [28] Sauer, H.J., G.W. Davidson, and S. Chongrungreong. "Nucleate boiling of refrigerant-oil mixtures from finned tubing." Paper presented at the Joint ASME/AIChE National Heat Transfer Conference, Orlando, Florida, July, 1980.
- [29] Chongrungreong, S. and H.J. Sauer. "Nucleate boiling performance of refrigerants and refrigerant-oil mixtures." *ASME Journal of Heat Transfer* 102 (1980): 701-705.
- [30] Webb, R.L. and W.F. McQuade. "Pool boiling of R-11 and R-123 oil-refrigerant mixtures on plain and enhanced tube geometries." *ASHRAE Transactions* 99, no. 1 (1993): 1225-1236.
- [31] Jensen, M.K. and D.L. Jackman. "Prediction of nucleate pool boiling heat transfer coefficients of refrigerant-oil mixtures." *ASME Journal of Heat Transfer* 106 (1984): 184-190.
- [32] Webb, R.L., and C. Pais. "Pool boiling data for five refrigerants on three tube geometries." *ASHRAE Transactions* 97, no. 1 (1991): 72-78.

- [33] Surface: W-SE, See Wieland Product Literature for the GEWA-SE Surface. (1993).
- [34] Surface: W-SC, See Wieland Product Literature for the GEWA-SC Surface. (1993).
- [35] Surface: Tu-B, See Wolverine Product Literature for the Turbo-B Surface. (1993).
- [36] Surface: Tu-Cii, See Wolverine Product Literature for the Turbo-Cii Surface. (1993).
- [37] Surface: W-26 fpi, See Wolverine Product Literature for the Wolverine 26 fpi Surface. (1993).
- [38] Surface: W-40 fpi, See Wolverine Product Literature for the Wolverine 40 fpi Surface. (1993).
- [39] Surface: Plain, See Wieland Product Literature for Annealed, Plain Surface Tube. (1993).
- [40] Huber, J.B., L.E. Rewerts, and M.B. Pate. "Shell-Side Condensation Heat Transfer of R-134a Part 1: Finned Tube Performance." Paper presented at the ASHRAE Summer Conference, Orlando, Florida, June, 1994.
- [41] Glamm, P. 1993. Personal communication.
- [42] Huber, J.B., L.E. Rewerts, and M.B. Pate. "Shell-Side Condensation Heat Transfer of R-134a Part 2: Enhanced Tube Performance." Paper presented at the ASHRAE Summer Conference, Orlando, Florida, 1994.
- [43] ASHRAE. 1984. *ANSI/ASHRAE Standard 41.4-1984, Standard method for measurements of proportion of oil in liquid refrigerant*. Atlanta: American Society of Heating, Refrigerating, and Air-Conditioning Engineers, Inc.
- [44] Incropera, F.P., and D.P. De Witt. Fundamentals of Heat and Mass Transfer (Third Edition), New York: Wiley, 1990.
- [45] Beckwith, T.G., N.L. Buck, and R.D. Marangoni. Mechanical Measurements, Reading, Massachusetts: Addison-Wesley Publishing Company, 1982.
- [46] Eckels, S.J., T.M. Doerr, and M.B. Pate. "Heat transfer and pressure drop during condensation and evaporation of R-134a/oil mixtures in smooth and micro-fin tubes." Ph.D. dissertation, Iowa State University, 1993.

- [47] Kang H.M., S.C. Zoz, and M.B. Pate. "Solubility of HFC-32, HFC-125, and HFC-134a with three potential lubricants." Paper presented at the International Refrigeration Conference, Purdue University, 1994.
- [48] Stephan, K., and M. Abdelsalam. "Heat transfer correlations for natural convection boiling." *Int. J. Heat Mass Transfer* 23: pp.73-87.
- [49] Zeng, X., M.C. Chyu, and Z.H. Ayub. "Characteristic study of sprayed fluid in a tube bundle." Paper presented at the Winter ASHRAE Conference, New Orleans, LA, January, 1994.
- [50] Webb, R.L., and C. Pais. "Nucleate pool boiling data for five refrigerants on plain, integral-fin and enhanced tube geometries." *Int. J. Heat Mass Transfer* 35, no. 8 (1992): 1893-1904.

ACKNOWLEDGMENTS

This work was sponsored by the American Society of Heating, Refrigerating and Air-Conditioning Engineers as research project RP-668. The advise and technical guidance of Committee TC1.3, Heat Transfer and Fluid Flow, was greatly appreciated. Special appreciation is given to the ASHRAE Oversight Committee (Mr. Paul Glamm, Mr. Keith Starner, and Dr. Zahid Ayub).

The support of the Department of Mechanical Engineering, and the Engineering Research Institute at Iowa State University is also greatly appreciated by the authors.

APPENDIX A. MULTI-TUBE TEST FACILITY TABULATED DATA

The experimental data from the 19.1 mm diameter tube, HFC-134a tests conducted on the multi-tube test facility are reported in this Appendix. These results are presented and discussed in Chapter 8. The pure refrigerant results from surfaces not evaluated in the lubricant effects testing are presented first, and are followed by the 160 SUS and 340 SUS viscosity, polyol-ester oil lubricant effects testing results.

The data reported for each run are the wall heat flux, the average shell-side heat transfer coefficient, and the average wall superheat. The method used for calculating the average shell-side heat transfer coefficient is presented in Chapter 5. The heat flux was calculated with a watt transducer reading and the active heater length of the cartridge heater. The average shell-side heat transfer coefficient is based upon a nominal 19.1 mm diameter for all results presented in this Appendix.

The film-feed supply rate used in this testing was $1.26\text{E-}02$ kg/(s*m) corresponding to a refrigerant supply rate of 2.8 kg/min. Similar to the wall heat flux, this film-feed supply rate is based upon the active length of the cartridge heater, and was calculated from the known mass flow rate of refrigerant supplied to the spray manifold and collector test results. Collector testing was performed in parallel with the heat transfer analysis experiments.

Table A.1 Refrigerant: HFC-134a, Plain Surface, Diameter: 19.1 mm,
Pool Boiling, T-sat: 2.0 °C, Pure Refrigerant Testing

| q'' ($\frac{kW}{m^2}$) | h ($\frac{kW}{m^2 \cdot K}$) | $T_w - T_r$ (°K) |
|-------------------------------|-------------------------------------|---------------------|
| 5.13 | 1.74 | 2.95 |
| 10.20 | 2.63 | 3.88 |
| 15.26 | 3.29 | 4.63 |
| 20.19 | 3.75 | 5.38 |
| 25.26 | 4.14 | 6.11 |
| 29.97 | 4.49 | 6.67 |
| 35.38 | 4.85 | 7.29 |
| 40.35 | 5.14 | 7.84 |

Table A.2 Refrigerant: HFC-134a, W-26 fpi Surface, Diameter: 19.1 mm,
Film Feed Supply Rate: 1.26E-02 kg/(s*m), T-sat: 2.0 °C,
Pure Refrigerant Testing

| q'' ($\frac{kW}{m^2}$) | h ($\frac{kW}{m^2 \cdot K}$) | $T_w - T_r$ (°K) |
|-------------------------------|-------------------------------------|---------------------|
| 10.23 | 7.68 | 1.33 |
| 14.86 | 7.52 | 1.98 |
| 20.05 | 7.49 | 2.68 |
| 25.36 | 7.53 | 3.37 |
| 30.08 | 7.44 | 4.04 |
| 35.32 | 7.32 | 4.82 |
| 40.28 | 6.01 | 6.70 |

Table A.3 Refrigerant: HFC-134a, Tu-B Surface, Diameter: 19.1 mm,
Film Feed Supply Rate: 1.26E-02 kg/(s*m), T-sat: 2.0 °C,
Pure Refrigerant Testing

| q'' ($\frac{kW}{m^2}$) | h ($\frac{kW}{m^2 \cdot K}$) | $T_w - T_r$ (°K) |
|-------------------------------|-------------------------------------|---------------------|
| 5.06 | 8.29 | 0.61 |
| 10.37 | 9.43 | 1.10 |
| 15.37 | 9.19 | 1.67 |
| 20.37 | 8.41 | 2.42 |
| 25.33 | 7.74 | 3.27 |
| 30.37 | 7.45 | 4.08 |
| 35.18 | 7.39 | 4.76 |
| 41.15 | 5.35 | 7.68 |

Table A.4 Refrigerant: HFC-134a, W-SE Surface, Diameter: 19.1 mm,
Film Feed Supply Rate: 1.26E-02 kg/(s*m), T-sat: 2.0 °C,
Pure Refrigerant Testing

| q'' ($\frac{\text{kW}}{\text{m}^2}$) | h ($\frac{\text{kW}}{\text{m}^2 \cdot \text{K}}$) | $T_w - T_r$ ($^{\circ}\text{K}$) |
|---|--|---------------------------------------|
| 5.27 | 7.57 | 0.70 |
| 10.25 | 7.75 | 1.32 |
| 15.32 | 8.28 | 1.85 |
| 20.04 | 8.54 | 2.35 |
| 25.42 | 8.55 | 2.97 |
| 30.23 | 8.49 | 3.56 |
| 35.55 | 8.45 | 4.21 |
| 40.98 | 6.92 | 5.92 |

Table A.5 Refrigerant: HFC-134a, W-SC Surface, Diameter: 19.1 mm,
Film Feed Supply Rate: 1.26E-02 kg/(s*m), T-sat: 2.0 °C,
Pure Refrigerant Testing

| q'' ($\frac{\text{kW}}{\text{m}^2}$) | h ($\frac{\text{kW}}{\text{m}^2 \cdot \text{K}}$) | $T_w - T_r$ ($^{\circ}\text{K}$) |
|---|--|---------------------------------------|
| 5.09 | 9.24 | 0.55 |
| 10.18 | 9.23 | 1.10 |
| 15.16 | 9.56 | 1.59 |
| 20.37 | 9.40 | 2.17 |
| 25.44 | 8.84 | 2.88 |
| 30.31 | 8.76 | 3.46 |
| 35.33 | 8.74 | 4.04 |
| 41.34 | 8.51 | 4.86 |

Table A.6 Refrigerant: HFC-134a, Plain Surface, Diameter: 19.1 mm,
Film Feed Supply Rate: 1.26E-02 kg/(s*m), P-sat: 314.5 kPa,
Lubricant Concentration: 0.0 % (160 SUS oil testing)

| q'' ($\frac{\text{kW}}{\text{m}^2}$) | h ($\frac{\text{kW}}{\text{m}^2 \cdot \text{K}}$) | $T_w - T_r$ ($^{\circ}\text{K}$) |
|---|--|---------------------------------------|
| 5.21 | 1.95 | 2.67 |
| 10.33 | 2.70 | 3.83 |
| 15.30 | 3.25 | 4.71 |
| 20.37 | 3.63 | 5.62 |
| 25.39 | 3.75 | 6.77 |
| 30.56 | 3.69 | 8.29 |
| 35.56 | 3.36 | 10.58 |
| 40.73 | 2.49 | 16.38 |

Table A.7 Refrigerant: HFC-134a, Plain Surface, Diameter: 19.1 mm,
 Film Feed Supply Rate: 1.26E-02 kg/(s*m), P-sat: 314.5 kPa,
 Lubricant Concentration: 1.0 % (160 SUS oil testing)

| q'' ($\frac{kW}{m^2}$) | h ($\frac{kW}{m^2 \cdot K}$) | $T_w - T_r$ ($^{\circ}K$) |
|-------------------------------|-------------------------------------|--------------------------------|
| 5.29 | 2.09 | 2.53 |
| 10.19 | 2.83 | 3.61 |
| 15.34 | 3.43 | 4.48 |
| 20.40 | 3.92 | 5.20 |
| 25.49 | 4.37 | 5.84 |
| 30.43 | 4.75 | 6.41 |
| 35.34 | 5.05 | 7.00 |
| 39.33 | 4.84 | 8.12 |

Table A.8 Refrigerant: HFC-134a, Plain Surface, Diameter: 19.1 mm,
 Film Feed Supply Rate: 1.26E-02 kg/(s*m), P-sat: 314.5 kPa,
 Lubricant Concentration: 2.0 % (160 SUS oil testing)

| q'' ($\frac{kW}{m^2}$) | h ($\frac{kW}{m^2 \cdot K}$) | $T_w - T_r$ ($^{\circ}K$) |
|-------------------------------|-------------------------------------|--------------------------------|
| 5.25 | 3.41 | 1.54 |
| 10.43 | 4.25 | 2.45 |
| 15.39 | 4.87 | 3.16 |
| 20.43 | 5.30 | 3.85 |
| 25.49 | 5.61 | 4.55 |
| 30.33 | 5.81 | 5.22 |
| 35.31 | 5.99 | 5.90 |
| 37.98 | 5.84 | 6.50 |

Table A.9 Refrigerant: HFC-134a, Plain Surface, Diameter: 19.1 mm,
 Film Feed Supply Rate: 1.26E-02 kg/(s*m), P-sat: 314.5 kPa,
 Lubricant Concentration: 3.0 % (160 SUS oil testing)

| q'' ($\frac{kW}{m^2}$) | h ($\frac{kW}{m^2 \cdot K}$) | $T_w - T_r$ ($^{\circ}K$) |
|-------------------------------|-------------------------------------|--------------------------------|
| 5.22 | 4.13 | 1.27 |
| 10.66 | 4.84 | 2.20 |
| 15.36 | 5.24 | 2.93 |
| 20.66 | 5.58 | 3.70 |
| 25.61 | 5.82 | 4.40 |
| 30.62 | 5.87 | 5.22 |
| 35.30 | 5.15 | 6.85 |

Table A.10 Refrigerant: HFC-134a, W-40 fpi Surface, Diameter: 19.1 mm,
Film Feed Supply Rate: 1.26E-02 kg/(s*m), P-sat: 314.5 kPa,
Lubricant Concentration: 0.0 % (160 SUS oil testing)

| q'' $\left(\frac{\text{kW}}{\text{m}^2}\right)$ | h $\left(\frac{\text{kW}}{\text{m}^2 \cdot \text{K}}\right)$ | $T_w - T_r$ $(^\circ\text{K})$ |
|--|---|-----------------------------------|
| 10.28 | 7.00 | 1.47 |
| 15.35 | 6.92 | 2.22 |
| 20.40 | 6.87 | 2.97 |
| 25.44 | 6.83 | 3.72 |
| 30.32 | 6.82 | 4.44 |
| 35.14 | 6.64 | 5.29 |
| 39.73 | 5.30 | 7.50 |

Table A.11 Refrigerant: HFC-134a, W-40 fpi Surface, Diameter: 19.1 mm,
Film Feed Supply Rate: 1.26E-02 kg/(s*m), P-sat: 314.5 kPa,
Lubricant Concentration: 1.0 % (160 SUS oil testing)

| q'' $\left(\frac{\text{kW}}{\text{m}^2}\right)$ | h $\left(\frac{\text{kW}}{\text{m}^2 \cdot \text{K}}\right)$ | $T_w - T_r$ $(^\circ\text{K})$ |
|--|---|-----------------------------------|
| 10.45 | 8.35 | 1.25 |
| 15.20 | 8.49 | 1.79 |
| 20.36 | 8.93 | 2.28 |
| 25.51 | 9.30 | 2.74 |
| 30.67 | 9.53 | 3.22 |
| 35.34 | 9.45 | 3.74 |
| 39.70 | 9.58 | 4.15 |

Table A.12 Refrigerant: HFC-134a, W-40 fpi Surface, Diameter: 19.1 mm,
Film Feed Supply Rate: 1.26E-02 kg/(s*m), P-sat: 314.5 kPa,
Lubricant Concentration: 2.0 % (160 SUS oil testing)

| q'' $\left(\frac{\text{kW}}{\text{m}^2}\right)$ | h $\left(\frac{\text{kW}}{\text{m}^2 \cdot \text{K}}\right)$ | $T_w - T_r$ $(^\circ\text{K})$ |
|--|---|-----------------------------------|
| 10.47 | 9.75 | 1.07 |
| 15.38 | 9.30 | 1.65 |
| 20.51 | 9.58 | 2.14 |
| 25.26 | 9.68 | 2.61 |
| 30.55 | 9.82 | 3.11 |
| 35.61 | 9.97 | 3.57 |
| 40.33 | 10.12 | 3.98 |

Table A.13 Refrigerant: HFC-134a, W-40 fpi Surface, Diameter: 19.1 mm,
Film Feed Supply Rate: 1.26E-02 kg/(s*m), P-sat: 314.5 kPa,
Lubricant Concentration: 3.0 % (160 SUS oil testing)

| q'' $\left(\frac{\text{kW}}{\text{m}^2}\right)$ | h $\left(\frac{\text{kW}}{\text{m}^2 \cdot \text{K}}\right)$ | $T_w - T_r$ $(^\circ\text{K})$ |
|--|---|-----------------------------------|
| 10.40 | 10.24 | 1.02 |
| 15.16 | 10.05 | 1.51 |
| 20.60 | 9.81 | 2.10 |
| 25.67 | 9.93 | 2.59 |
| 30.74 | 9.79 | 3.14 |
| 35.41 | 9.95 | 3.56 |
| 39.64 | 9.97 | 3.98 |

Table A.14 Refrigerant: HFC-134a, Tu-Cii Surface, Diameter: 19.1 mm,
Film Feed Supply Rate: 1.26E-02 kg/(s*m), P-sat: 314.5 kPa,
Lubricant Concentration: 0.0 % (160 SUS oil testing)

| q'' $\left(\frac{\text{kW}}{\text{m}^2}\right)$ | h $\left(\frac{\text{kW}}{\text{m}^2 \cdot \text{K}}\right)$ | $T_w - T_r$ $(^\circ\text{K})$ |
|--|---|-----------------------------------|
| 5.33 | 7.79 | 0.68 |
| 10.30 | 8.77 | 1.18 |
| 15.51 | 9.66 | 1.61 |
| 20.37 | 10.10 | 2.02 |
| 25.87 | 10.27 | 2.52 |
| 30.79 | 10.03 | 3.07 |
| 35.70 | 9.58 | 3.73 |
| 40.72 | 8.03 | 5.08 |

Table A.15 Refrigerant: HFC-134a, Tu-Cii Surface, Diameter: 19.1 mm,
Film Feed Supply Rate: 1.26E-02 kg/(s*m), P-sat: 314.5 kPa,
Lubricant Concentration: 1.0 % (160 SUS oil testing)

| q'' $\left(\frac{\text{kW}}{\text{m}^2}\right)$ | h $\left(\frac{\text{kW}}{\text{m}^2 \cdot \text{K}}\right)$ | $T_w - T_r$ $(^\circ\text{K})$ |
|--|---|-----------------------------------|
| 5.21 | 7.89 | 0.66 |
| 10.16 | 8.54 | 1.19 |
| 14.96 | 9.39 | 1.59 |
| 20.43 | 10.23 | 2.00 |
| 25.39 | 10.89 | 2.33 |
| 30.57 | 11.37 | 2.69 |
| 35.38 | 11.65 | 3.04 |
| 40.60 | 12.07 | 3.36 |

Table A.16 Refrigerant: HFC-134a, Tu-Cii Surface, Diameter: 19.1 mm,
 Film Feed Supply Rate: 1.26E-02 kg/(s*m), P-sat: 314.5 kPa,
 Lubricant Concentration: 2.0 % (160 SUS oil testing)

| q'' ($\frac{kW}{m^2}$) | h ($\frac{kW}{m^2 \cdot K}$) | $T_w - T_r$ ($^{\circ}K$) |
|-------------------------------|-------------------------------------|--------------------------------|
| 5.30 | 10.09 | 0.53 |
| 10.41 | 10.34 | 1.01 |
| 15.46 | 10.70 | 1.45 |
| 20.47 | 11.31 | 1.81 |
| 25.52 | 11.58 | 2.20 |
| 30.77 | 12.00 | 2.57 |
| 35.43 | 12.20 | 2.91 |
| 39.95 | 12.28 | 3.25 |

Table A.17 Refrigerant: HFC-134a, Tu-Cii Surface, Diameter: 19.1 mm,
 Film Feed Supply Rate: 1.26E-02 kg/(s*m), P-sat: 314.5 kPa,
 Lubricant Concentration: 3.0 % (160 SUS oil testing)

| q'' ($\frac{kW}{m^2}$) | h ($\frac{kW}{m^2 \cdot K}$) | $T_w - T_r$ ($^{\circ}K$) |
|-------------------------------|-------------------------------------|--------------------------------|
| 5.34 | 10.12 | 0.53 |
| 10.32 | 11.32 | 0.91 |
| 15.46 | 11.48 | 1.35 |
| 20.33 | 11.49 | 1.77 |
| 25.24 | 11.67 | 2.16 |
| 30.55 | 11.72 | 2.61 |
| 35.65 | 11.49 | 3.10 |
| 40.52 | 10.21 | 3.97 |

Table A.18 Refrigerant: HFC-134a, W-40 fpi Surface, Diameter: 19.1 mm,
 Film Feed Supply Rate: 1.26E-02 kg/(s*m), P-sat: 314.5 kPa,
 Lubricant Concentration: 0.0 % (340 SUS oil testing)

| q'' ($\frac{kW}{m^2}$) | h ($\frac{kW}{m^2 \cdot K}$) | $T_w - T_r$ ($^{\circ}K$) |
|-------------------------------|-------------------------------------|--------------------------------|
| 10.53 | 6.40 | 1.65 |
| 15.38 | 6.67 | 2.31 |
| 20.16 | 6.81 | 2.96 |
| 25.41 | 6.84 | 3.72 |
| 30.72 | 6.59 | 4.67 |
| 35.62 | 6.38 | 5.58 |

Table A.19 Refrigerant: HFC-134a, W-40 fpi Surface, Diameter: 19.1 mm,
 Film Feed Supply Rate: 1.26E-02 kg/(s*m), P-sat: 314.5 kPa,
 Lubricant Concentration: 0.5 % (340 SUS oil testing)

| q'' $\left(\frac{\text{kW}}{\text{m}^2}\right)$ | h $\left(\frac{\text{kW}}{\text{m}^2 \cdot \text{K}}\right)$ | $T_w - T_r$ $(^\circ\text{K})$ |
|--|---|-----------------------------------|
| 10.35 | 7.31 | 1.42 |
| 15.46 | 7.58 | 2.04 |
| 20.42 | 7.91 | 2.58 |
| 25.60 | 8.24 | 3.11 |
| 30.43 | 8.33 | 3.66 |
| 35.52 | 8.39 | 4.24 |

Table A.20 Refrigerant: HFC-134a, W-40 fpi Surface, Diameter: 19.1 mm,
 Film Feed Supply Rate: 1.26E-02 kg/(s*m), P-sat: 314.5 kPa,
 Lubricant Concentration: 1.0 % (340 SUS oil testing)

| q'' $\left(\frac{\text{kW}}{\text{m}^2}\right)$ | h $\left(\frac{\text{kW}}{\text{m}^2 \cdot \text{K}}\right)$ | $T_w - T_r$ $(^\circ\text{K})$ |
|--|---|-----------------------------------|
| 10.54 | 7.76 | 1.36 |
| 15.45 | 8.39 | 1.84 |
| 20.37 | 8.61 | 2.37 |
| 25.57 | 9.17 | 2.79 |
| 30.19 | 9.29 | 3.25 |
| 35.73 | 9.54 | 3.74 |

Table A.21 Refrigerant: HFC-134a, W-40 fpi Surface, Diameter: 19.1 mm,
 Film Feed Supply Rate: 1.26E-02 kg/(s*m), P-sat: 314.5 kPa,
 Lubricant Concentration: 3.0 % (340 SUS oil testing)

| q'' $\left(\frac{\text{kW}}{\text{m}^2}\right)$ | h $\left(\frac{\text{kW}}{\text{m}^2 \cdot \text{K}}\right)$ | $T_w - T_r$ $(^\circ\text{K})$ |
|--|---|-----------------------------------|
| 10.54 | 9.55 | 1.11 |
| 15.36 | 8.97 | 1.71 |
| 20.43 | 9.09 | 2.25 |
| 25.62 | 9.19 | 2.79 |
| 30.79 | 9.21 | 3.34 |
| 35.46 | 9.14 | 3.88 |

Table A.22 Refrigerant: HFC-134a, W-40 fpi Surface, Diameter: 19.1 mm,
 Film Feed Supply Rate: 1.26E-02 kg/(s*m), P-sat: 314.5 kPa,
 Lubricant Concentration: 5.0 % (340 SUS oil testing)

| q'' ($\frac{kW}{m^2}$) | h ($\frac{kW}{m^2 \cdot K}$) | $T_w - T_r$ ($^{\circ}K$) |
|-------------------------------|-------------------------------------|--------------------------------|
| 10.66 | 8.76 | 1.23 |
| 15.53 | 8.98 | 1.73 |
| 20.65 | 8.95 | 2.31 |
| 25.48 | 8.72 | 2.92 |
| 30.43 | 8.37 | 3.64 |
| 35.62 | 7.92 | 4.50 |

Table A.23 Refrigerant: HFC-134a, Tu-Cii Surface, Diameter: 19.1 mm,
 Film Feed Supply Rate: 1.26E-02 kg/(s*m), P-sat: 314.5 kPa,
 Lubricant Concentration: 0.0 % (340 SUS oil testing)

| q'' ($\frac{kW}{m^2}$) | h ($\frac{kW}{m^2 \cdot K}$) | $T_w - T_r$ ($^{\circ}K$) |
|-------------------------------|-------------------------------------|--------------------------------|
| 5.54 | 7.97 | 0.70 |
| 10.60 | 8.27 | 1.29 |
| 15.49 | 8.51 | 1.82 |
| 20.60 | 8.80 | 2.34 |
| 25.53 | 8.89 | 2.87 |
| 30.44 | 8.85 | 3.44 |
| 35.24 | 8.46 | 4.16 |

Table A.24 Refrigerant: HFC-134a, Tu-Cii Surface, Diameter: 19.1 mm,
 Film Feed Supply Rate: 1.26E-02 kg/(s*m), P-sat: 314.5 kPa,
 Lubricant Concentration: 0.5 % (340 SUS oil testing)

| q'' ($\frac{kW}{m^2}$) | h ($\frac{kW}{m^2 \cdot K}$) | $T_w - T_r$ ($^{\circ}K$) |
|-------------------------------|-------------------------------------|--------------------------------|
| 5.26 | 9.99 | 0.53 |
| 10.33 | 10.27 | 1.01 |
| 15.11 | 10.59 | 1.43 |
| 20.47 | 11.16 | 1.83 |
| 25.54 | 11.53 | 2.21 |
| 30.79 | 11.95 | 2.58 |
| 35.32 | 12.36 | 2.86 |

Table A.25 Refrigerant: HFC-134a, Tu-Cii Surface, Diameter: 19.1 mm,
 Film Feed Supply Rate: 1.26E-02 kg/(s*m), P-sat: 314.5 kPa,
 Lubricant Concentration: 1.0 % (340 SUS oil testing)

| q'' ($\frac{kW}{m^2}$) | h ($\frac{kW}{m^2 \cdot K}$) | $T_w - T_r$ ($^{\circ}K$) |
|-------------------------------|-------------------------------------|--------------------------------|
| 5.27 | 8.88 | 0.60 |
| 10.53 | 9.54 | 1.10 |
| 15.37 | 10.46 | 1.47 |
| 20.68 | 11.32 | 1.83 |
| 25.56 | 11.98 | 2.13 |
| 30.66 | 12.85 | 2.39 |
| 35.55 | 13.03 | 2.73 |

Table A.26 Refrigerant: HFC-134a, Tu-Cii Surface, Diameter: 19.1 mm,
 Film Feed Supply Rate: 1.26E-02 kg/(s*m), P-sat: 314.5 kPa,
 Lubricant Concentration: 3.0 % (340 SUS oil testing)

| q'' ($\frac{kW}{m^2}$) | h ($\frac{kW}{m^2 \cdot K}$) | $T_w - T_r$ ($^{\circ}K$) |
|-------------------------------|-------------------------------------|--------------------------------|
| 5.37 | 9.61 | 0.57 |
| 10.23 | 11.69 | 0.88 |
| 15.15 | 13.27 | 1.15 |
| 20.71 | 13.26 | 1.57 |
| 25.45 | 13.13 | 1.94 |
| 30.37 | 12.87 | 2.36 |
| 35.68 | 12.43 | 2.87 |

Table A.27 Refrigerant: HFC-134a, Tu-Cii Surface, Diameter: 19.1 mm,
 Film Feed Supply Rate: 1.26E-02 kg/(s*m), P-sat: 314.5 kPa,
 Lubricant Concentration: 5.0 % (340 SUS oil testing)

| q'' ($\frac{kW}{m^2}$) | h ($\frac{kW}{m^2 \cdot K}$) | $T_w - T_r$ ($^{\circ}K$) |
|-------------------------------|-------------------------------------|--------------------------------|
| 5.19 | 10.01 | 0.54 |
| 10.61 | 11.70 | 0.92 |
| 15.60 | 12.58 | 1.24 |
| 20.70 | 12.55 | 1.65 |
| 25.49 | 11.60 | 2.20 |
| 30.58 | 10.87 | 2.81 |
| 35.38 | 9.86 | 3.59 |

APPENDIX B. BUNDLE TEST FACILITY HFC-134a TABULATED DATA

The experimental data from HFC-134a tests conducted on the bundle test facility are reported in this Appendix. The pure HFC-134a results from the film feed supply rate effects testing along with the surface enhancement and bundle geometry effects testing are presented first in Tables B.1 to B.22. These data are followed by results from the nozzle configuration geometry effects testing conducted with the W-40 fpi bundle, which are shown in Tables B.23 to B.30. Pool-boiling results for the W-40 fpi and Tu-B bundles are presented in Tables B.31 and B.32. Finally, data from the lubricant effects testing done with a 340 SUS polyol-ester oil are presented in Tables B.33 to B.48. These HFC-134a results are presented and discussed in Chapters 9, 10 and 11.

Bundle and row heat transfer coefficients are presented for each run. These heat transfer coefficients are based upon the nominal cylindrical area over the shell-side surface enhancement or low-finned structure for a given tube. Geometric specifications for the tubes used in this work are presented in Table 4.1. The method used for the calculation of these shell-side heat transfer coefficients is presented in Chapter 5.

The bundle overfeed ratio and the film-feed supply rate seen by the fourth (bottom) row of the tube bundle are presented at the respective wall heat fluxes for all tests except those done during the nozzle configuration geometry effects testing, shown in Tables B.23 to B.30. Pure HFC-134a results presented in Tables B.1 to B.22 include the Reynolds number and Prandtl number as well.

To calculate the film-feed supply rate, Reynolds number, and Prandtl number on the shell-side of the bottom row within the tube bundle the following assumptions are applied:

1. No variation in refrigerant mass flux in the lateral direction across the tube bundle exists. Note, marginal axial variation is accounted for inherently by the energy balance and log mean temperature difference analysis technique applied to the tube bundle.
2. Refrigerant properties may be calculated at the mean temperature of the refrigerant space and tube wall (i.e. the film temperature).
3. This tube wall temperature may be calculated with a thermal resistance circuit whose single resistance is the inverse of the shell-side heat transfer coefficient. End-nodes of the circuit are the refrigerant space and the unknown tube wall temperature.
4. The heat transfer performance of a given row may be represented by that found on the third tube in each row.
5. An energy balance may be used to calculate the variation in the film-feed supply rate with bundle depth. The local film-feed supply rate decreases with bundle depth with the top row receiving the highest and the bottom row receiving the lowest film-feed supply rates. The variation with row depth is calculated using the known energy transfer rate in each row and the latent heat of vaporization of the refrigerant.

Table B.1 Refrigerant: HFC-134a, Plain Surface, Triangular Pitch, Nozzle Configuration: 30WHCRC,
Refrigerant Supply Rate: 15 kg/min, Pure Refrigerant Data

| q'' $\left(\frac{\text{kW}}{\text{m}^2 \cdot \text{K}}\right)$ | h_b $\left(\frac{\text{kW}}{\text{m}^2 \cdot \text{K}}\right)$ | h_1 $\left(\frac{\text{kW}}{\text{m}^2 \cdot \text{K}}\right)$ | h_2 $\left(\frac{\text{kW}}{\text{m}^2 \cdot \text{K}}\right)$ | h_3 $\left(\frac{\text{kW}}{\text{m}^2 \cdot \text{K}}\right)$ | h_4 $\left(\frac{\text{kW}}{\text{m}^2 \cdot \text{K}}\right)$ | OFR | Γ_4 $\left(\frac{\text{kg}}{\text{s} \cdot \text{m}}\right)$ | Re_4 | Pr_4 |
|---|---|---|---|---|---|----------|--|----------|----------|
| 4.00E+01 | 3.83E+00 | 5.14E+00 | 4.71E+00 | 3.64E+00 | 3.13E+00 | 1.42E+00 | 1.50E-02 | 2.30E+02 | 3.93E+00 |
| 3.67E+01 | 3.87E+00 | 4.88E+00 | 4.56E+00 | 3.74E+00 | 3.13E+00 | 1.59E+00 | 1.73E-02 | 2.65E+02 | 3.94E+00 |
| 3.31E+01 | 3.84E+00 | 4.61E+00 | 4.39E+00 | 3.75E+00 | 3.07E+00 | 1.75E+00 | 1.90E-02 | 2.88E+02 | 3.95E+00 |
| 2.95E+01 | 3.78E+00 | 4.36E+00 | 4.20E+00 | 3.72E+00 | 3.03E+00 | 1.95E+00 | 2.05E-02 | 3.09E+02 | 3.95E+00 |
| 2.62E+01 | 3.70E+00 | 4.08E+00 | 3.94E+00 | 3.60E+00 | 2.95E+00 | 2.20E+00 | 2.21E-02 | 3.33E+02 | 3.96E+00 |
| 2.28E+01 | 3.56E+00 | 3.75E+00 | 3.65E+00 | 3.41E+00 | 2.87E+00 | 2.51E+00 | 2.36E-02 | 3.54E+02 | 3.96E+00 |
| 1.89E+01 | 3.37E+00 | 3.42E+00 | 3.36E+00 | 3.16E+00 | 2.80E+00 | 3.01E+00 | 2.56E-02 | 3.81E+02 | 3.97E+00 |

Table B.2 Refrigerant: HFC-134a, Plain Surface, Triangular Pitch, Nozzle Configuration: 30WHCRC,
Refrigerant Supply Rate: 35 kg/min, Pure Refrigerant Data

| q'' $\left(\frac{\text{kW}}{\text{m}^2 \cdot \text{K}}\right)$ | h_b $\left(\frac{\text{kW}}{\text{m}^2 \cdot \text{K}}\right)$ | h_1 $\left(\frac{\text{kW}}{\text{m}^2 \cdot \text{K}}\right)$ | h_2 $\left(\frac{\text{kW}}{\text{m}^2 \cdot \text{K}}\right)$ | h_3 $\left(\frac{\text{kW}}{\text{m}^2 \cdot \text{K}}\right)$ | h_4 $\left(\frac{\text{kW}}{\text{m}^2 \cdot \text{K}}\right)$ | OFR | Γ_4 $\left(\frac{\text{kg}}{\text{s} \cdot \text{m}}\right)$ | Re_4 | Pr_4 |
|---|---|---|---|---|---|----------|--|----------|----------|
| 4.03E+01 | 4.58E+00 | 4.98E+00 | 4.71E+00 | 4.26E+00 | 3.81E+00 | 3.18E+00 | 5.77E-02 | 8.77E+02 | 3.94E+00 |
| 3.67E+01 | 4.51E+00 | 4.77E+00 | 4.54E+00 | 4.21E+00 | 3.79E+00 | 3.35E+00 | 5.66E-02 | 8.57E+02 | 3.95E+00 |
| 3.31E+01 | 4.43E+00 | 4.60E+00 | 4.38E+00 | 4.12E+00 | 3.72E+00 | 3.79E+00 | 6.01E-02 | 9.07E+02 | 3.96E+00 |
| 2.95E+01 | 4.28E+00 | 4.36E+00 | 4.13E+00 | 3.92E+00 | 3.64E+00 | 4.25E+00 | 6.18E-02 | 9.27E+02 | 3.96E+00 |
| 2.62E+01 | 4.11E+00 | 4.14E+00 | 3.89E+00 | 3.72E+00 | 3.53E+00 | 4.82E+00 | 6.42E-02 | 9.60E+02 | 3.97E+00 |
| 2.26E+01 | 3.90E+00 | 3.87E+00 | 3.62E+00 | 3.48E+00 | 3.32E+00 | 5.47E+00 | 6.45E-02 | 9.61E+02 | 3.97E+00 |
| 1.92E+01 | 3.67E+00 | 3.63E+00 | 3.41E+00 | 3.24E+00 | 3.12E+00 | 6.44E+00 | 6.69E-02 | 9.94E+02 | 3.98E+00 |

Table B.3 Refrigerant: HFC-134a, W-40 fpi surface, Triangular Pitch, Nozzle Configuration: 30WHCRC,
Refrigerant Supply Rate: 15 kg/min, Pure Refrigerant Data

| q'' $\left(\frac{\text{kW}}{\text{m}^2 \cdot \text{K}}\right)$ | h_b $\left(\frac{\text{kW}}{\text{m}^2 \cdot \text{K}}\right)$ | h_1 $\left(\frac{\text{kW}}{\text{m}^2 \cdot \text{K}}\right)$ | h_2 $\left(\frac{\text{kW}}{\text{m}^2 \cdot \text{K}}\right)$ | h_3 $\left(\frac{\text{kW}}{\text{m}^2 \cdot \text{K}}\right)$ | h_4 $\left(\frac{\text{kW}}{\text{m}^2 \cdot \text{K}}\right)$ | OFR | Γ_4 $\left(\frac{\text{kg}}{\text{s} \cdot \text{m}}\right)$ | Re_4 | Pr_4 |
|---|---|---|---|---|---|----------|--|----------|----------|
| 4.10E+01 | 9.49E+00 | 1.59E+01 | 1.17E+01 | 9.01E+00 | 4.72E+00 | 1.38E+00 | 1.38E-02 | 2.06E+02 | 3.97E+00 |
| 3.73E+01 | 9.71E+00 | 1.58E+01 | 1.15E+01 | 8.83E+00 | 5.08E+00 | 1.51E+00 | 1.57E-02 | 2.33E+02 | 3.98E+00 |
| 3.40E+01 | 9.88E+00 | 1.56E+01 | 1.13E+01 | 8.53E+00 | 5.32E+00 | 1.65E+00 | 1.73E-02 | 2.56E+02 | 3.98E+00 |
| 2.95E+01 | 9.88E+00 | 1.45E+01 | 1.08E+01 | 8.04E+00 | 5.69E+00 | 1.89E+00 | 1.94E-02 | 2.86E+02 | 3.99E+00 |
| 2.64E+01 | 9.60E+00 | 1.32E+01 | 1.00E+01 | 7.33E+00 | 5.72E+00 | 2.11E+00 | 2.11E-02 | 3.10E+02 | 3.99E+00 |
| 2.35E+01 | 8.77E+00 | 1.09E+01 | 8.64E+00 | 6.48E+00 | 5.50E+00 | 2.37E+00 | 2.24E-02 | 3.29E+02 | 3.99E+00 |
| 1.95E+01 | 7.40E+00 | 8.57E+00 | 6.98E+00 | 5.54E+00 | 4.80E+00 | 2.84E+00 | 2.43E-02 | 3.56E+02 | 3.99E+00 |

Table B.4 Refrigerant: HFC-134a, W-40 fpi surface, Triangular Pitch, Nozzle Configuration: 30WHCRC,
Refrigerant Supply Rate: 25 kg/min, Pure Refrigerant Data

| q'' $\left(\frac{\text{kW}}{\text{m}^2 \cdot \text{K}}\right)$ | h_b $\left(\frac{\text{kW}}{\text{m}^2 \cdot \text{K}}\right)$ | h_1 $\left(\frac{\text{kW}}{\text{m}^2 \cdot \text{K}}\right)$ | h_2 $\left(\frac{\text{kW}}{\text{m}^2 \cdot \text{K}}\right)$ | h_3 $\left(\frac{\text{kW}}{\text{m}^2 \cdot \text{K}}\right)$ | h_4 $\left(\frac{\text{kW}}{\text{m}^2 \cdot \text{K}}\right)$ | OFR | Γ_4 $\left(\frac{\text{kg}}{\text{s} \cdot \text{m}}\right)$ | Re_4 | Pr_4 |
|---|---|---|---|---|---|----------|--|----------|----------|
| 4.08E+01 | 1.01E+01 | 1.68E+01 | 1.13E+01 | 9.27E+00 | 4.34E+00 | 2.26E+00 | 3.47E-02 | 5.17E+02 | 3.97E+00 |
| 3.70E+01 | 1.04E+01 | 1.69E+01 | 1.12E+01 | 9.13E+00 | 4.69E+00 | 2.57E+00 | 3.85E-02 | 5.72E+02 | 3.98E+00 |
| 3.35E+01 | 1.05E+01 | 1.67E+01 | 1.09E+01 | 8.81E+00 | 4.92E+00 | 2.75E+00 | 3.89E-02 | 5.75E+02 | 3.98E+00 |
| 3.04E+01 | 1.05E+01 | 1.59E+01 | 1.04E+01 | 8.36E+00 | 5.17E+00 | 2.99E+00 | 3.99E-02 | 5.89E+02 | 3.99E+00 |
| 2.63E+01 | 1.01E+01 | 1.42E+01 | 9.57E+00 | 7.62E+00 | 5.29E+00 | 3.50E+00 | 4.27E-02 | 6.28E+02 | 3.99E+00 |
| 2.29E+01 | 9.24E+00 | 1.20E+01 | 8.29E+00 | 6.79E+00 | 5.18E+00 | 4.04E+00 | 4.50E-02 | 6.61E+02 | 3.99E+00 |
| 1.92E+01 | 7.57E+00 | 8.66E+00 | 6.30E+00 | 5.52E+00 | 4.61E+00 | 4.70E+00 | 4.59E-02 | 6.73E+02 | 3.99E+00 |

Table B.5 Refrigerant: HFC-134a, W-40 fpi surface, Triangular Pitch, Nozzle Configuration: 30WHCRC,
Refrigerant Supply Rate: 35 kg/min, Pure Refrigerant Data

| q'' $\left(\frac{\text{kW}}{\text{m}^2 \cdot \text{K}}\right)$ | h_b $\left(\frac{\text{kW}}{\text{m}^2 \cdot \text{K}}\right)$ | h_1 $\left(\frac{\text{kW}}{\text{m}^2 \cdot \text{K}}\right)$ | h_2 $\left(\frac{\text{kW}}{\text{m}^2 \cdot \text{K}}\right)$ | h_3 $\left(\frac{\text{kW}}{\text{m}^2 \cdot \text{K}}\right)$ | h_4 $\left(\frac{\text{kW}}{\text{m}^2 \cdot \text{K}}\right)$ | OFR | Γ_4 $\left(\frac{\text{kg}}{\text{s} \cdot \text{m}}\right)$ | Re_4 | Pr_4 |
|---|---|---|---|---|---|----------|--|----------|----------|
| 4.05E+01 | 1.05E+01 | 1.71E+01 | 1.19E+01 | 9.72E+00 | 4.99E+00 | 3.16E+00 | 5.64E-02 | 8.39E+02 | 3.97E+00 |
| 3.72E+01 | 1.06E+01 | 1.75E+01 | 1.17E+01 | 9.34E+00 | 5.21E+00 | 3.33E+00 | 5.57E-02 | 8.25E+02 | 3.98E+00 |
| 3.39E+01 | 1.05E+01 | 1.74E+01 | 1.15E+01 | 8.99E+00 | 5.36E+00 | 3.59E+00 | 5.65E-02 | 8.35E+02 | 3.98E+00 |
| 2.93E+01 | 1.04E+01 | 1.61E+01 | 1.07E+01 | 8.49E+00 | 5.58E+00 | 4.14E+00 | 5.90E-02 | 8.68E+02 | 3.99E+00 |
| 2.59E+01 | 9.86E+00 | 1.44E+01 | 9.85E+00 | 7.74E+00 | 5.64E+00 | 4.68E+00 | 6.10E-02 | 8.96E+02 | 3.99E+00 |
| 2.24E+01 | 8.87E+00 | 1.22E+01 | 8.47E+00 | 6.78E+00 | 5.43E+00 | 5.33E+00 | 6.19E-02 | 9.07E+02 | 3.99E+00 |
| 1.95E+01 | 7.33E+00 | 8.94E+00 | 6.57E+00 | 5.65E+00 | 4.82E+00 | 6.24E+00 | 6.54E-02 | 9.59E+02 | 3.99E+00 |

Table B.6 Refrigerant: HFC-134a, W-40 fpi surface, Triangular Pitch, Nozzle Configuration: 30WHCRC,
Refrigerant Supply Rate: 45 kg/min, Pure Refrigerant Data

| q'' $\left(\frac{\text{kW}}{\text{m}^2 \cdot \text{K}}\right)$ | h_b $\left(\frac{\text{kW}}{\text{m}^2 \cdot \text{K}}\right)$ | h_1 $\left(\frac{\text{kW}}{\text{m}^2 \cdot \text{K}}\right)$ | h_2 $\left(\frac{\text{kW}}{\text{m}^2 \cdot \text{K}}\right)$ | h_3 $\left(\frac{\text{kW}}{\text{m}^2 \cdot \text{K}}\right)$ | h_4 $\left(\frac{\text{kW}}{\text{m}^2 \cdot \text{K}}\right)$ | OFR | Γ_4 $\left(\frac{\text{kg}}{\text{s} \cdot \text{m}}\right)$ | Re_4 | Pr_4 |
|---|---|---|---|---|---|----------|--|----------|----------|
| 3.99E+01 | 1.05E+01 | 1.70E+01 | 1.20E+01 | 9.55E+00 | 5.39E+00 | 3.78E+00 | 7.05E-02 | 1.05E+03 | 3.98E+00 |
| 3.69E+01 | 1.06E+01 | 1.73E+01 | 1.19E+01 | 9.34E+00 | 5.56E+00 | 4.10E+00 | 7.28E-02 | 1.08E+03 | 3.98E+00 |
| 3.34E+01 | 1.05E+01 | 1.68E+01 | 1.15E+01 | 9.09E+00 | 5.78E+00 | 4.84E+00 | 8.11E-02 | 1.20E+03 | 3.99E+00 |
| 2.97E+01 | 1.03E+01 | 1.59E+01 | 1.10E+01 | 8.29E+00 | 5.95E+00 | 5.01E+00 | 7.56E-02 | 1.11E+03 | 3.99E+00 |
| 2.64E+01 | 9.90E+00 | 1.45E+01 | 1.02E+01 | 7.69E+00 | 6.02E+00 | 5.82E+00 | 8.09E-02 | 1.19E+03 | 3.99E+00 |
| 2.28E+01 | 8.86E+00 | 1.19E+01 | 8.58E+00 | 6.71E+00 | 5.71E+00 | 6.91E+00 | 8.59E-02 | 1.26E+03 | 3.99E+00 |
| 1.97E+01 | 7.12E+00 | 8.56E+00 | 6.47E+00 | 5.38E+00 | 4.91E+00 | 7.31E+00 | 7.96E-02 | 1.17E+03 | 3.99E+00 |

Table B.7 Refrigerant: HFC-134a, W-SC surface, Triangular Pitch, Nozzle Configuration: 30WHCRC,
Refrigerant Supply Rate: 15 kg/min, Pure Refrigerant Data

| q'' $\left(\frac{\text{kW}}{\text{m}^2 \cdot \text{K}}\right)$ | h_b $\left(\frac{\text{kW}}{\text{m}^2 \cdot \text{K}}\right)$ | h_1 $\left(\frac{\text{kW}}{\text{m}^2 \cdot \text{K}}\right)$ | h_2 $\left(\frac{\text{kW}}{\text{m}^2 \cdot \text{K}}\right)$ | h_3 $\left(\frac{\text{kW}}{\text{m}^2 \cdot \text{K}}\right)$ | h_4 $\left(\frac{\text{kW}}{\text{m}^2 \cdot \text{K}}\right)$ | OFR | Γ_4 $\left(\frac{\text{kg}}{\text{s} \cdot \text{m}}\right)$ | Re_4 | Pr_4 |
|---|---|---|---|---|---|----------|--|----------|----------|
| 4.00E+01 | 1.33E+01 | 1.99E+01 | 1.36E+01 | 1.16E+01 | 4.39E+00 | 1.42E+00 | 1.40E-02 | 2.08E+02 | 3.98E+00 |
| 3.66E+01 | 1.39E+01 | 1.96E+01 | 1.36E+01 | 1.23E+01 | 4.82E+00 | 1.58E+00 | 1.65E-02 | 2.44E+02 | 3.98E+00 |
| 3.30E+01 | 1.47E+01 | 2.05E+01 | 1.35E+01 | 1.27E+01 | 5.32E+00 | 1.73E+00 | 1.82E-02 | 2.68E+02 | 3.99E+00 |
| 2.96E+01 | 1.48E+01 | 2.00E+01 | 1.32E+01 | 1.40E+01 | 5.90E+00 | 1.93E+00 | 2.01E-02 | 2.95E+02 | 3.99E+00 |
| 2.59E+01 | 1.50E+01 | 1.97E+01 | 1.24E+01 | 1.44E+01 | 6.19E+00 | 2.19E+00 | 2.19E-02 | 3.20E+02 | 4.00E+00 |
| 2.27E+01 | 1.36E+01 | 1.64E+01 | 1.06E+01 | 1.35E+01 | 6.35E+00 | 2.48E+00 | 2.34E-02 | 3.42E+02 | 4.00E+00 |
| 1.89E+01 | 1.10E+01 | 1.20E+01 | 8.04E+00 | 1.08E+01 | 5.85E+00 | 3.04E+00 | 2.60E-02 | 3.80E+02 | 4.00E+00 |

Table B.8 Refrigerant: HFC-134a, W-SC surface, Triangular Pitch, Nozzle Configuration: 30WHCRC,
Refrigerant Supply Rate: 25 kg/min, Pure Refrigerant Data

| q'' $\left(\frac{\text{kW}}{\text{m}^2 \cdot \text{K}}\right)$ | h_b $\left(\frac{\text{kW}}{\text{m}^2 \cdot \text{K}}\right)$ | h_1 $\left(\frac{\text{kW}}{\text{m}^2 \cdot \text{K}}\right)$ | h_2 $\left(\frac{\text{kW}}{\text{m}^2 \cdot \text{K}}\right)$ | h_3 $\left(\frac{\text{kW}}{\text{m}^2 \cdot \text{K}}\right)$ | h_4 $\left(\frac{\text{kW}}{\text{m}^2 \cdot \text{K}}\right)$ | OFR | Γ_4 $\left(\frac{\text{kg}}{\text{s} \cdot \text{m}}\right)$ | Re_4 | Pr_4 |
|---|---|---|---|---|---|----------|--|----------|----------|
| 4.04E+01 | 1.40E+01 | 1.99E+01 | 1.35E+01 | 1.23E+01 | 4.14E+00 | 2.32E+00 | 3.59E-02 | 5.33E+02 | 3.97E+00 |
| 3.70E+01 | 1.47E+01 | 2.05E+01 | 1.36E+01 | 1.31E+01 | 4.51E+00 | 2.49E+00 | 3.69E-02 | 5.46E+02 | 3.98E+00 |
| 3.30E+01 | 1.52E+01 | 2.06E+01 | 1.34E+01 | 1.37E+01 | 4.84E+00 | 2.80E+00 | 3.94E-02 | 5.81E+02 | 3.99E+00 |
| 2.98E+01 | 1.58E+01 | 2.12E+01 | 1.32E+01 | 1.47E+01 | 5.22E+00 | 3.09E+00 | 4.10E-02 | 6.02E+02 | 3.99E+00 |
| 2.63E+01 | 1.55E+01 | 2.02E+01 | 1.22E+01 | 1.53E+01 | 5.62E+00 | 3.43E+00 | 4.19E-02 | 6.14E+02 | 3.99E+00 |
| 2.28E+01 | 1.46E+01 | 1.78E+01 | 1.09E+01 | 1.48E+01 | 5.90E+00 | 3.98E+00 | 4.44E-02 | 6.49E+02 | 4.00E+00 |
| 1.92E+01 | 1.16E+01 | 1.31E+01 | 8.31E+00 | 1.27E+01 | 5.61E+00 | 4.66E+00 | 4.57E-02 | 6.67E+02 | 4.00E+00 |

Table B.9 Refrigerant: HFC-134a, W-SC surface, Triangular Pitch, Nozzle Configuration: 30WHCRC,
Refrigerant Supply Rate: 35 kg/min, Pure Refrigerant Data

| q'' $\left(\frac{\text{kW}}{\text{m}^2 \cdot \text{K}}\right)$ | h_b $\left(\frac{\text{kW}}{\text{m}^2 \cdot \text{K}}\right)$ | h_1 $\left(\frac{\text{kW}}{\text{m}^2 \cdot \text{K}}\right)$ | h_2 $\left(\frac{\text{kW}}{\text{m}^2 \cdot \text{K}}\right)$ | h_3 $\left(\frac{\text{kW}}{\text{m}^2 \cdot \text{K}}\right)$ | h_4 $\left(\frac{\text{kW}}{\text{m}^2 \cdot \text{K}}\right)$ | OFR | Γ_4 $\left(\frac{\text{kg}}{\text{s} \cdot \text{m}}\right)$ | Re_4 | Pr_4 |
|---|---|---|---|---|---|----------|--|----------|----------|
| 4.01E+01 | 1.44E+01 | 1.94E+01 | 1.33E+01 | 1.32E+01 | 4.57E+00 | 3.13E+00 | 5.51E-02 | 8.18E+02 | 3.98E+00 |
| 3.67E+01 | 1.48E+01 | 1.98E+01 | 1.34E+01 | 1.38E+01 | 4.90E+00 | 3.47E+00 | 5.82E-02 | 8.61E+02 | 3.98E+00 |
| 3.33E+01 | 1.53E+01 | 2.00E+01 | 1.32E+01 | 1.45E+01 | 5.16E+00 | 3.70E+00 | 5.79E-02 | 8.54E+02 | 3.99E+00 |
| 2.94E+01 | 1.53E+01 | 1.97E+01 | 1.27E+01 | 1.52E+01 | 5.47E+00 | 4.27E+00 | 6.16E-02 | 9.05E+02 | 3.99E+00 |
| 2.57E+01 | 1.51E+01 | 1.92E+01 | 1.19E+01 | 1.56E+01 | 5.87E+00 | 4.77E+00 | 6.22E-02 | 9.11E+02 | 4.00E+00 |
| 2.31E+01 | 1.42E+01 | 1.69E+01 | 1.05E+01 | 1.53E+01 | 6.06E+00 | 5.26E+00 | 6.33E-02 | 9.25E+02 | 4.00E+00 |
| 1.93E+01 | 1.12E+01 | 1.22E+01 | 7.95E+00 | 1.21E+01 | 5.68E+00 | 6.32E+00 | 6.59E-02 | 9.61E+02 | 4.00E+00 |

Table B.10 Refrigerant: HFC-134a, W-SC surface, Triangular Pitch, Nozzle Configuration: 30WHCRC,
Refrigerant Supply Rate: 45 kg/min, Pure Refrigerant Data

| q'' $\left(\frac{\text{kW}}{\text{m}^2 \cdot \text{K}}\right)$ | h_b $\left(\frac{\text{kW}}{\text{m}^2 \cdot \text{K}}\right)$ | h_1 $\left(\frac{\text{kW}}{\text{m}^2 \cdot \text{K}}\right)$ | h_2 $\left(\frac{\text{kW}}{\text{m}^2 \cdot \text{K}}\right)$ | h_3 $\left(\frac{\text{kW}}{\text{m}^2 \cdot \text{K}}\right)$ | h_4 $\left(\frac{\text{kW}}{\text{m}^2 \cdot \text{K}}\right)$ | OFR | Γ_4 $\left(\frac{\text{kg}}{\text{s} \cdot \text{m}}\right)$ | Re_4 | Pr_4 |
|---|---|---|---|---|---|----------|--|----------|----------|
| 4.04E+01 | 1.46E+01 | 1.89E+01 | 1.35E+01 | 1.31E+01 | 4.96E+00 | 3.89E+00 | 7.44E-02 | 1.10E+03 | 3.98E+00 |
| 3.68E+01 | 1.49E+01 | 1.94E+01 | 1.34E+01 | 1.39E+01 | 5.17E+00 | 4.17E+00 | 7.45E-02 | 1.10E+03 | 3.98E+00 |
| 3.36E+01 | 1.50E+01 | 1.93E+01 | 1.31E+01 | 1.43E+01 | 5.45E+00 | 4.67E+00 | 7.84E-02 | 1.15E+03 | 3.99E+00 |
| 2.94E+01 | 1.50E+01 | 1.90E+01 | 1.25E+01 | 1.45E+01 | 5.61E+00 | 4.90E+00 | 7.32E-02 | 1.07E+03 | 3.99E+00 |
| 2.62E+01 | 1.45E+01 | 1.78E+01 | 1.15E+01 | 1.52E+01 | 6.11E+00 | 5.85E+00 | 8.11E-02 | 1.19E+03 | 4.00E+00 |
| 2.27E+01 | 1.35E+01 | 1.54E+01 | 1.02E+01 | 1.44E+01 | 6.37E+00 | 6.45E+00 | 7.93E-02 | 1.16E+03 | 4.00E+00 |
| 1.90E+01 | 1.10E+01 | 1.20E+01 | 7.93E+00 | 1.25E+01 | 6.06E+00 | 7.97E+00 | 8.51E-02 | 1.24E+03 | 4.00E+00 |

Table B.11 Refrigerant: HFC-134a, Tu-Cii surface, Triangular Pitch, Nozzle Configuration: 30WHCRC,
Refrigerant Supply Rate: 15 kg/min, Pure Refrigerant Data

| q'' $\left(\frac{\text{kW}}{\text{m}^2 \cdot \text{K}}\right)$ | h_b $\left(\frac{\text{kW}}{\text{m}^2 \cdot \text{K}}\right)$ | h_1 $\left(\frac{\text{kW}}{\text{m}^2 \cdot \text{K}}\right)$ | h_2 $\left(\frac{\text{kW}}{\text{m}^2 \cdot \text{K}}\right)$ | h_3 $\left(\frac{\text{kW}}{\text{m}^2 \cdot \text{K}}\right)$ | h_4 $\left(\frac{\text{kW}}{\text{m}^2 \cdot \text{K}}\right)$ | OFR | Γ_4 $\left(\frac{\text{kg}}{\text{s} \cdot \text{m}}\right)$ | Re_4 | Pr_4 |
|---|---|---|---|---|---|----------|--|----------|----------|
| 4.06E+01 | 3.40E+01 | 3.45E+01 | 4.87E+01 | 3.37E+01 | 2.22E+01 | 1.42E+00 | 1.57E-02 | 2.28E+02 | 4.01E+00 |
| 3.69E+01 | 3.64E+01 | 3.51E+01 | 5.11E+01 | 3.37E+01 | 2.47E+01 | 1.56E+00 | 1.74E-02 | 2.52E+02 | 4.01E+00 |
| 3.34E+01 | 3.82E+01 | 3.61E+01 | 5.27E+01 | 3.27E+01 | 2.63E+01 | 1.71E+00 | 1.89E-02 | 2.73E+02 | 4.01E+00 |
| 2.97E+01 | 3.77E+01 | 3.44E+01 | 4.98E+01 | 3.06E+01 | 2.68E+01 | 1.93E+00 | 2.08E-02 | 3.00E+02 | 4.02E+00 |
| 2.61E+01 | 3.80E+01 | 3.41E+01 | 4.92E+01 | 2.86E+01 | 2.64E+01 | 2.18E+00 | 2.23E-02 | 3.21E+02 | 4.02E+00 |
| 2.29E+01 | 3.73E+01 | 3.26E+01 | 4.68E+01 | 2.69E+01 | 2.58E+01 | 2.48E+00 | 2.38E-02 | 3.44E+02 | 4.02E+00 |
| 1.93E+01 | 3.33E+01 | 2.82E+01 | 3.96E+01 | 2.28E+01 | 2.35E+01 | 2.92E+00 | 2.53E-02 | 3.65E+02 | 4.02E+00 |

Table B.12 Refrigerant: HFC-134a, Tu-Cii surface, Triangular Pitch, Nozzle Configuration: 30WHCRC,
Refrigerant Supply Rate: 25 kg/min, Pure Refrigerant Data

| q'' $\left(\frac{\text{kW}}{\text{m}^2 \cdot \text{K}}\right)$ | h_b $\left(\frac{\text{kW}}{\text{m}^2 \cdot \text{K}}\right)$ | h_1 $\left(\frac{\text{kW}}{\text{m}^2 \cdot \text{K}}\right)$ | h_2 $\left(\frac{\text{kW}}{\text{m}^2 \cdot \text{K}}\right)$ | h_3 $\left(\frac{\text{kW}}{\text{m}^2 \cdot \text{K}}\right)$ | h_4 $\left(\frac{\text{kW}}{\text{m}^2 \cdot \text{K}}\right)$ | OFR | Γ_4 $\left(\frac{\text{kg}}{\text{s} \cdot \text{m}}\right)$ | Re_4 | Pr_4 |
|---|---|---|---|---|---|----------|--|----------|----------|
| 4.06E+01 | 3.61E+01 | 3.45E+01 | 4.81E+01 | 3.42E+01 | 2.39E+01 | 2.23E+00 | 3.53E-02 | 5.12E+02 | 4.01E+00 |
| 3.66E+01 | 3.78E+01 | 3.52E+01 | 5.01E+01 | 3.34E+01 | 2.60E+01 | 2.41E+00 | 3.59E-02 | 5.20E+02 | 4.01E+00 |
| 3.29E+01 | 3.91E+01 | 3.56E+01 | 5.20E+01 | 3.24E+01 | 2.68E+01 | 2.78E+00 | 3.97E-02 | 5.74E+02 | 4.01E+00 |
| 2.97E+01 | 3.86E+01 | 3.38E+01 | 4.95E+01 | 3.10E+01 | 2.73E+01 | 2.98E+00 | 3.97E-02 | 5.73E+02 | 4.02E+00 |
| 2.60E+01 | 3.88E+01 | 3.43E+01 | 4.92E+01 | 2.89E+01 | 2.72E+01 | 3.38E+00 | 4.11E-02 | 5.93E+02 | 4.02E+00 |
| 2.28E+01 | 3.73E+01 | 3.17E+01 | 4.43E+01 | 2.64E+01 | 2.60E+01 | 3.88E+00 | 4.31E-02 | 6.22E+02 | 4.02E+00 |
| 1.92E+01 | 3.29E+01 | 2.74E+01 | 3.77E+01 | 2.26E+01 | 2.36E+01 | 4.51E+00 | 4.40E-02 | 6.35E+02 | 4.02E+00 |

Table B.13 Refrigerant: HFC-134a, Tu-Cii surface, Triangular Pitch, Nozzle Configuration: 30WHCRC,
Refrigerant Supply Rate: 35 kg/min, Pure Refrigerant Data

| q'' $\left(\frac{\text{kW}}{\text{m}^2 \cdot \text{K}}\right)$ | h_b $\left(\frac{\text{kW}}{\text{m}^2 \cdot \text{K}}\right)$ | h_1 $\left(\frac{\text{kW}}{\text{m}^2 \cdot \text{K}}\right)$ | h_2 $\left(\frac{\text{kW}}{\text{m}^2 \cdot \text{K}}\right)$ | h_3 $\left(\frac{\text{kW}}{\text{m}^2 \cdot \text{K}}\right)$ | h_4 $\left(\frac{\text{kW}}{\text{m}^2 \cdot \text{K}}\right)$ | OFR | Γ_4 $\left(\frac{\text{kg}}{\text{s} \cdot \text{m}}\right)$ | Re_4 | Pr_4 |
|---|---|---|---|---|---|----------|--|----------|----------|
| 4.05E+01 | 3.82E+01 | 3.46E+01 | 5.16E+01 | 3.59E+01 | 2.78E+01 | 3.15E+00 | 5.78E-02 | 8.36E+02 | 4.01E+00 |
| 3.65E+01 | 3.96E+01 | 3.54E+01 | 5.30E+01 | 3.49E+01 | 2.89E+01 | 3.45E+00 | 5.88E-02 | 8.50E+02 | 4.01E+00 |
| 3.34E+01 | 4.08E+01 | 3.55E+01 | 5.47E+01 | 3.39E+01 | 2.97E+01 | 3.71E+00 | 5.93E-02 | 8.56E+02 | 4.02E+00 |
| 2.98E+01 | 3.89E+01 | 3.31E+01 | 5.15E+01 | 3.13E+01 | 2.93E+01 | 4.00E+00 | 5.83E-02 | 8.42E+02 | 4.02E+00 |
| 2.61E+01 | 3.80E+01 | 3.26E+01 | 4.88E+01 | 2.92E+01 | 2.77E+01 | 4.80E+00 | 6.41E-02 | 9.25E+02 | 4.02E+00 |
| 2.28E+01 | 3.53E+01 | 3.09E+01 | 4.54E+01 | 2.66E+01 | 2.61E+01 | 5.30E+00 | 6.32E-02 | 9.12E+02 | 4.02E+00 |
| 1.91E+01 | 2.95E+01 | 2.55E+01 | 3.67E+01 | 2.18E+01 | 2.22E+01 | 6.36E+00 | 6.59E-02 | 9.50E+02 | 4.02E+00 |

Table B.14 Refrigerant: HFC-134a, Tu-Cii surface, Triangular Pitch, Nozzle Configuration: 30WHCRC,
Refrigerant Supply Rate: 45 kg/min, Pure Refrigerant Data

| q'' $\left(\frac{\text{kW}}{\text{m}^2 \cdot \text{K}}\right)$ | h_b $\left(\frac{\text{kW}}{\text{m}^2 \cdot \text{K}}\right)$ | h_1 $\left(\frac{\text{kW}}{\text{m}^2 \cdot \text{K}}\right)$ | h_2 $\left(\frac{\text{kW}}{\text{m}^2 \cdot \text{K}}\right)$ | h_3 $\left(\frac{\text{kW}}{\text{m}^2 \cdot \text{K}}\right)$ | h_4 $\left(\frac{\text{kW}}{\text{m}^2 \cdot \text{K}}\right)$ | OFR | Γ_4 $\left(\frac{\text{kg}}{\text{s} \cdot \text{m}}\right)$ | Re_4 | Pr_4 |
|---|---|---|---|---|---|----------|--|----------|----------|
| 4.04E+01 | 4.12E+01 | 3.51E+01 | 5.18E+01 | 3.66E+01 | 3.23E+01 | 3.77E+00 | 7.30E-02 | 1.06E+03 | 4.01E+00 |
| 3.67E+01 | 4.25E+01 | 3.59E+01 | 5.48E+01 | 3.58E+01 | 3.33E+01 | 4.24E+00 | 7.71E-02 | 1.11E+03 | 4.02E+00 |
| 3.30E+01 | 4.28E+01 | 3.58E+01 | 5.49E+01 | 3.37E+01 | 3.26E+01 | 4.78E+00 | 8.07E-02 | 1.17E+03 | 4.02E+00 |
| 2.99E+01 | 4.00E+01 | 3.28E+01 | 5.09E+01 | 2.96E+01 | 3.22E+01 | 5.18E+00 | 8.03E-02 | 1.16E+03 | 4.02E+00 |
| 2.59E+01 | 3.82E+01 | 3.18E+01 | 4.85E+01 | 2.63E+01 | 2.90E+01 | 6.07E+00 | 8.43E-02 | 1.22E+03 | 4.02E+00 |
| 2.28E+01 | 3.50E+01 | 2.98E+01 | 4.21E+01 | 2.28E+01 | 2.61E+01 | 6.82E+00 | 8.53E-02 | 1.23E+03 | 4.02E+00 |
| 1.92E+01 | 2.94E+01 | 2.55E+01 | 3.34E+01 | 1.89E+01 | 2.26E+01 | 7.98E+00 | 8.63E-02 | 1.25E+03 | 4.02E+00 |

Table B.15 Refrigerant: HFC-134a, Tu-B surface, Triangular Pitch, Nozzle Configuration: 30WHCRC,
Refrigerant Supply Rate: 15 kg/min, Pure Refrigerant Data

| q'' $\left(\frac{\text{kW}}{\text{m}^2 \cdot \text{K}}\right)$ | h_b $\left(\frac{\text{kW}}{\text{m}^2 \cdot \text{K}}\right)$ | h_1 $\left(\frac{\text{kW}}{\text{m}^2 \cdot \text{K}}\right)$ | h_2 $\left(\frac{\text{kW}}{\text{m}^2 \cdot \text{K}}\right)$ | h_3 $\left(\frac{\text{kW}}{\text{m}^2 \cdot \text{K}}\right)$ | h_4 $\left(\frac{\text{kW}}{\text{m}^2 \cdot \text{K}}\right)$ | OFR | Γ_4 $\left(\frac{\text{kg}}{\text{s} \cdot \text{m}}\right)$ | Re_4 | Pr_4 |
|---|---|---|---|---|---|----------|--|----------|----------|
| 4.05E+01 | 1.46E+01 | 1.76E+01 | 1.52E+01 | 1.39E+01 | 1.40E+01 | 1.46E+00 | 1.66E-02 | 2.42E+02 | 4.00E+00 |
| 3.70E+01 | 1.46E+01 | 1.74E+01 | 1.49E+01 | 1.39E+01 | 1.46E+01 | 1.59E+00 | 1.80E-02 | 2.62E+02 | 4.00E+00 |
| 3.35E+01 | 1.43E+01 | 1.69E+01 | 1.43E+01 | 1.34E+01 | 1.47E+01 | 1.74E+00 | 1.94E-02 | 2.82E+02 | 4.01E+00 |
| 2.98E+01 | 1.39E+01 | 1.58E+01 | 1.36E+01 | 1.27E+01 | 1.50E+01 | 1.95E+00 | 2.12E-02 | 3.07E+02 | 4.01E+00 |
| 2.66E+01 | 1.33E+01 | 1.52E+01 | 1.33E+01 | 1.19E+01 | 1.42E+01 | 2.16E+00 | 2.23E-02 | 3.24E+02 | 4.01E+00 |
| 2.29E+01 | 1.27E+01 | 1.40E+01 | 1.23E+01 | 1.09E+01 | 1.39E+01 | 2.53E+00 | 2.42E-02 | 3.51E+02 | 4.01E+00 |
| 1.93E+01 | 1.16E+01 | 1.29E+01 | 1.17E+01 | 9.85E+00 | 1.25E+01 | 2.98E+00 | 2.57E-02 | 3.73E+02 | 4.01E+00 |

Table B.16 Refrigerant: HFC-134a, Tu-B surface, Triangular Pitch, Nozzle Configuration: 30WHCRC,
Refrigerant Supply Rate: 25 kg/min, Pure Refrigerant Data

| q'' $\left(\frac{\text{kW}}{\text{m}^2 \cdot \text{K}}\right)$ | h_b $\left(\frac{\text{kW}}{\text{m}^2 \cdot \text{K}}\right)$ | h_1 $\left(\frac{\text{kW}}{\text{m}^2 \cdot \text{K}}\right)$ | h_2 $\left(\frac{\text{kW}}{\text{m}^2 \cdot \text{K}}\right)$ | h_3 $\left(\frac{\text{kW}}{\text{m}^2 \cdot \text{K}}\right)$ | h_4 $\left(\frac{\text{kW}}{\text{m}^2 \cdot \text{K}}\right)$ | OFR | Γ_4 $\left(\frac{\text{kg}}{\text{s} \cdot \text{m}}\right)$ | Re_4 | Pr_4 |
|---|---|---|---|---|---|----------|--|----------|----------|
| 4.06E+01 | 1.54E+01 | 1.90E+01 | 1.63E+01 | 1.31E+01 | 1.44E+01 | 2.35E+00 | 3.80E-02 | 5.55E+02 | 4.00E+00 |
| 3.69E+01 | 1.50E+01 | 1.85E+01 | 1.57E+01 | 1.26E+01 | 1.41E+01 | 2.54E+00 | 3.88E-02 | 5.65E+02 | 4.00E+00 |
| 3.36E+01 | 1.45E+01 | 1.78E+01 | 1.50E+01 | 1.22E+01 | 1.41E+01 | 2.79E+00 | 4.05E-02 | 5.90E+02 | 4.00E+00 |
| 2.98E+01 | 1.41E+01 | 1.67E+01 | 1.43E+01 | 1.17E+01 | 1.41E+01 | 3.15E+00 | 4.22E-02 | 6.13E+02 | 4.01E+00 |
| 2.63E+01 | 1.35E+01 | 1.61E+01 | 1.37E+01 | 1.11E+01 | 1.34E+01 | 3.59E+00 | 4.43E-02 | 6.44E+02 | 4.01E+00 |
| 2.31E+01 | 1.29E+01 | 1.52E+01 | 1.32E+01 | 1.06E+01 | 1.30E+01 | 4.07E+00 | 4.56E-02 | 6.61E+02 | 4.01E+00 |
| 1.91E+01 | 1.20E+01 | 1.37E+01 | 1.24E+01 | 9.57E+00 | 1.20E+01 | 4.83E+00 | 4.69E-02 | 6.79E+02 | 4.01E+00 |

Table B.17 Refrigerant: HFC-134a, Tu-B surface, Triangular Pitch, Nozzle Configuration: 30WHCRC,
Refrigerant Supply Rate: 35 kg/min, Pure Refrigerant Data

| q'' $\left(\frac{\text{kW}}{\text{m}^2 \cdot \text{K}}\right)$ | h_b $\left(\frac{\text{kW}}{\text{m}^2 \cdot \text{K}}\right)$ | h_1 $\left(\frac{\text{kW}}{\text{m}^2 \cdot \text{K}}\right)$ | h_2 $\left(\frac{\text{kW}}{\text{m}^2 \cdot \text{K}}\right)$ | h_3 $\left(\frac{\text{kW}}{\text{m}^2 \cdot \text{K}}\right)$ | h_4 $\left(\frac{\text{kW}}{\text{m}^2 \cdot \text{K}}\right)$ | OFR | Γ_4 $\left(\frac{\text{kg}}{\text{s} \cdot \text{m}}\right)$ | Re_4 | Pr_4 |
|---|---|---|---|---|---|----------|--|----------|----------|
| 4.07E+01 | 1.62E+01 | 2.02E+01 | 1.71E+01 | 1.38E+01 | 1.46E+01 | 2.97E+00 | 5.30E-02 | 7.74E+02 | 4.00E+00 |
| 3.72E+01 | 1.59E+01 | 1.96E+01 | 1.66E+01 | 1.33E+01 | 1.45E+01 | 3.36E+00 | 5.74E-02 | 8.36E+02 | 4.00E+00 |
| 3.34E+01 | 1.54E+01 | 1.90E+01 | 1.61E+01 | 1.28E+01 | 1.41E+01 | 3.69E+00 | 5.81E-02 | 8.45E+02 | 4.00E+00 |
| 3.02E+01 | 1.51E+01 | 1.81E+01 | 1.56E+01 | 1.23E+01 | 1.42E+01 | 4.03E+00 | 5.87E-02 | 8.53E+02 | 4.01E+00 |
| 2.67E+01 | 1.44E+01 | 1.78E+01 | 1.52E+01 | 1.17E+01 | 1.35E+01 | 4.54E+00 | 6.03E-02 | 8.75E+02 | 4.01E+00 |
| 2.29E+01 | 1.39E+01 | 1.68E+01 | 1.48E+01 | 1.10E+01 | 1.31E+01 | 5.34E+00 | 6.28E-02 | 9.11E+02 | 4.01E+00 |
| 1.91E+01 | 1.28E+01 | 1.52E+01 | 1.38E+01 | 9.85E+00 | 1.21E+01 | 6.28E+00 | 6.42E-02 | 9.30E+02 | 4.01E+00 |

Table B.18 Refrigerant: HFC-134a, Tu-B surface, Triangular Pitch, Nozzle Configuration: 30WHCRC,
Refrigerant Supply Rate: 45 kg/min, Pure Refrigerant Data

| q'' $\left(\frac{\text{kW}}{\text{m}^2 \cdot \text{K}}\right)$ | h_b $\left(\frac{\text{kW}}{\text{m}^2 \cdot \text{K}}\right)$ | h_1 $\left(\frac{\text{kW}}{\text{m}^2 \cdot \text{K}}\right)$ | h_2 $\left(\frac{\text{kW}}{\text{m}^2 \cdot \text{K}}\right)$ | h_3 $\left(\frac{\text{kW}}{\text{m}^2 \cdot \text{K}}\right)$ | h_4 $\left(\frac{\text{kW}}{\text{m}^2 \cdot \text{K}}\right)$ | OFR | Γ_4 $\left(\frac{\text{kg}}{\text{s} \cdot \text{m}}\right)$ | Re_4 | Pr_4 |
|---|---|---|---|---|---|----------|--|----------|----------|
| 4.07E+01 | 1.64E+01 | 2.02E+01 | 1.70E+01 | 1.35E+01 | 1.48E+01 | 3.93E+00 | 7.64E-02 | 1.11E+03 | 4.00E+00 |
| 3.73E+01 | 1.60E+01 | 1.98E+01 | 1.67E+01 | 1.31E+01 | 1.45E+01 | 4.33E+00 | 7.87E-02 | 1.15E+03 | 4.00E+00 |
| 3.35E+01 | 1.54E+01 | 1.92E+01 | 1.60E+01 | 1.26E+01 | 1.40E+01 | 4.74E+00 | 7.93E-02 | 1.15E+03 | 4.00E+00 |
| 3.01E+01 | 1.51E+01 | 1.85E+01 | 1.55E+01 | 1.22E+01 | 1.40E+01 | 5.28E+00 | 8.08E-02 | 1.17E+03 | 4.01E+00 |
| 2.64E+01 | 1.44E+01 | 1.80E+01 | 1.51E+01 | 1.14E+01 | 1.31E+01 | 6.03E+00 | 8.32E-02 | 1.21E+03 | 4.01E+00 |
| 2.28E+01 | 1.36E+01 | 1.69E+01 | 1.42E+01 | 1.06E+01 | 1.23E+01 | 6.89E+00 | 8.41E-02 | 1.22E+03 | 4.01E+00 |
| 1.95E+01 | 1.27E+01 | 1.55E+01 | 1.34E+01 | 9.67E+00 | 1.16E+01 | 7.96E+00 | 8.51E-02 | 1.23E+03 | 4.01E+00 |

Table B.19 Refrigerant: HFC-134a, Tu-B surface, Square Pitch, Nozzle Configuration: 30WHCRC,
Refrigerant Supply Rate: 15 kg/min, Pure Refrigerant Data

| q'' ($\frac{kW}{m^2 \cdot K}$) | h_b ($\frac{kW}{m^2 \cdot K}$) | h_1 ($\frac{kW}{m^2 \cdot K}$) | h_2 ($\frac{kW}{m^2 \cdot K}$) | h_3 ($\frac{kW}{m^2 \cdot K}$) | h_4 ($\frac{kW}{m^2 \cdot K}$) | OFR | Γ_4 ($\frac{kg}{s \cdot m}$) | Re_4 | Pr_4 |
|---------------------------------------|---------------------------------------|---------------------------------------|---------------------------------------|---------------------------------------|---------------------------------------|----------|--|----------|----------|
| 4.10E+01 | 1.43E+01 | 1.63E+01 | 1.53E+01 | 1.57E+01 | 1.37E+01 | 1.34E+00 | 1.39E-02 | 2.04E+02 | 4.00E+00 |
| 3.73E+01 | 1.42E+01 | 1.61E+01 | 1.50E+01 | 1.56E+01 | 1.36E+01 | 1.47E+00 | 1.56E-02 | 2.28E+02 | 4.00E+00 |
| 3.31E+01 | 1.38E+01 | 1.58E+01 | 1.45E+01 | 1.51E+01 | 1.33E+01 | 1.65E+00 | 1.75E-02 | 2.54E+02 | 4.00E+00 |
| 2.99E+01 | 1.36E+01 | 1.59E+01 | 1.43E+01 | 1.46E+01 | 1.32E+01 | 1.83E+00 | 1.90E-02 | 2.77E+02 | 4.01E+00 |
| 2.59E+01 | 1.33E+01 | 1.58E+01 | 1.39E+01 | 1.37E+01 | 1.30E+01 | 2.09E+00 | 2.06E-02 | 3.00E+02 | 4.01E+00 |
| 2.27E+01 | 1.31E+01 | 1.62E+01 | 1.37E+01 | 1.31E+01 | 1.29E+01 | 2.38E+00 | 2.20E-02 | 3.19E+02 | 4.01E+00 |
| 1.94E+01 | 1.26E+01 | 1.61E+01 | 1.32E+01 | 1.20E+01 | 1.25E+01 | 2.77E+00 | 2.35E-02 | 3.41E+02 | 4.01E+00 |

Table B.20 Refrigerant: HFC-134a, Tu-B surface, Square Pitch, Nozzle Configuration: 30WHCRC,
Refrigerant Supply Rate: 25 kg/min, Pure Refrigerant Data

| q'' ($\frac{kW}{m^2 \cdot K}$) | h_b ($\frac{kW}{m^2 \cdot K}$) | h_1 ($\frac{kW}{m^2 \cdot K}$) | h_2 ($\frac{kW}{m^2 \cdot K}$) | h_3 ($\frac{kW}{m^2 \cdot K}$) | h_4 ($\frac{kW}{m^2 \cdot K}$) | OFR | Γ_4 ($\frac{kg}{s \cdot m}$) | Re_4 | Pr_4 |
|---------------------------------------|---------------------------------------|---------------------------------------|---------------------------------------|---------------------------------------|---------------------------------------|----------|--|----------|----------|
| 4.06E+01 | 1.44E+01 | 1.46E+01 | 1.39E+01 | 1.51E+01 | 1.32E+01 | 2.15E+00 | 3.33E-02 | 4.86E+02 | 4.00E+00 |
| 3.72E+01 | 1.43E+01 | 1.47E+01 | 1.37E+01 | 1.49E+01 | 1.30E+01 | 2.37E+00 | 3.55E-02 | 5.19E+02 | 4.00E+00 |
| 3.35E+01 | 1.41E+01 | 1.46E+01 | 1.34E+01 | 1.46E+01 | 1.28E+01 | 2.61E+00 | 3.69E-02 | 5.37E+02 | 4.00E+00 |
| 2.98E+01 | 1.40E+01 | 1.49E+01 | 1.31E+01 | 1.40E+01 | 1.27E+01 | 2.87E+00 | 3.77E-02 | 5.48E+02 | 4.01E+00 |
| 2.62E+01 | 1.37E+01 | 1.51E+01 | 1.28E+01 | 1.33E+01 | 1.26E+01 | 3.25E+00 | 3.93E-02 | 5.71E+02 | 4.01E+00 |
| 2.29E+01 | 1.35E+01 | 1.56E+01 | 1.25E+01 | 1.26E+01 | 1.22E+01 | 3.68E+00 | 4.05E-02 | 5.88E+02 | 4.01E+00 |
| 1.95E+01 | 1.29E+01 | 1.57E+01 | 1.17E+01 | 1.15E+01 | 1.16E+01 | 4.46E+00 | 4.38E-02 | 6.35E+02 | 4.01E+00 |

Table B.21 Refrigerant: HFC-134a, Tu-B surface, Square Pitch, Nozzle Configuration: 30WHCRC,
Refrigerant Supply Rate: 35 kg/min, Pure Refrigerant Data

| q'' $\left(\frac{\text{kW}}{\text{m}^2 \cdot \text{K}}\right)$ | h_b $\left(\frac{\text{kW}}{\text{m}^2 \cdot \text{K}}\right)$ | h_1 $\left(\frac{\text{kW}}{\text{m}^2 \cdot \text{K}}\right)$ | h_2 $\left(\frac{\text{kW}}{\text{m}^2 \cdot \text{K}}\right)$ | h_3 $\left(\frac{\text{kW}}{\text{m}^2 \cdot \text{K}}\right)$ | h_4 $\left(\frac{\text{kW}}{\text{m}^2 \cdot \text{K}}\right)$ | OFR | Γ_4 $\left(\frac{\text{kg}}{\text{s} \cdot \text{m}}\right)$ | Re_4 | Pr_4 |
|---|---|---|---|---|---|----------|--|----------|----------|
| 4.04E+01 | 1.47E+01 | 1.55E+01 | 1.37E+01 | 1.45E+01 | 1.35E+01 | 2.96E+00 | 5.26E-02 | 7.68E+02 | 4.00E+00 |
| 3.71E+01 | 1.49E+01 | 1.59E+01 | 1.37E+01 | 1.44E+01 | 1.36E+01 | 3.16E+00 | 5.24E-02 | 7.64E+02 | 4.00E+00 |
| 3.38E+01 | 1.48E+01 | 1.63E+01 | 1.34E+01 | 1.42E+01 | 1.34E+01 | 3.49E+00 | 5.42E-02 | 7.90E+02 | 4.00E+00 |
| 3.05E+01 | 1.47E+01 | 1.66E+01 | 1.33E+01 | 1.37E+01 | 1.33E+01 | 3.88E+00 | 5.66E-02 | 8.24E+02 | 4.01E+00 |
| 2.68E+01 | 1.44E+01 | 1.70E+01 | 1.29E+01 | 1.29E+01 | 1.31E+01 | 4.31E+00 | 5.72E-02 | 8.31E+02 | 4.01E+00 |
| 2.34E+01 | 1.42E+01 | 1.76E+01 | 1.26E+01 | 1.21E+01 | 1.27E+01 | 4.94E+00 | 5.90E-02 | 8.56E+02 | 4.01E+00 |
| 1.90E+01 | 1.33E+01 | 1.77E+01 | 1.19E+01 | 1.07E+01 | 1.18E+01 | 5.95E+00 | 6.00E-02 | 8.69E+02 | 4.01E+00 |

Table B.22 Refrigerant: HFC-134a, Tu-B surface, Square Pitch, Nozzle Configuration: 30WHCRC,
Refrigerant Supply Rate: 45 kg/min, Pure Refrigerant Data

| q'' $\left(\frac{\text{kW}}{\text{m}^2 \cdot \text{K}}\right)$ | h_b $\left(\frac{\text{kW}}{\text{m}^2 \cdot \text{K}}\right)$ | h_1 $\left(\frac{\text{kW}}{\text{m}^2 \cdot \text{K}}\right)$ | h_2 $\left(\frac{\text{kW}}{\text{m}^2 \cdot \text{K}}\right)$ | h_3 $\left(\frac{\text{kW}}{\text{m}^2 \cdot \text{K}}\right)$ | h_4 $\left(\frac{\text{kW}}{\text{m}^2 \cdot \text{K}}\right)$ | OFR | Γ_4 $\left(\frac{\text{kg}}{\text{s} \cdot \text{m}}\right)$ | Re_4 | Pr_4 |
|---|---|---|---|---|---|----------|--|----------|----------|
| 4.08E+01 | 1.50E+01 | 1.52E+01 | 1.35E+01 | 1.50E+01 | 1.43E+01 | 3.70E+00 | 6.98E-02 | 1.02E+03 | 4.00E+00 |
| 3.66E+01 | 1.49E+01 | 1.57E+01 | 1.33E+01 | 1.45E+01 | 1.39E+01 | 3.97E+00 | 7.03E-02 | 1.02E+03 | 4.00E+00 |
| 3.34E+01 | 1.49E+01 | 1.62E+01 | 1.31E+01 | 1.42E+01 | 1.37E+01 | 4.31E+00 | 7.13E-02 | 1.04E+03 | 4.00E+00 |
| 3.02E+01 | 1.49E+01 | 1.72E+01 | 1.29E+01 | 1.36E+01 | 1.35E+01 | 4.73E+00 | 7.23E-02 | 1.05E+03 | 4.01E+00 |
| 2.66E+01 | 1.48E+01 | 1.80E+01 | 1.27E+01 | 1.29E+01 | 1.32E+01 | 5.35E+00 | 7.44E-02 | 1.08E+03 | 4.01E+00 |
| 2.33E+01 | 1.47E+01 | 1.92E+01 | 1.24E+01 | 1.22E+01 | 1.29E+01 | 6.05E+00 | 7.56E-02 | 1.10E+03 | 4.01E+00 |
| 1.97E+01 | 1.41E+01 | 1.97E+01 | 1.19E+01 | 1.10E+01 | 1.21E+01 | 7.03E+00 | 7.66E-02 | 1.11E+03 | 4.01E+00 |

Table B.23 Refrigerant: HFC-134a, W-40 fpi surface, Triangular Pitch, Nozzle Configuration: 17WHCRC, Refrigerant Supply Rate: 25 kg/min, Pure Refrigerant Data

| q'' $\left(\frac{\text{kW}}{\text{m}^2 \cdot \text{K}}\right)$ | h_b $\left(\frac{\text{kW}}{\text{m}^2 \cdot \text{K}}\right)$ | h_1 $\left(\frac{\text{kW}}{\text{m}^2 \cdot \text{K}}\right)$ | h_2 $\left(\frac{\text{kW}}{\text{m}^2 \cdot \text{K}}\right)$ | h_3 $\left(\frac{\text{kW}}{\text{m}^2 \cdot \text{K}}\right)$ | h_4 $\left(\frac{\text{kW}}{\text{m}^2 \cdot \text{K}}\right)$ |
|---|---|---|---|---|---|
| 4.06E+01 | 6.08E+00 | 1.82E+01 | 4.58E+00 | 8.41E+00 | 7.18E-01 |
| 3.67E+01 | 6.57E+00 | 1.81E+01 | 5.22E+00 | 8.92E+00 | 9.02E-01 |
| 3.35E+01 | 6.96E+00 | 1.78E+01 | 5.82E+00 | 9.28E+00 | 1.09E+00 |
| 3.01E+01 | 7.22E+00 | 1.67E+01 | 6.29E+00 | 9.25E+00 | 1.26E+00 |
| 2.67E+01 | 7.14E+00 | 1.53E+01 | 6.46E+00 | 8.76E+00 | 1.43E+00 |
| 2.32E+01 | 6.91E+00 | 1.26E+01 | 6.10E+00 | 7.87E+00 | 1.73E+00 |
| 2.00E+01 | 6.19E+00 | 9.05E+00 | 5.23E+00 | 6.54E+00 | 1.98E+00 |

Table B.24 Refrigerant: HFC-134a, W-40 fpi surface, Triangular Pitch, Nozzle Configuration: 17WLCRC, Refrigerant Supply Rate: 25 kg/min, Pure Refrigerant Data

| q'' $\left(\frac{\text{kW}}{\text{m}^2 \cdot \text{K}}\right)$ | h_b $\left(\frac{\text{kW}}{\text{m}^2 \cdot \text{K}}\right)$ | h_1 $\left(\frac{\text{kW}}{\text{m}^2 \cdot \text{K}}\right)$ | h_2 $\left(\frac{\text{kW}}{\text{m}^2 \cdot \text{K}}\right)$ | h_3 $\left(\frac{\text{kW}}{\text{m}^2 \cdot \text{K}}\right)$ | h_4 $\left(\frac{\text{kW}}{\text{m}^2 \cdot \text{K}}\right)$ |
|---|---|---|---|---|---|
| 4.03E+01 | 6.55E+00 | 1.82E+01 | 6.42E+00 | 8.69E+00 | 1.38E+00 |
| 3.66E+01 | 7.00E+00 | 1.83E+01 | 6.99E+00 | 9.25E+00 | 1.57E+00 |
| 3.34E+01 | 7.30E+00 | 1.80E+01 | 7.46E+00 | 9.32E+00 | 1.82E+00 |
| 2.98E+01 | 7.55E+00 | 1.71E+01 | 7.64E+00 | 9.10E+00 | 2.08E+00 |
| 2.61E+01 | 7.52E+00 | 1.53E+01 | 7.47E+00 | 8.57E+00 | 2.40E+00 |
| 2.29E+01 | 7.14E+00 | 1.27E+01 | 6.82E+00 | 7.57E+00 | 2.64E+00 |
| 1.98E+01 | 6.23E+00 | 9.19E+00 | 5.55E+00 | 6.21E+00 | 2.74E+00 |

Table B.25 Refrigerant: HFC-134a, W-40 fpi surface, Triangular Pitch, Nozzle Configuration: 24WHCRC, Refrigerant Supply Rate: 25 kg/min, Pure Refrigerant Data

| q'' $\left(\frac{\text{kW}}{\text{m}^2 \cdot \text{K}}\right)$ | h_b $\left(\frac{\text{kW}}{\text{m}^2 \cdot \text{K}}\right)$ | h_1 $\left(\frac{\text{kW}}{\text{m}^2 \cdot \text{K}}\right)$ | h_2 $\left(\frac{\text{kW}}{\text{m}^2 \cdot \text{K}}\right)$ | h_3 $\left(\frac{\text{kW}}{\text{m}^2 \cdot \text{K}}\right)$ | h_4 $\left(\frac{\text{kW}}{\text{m}^2 \cdot \text{K}}\right)$ |
|---|---|---|---|---|---|
| 4.06E+01 | 7.76E+00 | 1.86E+01 | 7.19E+00 | 1.08E+01 | 1.40E+00 |
| 3.69E+01 | 8.19E+00 | 1.85E+01 | 7.76E+00 | 1.05E+01 | 1.62E+00 |
| 3.35E+01 | 8.48E+00 | 1.86E+01 | 8.11E+00 | 1.05E+01 | 1.86E+00 |
| 2.96E+01 | 8.68E+00 | 1.75E+01 | 8.31E+00 | 9.87E+00 | 2.14E+00 |
| 2.60E+01 | 8.58E+00 | 1.58E+01 | 8.04E+00 | 9.06E+00 | 2.45E+00 |
| 2.28E+01 | 8.16E+00 | 1.27E+01 | 7.23E+00 | 8.19E+00 | 2.71E+00 |
| 1.93E+01 | 7.00E+00 | 9.08E+00 | 5.87E+00 | 6.62E+00 | 2.81E+00 |

Table B.26 Refrigerant: HFC-134a, W-40 fpi surface, Triangular Pitch, Nozzle Configuration: 24WLCRC, Refrigerant Supply Rate: 25 kg/min, Pure Refrigerant Data

| q'' $\left(\frac{\text{kW}}{\text{m}^2 \cdot \text{K}}\right)$ | h_b $\left(\frac{\text{kW}}{\text{m}^2 \cdot \text{K}}\right)$ | h_1 $\left(\frac{\text{kW}}{\text{m}^2 \cdot \text{K}}\right)$ | h_2 $\left(\frac{\text{kW}}{\text{m}^2 \cdot \text{K}}\right)$ | h_3 $\left(\frac{\text{kW}}{\text{m}^2 \cdot \text{K}}\right)$ | h_4 $\left(\frac{\text{kW}}{\text{m}^2 \cdot \text{K}}\right)$ |
|---|---|---|---|---|---|
| 4.08E+01 | 7.63E+00 | 1.85E+01 | 8.36E+00 | 9.28E+00 | 2.13E+00 |
| 3.70E+01 | 7.99E+00 | 1.87E+01 | 8.96E+00 | 9.45E+00 | 2.36E+00 |
| 3.40E+01 | 8.34E+00 | 1.88E+01 | 9.24E+00 | 9.65E+00 | 2.60E+00 |
| 3.03E+01 | 8.49E+00 | 1.75E+01 | 9.17E+00 | 9.20E+00 | 2.87E+00 |
| 2.68E+01 | 8.49E+00 | 1.59E+01 | 8.77E+00 | 8.70E+00 | 3.18E+00 |
| 2.32E+01 | 8.02E+00 | 1.31E+01 | 7.75E+00 | 7.72E+00 | 3.38E+00 |
| 1.97E+01 | 6.97E+00 | 9.54E+00 | 6.28E+00 | 6.49E+00 | 3.39E+00 |

Table B.27 Refrigerant: HFC-134a, W-40 fpi surface, Triangular Pitch, Nozzle Configuration: 24WHSQR, Refrigerant Supply Rate: 25 kg/min, Pure Refrigerant Data

| q'' $\left(\frac{\text{kW}}{\text{m}^2 \cdot \text{K}}\right)$ | h_b $\left(\frac{\text{kW}}{\text{m}^2 \cdot \text{K}}\right)$ | h_1 $\left(\frac{\text{kW}}{\text{m}^2 \cdot \text{K}}\right)$ | h_2 $\left(\frac{\text{kW}}{\text{m}^2 \cdot \text{K}}\right)$ | h_3 $\left(\frac{\text{kW}}{\text{m}^2 \cdot \text{K}}\right)$ | h_4 $\left(\frac{\text{kW}}{\text{m}^2 \cdot \text{K}}\right)$ |
|---|---|---|---|---|---|
| 4.04E+01 | 7.67E+00 | 1.84E+01 | 6.81E+00 | 1.00E+01 | 1.38E+00 |
| 3.70E+01 | 8.09E+00 | 1.86E+01 | 7.50E+00 | 1.00E+01 | 1.57E+00 |
| 3.35E+01 | 8.46E+00 | 1.82E+01 | 7.98E+00 | 9.94E+00 | 1.80E+00 |
| 2.98E+01 | 8.64E+00 | 1.72E+01 | 8.17E+00 | 9.53E+00 | 2.07E+00 |
| 2.63E+01 | 8.57E+00 | 1.57E+01 | 7.96E+00 | 8.83E+00 | 2.34E+00 |
| 2.27E+01 | 8.09E+00 | 1.28E+01 | 7.16E+00 | 7.90E+00 | 2.58E+00 |
| 1.91E+01 | 6.96E+00 | 8.97E+00 | 5.85E+00 | 6.47E+00 | 2.69E+00 |

Table B.28 Refrigerant: HFC-134a, W-40 fpi surface, Triangular Pitch, Nozzle Configuration: 24WLSQR, Refrigerant Supply Rate: 25 kg/min, Pure Refrigerant Data

| q'' $\left(\frac{\text{kW}}{\text{m}^2 \cdot \text{K}}\right)$ | h_b $\left(\frac{\text{kW}}{\text{m}^2 \cdot \text{K}}\right)$ | h_1 $\left(\frac{\text{kW}}{\text{m}^2 \cdot \text{K}}\right)$ | h_2 $\left(\frac{\text{kW}}{\text{m}^2 \cdot \text{K}}\right)$ | h_3 $\left(\frac{\text{kW}}{\text{m}^2 \cdot \text{K}}\right)$ | h_4 $\left(\frac{\text{kW}}{\text{m}^2 \cdot \text{K}}\right)$ |
|---|---|---|---|---|---|
| 4.01E+01 | 7.76E+00 | 1.80E+01 | 8.93E+00 | 9.83E+00 | 1.99E+00 |
| 3.67E+01 | 8.20E+00 | 1.83E+01 | 9.34E+00 | 9.90E+00 | 2.21E+00 |
| 3.33E+01 | 8.48E+00 | 1.78E+01 | 9.57E+00 | 9.81E+00 | 2.52E+00 |
| 2.96E+01 | 8.72E+00 | 1.71E+01 | 9.48E+00 | 9.45E+00 | 2.93E+00 |
| 2.62E+01 | 8.64E+00 | 1.56E+01 | 9.11E+00 | 8.65E+00 | 3.16E+00 |
| 2.28E+01 | 8.12E+00 | 1.28E+01 | 7.90E+00 | 7.78E+00 | 3.36E+00 |
| 1.95E+01 | 6.88E+00 | 9.02E+00 | 6.20E+00 | 6.36E+00 | 3.28E+00 |

Table B.29 Refrigerant: HFC-134a, W-40 fpi surface, Triangular Pitch, Nozzle Configuration: 30WHSQR, Refrigerant Supply Rate: 25 kg/min, Pure Refrigerant Data

| q'' $\left(\frac{\text{kW}}{\text{m}^2 \cdot \text{K}}\right)$ | h_b $\left(\frac{\text{kW}}{\text{m}^2 \cdot \text{K}}\right)$ | h_1 $\left(\frac{\text{kW}}{\text{m}^2 \cdot \text{K}}\right)$ | h_2 $\left(\frac{\text{kW}}{\text{m}^2 \cdot \text{K}}\right)$ | h_3 $\left(\frac{\text{kW}}{\text{m}^2 \cdot \text{K}}\right)$ | h_4 $\left(\frac{\text{kW}}{\text{m}^2 \cdot \text{K}}\right)$ |
|---|---|---|---|---|---|
| 4.07E+01 | 1.05E+01 | 1.90E+01 | 1.17E+01 | 1.13E+01 | 3.87E+00 |
| 3.70E+01 | 1.08E+01 | 1.93E+01 | 1.20E+01 | 1.11E+01 | 4.07E+00 |
| 3.33E+01 | 1.10E+01 | 1.90E+01 | 1.21E+01 | 1.07E+01 | 4.32E+00 |
| 3.00E+01 | 1.09E+01 | 1.86E+01 | 1.19E+01 | 1.03E+01 | 4.56E+00 |
| 2.63E+01 | 1.05E+01 | 1.68E+01 | 1.09E+01 | 9.42E+00 | 4.68E+00 |
| 2.28E+01 | 9.49E+00 | 1.36E+01 | 9.36E+00 | 8.25E+00 | 4.77E+00 |
| 1.97E+01 | 7.75E+00 | 9.48E+00 | 7.20E+00 | 6.67E+00 | 4.31E+00 |

Table B.30 Refrigerant: HFC-134a, W-40 fpi surface, Triangular Pitch, Nozzle Configuration: 30WHSQR, Refrigerant Supply Rate: 45 kg/min, Pure Refrigerant Data

| q'' $\left(\frac{\text{kW}}{\text{m}^2 \cdot \text{K}}\right)$ | h_b $\left(\frac{\text{kW}}{\text{m}^2 \cdot \text{K}}\right)$ | h_1 $\left(\frac{\text{kW}}{\text{m}^2 \cdot \text{K}}\right)$ | h_2 $\left(\frac{\text{kW}}{\text{m}^2 \cdot \text{K}}\right)$ | h_3 $\left(\frac{\text{kW}}{\text{m}^2 \cdot \text{K}}\right)$ | h_4 $\left(\frac{\text{kW}}{\text{m}^2 \cdot \text{K}}\right)$ |
|---|---|---|---|---|---|
| 4.06E+01 | 1.13E+01 | 1.81E+01 | 1.29E+01 | 1.12E+01 | 5.19E+00 |
| 3.69E+01 | 1.14E+01 | 1.81E+01 | 1.30E+01 | 1.13E+01 | 5.64E+00 |
| 3.35E+01 | 1.14E+01 | 1.79E+01 | 1.31E+01 | 1.09E+01 | 5.95E+00 |
| 2.97E+01 | 1.10E+01 | 1.70E+01 | 1.25E+01 | 1.04E+01 | 6.30E+00 |
| 2.61E+01 | 1.05E+01 | 1.53E+01 | 1.15E+01 | 9.77E+00 | 6.46E+00 |
| 2.30E+01 | 9.33E+00 | 1.24E+01 | 9.69E+00 | 8.53E+00 | 6.28E+00 |
| 1.94E+01 | 7.50E+00 | 8.88E+00 | 7.41E+00 | 6.93E+00 | 5.35E+00 |

Table B.31 Refrigerant: HFC-134a, W-40 fpi surface, Triangular Pitch, Pool Boiling, Pure Refrigerant Data

| q'' $\left(\frac{\text{kW}}{\text{m}^2 \cdot \text{K}}\right)$ | h_b $\left(\frac{\text{kW}}{\text{m}^2 \cdot \text{K}}\right)$ | h_1 $\left(\frac{\text{kW}}{\text{m}^2 \cdot \text{K}}\right)$ | h_2 $\left(\frac{\text{kW}}{\text{m}^2 \cdot \text{K}}\right)$ | h_3 $\left(\frac{\text{kW}}{\text{m}^2 \cdot \text{K}}\right)$ | h_4 $\left(\frac{\text{kW}}{\text{m}^2 \cdot \text{K}}\right)$ |
|---|---|---|---|---|---|
| 3.71E+01 | 1.04E+01 | 1.23E+01 | 9.66E+00 | 9.29E+00 | 6.21E+00 |
| 3.32E+01 | 1.01E+01 | 1.19E+01 | 9.28E+00 | 8.78E+00 | 6.11E+00 |
| 2.96E+01 | 9.59E+00 | 1.10E+01 | 8.68E+00 | 8.15E+00 | 6.03E+00 |
| 2.64E+01 | 8.82E+00 | 1.01E+01 | 7.99E+00 | 7.25E+00 | 5.63E+00 |
| 2.29E+01 | 7.80E+00 | 8.67E+00 | 6.76E+00 | 6.25E+00 | 5.10E+00 |
| 1.90E+01 | 6.20E+00 | 6.55E+00 | 5.30E+00 | 5.06E+00 | 4.21E+00 |

Table B.32 Refrigerant: HFC-134a, Tu-B surface, Triangular Pitch,
Pool Boiling, Pure Refrigerant Data

| q'' $\left(\frac{\text{kW}}{\text{m}^2 \cdot \text{K}}\right)$ | h_b $\left(\frac{\text{kW}}{\text{m}^2 \cdot \text{K}}\right)$ | h_1 $\left(\frac{\text{kW}}{\text{m}^2 \cdot \text{K}}\right)$ | h_2 $\left(\frac{\text{kW}}{\text{m}^2 \cdot \text{K}}\right)$ | h_3 $\left(\frac{\text{kW}}{\text{m}^2 \cdot \text{K}}\right)$ | h_4 $\left(\frac{\text{kW}}{\text{m}^2 \cdot \text{K}}\right)$ |
|---|---|---|---|---|---|
| 3.69E+01 | 1.63E+01 | 1.66E+01 | 1.70E+01 | 1.19E+01 | 1.41E+01 |
| 3.35E+01 | 1.69E+01 | 1.68E+01 | 1.77E+01 | 1.21E+01 | 1.45E+01 |
| 3.00E+01 | 1.72E+01 | 1.66E+01 | 1.82E+01 | 1.21E+01 | 1.50E+01 |
| 2.70E+01 | 1.75E+01 | 1.58E+01 | 1.86E+01 | 1.21E+01 | 1.53E+01 |
| 2.30E+01 | 1.76E+01 | 1.44E+01 | 1.76E+01 | 1.19E+01 | 1.62E+01 |
| 1.94E+01 | 1.65E+01 | 1.22E+01 | 1.57E+01 | 1.10E+01 | 1.56E+01 |

Table B.33 Refrigerant: HFC-134a, Plain surface, Triangular Pitch, Nozzle Configuration:
30WHCRC, Refrigerant Supply Rate: 15 kg/min, 1.0 % Oil Concentration

| q'' $\left(\frac{\text{kW}}{\text{m}^2 \cdot \text{K}}\right)$ | h_b $\left(\frac{\text{kW}}{\text{m}^2 \cdot \text{K}}\right)$ | h_1 $\left(\frac{\text{kW}}{\text{m}^2 \cdot \text{K}}\right)$ | h_2 $\left(\frac{\text{kW}}{\text{m}^2 \cdot \text{K}}\right)$ | h_3 $\left(\frac{\text{kW}}{\text{m}^2 \cdot \text{K}}\right)$ | h_4 $\left(\frac{\text{kW}}{\text{m}^2 \cdot \text{K}}\right)$ | OFR | Γ_4 $\left(\frac{\text{kg}}{\text{s} \cdot \text{m}}\right)$ |
|---|---|---|---|---|---|----------|--|
| 4.04E+01 | 5.65E+00 | 5.35E+00 | 5.79E+00 | 5.19E+00 | 5.43E+00 | 1.43E+00 | 1.62E-02 |
| 3.67E+01 | 5.58E+00 | 5.22E+00 | 5.68E+00 | 4.92E+00 | 5.29E+00 | 1.57E+00 | 1.79E-02 |
| 3.30E+01 | 5.46E+00 | 4.95E+00 | 5.53E+00 | 4.34E+00 | 5.04E+00 | 1.75E+00 | 1.97E-02 |
| 2.96E+01 | 5.33E+00 | 4.70E+00 | 5.40E+00 | 3.97E+00 | 4.74E+00 | 1.94E+00 | 2.11E-02 |
| 2.65E+01 | 5.20E+00 | 4.40E+00 | 5.21E+00 | 3.86E+00 | 4.44E+00 | 2.18E+00 | 2.27E-02 |
| 2.31E+01 | 5.01E+00 | 4.12E+00 | 4.92E+00 | 3.99E+00 | 4.30E+00 | 2.49E+00 | 2.40E-02 |
| 1.90E+01 | 4.80E+00 | 3.90E+00 | 4.65E+00 | 4.26E+00 | 4.31E+00 | 3.03E+00 | 2.60E-02 |

Table B.34 Refrigerant: HFC-134a, Plain surface, Triangular Pitch, Nozzle Configuration:
30WHCRC, Refrigerant Supply Rate: 35 kg/min, 1.0 % Oil Concentration

| q'' $\left(\frac{\text{kW}}{\text{m}^2 \cdot \text{K}}\right)$ | h_b $\left(\frac{\text{kW}}{\text{m}^2 \cdot \text{K}}\right)$ | h_1 $\left(\frac{\text{kW}}{\text{m}^2 \cdot \text{K}}\right)$ | h_2 $\left(\frac{\text{kW}}{\text{m}^2 \cdot \text{K}}\right)$ | h_3 $\left(\frac{\text{kW}}{\text{m}^2 \cdot \text{K}}\right)$ | h_4 $\left(\frac{\text{kW}}{\text{m}^2 \cdot \text{K}}\right)$ | OFR | Γ_4 $\left(\frac{\text{kg}}{\text{s} \cdot \text{m}}\right)$ |
|---|---|---|---|---|---|----------|--|
| 4.03E+01 | 6.31E+00 | 5.16E+00 | 5.42E+00 | 5.91E+00 | 5.72E+00 | 3.05E+00 | 5.55E-02 |
| 3.68E+01 | 6.35E+00 | 5.14E+00 | 5.57E+00 | 5.78E+00 | 5.63E+00 | 3.35E+00 | 5.73E-02 |
| 3.30E+01 | 6.20E+00 | 5.02E+00 | 5.55E+00 | 5.59E+00 | 5.51E+00 | 3.75E+00 | 5.95E-02 |
| 2.96E+01 | 5.96E+00 | 4.76E+00 | 5.43E+00 | 5.00E+00 | 5.32E+00 | 4.00E+00 | 5.81E-02 |
| 2.63E+01 | 5.66E+00 | 4.51E+00 | 5.26E+00 | 4.57E+00 | 5.10E+00 | 4.62E+00 | 6.19E-02 |
| 2.28E+01 | 5.38E+00 | 4.29E+00 | 5.00E+00 | 4.34E+00 | 4.82E+00 | 5.42E+00 | 6.53E-02 |
| 1.88E+01 | 5.03E+00 | 4.01E+00 | 4.63E+00 | 4.45E+00 | 4.57E+00 | 6.28E+00 | 6.45E-02 |

Table B.35 Refrigerant: HFC-134a, Plain surface, Triangular Pitch, Nozzle Configuration: 30WHCRC, Refrigerant Supply Rate: 15 kg/min, 2.5 % Oil Concentration

| q'' $\left(\frac{\text{kW}}{\text{m}^2 \cdot \text{K}}\right)$ | h_b $\left(\frac{\text{kW}}{\text{m}^2 \cdot \text{K}}\right)$ | h_1 $\left(\frac{\text{kW}}{\text{m}^2 \cdot \text{K}}\right)$ | h_2 $\left(\frac{\text{kW}}{\text{m}^2 \cdot \text{K}}\right)$ | h_3 $\left(\frac{\text{kW}}{\text{m}^2 \cdot \text{K}}\right)$ | h_4 $\left(\frac{\text{kW}}{\text{m}^2 \cdot \text{K}}\right)$ | OFR | Γ_4 $\left(\frac{\text{kg}}{\text{s} \cdot \text{m}}\right)$ |
|---|---|---|---|---|---|----------|--|
| 4.03E+01 | 6.92E+00 | 7.30E+00 | 7.71E+00 | 7.25E+00 | 6.73E+00 | 1.44E+00 | 1.63E-02 |
| 3.71E+01 | 7.14E+00 | 7.18E+00 | 7.61E+00 | 7.29E+00 | 7.10E+00 | 1.56E+00 | 1.79E-02 |
| 3.34E+01 | 7.28E+00 | 7.00E+00 | 7.45E+00 | 7.20E+00 | 7.17E+00 | 1.74E+00 | 1.96E-02 |
| 2.97E+01 | 7.28E+00 | 6.61E+00 | 7.36E+00 | 7.15E+00 | 6.98E+00 | 1.96E+00 | 2.14E-02 |
| 2.61E+01 | 7.16E+00 | 6.21E+00 | 7.20E+00 | 7.03E+00 | 6.71E+00 | 2.18E+00 | 2.24E-02 |
| 2.27E+01 | 6.98E+00 | 5.92E+00 | 6.87E+00 | 6.88E+00 | 6.37E+00 | 2.51E+00 | 2.40E-02 |
| 1.94E+01 | 6.63E+00 | 5.58E+00 | 6.67E+00 | 6.40E+00 | 5.54E+00 | 2.94E+00 | 2.56E-02 |

Table B.36 Refrigerant: HFC-134a, Plain surface, Triangular Pitch, Nozzle Configuration: 30WHCRC, Refrigerant Supply Rate: 35 kg/min, 2.5 % Oil Concentration

| q'' $\left(\frac{\text{kW}}{\text{m}^2 \cdot \text{K}}\right)$ | h_b $\left(\frac{\text{kW}}{\text{m}^2 \cdot \text{K}}\right)$ | h_1 $\left(\frac{\text{kW}}{\text{m}^2 \cdot \text{K}}\right)$ | h_2 $\left(\frac{\text{kW}}{\text{m}^2 \cdot \text{K}}\right)$ | h_3 $\left(\frac{\text{kW}}{\text{m}^2 \cdot \text{K}}\right)$ | h_4 $\left(\frac{\text{kW}}{\text{m}^2 \cdot \text{K}}\right)$ | OFR | Γ_4 $\left(\frac{\text{kg}}{\text{s} \cdot \text{m}}\right)$ |
|---|---|---|---|---|---|----------|--|
| 4.03E+01 | 8.28E+00 | 6.98E+00 | 7.54E+00 | 8.35E+00 | 8.02E+00 | 3.03E+00 | 5.48E-02 |
| 3.69E+01 | 8.35E+00 | 6.96E+00 | 7.54E+00 | 8.21E+00 | 7.97E+00 | 3.30E+00 | 5.63E-02 |
| 3.32E+01 | 8.28E+00 | 6.76E+00 | 7.46E+00 | 8.09E+00 | 7.82E+00 | 3.69E+00 | 5.78E-02 |
| 2.98E+01 | 8.23E+00 | 6.49E+00 | 7.47E+00 | 7.88E+00 | 7.47E+00 | 4.14E+00 | 5.95E-02 |
| 2.63E+01 | 8.08E+00 | 6.08E+00 | 7.28E+00 | 7.51E+00 | 7.13E+00 | 4.80E+00 | 6.25E-02 |
| 2.28E+01 | 7.78E+00 | 5.79E+00 | 7.02E+00 | 7.18E+00 | 6.57E+00 | 5.46E+00 | 6.22E-02 |
| 1.90E+01 | 7.31E+00 | 5.49E+00 | 6.74E+00 | 6.90E+00 | 6.09E+00 | 6.74E+00 | 6.63E-02 |

Table B.37 Refrigerant: HFC-134a, W-40 fpi surface, Triangular Pitch, Nozzle Configuration: 30WHCRC, Refrigerant Supply Rate: 15 kg/min, 1.0 % Oil Concentration

| q'' $\left(\frac{\text{kW}}{\text{m}^2 \cdot \text{K}}\right)$ | h_b $\left(\frac{\text{kW}}{\text{m}^2 \cdot \text{K}}\right)$ | h_1 $\left(\frac{\text{kW}}{\text{m}^2 \cdot \text{K}}\right)$ | h_2 $\left(\frac{\text{kW}}{\text{m}^2 \cdot \text{K}}\right)$ | h_3 $\left(\frac{\text{kW}}{\text{m}^2 \cdot \text{K}}\right)$ | h_4 $\left(\frac{\text{kW}}{\text{m}^2 \cdot \text{K}}\right)$ | OFR | Γ_4 $\left(\frac{\text{kg}}{\text{s} \cdot \text{m}}\right)$ |
|---|---|---|---|---|---|----------|--|
| 4.07E+01 | 1.31E+01 | 2.35E+01 | 1.56E+01 | 7.11E+00 | 3.06E+00 | 1.44E+00 | 1.42E-02 |
| 3.70E+01 | 1.33E+01 | 2.35E+01 | 1.55E+01 | 6.78E+00 | 3.45E+00 | 1.58E+00 | 1.61E-02 |
| 3.35E+01 | 1.34E+01 | 2.36E+01 | 1.52E+01 | 6.79E+00 | 4.00E+00 | 1.73E+00 | 1.80E-02 |
| 2.99E+01 | 1.34E+01 | 2.23E+01 | 1.45E+01 | 6.94E+00 | 5.06E+00 | 1.92E+00 | 1.99E-02 |
| 2.62E+01 | 1.31E+01 | 2.05E+01 | 1.29E+01 | 7.50E+00 | 6.46E+00 | 2.18E+00 | 2.19E-02 |
| 2.26E+01 | 1.21E+01 | 1.57E+01 | 1.09E+01 | 7.41E+00 | 7.58E+00 | 2.53E+00 | 2.40E-02 |
| 1.92E+01 | 9.73E+00 | 1.05E+01 | 7.85E+00 | 6.39E+00 | 7.25E+00 | 2.96E+00 | 2.55E-02 |

Table B.38 Refrigerant: HFC-134a, W-40 fpi surface, Triangular Pitch, Nozzle Configuration: 30WHCRC, Refrigerant Supply Rate: 35 kg/min, 1.0 % Oil Concentration

| q'' $\left(\frac{\text{kW}}{\text{m}^2 \cdot \text{K}}\right)$ | h_b $\left(\frac{\text{kW}}{\text{m}^2 \cdot \text{K}}\right)$ | h_1 $\left(\frac{\text{kW}}{\text{m}^2 \cdot \text{K}}\right)$ | h_2 $\left(\frac{\text{kW}}{\text{m}^2 \cdot \text{K}}\right)$ | h_3 $\left(\frac{\text{kW}}{\text{m}^2 \cdot \text{K}}\right)$ | h_4 $\left(\frac{\text{kW}}{\text{m}^2 \cdot \text{K}}\right)$ | OFR | Γ_4 $\left(\frac{\text{kg}}{\text{s} \cdot \text{m}}\right)$ |
|---|---|---|---|---|---|----------|--|
| 4.08E+01 | 1.77E+01 | 2.51E+01 | 1.65E+01 | 1.04E+01 | 6.43E+00 | 3.03E+00 | 5.41E-02 |
| 3.67E+01 | 1.61E+01 | 2.48E+01 | 1.62E+01 | 6.84E+00 | 5.58E+00 | 3.39E+00 | 5.65E-02 |
| 3.32E+01 | 1.48E+01 | 2.46E+01 | 1.62E+01 | 5.39E+00 | 4.91E+00 | 3.78E+00 | 5.87E-02 |
| 2.95E+01 | 1.30E+01 | 2.31E+01 | 1.55E+01 | 4.19E+00 | 4.92E+00 | 4.17E+00 | 5.92E-02 |
| 2.62E+01 | 1.14E+01 | 2.05E+01 | 1.40E+01 | 3.94E+00 | 5.77E+00 | 4.71E+00 | 6.17E-02 |
| 2.29E+01 | 9.80E+00 | 1.61E+01 | 1.15E+01 | 4.28E+00 | 7.05E+00 | 5.26E+00 | 6.22E-02 |
| 1.94E+01 | 7.97E+00 | 1.09E+01 | 8.40E+00 | 4.52E+00 | 6.96E+00 | 6.20E+00 | 6.35E-02 |

Table B.39 Refrigerant: HFC-134a, W-40 fpi surface, Triangular Pitch, Nozzle Configuration: 30WHCRC, Refrigerant Supply Rate: 15 kg/min, 2.5 % Oil Concentration

| q'' $\left(\frac{\text{kW}}{\text{m}^2 \cdot \text{K}}\right)$ | h_b $\left(\frac{\text{kW}}{\text{m}^2 \cdot \text{K}}\right)$ | h_1 $\left(\frac{\text{kW}}{\text{m}^2 \cdot \text{K}}\right)$ | h_2 $\left(\frac{\text{kW}}{\text{m}^2 \cdot \text{K}}\right)$ | h_3 $\left(\frac{\text{kW}}{\text{m}^2 \cdot \text{K}}\right)$ | h_4 $\left(\frac{\text{kW}}{\text{m}^2 \cdot \text{K}}\right)$ | OFR | Γ_4 $\left(\frac{\text{kg}}{\text{s} \cdot \text{m}}\right)$ |
|---|---|---|---|---|---|----------|--|
| 4.06E+01 | 2.32E+01 | 2.96E+01 | 2.28E+01 | 1.63E+01 | 2.13E+01 | 1.43E+00 | 1.61E-02 |
| 3.71E+01 | 2.31E+01 | 2.95E+01 | 2.25E+01 | 1.50E+01 | 1.86E+01 | 1.58E+00 | 1.81E-02 |
| 3.31E+01 | 2.16E+01 | 2.90E+01 | 2.13E+01 | 1.09E+01 | 1.46E+01 | 1.77E+00 | 1.98E-02 |
| 2.99E+01 | 1.96E+01 | 2.69E+01 | 1.96E+01 | 7.68E+00 | 1.04E+01 | 1.94E+00 | 2.08E-02 |
| 2.61E+01 | 1.60E+01 | 2.38E+01 | 1.70E+01 | 5.38E+00 | 6.53E+00 | 2.21E+00 | 2.22E-02 |
| 2.28E+01 | 1.26E+01 | 1.81E+01 | 1.32E+01 | 4.57E+00 | 5.62E+00 | 2.53E+00 | 2.39E-02 |
| 1.90E+01 | 9.45E+00 | 1.17E+01 | 8.78E+00 | 4.45E+00 | 5.58E+00 | 3.00E+00 | 2.54E-02 |

Table B.40 Refrigerant: HFC-134a, W-40 fpi surface, Triangular Pitch, Nozzle Configuration: 30WHCRC, Refrigerant Supply Rate: 35 kg/min, 2.5 % Oil Concentration

| q'' $\left(\frac{\text{kW}}{\text{m}^2 \cdot \text{K}}\right)$ | h_b $\left(\frac{\text{kW}}{\text{m}^2 \cdot \text{K}}\right)$ | h_1 $\left(\frac{\text{kW}}{\text{m}^2 \cdot \text{K}}\right)$ | h_2 $\left(\frac{\text{kW}}{\text{m}^2 \cdot \text{K}}\right)$ | h_3 $\left(\frac{\text{kW}}{\text{m}^2 \cdot \text{K}}\right)$ | h_4 $\left(\frac{\text{kW}}{\text{m}^2 \cdot \text{K}}\right)$ | OFR | Γ_4 $\left(\frac{\text{kg}}{\text{s} \cdot \text{m}}\right)$ |
|---|---|---|---|---|---|----------|--|
| 4.09E+01 | 3.17E+01 | 2.95E+01 | 2.19E+01 | 1.86E+01 | 2.76E+01 | 3.06E+00 | 5.60E-02 |
| 3.71E+01 | 3.35E+01 | 3.06E+01 | 2.26E+01 | 1.83E+01 | 3.02E+01 | 3.40E+00 | 5.82E-02 |
| 3.33E+01 | 3.36E+01 | 3.03E+01 | 2.26E+01 | 1.71E+01 | 3.12E+01 | 3.86E+00 | 6.06E-02 |
| 2.97E+01 | 3.20E+01 | 2.82E+01 | 2.11E+01 | 1.43E+01 | 2.53E+01 | 4.28E+00 | 6.15E-02 |
| 2.64E+01 | 2.46E+01 | 2.47E+01 | 1.83E+01 | 9.41E+00 | 1.52E+01 | 4.67E+00 | 6.02E-02 |
| 2.30E+01 | 1.64E+01 | 1.85E+01 | 1.40E+01 | 5.33E+00 | 8.87E+00 | 5.69E+00 | 6.54E-02 |
| 1.93E+01 | 1.04E+01 | 1.18E+01 | 9.03E+00 | 3.51E+00 | 4.52E+00 | 6.90E+00 | 6.77E-02 |

Table B.41 Refrigerant: HFC-134a, W-SC surface, Triangular Pitch, Nozzle Configuration:
30WHCRC, Refrigerant Supply Rate: 15 kg/min, 1.0 % Oil Concentration

| q'' $\left(\frac{\text{kW}}{\text{m}^2 \cdot \text{K}}\right)$ | h_b $\left(\frac{\text{kW}}{\text{m}^2 \cdot \text{K}}\right)$ | h_1 $\left(\frac{\text{kW}}{\text{m}^2 \cdot \text{K}}\right)$ | h_2 $\left(\frac{\text{kW}}{\text{m}^2 \cdot \text{K}}\right)$ | h_3 $\left(\frac{\text{kW}}{\text{m}^2 \cdot \text{K}}\right)$ | h_4 $\left(\frac{\text{kW}}{\text{m}^2 \cdot \text{K}}\right)$ | OFR | Γ_4 $\left(\frac{\text{kg}}{\text{s} \cdot \text{m}}\right)$ |
|---|---|---|---|---|---|----------|--|
| 4.00E+01 | 1.54E+01 | 2.38E+01 | 1.77E+01 | 1.21E+01 | 4.57E+00 | 1.42E+00 | 1.41E-02 |
| 3.68E+01 | 1.68E+01 | 2.44E+01 | 1.77E+01 | 1.33E+01 | 5.54E+00 | 1.53E+00 | 1.57E-02 |
| 3.28E+01 | 1.86E+01 | 2.52E+01 | 1.75E+01 | 1.45E+01 | 6.64E+00 | 1.72E+00 | 1.81E-02 |
| 2.96E+01 | 1.85E+01 | 2.42E+01 | 1.70E+01 | 1.64E+01 | 7.80E+00 | 1.84E+00 | 1.88E-02 |
| 2.60E+01 | 1.83E+01 | 2.31E+01 | 1.52E+01 | 1.73E+01 | 7.94E+00 | 2.22E+00 | 2.24E-02 |
| 2.26E+01 | 1.68E+01 | 2.04E+01 | 1.33E+01 | 1.82E+01 | 8.28E+00 | 2.53E+00 | 2.39E-02 |
| 1.92E+01 | 1.29E+01 | 1.48E+01 | 9.67E+00 | 1.51E+01 | 7.54E+00 | 2.95E+00 | 2.52E-02 |

Table B.42 Refrigerant: HFC-134a, W-SC surface, Triangular Pitch, Nozzle Configuration:
30WHCRC, Refrigerant Supply Rate: 35 kg/min, 1.0 % Oil Concentration

| q'' $\left(\frac{\text{kW}}{\text{m}^2 \cdot \text{K}}\right)$ | h_b $\left(\frac{\text{kW}}{\text{m}^2 \cdot \text{K}}\right)$ | h_1 $\left(\frac{\text{kW}}{\text{m}^2 \cdot \text{K}}\right)$ | h_2 $\left(\frac{\text{kW}}{\text{m}^2 \cdot \text{K}}\right)$ | h_3 $\left(\frac{\text{kW}}{\text{m}^2 \cdot \text{K}}\right)$ | h_4 $\left(\frac{\text{kW}}{\text{m}^2 \cdot \text{K}}\right)$ | OFR | Γ_4 $\left(\frac{\text{kg}}{\text{s} \cdot \text{m}}\right)$ |
|---|---|---|---|---|---|----------|--|
| 4.01E+01 | 1.91E+01 | 2.21E+01 | 1.67E+01 | 1.33E+01 | 6.53E+00 | 2.98E+00 | 5.17E-02 |
| 3.66E+01 | 1.98E+01 | 2.26E+01 | 1.67E+01 | 1.37E+01 | 7.02E+00 | 3.33E+00 | 5.53E-02 |
| 3.31E+01 | 2.05E+01 | 2.32E+01 | 1.65E+01 | 1.47E+01 | 7.69E+00 | 3.55E+00 | 5.46E-02 |
| 2.97E+01 | 2.05E+01 | 2.32E+01 | 1.73E+01 | 1.81E+01 | 8.72E+00 | 3.96E+00 | 5.62E-02 |
| 2.64E+01 | 1.96E+01 | 2.20E+01 | 1.57E+01 | 1.85E+01 | 8.69E+00 | 4.39E+00 | 5.81E-02 |
| 2.28E+01 | 1.68E+01 | 1.92E+01 | 1.35E+01 | 1.84E+01 | 8.25E+00 | 5.08E+00 | 5.93E-02 |
| 1.93E+01 | 1.26E+01 | 1.40E+01 | 9.31E+00 | 1.54E+01 | 7.38E+00 | 6.07E+00 | 6.22E-02 |

Table B.43 Refrigerant: HFC-134a, W-SC surface, Triangular Pitch, Nozzle Configuration:
30WHCRC, Refrigerant Supply Rate: 15 kg/min, 2.5 % Oil Concentration

| q'' $\left(\frac{\text{kW}}{\text{m}^2 \cdot \text{K}}\right)$ | h_b $\left(\frac{\text{kW}}{\text{m}^2 \cdot \text{K}}\right)$ | h_1 $\left(\frac{\text{kW}}{\text{m}^2 \cdot \text{K}}\right)$ | h_2 $\left(\frac{\text{kW}}{\text{m}^2 \cdot \text{K}}\right)$ | h_3 $\left(\frac{\text{kW}}{\text{m}^2 \cdot \text{K}}\right)$ | h_4 $\left(\frac{\text{kW}}{\text{m}^2 \cdot \text{K}}\right)$ | OFR | Γ_4 $\left(\frac{\text{kg}}{\text{s} \cdot \text{m}}\right)$ |
|---|---|---|---|---|---|----------|--|
| 4.01E+01 | 1.81E+01 | 2.70E+01 | 1.86E+01 | 1.96E+01 | 5.13E+00 | 1.45E+00 | 1.48E-02 |
| 3.67E+01 | 1.85E+01 | 2.76E+01 | 1.84E+01 | 1.99E+01 | 4.71E+00 | 1.59E+00 | 1.65E-02 |
| 3.31E+01 | 1.91E+01 | 2.80E+01 | 1.79E+01 | 2.03E+01 | 4.49E+00 | 1.75E+00 | 1.80E-02 |
| 2.95E+01 | 1.93E+01 | 2.60E+01 | 1.70E+01 | 2.13E+01 | 4.59E+00 | 1.96E+00 | 1.97E-02 |
| 2.61E+01 | 1.96E+01 | 2.60E+01 | 1.57E+01 | 2.28E+01 | 5.39E+00 | 2.21E+00 | 2.17E-02 |
| 2.28E+01 | 1.89E+01 | 2.24E+01 | 1.36E+01 | 2.30E+01 | 6.46E+00 | 2.58E+00 | 2.44E-02 |
| 1.90E+01 | 1.41E+01 | 1.55E+01 | 9.77E+00 | 1.90E+01 | 6.51E+00 | 3.04E+00 | 2.59E-02 |

Table B.44 Refrigerant: HFC-134a, W-SC surface, Triangular Pitch, Nozzle Configuration:
30WHCRC, Refrigerant Supply Rate: 35 kg/min, 2.5 % Oil Concentration

| q'' $\left(\frac{\text{kW}}{\text{m}^2 \cdot \text{K}}\right)$ | h_b $\left(\frac{\text{kW}}{\text{m}^2 \cdot \text{K}}\right)$ | h_1 $\left(\frac{\text{kW}}{\text{m}^2 \cdot \text{K}}\right)$ | h_2 $\left(\frac{\text{kW}}{\text{m}^2 \cdot \text{K}}\right)$ | h_3 $\left(\frac{\text{kW}}{\text{m}^2 \cdot \text{K}}\right)$ | h_4 $\left(\frac{\text{kW}}{\text{m}^2 \cdot \text{K}}\right)$ | OFR | Γ_4 $\left(\frac{\text{kg}}{\text{s} \cdot \text{m}}\right)$ |
|---|---|---|---|---|---|----------|--|
| 4.03E+01 | 2.63E+01 | 2.67E+01 | 1.90E+01 | 2.27E+01 | 1.29E+01 | 3.06E+00 | 5.47E-02 |
| 3.66E+01 | 2.70E+01 | 2.71E+01 | 1.87E+01 | 2.37E+01 | 1.28E+01 | 3.33E+00 | 5.56E-02 |
| 3.30E+01 | 2.70E+01 | 2.68E+01 | 1.82E+01 | 2.47E+01 | 1.22E+01 | 3.71E+00 | 5.71E-02 |
| 2.97E+01 | 2.63E+01 | 2.58E+01 | 1.71E+01 | 2.55E+01 | 1.14E+01 | 4.19E+00 | 5.99E-02 |
| 2.61E+01 | 2.52E+01 | 2.50E+01 | 1.61E+01 | 2.81E+01 | 1.08E+01 | 4.88E+00 | 6.29E-02 |
| 2.27E+01 | 2.23E+01 | 2.17E+01 | 1.38E+01 | 2.76E+01 | 9.80E+00 | 5.56E+00 | 6.34E-02 |
| 1.92E+01 | 1.56E+01 | 1.53E+01 | 9.68E+00 | 2.19E+01 | 8.87E+00 | 6.71E+00 | 6.63E-02 |

Table B.45 Refrigerant: HFC-134a, Tu-B surface, Triangular Pitch, Nozzle Configuration:
30WHCRC, Refrigerant Supply Rate: 15 kg/min, 1.0 % Oil Concentration

| q'' $\left(\frac{\text{kW}}{\text{m}^2 \cdot \text{K}}\right)$ | h_b $\left(\frac{\text{kW}}{\text{m}^2 \cdot \text{K}}\right)$ | h_1 $\left(\frac{\text{kW}}{\text{m}^2 \cdot \text{K}}\right)$ | h_2 $\left(\frac{\text{kW}}{\text{m}^2 \cdot \text{K}}\right)$ | h_3 $\left(\frac{\text{kW}}{\text{m}^2 \cdot \text{K}}\right)$ | h_4 $\left(\frac{\text{kW}}{\text{m}^2 \cdot \text{K}}\right)$ | OFR | Γ_4 $\left(\frac{\text{kg}}{\text{s} \cdot \text{m}}\right)$ |
|---|---|---|---|---|---|----------|--|
| 4.10E+01 | 2.34E+01 | 2.59E+01 | 2.52E+01 | 2.17E+01 | 1.88E+01 | 1.43E+00 | 1.61E-02 |
| 3.71E+01 | 2.67E+01 | 2.69E+01 | 2.68E+01 | 2.27E+01 | 2.45E+01 | 1.61E+00 | 1.87E-02 |
| 3.33E+01 | 3.03E+01 | 2.77E+01 | 2.81E+01 | 2.33E+01 | 3.07E+01 | 1.76E+00 | 1.99E-02 |
| 2.99E+01 | 3.38E+01 | 2.70E+01 | 2.87E+01 | 2.31E+01 | 3.67E+01 | 1.95E+00 | 2.13E-02 |
| 2.65E+01 | 3.64E+01 | 2.59E+01 | 2.93E+01 | 2.27E+01 | 4.25E+01 | 2.22E+00 | 2.31E-02 |
| 2.28E+01 | 3.69E+01 | 2.39E+01 | 2.81E+01 | 2.15E+01 | 4.74E+01 | 2.55E+00 | 2.44E-02 |
| 1.93E+01 | 3.34E+01 | 1.97E+01 | 2.53E+01 | 1.90E+01 | 4.56E+01 | 3.00E+00 | 2.61E-02 |

Table B.46 Refrigerant: HFC-134a, Tu-B surface, Triangular Pitch, Nozzle Configuration:
30WHCRC, Refrigerant Supply Rate: 35 kg/min, 1.0 % Oil Concentration

| q'' $\left(\frac{\text{kW}}{\text{m}^2 \cdot \text{K}}\right)$ | h_b $\left(\frac{\text{kW}}{\text{m}^2 \cdot \text{K}}\right)$ | h_1 $\left(\frac{\text{kW}}{\text{m}^2 \cdot \text{K}}\right)$ | h_2 $\left(\frac{\text{kW}}{\text{m}^2 \cdot \text{K}}\right)$ | h_3 $\left(\frac{\text{kW}}{\text{m}^2 \cdot \text{K}}\right)$ | h_4 $\left(\frac{\text{kW}}{\text{m}^2 \cdot \text{K}}\right)$ | OFR | Γ_4 $\left(\frac{\text{kg}}{\text{s} \cdot \text{m}}\right)$ |
|---|---|---|---|---|---|----------|--|
| 4.05E+01 | 3.15E+01 | 2.85E+01 | 2.67E+01 | 2.22E+01 | 3.05E+01 | 3.18E+00 | 5.80E-02 |
| 3.72E+01 | 3.39E+01 | 2.98E+01 | 2.86E+01 | 2.33E+01 | 3.33E+01 | 3.42E+00 | 5.88E-02 |
| 3.35E+01 | 3.64E+01 | 3.01E+01 | 2.95E+01 | 2.33E+01 | 3.58E+01 | 3.75E+00 | 5.98E-02 |
| 2.99E+01 | 3.93E+01 | 3.00E+01 | 3.04E+01 | 2.33E+01 | 3.95E+01 | 4.11E+00 | 6.00E-02 |
| 2.62E+01 | 4.09E+01 | 2.84E+01 | 3.03E+01 | 2.30E+01 | 4.46E+01 | 4.73E+00 | 6.25E-02 |
| 2.29E+01 | 4.06E+01 | 2.59E+01 | 2.92E+01 | 2.17E+01 | 4.85E+01 | 5.35E+00 | 6.34E-02 |
| 1.92E+01 | 3.66E+01 | 2.11E+01 | 2.62E+01 | 1.91E+01 | 4.79E+01 | 6.19E+00 | 6.38E-02 |

Table B.47 Refrigerant: HFC-134a, Tu-B surface, Triangular Pitch, Nozzle Configuration:
30WHCRC, Refrigerant Supply Rate: 15 kg/min, 2.5 % Oil Concentration

| q'' $\left(\frac{\text{kW}}{\text{m}^2 \cdot \text{K}}\right)$ | h_b $\left(\frac{\text{kW}}{\text{m}^2 \cdot \text{K}}\right)$ | h_1 $\left(\frac{\text{kW}}{\text{m}^2 \cdot \text{K}}\right)$ | h_2 $\left(\frac{\text{kW}}{\text{m}^2 \cdot \text{K}}\right)$ | h_3 $\left(\frac{\text{kW}}{\text{m}^2 \cdot \text{K}}\right)$ | h_4 $\left(\frac{\text{kW}}{\text{m}^2 \cdot \text{K}}\right)$ | OFR | Γ_4 $\left(\frac{\text{kg}}{\text{s} \cdot \text{m}}\right)$ |
|---|---|---|---|---|---|----------|--|
| 4.10E+01 | 2.03E+01 | 2.79E+01 | 2.74E+01 | 1.84E+01 | 1.16E+01 | 1.43E+00 | 1.57E-02 |
| 3.70E+01 | 2.34E+01 | 2.84E+01 | 2.87E+01 | 2.12E+01 | 1.68E+01 | 1.58E+00 | 1.77E-02 |
| 3.35E+01 | 2.71E+01 | 2.88E+01 | 2.96E+01 | 2.33E+01 | 2.27E+01 | 1.74E+00 | 1.94E-02 |
| 3.01E+01 | 3.12E+01 | 2.90E+01 | 3.09E+01 | 2.51E+01 | 3.13E+01 | 1.93E+00 | 2.11E-02 |
| 2.63E+01 | 3.50E+01 | 2.85E+01 | 3.14E+01 | 2.53E+01 | 4.11E+01 | 2.20E+00 | 2.28E-02 |
| 2.28E+01 | 3.74E+01 | 2.59E+01 | 3.09E+01 | 2.41E+01 | 5.04E+01 | 2.54E+00 | 2.44E-02 |
| 1.91E+01 | 3.67E+01 | 2.18E+01 | 2.84E+01 | 2.12E+01 | 5.61E+01 | 3.01E+00 | 2.60E-02 |

Table B.48 Refrigerant: HFC-134a, Tu-B surface, Triangular Pitch, Nozzle Configuration:
30WHCRC, Refrigerant Supply Rate: 35 kg/min, 2.5 % Oil Concentration

| q'' $\left(\frac{\text{kW}}{\text{m}^2 \cdot \text{K}}\right)$ | h_b $\left(\frac{\text{kW}}{\text{m}^2 \cdot \text{K}}\right)$ | h_1 $\left(\frac{\text{kW}}{\text{m}^2 \cdot \text{K}}\right)$ | h_2 $\left(\frac{\text{kW}}{\text{m}^2 \cdot \text{K}}\right)$ | h_3 $\left(\frac{\text{kW}}{\text{m}^2 \cdot \text{K}}\right)$ | h_4 $\left(\frac{\text{kW}}{\text{m}^2 \cdot \text{K}}\right)$ | OFR | Γ_4 $\left(\frac{\text{kg}}{\text{s} \cdot \text{m}}\right)$ |
|---|---|---|---|---|---|----------|--|
| 4.06E+01 | 2.92E+01 | 3.04E+01 | 2.70E+01 | 2.21E+01 | 2.18E+01 | 3.05E+00 | 5.45E-02 |
| 3.71E+01 | 3.14E+01 | 3.22E+01 | 2.87E+01 | 2.26E+01 | 2.30E+01 | 3.28E+00 | 5.53E-02 |
| 3.37E+01 | 3.44E+01 | 3.27E+01 | 3.02E+01 | 2.32E+01 | 2.65E+01 | 3.85E+00 | 6.09E-02 |
| 3.00E+01 | 3.83E+01 | 3.30E+01 | 3.21E+01 | 2.37E+01 | 3.26E+01 | 4.39E+00 | 6.38E-02 |
| 2.65E+01 | 4.14E+01 | 3.20E+01 | 3.26E+01 | 2.38E+01 | 3.97E+01 | 4.75E+00 | 6.19E-02 |
| 2.31E+01 | 4.42E+01 | 2.99E+01 | 3.36E+01 | 2.33E+01 | 4.84E+01 | 5.30E+00 | 6.09E-02 |
| 1.95E+01 | 4.19E+01 | 2.50E+01 | 3.14E+01 | 2.11E+01 | 5.26E+01 | 6.38E+00 | 6.35E-02 |

APPENDIX C. BUNDLE TEST FACILITY HCFC-22 TABULATED DATA

The experimental data from the HCFC-22 testing conducted on the bundle test facility are reported in this Appendix. Pure refrigerant results are presented first followed by the lubricant effects data taken with a 300 SUS alkyl-benzene oil. These results are presented and discussed in Chapter 11.

Bundle and row heat transfer coefficients are presented for the plain-surface and Tu-B tube bundles. The shell-side heat transfer coefficients for both tubes are based upon the outer diameter of the tube, which is the diameter over the enhancement for the Tu-B tube. The geometric specifications for both tubes are presented in Table 4.1. The method used to calculate the shell-side heat transfer coefficients is presented in Chapter 5.

Bundle overfeed ratios and the film-feed supply rate seen by the fourth (bottom) row of the tube bundle are presented at each respective wall heat flux. The HCFC-22 data presented in Tables C.1 and C.2 includes the Reynolds numbers and Prandtl numbers for the refrigerant film flowing over the bottom tube, which are calculated using the assumptions stated in Appendix B.

Table C.1 Refrigerant: HCFC-22, Plain Surface, Triangular Pitch, Nozzle Configuration: 30WHCRC,
Refrigerant Supply Rate: 15 kg/min, Pure Refrigerant Data

| q'' $\left(\frac{\text{kW}}{\text{m}^2 \cdot \text{K}}\right)$ | h_b $\left(\frac{\text{kW}}{\text{m}^2 \cdot \text{K}}\right)$ | h_1 $\left(\frac{\text{kW}}{\text{m}^2 \cdot \text{K}}\right)$ | h_2 $\left(\frac{\text{kW}}{\text{m}^2 \cdot \text{K}}\right)$ | h_3 $\left(\frac{\text{kW}}{\text{m}^2 \cdot \text{K}}\right)$ | h_4 $\left(\frac{\text{kW}}{\text{m}^2 \cdot \text{K}}\right)$ | OFR | Γ_4 $\left(\frac{\text{kg}}{\text{s} \cdot \text{m}}\right)$ | Re_4 | Pr_4 |
|---|---|---|---|---|---|----------|--|----------|----------|
| 4.01E+01 | 4.92E+00 | 5.76E+00 | 5.01E+00 | 5.24E+00 | 3.98E+00 | 1.42E+00 | 1.47E-02 | 2.84E+02 | 2.44E+00 |
| 3.70E+01 | 4.88E+00 | 5.49E+00 | 4.82E+00 | 5.11E+00 | 3.96E+00 | 1.59E+00 | 1.72E-02 | 3.32E+02 | 2.44E+00 |
| 3.30E+01 | 4.80E+00 | 5.08E+00 | 4.61E+00 | 4.97E+00 | 4.14E+00 | 1.75E+00 | 1.87E-02 | 3.59E+02 | 2.44E+00 |
| 3.00E+01 | 4.74E+00 | 4.70E+00 | 4.44E+00 | 4.79E+00 | 4.23E+00 | 1.94E+00 | 2.03E-02 | 3.89E+02 | 2.44E+00 |
| 2.62E+01 | 4.58E+00 | 4.29E+00 | 4.16E+00 | 4.51E+00 | 4.27E+00 | 2.20E+00 | 2.19E-02 | 4.17E+02 | 2.44E+00 |
| 2.29E+01 | 4.41E+00 | 3.94E+00 | 3.89E+00 | 4.19E+00 | 4.25E+00 | 2.61E+00 | 2.46E-02 | 4.67E+02 | 2.44E+00 |
| 1.92E+01 | 4.12E+00 | 3.59E+00 | 3.60E+00 | 3.77E+00 | 4.09E+00 | 3.00E+00 | 2.52E-02 | 4.76E+02 | 2.44E+00 |

Table C.2 Refrigerant: HCFC-22, Tu-B Surface, Triangular Pitch, Nozzle Configuration: 30WHCRC,
Refrigerant Supply Rate: 15 kg/min, Pure Refrigerant Data

| q'' $\left(\frac{\text{kW}}{\text{m}^2 \cdot \text{K}}\right)$ | h_b $\left(\frac{\text{kW}}{\text{m}^2 \cdot \text{K}}\right)$ | h_1 $\left(\frac{\text{kW}}{\text{m}^2 \cdot \text{K}}\right)$ | h_2 $\left(\frac{\text{kW}}{\text{m}^2 \cdot \text{K}}\right)$ | h_3 $\left(\frac{\text{kW}}{\text{m}^2 \cdot \text{K}}\right)$ | h_4 $\left(\frac{\text{kW}}{\text{m}^2 \cdot \text{K}}\right)$ | OFR | Γ_4 $\left(\frac{\text{kg}}{\text{s} \cdot \text{m}}\right)$ | Re_4 | Pr_4 |
|---|---|---|---|---|---|----------|--|----------|----------|
| 4.06E+01 | 1.59E+01 | 2.01E+01 | 1.77E+01 | 1.25E+01 | 1.19E+01 | 1.49E+00 | 1.67E-02 | 3.13E+02 | 2.45E+00 |
| 3.70E+01 | 1.68E+01 | 2.02E+01 | 1.87E+01 | 1.29E+01 | 1.34E+01 | 1.58E+00 | 1.72E-02 | 3.23E+02 | 2.45E+00 |
| 3.35E+01 | 1.75E+01 | 2.03E+01 | 1.89E+01 | 1.35E+01 | 1.40E+01 | 1.78E+00 | 1.92E-02 | 3.59E+02 | 2.45E+00 |
| 3.02E+01 | 1.81E+01 | 1.97E+01 | 1.90E+01 | 1.42E+01 | 1.45E+01 | 1.98E+00 | 2.09E-02 | 3.90E+02 | 2.45E+00 |
| 2.68E+01 | 1.84E+01 | 1.92E+01 | 1.86E+01 | 1.41E+01 | 1.52E+01 | 2.28E+00 | 2.30E-02 | 4.29E+02 | 2.45E+00 |
| 2.32E+01 | 1.85E+01 | 1.75E+01 | 1.83E+01 | 1.33E+01 | 1.56E+01 | 2.55E+00 | 2.37E-02 | 4.41E+02 | 2.45E+00 |
| 1.96E+01 | 1.83E+01 | 1.57E+01 | 1.70E+01 | 1.21E+01 | 1.81E+01 | 3.05E+00 | 2.56E-02 | 4.77E+02 | 2.45E+00 |

Table C.3 Refrigerant: HCFC-22, Plain surface, Triangular Pitch, Nozzle Configuration:
30WHCRC, Refrigerant Supply Rate: 15 kg/min, 1.0 % Oil Concentration

| q'' $\left(\frac{\text{kW}}{\text{m}^2 \cdot \text{K}}\right)$ | h_b $\left(\frac{\text{kW}}{\text{m}^2 \cdot \text{K}}\right)$ | h_1 $\left(\frac{\text{kW}}{\text{m}^2 \cdot \text{K}}\right)$ | h_2 $\left(\frac{\text{kW}}{\text{m}^2 \cdot \text{K}}\right)$ | h_3 $\left(\frac{\text{kW}}{\text{m}^2 \cdot \text{K}}\right)$ | h_4 $\left(\frac{\text{kW}}{\text{m}^2 \cdot \text{K}}\right)$ | OFR | Γ_4 $\left(\frac{\text{kg}}{\text{s} \cdot \text{m}}\right)$ |
|---|---|---|---|---|---|----------|--|
| 4.03E+01 | 5.43E+00 | 6.25E+00 | 5.65E+00 | 4.25E+00 | 4.34E+00 | 1.50E+00 | 1.67E-02 |
| 3.70E+01 | 5.41E+00 | 6.01E+00 | 5.44E+00 | 4.29E+00 | 4.34E+00 | 1.64E+00 | 1.83E-02 |
| 3.31E+01 | 5.38E+00 | 5.67E+00 | 5.32E+00 | 4.32E+00 | 4.38E+00 | 1.80E+00 | 1.96E-02 |
| 2.94E+01 | 5.35E+00 | 5.26E+00 | 5.16E+00 | 4.44E+00 | 4.43E+00 | 2.00E+00 | 2.09E-02 |
| 2.63E+01 | 5.30E+00 | 4.90E+00 | 4.96E+00 | 4.49E+00 | 4.44E+00 | 2.29E+00 | 2.31E-02 |
| 2.28E+01 | 5.17E+00 | 4.56E+00 | 4.70E+00 | 4.49E+00 | 4.33E+00 | 2.59E+00 | 2.40E-02 |
| 1.93E+01 | 4.95E+00 | 4.20E+00 | 4.48E+00 | 4.32E+00 | 4.22E+00 | 3.08E+00 | 2.60E-02 |

Table C.4 Refrigerant: HCFC-22, Tu-B surface, Triangular Pitch, Nozzle Configuration:
30WHCRC, Refrigerant Supply Rate: 15 kg/min, 1.0 % Oil Concentration

| q'' $\left(\frac{\text{kW}}{\text{m}^2 \cdot \text{K}}\right)$ | h_b $\left(\frac{\text{kW}}{\text{m}^2 \cdot \text{K}}\right)$ | h_1 $\left(\frac{\text{kW}}{\text{m}^2 \cdot \text{K}}\right)$ | h_2 $\left(\frac{\text{kW}}{\text{m}^2 \cdot \text{K}}\right)$ | h_3 $\left(\frac{\text{kW}}{\text{m}^2 \cdot \text{K}}\right)$ | h_4 $\left(\frac{\text{kW}}{\text{m}^2 \cdot \text{K}}\right)$ | OFR | Γ_4 $\left(\frac{\text{kg}}{\text{s} \cdot \text{m}}\right)$ |
|---|---|---|---|---|---|----------|--|
| 4.06E+01 | 2.08E+01 | 1.99E+01 | 2.07E+01 | 1.95E+01 | 1.83E+01 | 1.53E+00 | 1.77E-02 |
| 3.72E+01 | 2.24E+01 | 1.98E+01 | 2.08E+01 | 1.97E+01 | 2.24E+01 | 1.64E+00 | 1.87E-02 |
| 3.34E+01 | 2.41E+01 | 1.96E+01 | 2.10E+01 | 1.97E+01 | 2.75E+01 | 1.79E+00 | 1.99E-02 |
| 3.00E+01 | 2.59E+01 | 1.98E+01 | 2.14E+01 | 1.94E+01 | 3.24E+01 | 1.99E+00 | 2.13E-02 |
| 2.66E+01 | 2.76E+01 | 1.93E+01 | 2.17E+01 | 1.93E+01 | 3.69E+01 | 2.26E+00 | 2.30E-02 |
| 2.31E+01 | 2.80E+01 | 1.86E+01 | 2.16E+01 | 1.85E+01 | 3.97E+01 | 2.58E+00 | 2.43E-02 |
| 1.94E+01 | 2.64E+01 | 1.69E+01 | 2.07E+01 | 1.68E+01 | 3.84E+01 | 2.97E+00 | 2.47E-02 |

APPENDIX D. BUNDLE TEST FACILITY HCFC-123 TABULATED DATA

The experimental data from the HFC-123 tests conducted on the bundle test facility are reported in this Appendix. Pure refrigerant results are presented first followed by data from the lubricant effects testing done with a 305 SUS naphthenic mineral oil. The HCFC-123 results are presented and discussed in Chapter 12.

Bundle and row heat transfer coefficients are presented for each run. These heat transfer coefficients are based upon the nominal cylindrical area over the shell-side surface enhancement for each tube. These diameters are presented in Table 4.1. The method used for the calculation of these shell-side heat transfer coefficients is presented in Chapter 5.

The bundle overfeed ratios and film-feed supply rates seen by the fourth (bottom) row of the tube bundle are presented at each wall heat flux. Pure HCFC-123 results presented in Tables D.1 to D.10 include the Reynolds numbers and Prandtl numbers for the bottom row, which are calculated using the assumptions stated in Appendix B.

Table D.1 Refrigerant: HCFC-123, Plain Surface, Triangular Pitch, Nozzle Configuration: 24WDCRC,
Refrigerant Supply Rate: 25 kg/min, Pure Refrigerant Data

| q'' $\left(\frac{\text{kW}}{\text{m}^2 \cdot \text{K}}\right)$ | h_b $\left(\frac{\text{kW}}{\text{m}^2 \cdot \text{K}}\right)$ | h_1 $\left(\frac{\text{kW}}{\text{m}^2 \cdot \text{K}}\right)$ | h_2 $\left(\frac{\text{kW}}{\text{m}^2 \cdot \text{K}}\right)$ | h_3 $\left(\frac{\text{kW}}{\text{m}^2 \cdot \text{K}}\right)$ | h_4 $\left(\frac{\text{kW}}{\text{m}^2 \cdot \text{K}}\right)$ | OFR | Γ_4 $\left(\frac{\text{kg}}{\text{s} \cdot \text{m}}\right)$ | Re_4 | Pr_4 |
|---|---|---|---|---|---|----------|--|----------|----------|
| 4.02E+01 | 1.91E+00 | 2.40E+00 | 2.01E+00 | 1.96E+00 | 1.37E+00 | 1.74E+00 | 2.36E-02 | 1.87E+02 | 6.16E+00 |
| 3.63E+01 | 1.83E+00 | 2.21E+00 | 1.86E+00 | 1.84E+00 | 1.32E+00 | 1.92E+00 | 2.59E-02 | 2.04E+02 | 6.19E+00 |
| 3.33E+01 | 1.77E+00 | 2.07E+00 | 1.74E+00 | 1.74E+00 | 1.27E+00 | 2.08E+00 | 2.74E-02 | 2.14E+02 | 6.21E+00 |
| 2.97E+01 | 1.75E+00 | 1.88E+00 | 1.62E+00 | 1.70E+00 | 1.39E+00 | 2.31E+00 | 2.93E-02 | 2.27E+02 | 6.26E+00 |
| 2.60E+01 | 1.76E+00 | 1.81E+00 | 1.57E+00 | 1.74E+00 | 1.57E+00 | 2.68E+00 | 3.22E-02 | 2.45E+02 | 6.33E+00 |
| 2.23E+01 | 1.75E+00 | 1.75E+00 | 1.57E+00 | 1.67E+00 | 1.62E+00 | 3.06E+00 | 3.35E-02 | 2.51E+02 | 6.38E+00 |
| 1.89E+01 | 1.75E+00 | 1.70E+00 | 1.58E+00 | 1.60E+00 | 1.59E+00 | 3.58E+00 | 3.52E-02 | 2.61E+02 | 6.43E+00 |

Table D.2 Refrigerant: HCFC-123, Plain Surface, Triangular Pitch, Nozzle Configuration: 24WDCRC,
Refrigerant Supply Rate: 35 kg/min, Pure Refrigerant Data

| q'' $\left(\frac{\text{kW}}{\text{m}^2 \cdot \text{K}}\right)$ | h_b $\left(\frac{\text{kW}}{\text{m}^2 \cdot \text{K}}\right)$ | h_1 $\left(\frac{\text{kW}}{\text{m}^2 \cdot \text{K}}\right)$ | h_2 $\left(\frac{\text{kW}}{\text{m}^2 \cdot \text{K}}\right)$ | h_3 $\left(\frac{\text{kW}}{\text{m}^2 \cdot \text{K}}\right)$ | h_4 $\left(\frac{\text{kW}}{\text{m}^2 \cdot \text{K}}\right)$ | OFR | Γ_4 $\left(\frac{\text{kg}}{\text{s} \cdot \text{m}}\right)$ | Re_4 | Pr_4 |
|---|---|---|---|---|---|----------|--|----------|----------|
| 3.99E+01 | 2.08E+00 | 2.49E+00 | 1.98E+00 | 2.08E+00 | 1.71E+00 | 2.06E+00 | 3.22E-02 | 2.51E+02 | 6.22E+00 |
| 3.62E+01 | 1.98E+00 | 2.33E+00 | 1.85E+00 | 1.94E+00 | 1.61E+00 | 2.28E+00 | 3.45E-02 | 2.68E+02 | 6.23E+00 |
| 3.34E+01 | 1.92E+00 | 2.24E+00 | 1.75E+00 | 1.84E+00 | 1.57E+00 | 2.50E+00 | 3.67E-02 | 2.84E+02 | 6.26E+00 |
| 2.99E+01 | 1.88E+00 | 2.15E+00 | 1.65E+00 | 1.77E+00 | 1.54E+00 | 2.78E+00 | 3.84E-02 | 2.95E+02 | 6.29E+00 |
| 2.63E+01 | 1.86E+00 | 2.11E+00 | 1.60E+00 | 1.72E+00 | 1.58E+00 | 3.12E+00 | 4.00E-02 | 3.03E+02 | 6.34E+00 |
| 2.23E+01 | 1.83E+00 | 2.04E+00 | 1.58E+00 | 1.63E+00 | 1.57E+00 | 3.60E+00 | 4.14E-02 | 3.10E+02 | 6.39E+00 |
| 1.89E+01 | 1.82E+00 | 1.99E+00 | 1.56E+00 | 1.57E+00 | 1.53E+00 | 4.13E+00 | 4.28E-02 | 3.17E+02 | 6.43E+00 |

Table D.3 Refrigerant: HCFC-123, Plain surface, Triangular Pitch, Nozzle Configuration: 30WDCRC,
Refrigerant Supply Rate: 25 kg/min, Pure Refrigerant Data

| q'' $\left(\frac{\text{kW}}{\text{m}^2 \cdot \text{K}}\right)$ | h_b $\left(\frac{\text{kW}}{\text{m}^2 \cdot \text{K}}\right)$ | h_1 $\left(\frac{\text{kW}}{\text{m}^2 \cdot \text{K}}\right)$ | h_2 $\left(\frac{\text{kW}}{\text{m}^2 \cdot \text{K}}\right)$ | h_3 $\left(\frac{\text{kW}}{\text{m}^2 \cdot \text{K}}\right)$ | h_4 $\left(\frac{\text{kW}}{\text{m}^2 \cdot \text{K}}\right)$ | OFR | Γ_4 $\left(\frac{\text{kg}}{\text{s} \cdot \text{m}}\right)$ | Re_4 | Pr_4 |
|---|---|---|---|---|---|----------|--|----------|----------|
| 4.03E+01 | 2.02E+00 | 2.25E+00 | 1.98E+00 | 1.96E+00 | 1.60E+00 | 2.14E+00 | 3.48E-02 | 2.74E+02 | 6.19E+00 |
| 3.66E+01 | 1.92E+00 | 2.07E+00 | 1.80E+00 | 1.85E+00 | 1.57E+00 | 2.35E+00 | 3.71E-02 | 2.90E+02 | 6.22E+00 |
| 3.30E+01 | 1.82E+00 | 1.93E+00 | 1.67E+00 | 1.75E+00 | 1.51E+00 | 2.61E+00 | 3.88E-02 | 3.01E+02 | 6.24E+00 |
| 2.99E+01 | 1.75E+00 | 1.85E+00 | 1.57E+00 | 1.67E+00 | 1.46E+00 | 2.84E+00 | 4.01E-02 | 3.09E+02 | 6.27E+00 |
| 2.64E+01 | 1.71E+00 | 1.80E+00 | 1.50E+00 | 1.58E+00 | 1.45E+00 | 3.21E+00 | 4.19E-02 | 3.20E+02 | 6.31E+00 |
| 2.26E+01 | 1.70E+00 | 1.76E+00 | 1.47E+00 | 1.51E+00 | 1.50E+00 | 3.73E+00 | 4.39E-02 | 3.31E+02 | 6.36E+00 |
| 1.90E+01 | 1.68E+00 | 1.71E+00 | 1.46E+00 | 1.46E+00 | 1.50E+00 | 4.43E+00 | 4.59E-02 | 3.41E+02 | 6.41E+00 |

Table D.4 Refrigerant: HCFC-123, Plain surface, Triangular Pitch, Nozzle Configuration: 30WDCRC,
Refrigerant Supply Rate: 35 kg/min, Pure Refrigerant Data

| q'' $\left(\frac{\text{kW}}{\text{m}^2 \cdot \text{K}}\right)$ | h_b $\left(\frac{\text{kW}}{\text{m}^2 \cdot \text{K}}\right)$ | h_1 $\left(\frac{\text{kW}}{\text{m}^2 \cdot \text{K}}\right)$ | h_2 $\left(\frac{\text{kW}}{\text{m}^2 \cdot \text{K}}\right)$ | h_3 $\left(\frac{\text{kW}}{\text{m}^2 \cdot \text{K}}\right)$ | h_4 $\left(\frac{\text{kW}}{\text{m}^2 \cdot \text{K}}\right)$ | OFR | Γ_4 $\left(\frac{\text{kg}}{\text{s} \cdot \text{m}}\right)$ | Re_4 | Pr_4 |
|---|---|---|---|---|---|----------|--|----------|----------|
| 3.99E+01 | 2.09E+00 | 2.36E+00 | 1.91E+00 | 1.95E+00 | 1.72E+00 | 2.56E+00 | 4.66E-02 | 3.64E+02 | 6.22E+00 |
| 3.66E+01 | 1.98E+00 | 2.23E+00 | 1.77E+00 | 1.81E+00 | 1.67E+00 | 2.78E+00 | 4.79E-02 | 3.73E+02 | 6.23E+00 |
| 3.30E+01 | 1.90E+00 | 2.15E+00 | 1.66E+00 | 1.71E+00 | 1.58E+00 | 3.15E+00 | 5.09E-02 | 3.93E+02 | 6.26E+00 |
| 2.93E+01 | 1.82E+00 | 2.09E+00 | 1.57E+00 | 1.63E+00 | 1.48E+00 | 3.48E+00 | 5.17E-02 | 3.97E+02 | 6.29E+00 |
| 2.60E+01 | 1.78E+00 | 2.07E+00 | 1.54E+00 | 1.55E+00 | 1.45E+00 | 3.93E+00 | 5.37E-02 | 4.08E+02 | 6.32E+00 |
| 2.26E+01 | 1.76E+00 | 2.02E+00 | 1.53E+00 | 1.51E+00 | 1.48E+00 | 4.47E+00 | 5.53E-02 | 4.16E+02 | 6.37E+00 |
| 1.94E+01 | 1.76E+00 | 1.97E+00 | 1.52E+00 | 1.49E+00 | 1.49E+00 | 5.06E+00 | 5.67E-02 | 4.22E+02 | 6.42E+00 |

Table D.5 Refrigerant: HCFC-123, Tu-Cii surface, Triangular Pitch, Nozzle Configuration: 24WDCRC,
Refrigerant Supply Rate: 25 kg/min, Pure Refrigerant Data

| q'' $\left(\frac{\text{kW}}{\text{m}^2 \cdot \text{K}}\right)$ | h_b $\left(\frac{\text{kW}}{\text{m}^2 \cdot \text{K}}\right)$ | h_1 $\left(\frac{\text{kW}}{\text{m}^2 \cdot \text{K}}\right)$ | h_2 $\left(\frac{\text{kW}}{\text{m}^2 \cdot \text{K}}\right)$ | h_3 $\left(\frac{\text{kW}}{\text{m}^2 \cdot \text{K}}\right)$ | h_4 $\left(\frac{\text{kW}}{\text{m}^2 \cdot \text{K}}\right)$ | OFR | Γ_4 $\left(\frac{\text{kg}}{\text{s} \cdot \text{m}}\right)$ | Re_4 | Pr_4 |
|---|---|---|---|---|---|----------|--|----------|----------|
| 3.99E+01 | 4.06E+00 | 1.12E+01 | 5.95E+00 | 1.49E+00 | 3.09E-01 | 1.76E+00 | 2.03E-02 | 1.54E+02 | 6.33E+00 |
| 3.64E+01 | 3.98E+00 | 1.10E+01 | 6.79E+00 | 1.53E+00 | 3.11E-01 | 1.88E+00 | 2.13E-02 | 1.61E+02 | 6.34E+00 |
| 3.34E+01 | 4.31E+00 | 1.09E+01 | 8.01E+00 | 2.24E+00 | 5.04E-01 | 2.05E+00 | 2.40E-02 | 1.79E+02 | 6.39E+00 |
| 2.99E+01 | 6.62E+00 | 1.10E+01 | 8.45E+00 | 4.52E+00 | 3.89E+00 | 2.26E+00 | 2.84E-02 | 2.04E+02 | 6.55E+00 |
| 2.64E+01 | 7.76E+00 | 1.15E+01 | 9.10E+00 | 5.69E+00 | 5.65E+00 | 2.60E+00 | 3.15E-02 | 2.23E+02 | 6.60E+00 |
| 2.27E+01 | 8.55E+00 | 1.16E+01 | 9.83E+00 | 6.41E+00 | 6.19E+00 | 2.98E+00 | 3.28E-02 | 2.32E+02 | 6.62E+00 |
| 1.91E+01 | 9.32E+00 | 1.15E+01 | 1.04E+01 | 6.74E+00 | 7.04E+00 | 3.53E+00 | 3.49E-02 | 2.45E+02 | 6.64E+00 |

Table D.6 Refrigerant: HCFC-123, Tu-Cii surface, Triangular Pitch, Nozzle Configuration: 24WDCRC,
Refrigerant Supply Rate: 35 kg/min, Pure Refrigerant Data

| q'' $\left(\frac{\text{kW}}{\text{m}^2 \cdot \text{K}}\right)$ | h_b $\left(\frac{\text{kW}}{\text{m}^2 \cdot \text{K}}\right)$ | h_1 $\left(\frac{\text{kW}}{\text{m}^2 \cdot \text{K}}\right)$ | h_2 $\left(\frac{\text{kW}}{\text{m}^2 \cdot \text{K}}\right)$ | h_3 $\left(\frac{\text{kW}}{\text{m}^2 \cdot \text{K}}\right)$ | h_4 $\left(\frac{\text{kW}}{\text{m}^2 \cdot \text{K}}\right)$ | OFR | Γ_4 $\left(\frac{\text{kg}}{\text{s} \cdot \text{m}}\right)$ | Re_4 | Pr_4 |
|---|---|---|---|---|---|----------|--|----------|----------|
| 4.04E+01 | 4.43E+00 | 1.19E+01 | 8.36E+00 | 1.55E+00 | 4.39E-01 | 2.02E+00 | 2.76E-02 | 2.09E+02 | 6.34E+00 |
| 3.65E+01 | 4.53E+00 | 1.16E+01 | 9.27E+00 | 2.08E+00 | 5.95E-01 | 2.22E+00 | 3.03E-02 | 2.27E+02 | 6.38E+00 |
| 3.36E+01 | 6.39E+00 | 1.15E+01 | 9.34E+00 | 4.31E+00 | 3.63E+00 | 2.41E+00 | 3.49E-02 | 2.52E+02 | 6.53E+00 |
| 2.92E+01 | 7.92E+00 | 1.16E+01 | 9.55E+00 | 5.70E+00 | 5.84E+00 | 2.73E+00 | 3.72E-02 | 2.65E+02 | 6.59E+00 |
| 2.61E+01 | 8.60E+00 | 1.17E+01 | 1.01E+01 | 6.31E+00 | 6.56E+00 | 3.06E+00 | 3.94E-02 | 2.79E+02 | 6.61E+00 |
| 2.24E+01 | 9.35E+00 | 1.16E+01 | 1.04E+01 | 6.79E+00 | 7.10E+00 | 3.59E+00 | 4.15E-02 | 2.93E+02 | 6.63E+00 |
| 1.90E+01 | 1.00E+01 | 1.13E+01 | 1.04E+01 | 7.18E+00 | 8.03E+00 | 4.16E+00 | 4.30E-02 | 3.02E+02 | 6.65E+00 |

Table D.7 Refrigerant: HCFC-123, Tu-Cii surface, Triangular Pitch, Nozzle Configuration: 30WDCRC,
Refrigerant Supply Rate: 25 kg/min, Pure Refrigerant Data

| q'' $\left(\frac{\text{kW}}{\text{m}^2 \cdot \text{K}}\right)$ | h_b $\left(\frac{\text{kW}}{\text{m}^2 \cdot \text{K}}\right)$ | h_1 $\left(\frac{\text{kW}}{\text{m}^2 \cdot \text{K}}\right)$ | h_2 $\left(\frac{\text{kW}}{\text{m}^2 \cdot \text{K}}\right)$ | h_3 $\left(\frac{\text{kW}}{\text{m}^2 \cdot \text{K}}\right)$ | h_4 $\left(\frac{\text{kW}}{\text{m}^2 \cdot \text{K}}\right)$ | OFR | Γ_4 $\left(\frac{\text{kg}}{\text{s} \cdot \text{m}}\right)$ | Re_4 | Pr_4 |
|---|---|---|---|---|---|----------|--|----------|----------|
| 4.01E+01 | 4.82E+00 | 1.09E+01 | 1.07E+01 | 2.16E+00 | 1.01E+00 | 2.17E+00 | 3.18E-02 | 2.38E+02 | 6.39E+00 |
| 3.63E+01 | 4.87E+00 | 1.09E+01 | 1.05E+01 | 2.74E+00 | 1.27E+00 | 2.35E+00 | 3.37E-02 | 2.50E+02 | 6.42E+00 |
| 3.30E+01 | 5.76E+00 | 1.09E+01 | 1.01E+01 | 4.01E+00 | 2.88E+00 | 2.54E+00 | 3.66E-02 | 2.66E+02 | 6.51E+00 |
| 2.95E+01 | 8.09E+00 | 1.13E+01 | 1.01E+01 | 5.50E+00 | 6.71E+00 | 2.80E+00 | 3.94E-02 | 2.80E+02 | 6.60E+00 |
| 2.62E+01 | 9.12E+00 | 1.16E+01 | 1.04E+01 | 6.39E+00 | 7.50E+00 | 3.22E+00 | 4.20E-02 | 2.97E+02 | 6.62E+00 |
| 2.27E+01 | 9.89E+00 | 1.16E+01 | 1.04E+01 | 7.05E+00 | 8.10E+00 | 3.71E+00 | 4.39E-02 | 3.09E+02 | 6.64E+00 |
| 1.93E+01 | 1.06E+01 | 1.14E+01 | 1.02E+01 | 7.66E+00 | 8.73E+00 | 4.31E+00 | 4.57E-02 | 3.20E+02 | 6.65E+00 |

Table D.8 Refrigerant: HCFC-123, Tu-Cii surface, Triangular Pitch, Nozzle Configuration: 30WDCRC,
Refrigerant Supply Rate: 35 kg/min, Pure Refrigerant Data

| q'' $\left(\frac{\text{kW}}{\text{m}^2 \cdot \text{K}}\right)$ | h_b $\left(\frac{\text{kW}}{\text{m}^2 \cdot \text{K}}\right)$ | h_1 $\left(\frac{\text{kW}}{\text{m}^2 \cdot \text{K}}\right)$ | h_2 $\left(\frac{\text{kW}}{\text{m}^2 \cdot \text{K}}\right)$ | h_3 $\left(\frac{\text{kW}}{\text{m}^2 \cdot \text{K}}\right)$ | h_4 $\left(\frac{\text{kW}}{\text{m}^2 \cdot \text{K}}\right)$ | OFR | Γ_4 $\left(\frac{\text{kg}}{\text{s} \cdot \text{m}}\right)$ | Re_4 | Pr_4 |
|---|---|---|---|---|---|----------|--|----------|----------|
| 4.01E+01 | 5.45E+00 | 1.10E+01 | 1.13E+01 | 3.90E+00 | 2.06E+00 | 2.61E+00 | 4.48E-02 | 3.31E+02 | 6.44E+00 |
| 3.65E+01 | 5.49E+00 | 1.10E+01 | 1.10E+01 | 4.08E+00 | 2.44E+00 | 2.88E+00 | 4.74E-02 | 3.47E+02 | 6.48E+00 |
| 3.32E+01 | 5.65E+00 | 1.11E+01 | 1.08E+01 | 4.03E+00 | 3.83E+00 | 3.11E+00 | 4.97E-02 | 3.60E+02 | 6.53E+00 |
| 2.93E+01 | 6.19E+00 | 1.11E+01 | 1.08E+01 | 4.37E+00 | 5.99E+00 | 3.49E+00 | 5.24E-02 | 3.74E+02 | 6.58E+00 |
| 2.64E+01 | 6.75E+00 | 1.12E+01 | 1.08E+01 | 4.80E+00 | 6.57E+00 | 3.87E+00 | 5.41E-02 | 3.84E+02 | 6.60E+00 |
| 2.26E+01 | 6.95E+00 | 1.09E+01 | 1.08E+01 | 4.81E+00 | 6.76E+00 | 4.56E+00 | 5.67E-02 | 4.01E+02 | 6.62E+00 |
| 1.90E+01 | 7.37E+00 | 1.06E+01 | 1.05E+01 | 4.98E+00 | 7.08E+00 | 5.23E+00 | 5.74E-02 | 4.04E+02 | 6.64E+00 |

Table D.9 Refrigerant: HCFC-123, Tu-B surface, Triangular Pitch, Nozzle Configuration: 30WDCRC,
Refrigerant Supply Rate: 25 kg/min, Pure Refrigerant Data

| q'' $\left(\frac{\text{kW}}{\text{m}^2 \cdot \text{K}}\right)$ | h_b $\left(\frac{\text{kW}}{\text{m}^2 \cdot \text{K}}\right)$ | h_1 $\left(\frac{\text{kW}}{\text{m}^2 \cdot \text{K}}\right)$ | h_2 $\left(\frac{\text{kW}}{\text{m}^2 \cdot \text{K}}\right)$ | h_3 $\left(\frac{\text{kW}}{\text{m}^2 \cdot \text{K}}\right)$ | h_4 $\left(\frac{\text{kW}}{\text{m}^2 \cdot \text{K}}\right)$ | OFR | Γ_4 $\left(\frac{\text{kg}}{\text{s} \cdot \text{m}}\right)$ | Re_4 | Pr_4 |
|---|---|---|---|---|---|----------|--|----------|----------|
| 4.10E+01 | 2.17E+01 | 2.69E+01 | 2.96E+01 | 1.72E+01 | 1.95E+01 | 2.11E+00 | 3.54E-02 | 2.48E+02 | 6.65E+00 |
| 3.71E+01 | 2.27E+01 | 2.71E+01 | 3.01E+01 | 1.77E+01 | 2.07E+01 | 2.31E+00 | 3.67E-02 | 2.57E+02 | 6.66E+00 |
| 3.32E+01 | 2.33E+01 | 2.68E+01 | 3.03E+01 | 1.77E+01 | 2.23E+01 | 2.62E+00 | 3.91E-02 | 2.73E+02 | 6.67E+00 |
| 2.99E+01 | 2.40E+01 | 2.63E+01 | 3.02E+01 | 1.77E+01 | 2.43E+01 | 2.88E+00 | 4.07E-02 | 2.84E+02 | 6.67E+00 |
| 2.63E+01 | 2.40E+01 | 2.49E+01 | 2.90E+01 | 1.76E+01 | 2.53E+01 | 3.27E+00 | 4.26E-02 | 2.97E+02 | 6.68E+00 |
| 2.27E+01 | 2.32E+01 | 2.24E+01 | 2.63E+01 | 1.69E+01 | 2.73E+01 | 3.78E+00 | 4.43E-02 | 3.09E+02 | 6.68E+00 |
| 1.91E+01 | 2.06E+01 | 1.84E+01 | 2.19E+01 | 1.50E+01 | 2.58E+01 | 4.44E+00 | 4.61E-02 | 3.21E+02 | 6.69E+00 |

Table D.10 Refrigerant: HCFC-123, Tu-B surface, Triangular Pitch, Nozzle Configuration: 30WDCRC,
Refrigerant Supply Rate: 35 kg/min, Pure Refrigerant Data

| q'' $\left(\frac{\text{kW}}{\text{m}^2 \cdot \text{K}}\right)$ | h_b $\left(\frac{\text{kW}}{\text{m}^2 \cdot \text{K}}\right)$ | h_1 $\left(\frac{\text{kW}}{\text{m}^2 \cdot \text{K}}\right)$ | h_2 $\left(\frac{\text{kW}}{\text{m}^2 \cdot \text{K}}\right)$ | h_3 $\left(\frac{\text{kW}}{\text{m}^2 \cdot \text{K}}\right)$ | h_4 $\left(\frac{\text{kW}}{\text{m}^2 \cdot \text{K}}\right)$ | OFR | Γ_4 $\left(\frac{\text{kg}}{\text{s} \cdot \text{m}}\right)$ | Re_4 | Pr_4 |
|---|---|---|---|---|---|----------|--|----------|----------|
| 4.09E+01 | 2.28E+01 | 2.80E+01 | 3.04E+01 | 1.77E+01 | 2.06E+01 | 2.56E+00 | 4.70E-02 | 3.29E+02 | 6.66E+00 |
| 3.72E+01 | 2.39E+01 | 2.81E+01 | 3.12E+01 | 1.80E+01 | 2.21E+01 | 2.77E+00 | 4.82E-02 | 3.37E+02 | 6.66E+00 |
| 3.38E+01 | 2.44E+01 | 2.81E+01 | 3.15E+01 | 1.81E+01 | 2.36E+01 | 3.17E+00 | 5.14E-02 | 3.59E+02 | 6.67E+00 |
| 3.04E+01 | 2.50E+01 | 2.77E+01 | 3.13E+01 | 1.81E+01 | 2.56E+01 | 3.44E+00 | 5.21E-02 | 3.63E+02 | 6.68E+00 |
| 2.67E+01 | 2.49E+01 | 2.60E+01 | 3.00E+01 | 1.79E+01 | 2.65E+01 | 3.83E+00 | 5.37E-02 | 3.75E+02 | 6.68E+00 |
| 2.31E+01 | 2.40E+01 | 2.32E+01 | 2.70E+01 | 1.70E+01 | 2.83E+01 | 4.39E+00 | 5.56E-02 | 3.87E+02 | 6.68E+00 |
| 1.96E+01 | 2.14E+01 | 1.92E+01 | 2.26E+01 | 1.53E+01 | 2.61E+01 | 5.15E+00 | 5.73E-02 | 3.98E+02 | 6.69E+00 |

Table D.11 Refrigerant: HCFC-123, Plain surface, Triangular Pitch, Nozzle Configuration:
30WDCRC, Refrigerant Supply Rate: 25 kg/min, 1.1 % Oil Concentration

| q'' $\left(\frac{\text{kW}}{\text{m}^2 \cdot \text{K}}\right)$ | h_b $\left(\frac{\text{kW}}{\text{m}^2 \cdot \text{K}}\right)$ | h_1 $\left(\frac{\text{kW}}{\text{m}^2 \cdot \text{K}}\right)$ | h_2 $\left(\frac{\text{kW}}{\text{m}^2 \cdot \text{K}}\right)$ | h_3 $\left(\frac{\text{kW}}{\text{m}^2 \cdot \text{K}}\right)$ | h_4 $\left(\frac{\text{kW}}{\text{m}^2 \cdot \text{K}}\right)$ | OFR | Γ_4 $\left(\frac{\text{kg}}{\text{s} \cdot \text{m}}\right)$ |
|---|---|---|---|---|---|----------|--|
| 4.04E+01 | 1.89E+00 | 2.44E+00 | 1.95E+00 | 1.89E+00 | 1.25E+00 | 2.14E+00 | 3.39E-02 |
| 3.68E+01 | 2.04E+00 | 2.38E+00 | 1.87E+00 | 1.90E+00 | 1.66E+00 | 2.32E+00 | 3.63E-02 |
| 3.33E+01 | 2.11E+00 | 2.41E+00 | 1.85E+00 | 1.87E+00 | 1.84E+00 | 2.60E+00 | 3.91E-02 |
| 2.96E+01 | 2.13E+00 | 2.41E+00 | 1.85E+00 | 1.84E+00 | 1.83E+00 | 2.88E+00 | 4.03E-02 |
| 2.63E+01 | 2.14E+00 | 2.43E+00 | 1.87E+00 | 1.84E+00 | 1.77E+00 | 3.24E+00 | 4.22E-02 |
| 2.25E+01 | 2.16E+00 | 2.38E+00 | 1.92E+00 | 1.87E+00 | 1.77E+00 | 3.73E+00 | 4.34E-02 |
| 1.95E+01 | 2.21E+00 | 2.35E+00 | 1.97E+00 | 1.93E+00 | 1.77E+00 | 4.29E+00 | 4.49E-02 |

Table D.12 Refrigerant: HCFC-123, Plain surface, Triangular Pitch, Nozzle Configuration:
30WDCRC, Refrigerant Supply Rate: 25 kg/min, 2.5 % Oil Concentration

| q'' $\left(\frac{\text{kW}}{\text{m}^2 \cdot \text{K}}\right)$ | h_b $\left(\frac{\text{kW}}{\text{m}^2 \cdot \text{K}}\right)$ | h_1 $\left(\frac{\text{kW}}{\text{m}^2 \cdot \text{K}}\right)$ | h_2 $\left(\frac{\text{kW}}{\text{m}^2 \cdot \text{K}}\right)$ | h_3 $\left(\frac{\text{kW}}{\text{m}^2 \cdot \text{K}}\right)$ | h_4 $\left(\frac{\text{kW}}{\text{m}^2 \cdot \text{K}}\right)$ | OFR | Γ_4 $\left(\frac{\text{kg}}{\text{s} \cdot \text{m}}\right)$ |
|---|---|---|---|---|---|----------|--|
| 3.98E+01 | 1.56E+00 | 2.34E+00 | 1.79E+00 | 1.42E+00 | 9.08E-01 | 2.18E+00 | 3.36E-02 |
| 3.63E+01 | 1.79E+00 | 2.41E+00 | 1.82E+00 | 1.72E+00 | 1.24E+00 | 2.37E+00 | 3.62E-02 |
| 3.32E+01 | 2.02E+00 | 2.52E+00 | 1.90E+00 | 1.83E+00 | 1.57E+00 | 2.57E+00 | 3.81E-02 |
| 2.97E+01 | 2.18E+00 | 2.61E+00 | 1.99E+00 | 1.84E+00 | 1.72E+00 | 2.89E+00 | 4.04E-02 |
| 2.61E+01 | 2.31E+00 | 2.69E+00 | 2.10E+00 | 1.91E+00 | 1.76E+00 | 3.26E+00 | 4.18E-02 |
| 2.25E+01 | 2.41E+00 | 2.72E+00 | 2.21E+00 | 2.01E+00 | 1.84E+00 | 3.75E+00 | 4.36E-02 |
| 1.96E+01 | 2.54E+00 | 2.78E+00 | 2.34E+00 | 2.13E+00 | 1.94E+00 | 4.27E+00 | 4.50E-02 |

Table D.13 Refrigerant: HCFC-123, Plain surface, Triangular Pitch, Nozzle Configuration:
30WDCRC, Refrigerant Supply Rate: 35 kg/min, 2.5 % Oil Concentration

| q'' $\left(\frac{\text{kW}}{\text{m}^2 \cdot \text{K}}\right)$ | h_b $\left(\frac{\text{kW}}{\text{m}^2 \cdot \text{K}}\right)$ | h_1 $\left(\frac{\text{kW}}{\text{m}^2 \cdot \text{K}}\right)$ | h_2 $\left(\frac{\text{kW}}{\text{m}^2 \cdot \text{K}}\right)$ | h_3 $\left(\frac{\text{kW}}{\text{m}^2 \cdot \text{K}}\right)$ | h_4 $\left(\frac{\text{kW}}{\text{m}^2 \cdot \text{K}}\right)$ | OFR | Γ_4 $\left(\frac{\text{kg}}{\text{s} \cdot \text{m}}\right)$ |
|---|---|---|---|---|---|----------|--|
| 4.03E+01 | 1.63E+00 | 2.61E+00 | 1.80E+00 | 1.40E+00 | 9.55E-01 | 2.63E+00 | 4.52E-02 |
| 3.69E+01 | 1.82E+00 | 2.75E+00 | 1.81E+00 | 1.66E+00 | 1.23E+00 | 2.87E+00 | 4.81E-02 |
| 3.34E+01 | 2.03E+00 | 2.87E+00 | 1.92E+00 | 1.80E+00 | 1.49E+00 | 3.16E+00 | 5.00E-02 |
| 2.99E+01 | 2.24E+00 | 3.00E+00 | 2.04E+00 | 1.80E+00 | 1.66E+00 | 3.50E+00 | 5.19E-02 |
| 2.62E+01 | 2.42E+00 | 3.10E+00 | 2.18E+00 | 1.87E+00 | 1.75E+00 | 3.98E+00 | 5.37E-02 |
| 2.22E+01 | 2.56E+00 | 3.17E+00 | 2.36E+00 | 2.02E+00 | 1.82E+00 | 4.63E+00 | 5.54E-02 |
| 1.91E+01 | 2.71E+00 | 3.21E+00 | 2.58E+00 | 2.18E+00 | 1.99E+00 | 5.35E+00 | 5.72E-02 |

Table D.14 Refrigerant: HCFC-123, Tu-Cii surface, Triangular Pitch, Nozzle Configuration:
30WDCRC, Refrigerant Supply Rate: 25 kg/min, 1.1 % Oil Concentration

| q'' $\left(\frac{\text{kW}}{\text{m}^2 \cdot \text{K}}\right)$ | h_b $\left(\frac{\text{kW}}{\text{m}^2 \cdot \text{K}}\right)$ | h_1 $\left(\frac{\text{kW}}{\text{m}^2 \cdot \text{K}}\right)$ | h_2 $\left(\frac{\text{kW}}{\text{m}^2 \cdot \text{K}}\right)$ | h_3 $\left(\frac{\text{kW}}{\text{m}^2 \cdot \text{K}}\right)$ | h_4 $\left(\frac{\text{kW}}{\text{m}^2 \cdot \text{K}}\right)$ | OFR | Γ_4 $\left(\frac{\text{kg}}{\text{s} \cdot \text{m}}\right)$ |
|---|---|---|---|---|---|----------|--|
| 4.04E+01 | 6.08E+00 | 9.94E+00 | 9.20E+00 | 4.82E+00 | 3.22E+00 | 2.14E+00 | 3.36E-02 |
| 3.69E+01 | 6.76E+00 | 1.04E+01 | 8.84E+00 | 4.90E+00 | 4.98E+00 | 2.30E+00 | 3.58E-02 |
| 3.32E+01 | 7.43E+00 | 1.09E+01 | 8.60E+00 | 4.89E+00 | 7.09E+00 | 2.59E+00 | 3.91E-02 |
| 2.92E+01 | 8.11E+00 | 1.14E+01 | 8.39E+00 | 5.04E+00 | 8.49E+00 | 2.92E+00 | 4.13E-02 |
| 2.54E+01 | 8.95E+00 | 1.17E+01 | 8.31E+00 | 5.61E+00 | 9.17E+00 | 3.32E+00 | 4.26E-02 |
| 2.24E+01 | 9.68E+00 | 1.17E+01 | 8.20E+00 | 6.27E+00 | 9.67E+00 | 3.74E+00 | 4.40E-02 |
| 1.90E+01 | 1.02E+01 | 1.13E+01 | 8.21E+00 | 6.77E+00 | 1.02E+01 | 4.39E+00 | 4.57E-02 |

Table D.15 Refrigerant: HCFC-123, Tu-Cii surface, Triangular Pitch, Nozzle Configuration:
30WDCRC, Refrigerant Supply Rate: 25 kg/min, 2.5 % Oil Concentration

| q'' $\left(\frac{\text{kW}}{\text{m}^2 \cdot \text{K}}\right)$ | h_b $\left(\frac{\text{kW}}{\text{m}^2 \cdot \text{K}}\right)$ | h_1 $\left(\frac{\text{kW}}{\text{m}^2 \cdot \text{K}}\right)$ | h_2 $\left(\frac{\text{kW}}{\text{m}^2 \cdot \text{K}}\right)$ | h_3 $\left(\frac{\text{kW}}{\text{m}^2 \cdot \text{K}}\right)$ | h_4 $\left(\frac{\text{kW}}{\text{m}^2 \cdot \text{K}}\right)$ | OFR | Γ_4 $\left(\frac{\text{kg}}{\text{s} \cdot \text{m}}\right)$ |
|---|---|---|---|---|---|----------|--|
| 3.99E+01 | 6.19E+00 | 9.19E+00 | 9.10E+00 | 5.46E+00 | 4.29E+00 | 2.18E+00 | 3.46E-02 |
| 3.61E+01 | 6.84E+00 | 9.79E+00 | 9.56E+00 | 6.04E+00 | 5.98E+00 | 2.37E+00 | 3.68E-02 |
| 3.31E+01 | 7.41E+00 | 1.03E+01 | 9.84E+00 | 6.61E+00 | 7.45E+00 | 2.59E+00 | 3.87E-02 |
| 2.96E+01 | 8.21E+00 | 1.13E+01 | 1.02E+01 | 7.34E+00 | 9.01E+00 | 2.86E+00 | 4.02E-02 |
| 2.63E+01 | 9.33E+00 | 1.19E+01 | 1.05E+01 | 8.77E+00 | 1.04E+01 | 3.21E+00 | 4.19E-02 |
| 2.24E+01 | 1.10E+01 | 1.25E+01 | 1.09E+01 | 1.05E+01 | 1.17E+01 | 3.77E+00 | 4.41E-02 |
| 1.90E+01 | 1.22E+01 | 1.28E+01 | 1.11E+01 | 1.09E+01 | 1.24E+01 | 4.38E+00 | 4.54E-02 |

Table D.16 Refrigerant: HCFC-123, Tu-Cii surface, Triangular Pitch, Nozzle Configuration:
30WDCRC, Refrigerant Supply Rate: 35 kg/min, 2.5 % Oil Concentration

| q'' $\left(\frac{\text{kW}}{\text{m}^2 \cdot \text{K}}\right)$ | h_b $\left(\frac{\text{kW}}{\text{m}^2 \cdot \text{K}}\right)$ | h_1 $\left(\frac{\text{kW}}{\text{m}^2 \cdot \text{K}}\right)$ | h_2 $\left(\frac{\text{kW}}{\text{m}^2 \cdot \text{K}}\right)$ | h_3 $\left(\frac{\text{kW}}{\text{m}^2 \cdot \text{K}}\right)$ | h_4 $\left(\frac{\text{kW}}{\text{m}^2 \cdot \text{K}}\right)$ | OFR | Γ_4 $\left(\frac{\text{kg}}{\text{s} \cdot \text{m}}\right)$ |
|---|---|---|---|---|---|----------|--|
| 4.01E+01 | 7.17E+00 | 1.07E+01 | 9.93E+00 | 6.92E+00 | 5.85E+00 | 2.65E+00 | 4.71E-02 |
| 3.64E+01 | 7.91E+00 | 1.16E+01 | 1.08E+01 | 7.40E+00 | 7.31E+00 | 2.89E+00 | 4.89E-02 |
| 3.28E+01 | 8.71E+00 | 1.24E+01 | 1.16E+01 | 8.53E+00 | 8.66E+00 | 3.21E+00 | 5.08E-02 |
| 2.91E+01 | 9.93E+00 | 1.34E+01 | 1.25E+01 | 1.05E+01 | 1.03E+01 | 3.59E+00 | 5.26E-02 |
| 2.60E+01 | 1.12E+01 | 1.41E+01 | 1.34E+01 | 1.19E+01 | 1.14E+01 | 4.02E+00 | 5.45E-02 |
| 2.24E+01 | 1.28E+01 | 1.47E+01 | 1.42E+01 | 1.28E+01 | 1.23E+01 | 4.61E+00 | 5.58E-02 |
| 1.89E+01 | 1.41E+01 | 1.46E+01 | 1.47E+01 | 1.26E+01 | 1.36E+01 | 5.46E+00 | 5.78E-02 |

Table D.17 Refrigerant: HCFC-123, Tu-B surface, Triangular Pitch, Nozzle Configuration:
30WDCRC, Refrigerant Supply Rate: 25 kg/min, 1.1 % Oil Concentration

| q'' $\left(\frac{\text{kW}}{\text{m}^2 \cdot \text{K}}\right)$ | h_b $\left(\frac{\text{kW}}{\text{m}^2 \cdot \text{K}}\right)$ | h_1 $\left(\frac{\text{kW}}{\text{m}^2 \cdot \text{K}}\right)$ | h_2 $\left(\frac{\text{kW}}{\text{m}^2 \cdot \text{K}}\right)$ | h_3 $\left(\frac{\text{kW}}{\text{m}^2 \cdot \text{K}}\right)$ | h_4 $\left(\frac{\text{kW}}{\text{m}^2 \cdot \text{K}}\right)$ | OFR | Γ_4 $\left(\frac{\text{kg}}{\text{s} \cdot \text{m}}\right)$ |
|---|---|---|---|---|---|----------|--|
| 4.07E+01 | 1.72E+01 | 1.91E+01 | 1.86E+01 | 1.37E+01 | 1.57E+01 | 2.16E+00 | 3.56E-02 |
| 3.73E+01 | 1.81E+01 | 1.95E+01 | 1.87E+01 | 1.44E+01 | 1.68E+01 | 2.35E+00 | 3.76E-02 |
| 3.38E+01 | 1.87E+01 | 1.97E+01 | 1.85E+01 | 1.48E+01 | 1.78E+01 | 2.57E+00 | 3.88E-02 |
| 3.05E+01 | 1.93E+01 | 1.99E+01 | 1.81E+01 | 1.49E+01 | 1.91E+01 | 2.83E+00 | 4.05E-02 |
| 2.64E+01 | 1.94E+01 | 1.91E+01 | 1.73E+01 | 1.48E+01 | 2.01E+01 | 3.22E+00 | 4.19E-02 |
| 2.31E+01 | 1.87E+01 | 1.80E+01 | 1.58E+01 | 1.41E+01 | 2.07E+01 | 3.68E+00 | 4.36E-02 |
| 1.94E+01 | 1.72E+01 | 1.60E+01 | 1.37E+01 | 1.27E+01 | 1.95E+01 | 4.35E+00 | 4.54E-02 |

Table D.18 Refrigerant: HCFC-123, Tu-B surface, Triangular Pitch, Nozzle Configuration:
30WDCRC, Refrigerant Supply Rate: 25 kg/min, 2.5 % Oil Concentration

| q'' $\left(\frac{\text{kW}}{\text{m}^2 \cdot \text{K}}\right)$ | h_b $\left(\frac{\text{kW}}{\text{m}^2 \cdot \text{K}}\right)$ | h_1 $\left(\frac{\text{kW}}{\text{m}^2 \cdot \text{K}}\right)$ | h_2 $\left(\frac{\text{kW}}{\text{m}^2 \cdot \text{K}}\right)$ | h_3 $\left(\frac{\text{kW}}{\text{m}^2 \cdot \text{K}}\right)$ | h_4 $\left(\frac{\text{kW}}{\text{m}^2 \cdot \text{K}}\right)$ | OFR | Γ_4 $\left(\frac{\text{kg}}{\text{s} \cdot \text{m}}\right)$ |
|---|---|---|---|---|---|----------|--|
| 4.09E+01 | 1.37E+01 | 1.91E+01 | 1.97E+01 | 1.07E+01 | 1.26E+01 | 2.14E+00 | 3.52E-02 |
| 3.74E+01 | 1.51E+01 | 1.93E+01 | 2.01E+01 | 1.17E+01 | 1.41E+01 | 2.32E+00 | 3.68E-02 |
| 3.40E+01 | 1.59E+01 | 1.91E+01 | 2.03E+01 | 1.23E+01 | 1.49E+01 | 2.56E+00 | 3.88E-02 |
| 3.01E+01 | 1.73E+01 | 1.96E+01 | 2.13E+01 | 1.33E+01 | 1.70E+01 | 2.85E+00 | 4.05E-02 |
| 2.66E+01 | 1.76E+01 | 1.88E+01 | 2.04E+01 | 1.35E+01 | 1.80E+01 | 3.22E+00 | 4.21E-02 |
| 2.26E+01 | 1.74E+01 | 1.75E+01 | 1.94E+01 | 1.31E+01 | 1.96E+01 | 3.77E+00 | 4.41E-02 |
| 1.93E+01 | 1.64E+01 | 1.49E+01 | 1.70E+01 | 1.21E+01 | 1.90E+01 | 4.34E+00 | 4.52E-02 |

Table D.19 Refrigerant: HCFC-123, Tu-B surface, Triangular Pitch, Nozzle Configuration:
30WDCRC, Refrigerant Supply Rate: 35 kg/min, 2.5 % Oil Concentration

| q'' $\left(\frac{\text{kW}}{\text{m}^2 \cdot \text{K}}\right)$ | h_b $\left(\frac{\text{kW}}{\text{m}^2 \cdot \text{K}}\right)$ | h_1 $\left(\frac{\text{kW}}{\text{m}^2 \cdot \text{K}}\right)$ | h_2 $\left(\frac{\text{kW}}{\text{m}^2 \cdot \text{K}}\right)$ | h_3 $\left(\frac{\text{kW}}{\text{m}^2 \cdot \text{K}}\right)$ | h_4 $\left(\frac{\text{kW}}{\text{m}^2 \cdot \text{K}}\right)$ | OFR | Γ_4 $\left(\frac{\text{kg}}{\text{s} \cdot \text{m}}\right)$ |
|---|---|---|---|---|---|----------|--|
| 4.09E+01 | 1.53E+01 | 2.04E+01 | 2.05E+01 | 1.15E+01 | 1.40E+01 | 2.64E+00 | 4.78E-02 |
| 3.71E+01 | 1.65E+01 | 2.06E+01 | 2.11E+01 | 1.22E+01 | 1.54E+01 | 2.87E+00 | 4.95E-02 |
| 3.33E+01 | 1.77E+01 | 2.10E+01 | 2.18E+01 | 1.32E+01 | 1.70E+01 | 3.20E+00 | 5.13E-02 |
| 2.98E+01 | 1.87E+01 | 2.13E+01 | 2.23E+01 | 1.38E+01 | 1.86E+01 | 3.55E+00 | 5.27E-02 |
| 2.65E+01 | 1.89E+01 | 2.01E+01 | 2.17E+01 | 1.40E+01 | 1.93E+01 | 3.96E+00 | 5.43E-02 |
| 2.33E+01 | 1.90E+01 | 1.90E+01 | 2.03E+01 | 1.38E+01 | 2.13E+01 | 4.48E+00 | 5.59E-02 |
| 1.97E+01 | 1.78E+01 | 1.62E+01 | 1.81E+01 | 1.28E+01 | 2.07E+01 | 5.27E+00 | 5.75E-02 |

APPENDIX E. HEAT TRANSFER COEFFICIENT PREDICTION MODEL DEVELOPMENT

This appendix is dedicated to the presentation of heat transfer prediction models which were created to allow design engineers the use of heat transfer coefficients measured on the bundle test facility for spray evaporation heat exchanger development. A total of 13 models are presented. The first 10 are dedicated to the HFC-134a experimental work and the last 3 are dedicated to the HCFC-123 work. Although not presented here, other modeling work was conducted during this investigation with the more traditional dimensionless approach similar that seen in Equation 2.14. Some of the data presented in this report do not correlate well with the dimensionless parameter approach, because of partial dryout effects occurring in the upper heat flux range. The pure HFC-134a results collected with the W-40 fpi tube bundle are some of the results which do not behave as a power-law function. It was desired by the investigators to present models in this section of the report which were consistent in form and could be applied to results taken with each refrigerant and tube bundle combination.

Application descriptions and a listing of the corresponding data runs incorporated into each respective model are provided below.

| | |
|---------|--|
| Model 1 | Pure HFC-134a data, plain-surface, triangular-pitch tube bundle, data presented in Tables B.1 and B.2. |
|---------|--|

- Model 2 Pure HFC-134a data, W-40 fpi, triangular-pitch tube bundle, data presented in Tables B.3, B.4, B.5, and B.6.
- Model 3 Pure HFC-134a data, W-SC, triangular-pitch tube bundle, data presented in Tables B.7, B.8, B.9, and B.10.
- Model 4 Pure HFC-134a data, Tu-Cii, triangular-pitch tube bundle, data presented in Tables B.11, B.12, B.13, and B.14.
- Model 5 Pure HFC-134a data, Tu-B, triangular-pitch tube bundle, data presented in Tables B.15, B.16, B.17, and B.18.
- Model 6 Pure HFC-134a data, Tu-B, square-pitch tube bundle, data presented in Tables B.19, B.20, B.21, and B.22.
- Model 7 HFC-134a lubricant effects data, plain-surface, triangular-pitch tube bundle, data presented in Tables B.1, B.2, B.33, B.34, B.35, B.36.
- Model 8 HFC-134a lubricant effects data, W-40 fpi, triangular-pitch tube bundle, data presented in Tables B.3, B.5, B.37, B.38, B.39, B.40.
- Model 9 HFC-134a lubricant effects data, W-SC, triangular-pitch tube bundle, data presented in Tables B.7, B.9, B.41, B.42, B.43, B.44.
- Model 10 HFC-134a lubricant effects data, Tu-B, triangular-pitch tube bundle, data presented in Tables B.15, B.17, B.45, B.46, B.47, B.48.
- Model 11 HCFC-123 lubricant effects data, plain-surface, triangular-pitch tube bundle, data presented in Tables D.3, D.4, D.11, D.12, D.13.
- Model 12 HCFC-123 lubricant effects data, Tu-Cii, triangular-pitch tube bundle, data presented in Tables D.7, D.8, D.14, D.15, D.16.

Model 13 HCFC-123 lubricant effects data, Tu-B, triangular-pitch tube bundle, data presented in Tables D.9, D.10, D.17, D.18, D.19.

In Models 1 through 6 the heat transfer coefficients are correlated with the bundle overfeed ratio and the bundle heat flux. In addition to overfeed ratio and heat flux, Models 7 through 13 were developed with the lubricant mass fraction expressed as a percent (1.0%, 2.5% etc.). The units used throughout this appendix are kW/(m²*K) for heat transfer coefficients and kW/m² for heat fluxes. The bundle overfeed ratios are dimensionless.

Heat Transfer Coefficient Prediction Models

Equation E.1 presents the model used to correlate the pure HFC-134a data. This equation is used for Models 1 through 6. The constants a_1 through a_8 were evaluated with a statistical software package and are presented along with constants b_1 and b_2 in Table E.1.

Equation E.2 presents the model used to correlate the HFC-134a and HCFC-123 lubricant effects results. This equation is used for models 7 through 13. The constants a_1 through a_{13} along with b_1 , b_2 , and b_3 are presented in Tables E.2 and E.3.

Pure Refrigerant Model

$$\begin{aligned}
 h_o = & \text{Intercept} + a_1[q''-b_1] + a_2[\text{OFR}-b_2] + \\
 & a_3[q''-b_1]^2 + a_4[\text{OFR}-b_2]^2 + \\
 & a_5[(\text{OFR}-b_2)(q''-b_1)] + a_6[(\text{OFR}-b_2)^2(q''-b_1)] + \\
 & a_7[(\text{OFR}-b_2)(q''-b_1)^2] + a_8[(\text{OFR}-b_2)^2(q''-b_1)^2]
 \end{aligned} \tag{E.1}$$

Table E.1: Models correlating the pure HFC-134a results

| | Model | | | | | |
|-----------|-----------|-----------|-----------|-----------|-----------|-----------|
| | 1 | 2 | 3 | 4 | 5 | 6 |
| Intercept | 4.077419 | 10.485407 | 15.629125 | 39.717144 | 14.648617 | 14.396073 |
| a_1 | 0.058353 | 0.119846 | 0.102981 | 0.347080 | 0.204362 | 0.101054 |
| a_2 | 0.217197 | 0.128623 | 0.019094 | 0.824331 | 0.353017 | 0.472313 |
| a_3 | -0.000556 | -0.013547 | -0.024171 | -0.024843 | -0.003891 | -0.005227 |
| a_4 | 0.000000 | -0.113110 | -0.202267 | 0.000000 | -0.049645 | 0.000000 |
| a_5 | 0.016770 | -0.024009 | -0.030266 | 0.179921 | 0.000000 | 0.000000 |
| a_6 | 0.000000 | -0.012957 | -0.022195 | 0.000000 | -0.005816 | -0.004884 |
| a_7 | 0.000365 | -0.003029 | -0.003782 | 0.000000 | 0.000000 | -0.002597 |
| a_8 | 0.000000 | -0.000858 | -0.000537 | 0.000000 | -0.000510 | 0.000000 |
| b_1 | 29.630000 | 29.960000 | 29.680000 | 29.740000 | 29.980000 | 30.020000 |
| b_2 | 3.270000 | 3.740000 | 3.780000 | 3.790000 | 3.830000 | 3.530000 |
| CV | 0.308400 | 1.690920 | 3.205720 | 1.788100 | 1.641240 | 0.754510 |
| R^2 | 0.999300 | 0.984200 | 0.922500 | 0.964900 | 0.973500 | 0.979900 |

Lubricant Effects Model

$$\begin{aligned}
h_o = & \text{Intercept} + a_1[q''-b_1] + a_2[\text{OFR}-b_2] + a_3[\text{oil}-b_3] + \\
& a_4[q''-b_1]^2 + a_5[\text{oil}-b_3]^2 + a_6[(\text{OFR}-b_2)(\text{oil}-b_3)] + \\
& a_7[(\text{OFR}-b_2)(q''-b_1)] + a_8[(\text{oil}-b_3)(q''-b_1)] + \\
& a_9[(\text{OFR}-b_2)(q''-b_1)^2] + a_{10}[(\text{OFR}-b_2)(\text{oil}-b_3)^2] + \\
& a_{11}[(q''-b_1)^2(\text{oil}-b_3)] + a_{12}[(\text{oil}-b_3)^2(q''-b_1)] + \\
& a_{13}[(\text{oil}-b_3)^2(q''-b_1)^2]
\end{aligned} \tag{E.2}$$

Table E.2: Models correlating the HFC-134a lubricant effects results

| | Model | | | |
|-----------|-----------|-----------|-----------|-----------|
| | 7 | 8 | 9 | 10 |
| Intercept | 5.827190 | 14.103588 | 19.547623 | 37.968025 |
| a_1 | 0.081327 | 0.309483 | 0.318167 | -0.279646 |
| a_2 | 0.288747 | 0.000000 | 1.346631 | 2.147666 |
| a_3 | 1.517194 | 5.723922 | 3.266205 | 9.603386 |
| a_4 | 0.000000 | 0.000000 | -0.026424 | -0.041045 |
| a_5 | 0.000000 | 2.096607 | 0.000000 | -8.866201 |
| a_6 | 0.070840 | 0.808781 | 0.798345 | 0.837431 |
| a_7 | 0.021554 | 0.152022 | 0.135539 | 0.124232 |
| a_8 | 0.009367 | 0.386403 | 0.168654 | -0.298673 |
| a_9 | 0.000000 | 0.000000 | 0.000000 | 0.000000 |
| a_{10} | 0.034965 | 1.196474 | 0.000000 | 0.000000 |
| a_{11} | -0.001224 | -0.018790 | -0.008516 | -0.012721 |
| a_{12} | -0.009497 | 0.229350 | 0.000000 | 0.137647 |
| a_{13} | -0.000919 | -0.015018 | 0.000000 | 0.022505 |
| b_1 | 29.710000 | 29.900000 | 29.620000 | 29.990000 |
| b_2 | 3.240000 | 3.220000 | 3.210000 | 3.220000 |
| b_3 | 1.166700 | 1.166700 | 1.166700 | 1.166700 |
| CV | 1.275510 | 11.262040 | 6.223880 | 4.537460 |
| R^2 | 0.998400 | 0.961100 | 0.945000 | 0.990100 |

The constants b_1 and b_2 in Equation E.1 and b_1 , b_2 , and b_3 in Equation E.2 are used to center the distribution of each respective parameter about its mean value. Centering the distributions was required for successful operation of the statistical software package used to develop these models.

Table E.3: Models correlating the HCFC-123 lubricant effects results

| | Model | | |
|-----------|-----------|-----------|-----------|
| | 11 | 12 | 13 |
| Intercept | 2.459309 | 9.215622 | 19.881033 |
| a_1 | 0.057907 | 0.000000 | 0.138831 |
| a_2 | 0.717789 | 1.811933 | 2.248126 |
| a_3 | 0.181199 | 1.188508 | -2.720698 |
| a_4 | -0.003184 | 0.000000 | -0.017638 |
| a_5 | -0.288416 | -0.833763 | 1.023097 |
| a_6 | 0.031467 | 1.885449 | 0.263250 |
| a_7 | 0.000000 | 0.097246 | 0.081583 |
| a_8 | -0.022682 | 0.174183 | -0.035610 |
| a_9 | 0.000000 | 0.000000 | -0.007600 |
| a_{10} | -0.375109 | -1.120478 | 0.000000 |
| a_{11} | -0.000886 | -0.005347 | 0.001524 |
| a_{12} | -0.037607 | -0.172865 | -0.023315 |
| a_{13} | 0.001728 | 0.009870 | 0.000000 |
| b_1 | 29.660000 | 29.510000 | 30.110000 |
| b_2 | 3.300000 | 3.320000 | 3.290000 |
| b_3 | 1.220000 | 1.220000 | 1.220000 |
| CV | 0.954670 | 5.200660 | 0.977380 |
| R^2 | 0.996900 | 0.976100 | 0.997600 |

Model Use

It is very important to note that these models were developed to predict the heat transfer coefficients measured on the bundle test facility, not values outside the operating range used with each refrigerant. The models also allow for interpolation between the data points. For example, each model could be used to generate lines of constant overfeed ratio for graphical representation.

The dependent variable for each model is the shell-side heat transfer coefficient with units of $\text{kW}/(\text{m}^2 \cdot \text{K})$. To obtain shell-side heat transfer coefficient values the independent

variables heat flux, bundle overfeed ratio, and oil concentration where applicable are required for input into the respective models. The variables should be used in the following form.

Example Values

| | | |
|----------------------|----------|--------------------------------------|
| Heat Flux | 22, 36 | units of kW/m ² |
| Overfeed Ratio (OFR) | 2.0, 2.4 | parameter has no units |
| Oil concentration | 0.7, 2.4 | mass fraction expressed as a percent |

It is especially important to exercise caution when using the models in the upper heat flux range. The overfeed ratios were lowest at this end of the heat flux range, and dryout conditions were sometimes present for some of the tube bundles evaluated in this study. Higher overfeed ratios than those used in this study would eventually eliminate dryout on the lower rows of a tube bundle and the bundle heat transfer coefficient would increase significantly once this condition was achieved. It is questionable that any of the models presented herein could predict heat transfer coefficients at high overfeed ratios in the upper heat flux range with accuracy.

Correlation Accuracy

Both the coefficient of determination (R^2) and the coefficient of variability (CV) are presented in Tables E.1, E.2, and E.3 for each model. The coefficients of determination are all greater than 0.92 with the majority approaching 0.99. Tables E.4 through E.16 present measured and predicted values for each data point used in the correlation of each model. In

these tables the 95 % confidence limit on means (columns 4 and 5) and 95 % confidence limit on individuals (columns 6 and 7) are presented.

Table E.4: Pure HFC-134a, plain-surface, triangular-pitch tube bundle, correlation results summary (Model 1)

| Observation | Measured Value | Predicted Value | Lower 95% | Upper 95% | Lower 95% | Upper 95% |
|-------------|----------------|-----------------|-----------|-----------|-----------|-----------|
| | h_o | h_o | Mean | Mean | Predict | Predict |
| 1 | 3.8300 | 3.8265 | 3.8017 | 3.8514 | 3.7890 | 3.8641 |
| 2 | 3.8700 | 3.8674 | 3.8524 | 3.8825 | 3.8355 | 3.8994 |
| 3 | 3.8400 | 3.8479 | 3.8323 | 3.8636 | 3.8157 | 3.8802 |
| 4 | 3.7800 | 3.7860 | 3.7701 | 3.8019 | 3.7537 | 3.8183 |
| 5 | 3.7000 | 3.6953 | 3.6812 | 3.7093 | 3.6638 | 3.7267 |
| 6 | 3.5600 | 3.5620 | 3.5469 | 3.5771 | 3.5300 | 3.5939 |
| 7 | 3.3700 | 3.3667 | 3.3432 | 3.3902 | 3.3300 | 3.4033 |
| 8 | 4.5800 | 4.5974 | 4.5742 | 4.6205 | 4.5609 | 4.6338 |
| 9 | 4.5100 | 4.4905 | 4.4756 | 4.5054 | 4.4587 | 4.5224 |
| 10 | 4.4300 | 4.4187 | 4.4051 | 4.4323 | 4.3874 | 4.4500 |
| 11 | 4.2800 | 4.2805 | 4.2652 | 4.2959 | 4.2485 | 4.3126 |
| 12 | 4.1100 | 4.1249 | 4.1077 | 4.1421 | 4.0919 | 4.1579 |
| 13 | 3.9000 | 3.8979 | 3.8819 | 3.9139 | 3.8655 | 3.9303 |
| 14 | 3.6700 | 3.6683 | 3.6417 | 3.6950 | 3.6296 | 3.7071 |

Table E.5: Pure HFC-134a, W-40 fpi, triangular-pitch tube bundle, correlation results summary (Model 2)

| Observation | Measured Value | Predicted Value | Lower 95% | Upper 95% | Lower 95% | Upper 95% |
|-------------|----------------|-----------------|-----------|-----------|-----------|-----------|
| | h_o | h_o | Mean | Mean | Predict | Predict |
| 1 | 9.4900 | 9.3414 | 9.0438 | 9.6390 | 8.8896 | 9.7932 |
| 2 | 9.7100 | 9.8399 | 9.6510 | 10.0289 | 9.4510 | 10.2289 |
| 3 | 9.8800 | 10.0018 | 9.7987 | 10.2049 | 9.6057 | 10.3978 |
| 4 | 9.8800 | 9.8029 | 9.6212 | 9.9845 | 9.4174 | 10.1883 |
| 5 | 9.6000 | 9.3938 | 9.2301 | 9.5575 | 9.0165 | 9.7711 |
| 6 | 8.7700 | 8.8079 | 8.6199 | 8.9960 | 8.4194 | 9.1965 |
| 7 | 7.4000 | 7.6482 | 7.3885 | 7.9080 | 7.2204 | 8.0761 |
| 8 | 10.1000 | 10.1380 | 9.9320 | 10.3439 | 9.7405 | 10.5355 |
| 9 | 10.4000 | 10.5427 | 10.4077 | 10.6777 | 10.1769 | 10.9085 |
| 10 | 10.5000 | 10.5679 | 10.4380 | 10.6978 | 10.2040 | 10.9319 |
| 11 | 10.5000 | 10.3805 | 10.2455 | 10.5155 | 10.0147 | 10.7463 |
| 12 | 10.1000 | 9.8186 | 9.6868 | 9.9505 | 9.4540 | 10.1833 |
| 13 | 9.2400 | 9.0024 | 8.8677 | 9.1371 | 8.6367 | 9.3681 |
| 14 | 7.5700 | 7.5949 | 7.3494 | 7.8403 | 7.1755 | 8.0142 |
| 15 | 10.5000 | 10.3949 | 10.1968 | 10.5930 | 10.0014 | 10.7884 |
| 16 | 10.6000 | 10.6843 | 10.5578 | 10.8108 | 10.3215 | 11.0470 |
| 17 | 10.5000 | 10.7453 | 10.6195 | 10.8710 | 10.3827 | 11.1078 |
| 18 | 10.4000 | 10.4409 | 10.2986 | 10.5831 | 10.0723 | 10.8094 |
| 19 | 9.8600 | 9.8752 | 9.7411 | 10.0092 | 9.5097 | 10.2406 |
| 20 | 8.8700 | 8.8606 | 8.7148 | 9.0064 | 8.4907 | 9.2305 |
| 21 | 7.3300 | 7.4237 | 7.2178 | 7.6295 | 7.0262 | 7.8211 |
| 22 | 10.5000 | 10.3213 | 10.1057 | 10.5368 | 9.9187 | 10.7238 |
| 23 | 10.6000 | 10.5668 | 10.3923 | 10.7413 | 10.1846 | 10.9489 |
| 24 | 10.5000 | 10.5455 | 10.3273 | 10.7636 | 10.1415 | 10.9494 |
| 25 | 10.3000 | 10.4473 | 10.2948 | 10.5997 | 10.0747 | 10.8198 |
| 26 | 9.9000 | 9.9157 | 9.7167 | 10.1146 | 9.5218 | 10.3096 |
| 27 | 8.8600 | 8.7467 | 8.4837 | 9.0097 | 8.3169 | 9.1765 |
| 28 | 7.1200 | 7.1312 | 6.8291 | 7.4333 | 6.6764 | 7.5860 |

Table E.6: Pure HFC-134a, W-SC, triangular-pitch tube bundle, correlation results summary (Model 3)

| Observation | Measured Value | Predicted Value | Lower 95% | Upper 95% | Lower 95% | Upper 95% |
|-------------|----------------|-----------------|-----------|-----------|-----------|-----------|
| | h_o | h_o | Mean | Mean | Predict | Predict |
| 1 | 13.3000 | 13.0392 | 12.2100 | 13.8685 | 11.7781 | 14.3003 |
| 2 | 13.9000 | 14.1546 | 13.6415 | 14.6677 | 13.0748 | 15.2344 |
| 3 | 14.7000 | 14.7723 | 14.2146 | 15.3300 | 13.6706 | 15.8740 |
| 4 | 14.8000 | 14.8948 | 14.3772 | 15.4124 | 13.8128 | 15.9767 |
| 5 | 15.0000 | 14.4495 | 13.9891 | 14.9099 | 13.3937 | 15.5053 |
| 6 | 13.6000 | 13.5485 | 13.0008 | 14.0962 | 12.4518 | 14.6452 |
| 7 | 11.0000 | 11.7659 | 11.0648 | 12.4669 | 10.5851 | 12.9466 |
| 8 | 14.0000 | 13.9658 | 13.3702 | 14.5614 | 12.8444 | 15.0872 |
| 9 | 14.7000 | 14.9555 | 14.5673 | 15.3437 | 13.9291 | 15.9819 |
| 10 | 15.2000 | 15.5545 | 15.1868 | 15.9222 | 14.5357 | 16.5733 |
| 11 | 15.8000 | 15.5329 | 15.1552 | 15.9106 | 14.5105 | 16.5554 |
| 12 | 15.5000 | 14.9612 | 14.5942 | 15.3282 | 13.9427 | 15.9798 |
| 13 | 14.6000 | 13.7832 | 13.4173 | 14.1490 | 12.7651 | 14.8013 |
| 14 | 11.6000 | 11.8035 | 11.1606 | 12.4463 | 10.6563 | 12.9506 |
| 15 | 14.4000 | 14.3295 | 13.7694 | 14.8895 | 13.2266 | 15.4324 |
| 16 | 14.8000 | 15.2417 | 14.8927 | 15.5906 | 14.2295 | 16.2538 |
| 17 | 15.3000 | 15.6945 | 15.3422 | 16.0468 | 14.6812 | 16.7079 |
| 18 | 15.3000 | 15.5647 | 15.1832 | 15.9462 | 14.5408 | 16.5885 |
| 19 | 15.1000 | 14.7952 | 14.4438 | 15.1467 | 13.7822 | 15.8083 |
| 20 | 14.2000 | 13.8116 | 13.4414 | 14.1818 | 12.7919 | 14.8313 |
| 21 | 11.2000 | 11.5754 | 10.9655 | 12.1854 | 10.4464 | 12.7045 |
| 22 | 14.6000 | 13.8680 | 13.1908 | 14.5451 | 12.7012 | 15.0347 |
| 23 | 14.9000 | 14.9267 | 14.4346 | 15.4189 | 13.8567 | 15.9967 |
| 24 | 15.0000 | 15.2854 | 14.7440 | 15.8268 | 14.1919 | 16.3789 |
| 25 | 15.0000 | 15.3830 | 14.9753 | 15.7906 | 14.3491 | 16.4168 |
| 26 | 14.5000 | 14.5772 | 13.9643 | 15.1901 | 13.4465 | 15.7078 |
| 27 | 13.5000 | 13.3317 | 12.6839 | 13.9795 | 12.1818 | 14.4817 |
| 28 | 11.0000 | 10.9341 | 10.0213 | 11.8469 | 9.6165 | 12.2516 |

Table E.7: Pure HFC-134a, Tu-Cii, triangular-pitch tube bundle, correlation results summary (Model 4)

| Observation | Measured Value | Predicted Value | Lower 95% | Upper 95% | Lower 95% | Upper 95% |
|-------------|----------------|-----------------|-----------|-----------|-----------|-----------|
| | h_o | h_o | Mean | Mean | Predict | Predict |
| 1 | 34.0000 | 33.9719 | 33.1623 | 34.7816 | 32.3717 | 35.5722 |
| 2 | 36.4000 | 36.2176 | 35.5948 | 36.8404 | 34.7033 | 37.7320 |
| 3 | 38.2000 | 37.5704 | 36.9985 | 38.1422 | 36.0762 | 39.0645 |
| 4 | 37.7000 | 38.1834 | 37.6485 | 38.7182 | 36.7030 | 39.6637 |
| 5 | 38.0000 | 37.8518 | 37.3321 | 38.3716 | 36.3769 | 39.3268 |
| 6 | 37.3000 | 36.7131 | 36.1038 | 37.3224 | 35.2042 | 38.2220 |
| 7 | 33.3000 | 34.3029 | 33.3996 | 35.2062 | 32.6533 | 35.9525 |
| 8 | 36.1000 | 36.2223 | 35.5850 | 36.8597 | 34.7020 | 37.7427 |
| 9 | 37.8000 | 38.0882 | 37.6727 | 38.5037 | 36.6466 | 39.5297 |
| 10 | 39.1000 | 39.1590 | 38.7575 | 39.5606 | 37.7215 | 40.5966 |
| 11 | 38.6000 | 39.0413 | 38.6239 | 39.4588 | 37.5992 | 40.4835 |
| 12 | 38.8000 | 38.0095 | 37.6193 | 38.3997 | 36.5750 | 39.4439 |
| 13 | 37.3000 | 36.0737 | 35.6604 | 36.4870 | 34.6328 | 37.5146 |
| 14 | 32.9000 | 32.5272 | 31.8778 | 33.1766 | 31.0017 | 34.0527 |
| 15 | 38.2000 | 38.8089 | 38.1468 | 39.4709 | 37.2780 | 40.3398 |
| 16 | 39.6000 | 40.2343 | 39.8351 | 40.6336 | 38.7974 | 41.6713 |
| 17 | 40.8000 | 40.5360 | 40.1459 | 40.9262 | 39.1016 | 41.9705 |
| 18 | 38.9000 | 39.9133 | 39.5077 | 40.3189 | 38.4745 | 41.3520 |
| 19 | 38.0000 | 38.2957 | 37.9081 | 38.6833 | 36.8620 | 39.7295 |
| 20 | 35.3000 | 35.4712 | 35.0851 | 35.8572 | 34.0378 | 36.9045 |
| 21 | 29.5000 | 30.4104 | 29.7365 | 31.0842 | 28.8743 | 31.9464 |
| 22 | 41.2000 | 40.5391 | 39.7370 | 41.3412 | 38.9426 | 42.1356 |
| 23 | 42.5000 | 41.8638 | 41.2777 | 42.4499 | 40.3642 | 43.3635 |
| 24 | 42.8000 | 41.9814 | 41.4306 | 42.5321 | 40.4952 | 43.4675 |
| 25 | 40.0000 | 40.9579 | 40.4298 | 41.4860 | 39.4799 | 42.4358 |
| 26 | 38.2000 | 38.3223 | 37.8040 | 38.8405 | 36.8478 | 39.7967 |
| 27 | 35.0000 | 34.8262 | 34.2446 | 35.4078 | 33.3283 | 36.3241 |
| 28 | 29.4000 | 28.8072 | 27.8531 | 29.7613 | 27.1292 | 30.4852 |

Table E.8: Pure HFC-134a, Tu-B, triangular-pitch tube bundle, correlation results summary (Model 5)

| Observation | Measured Value | Predicted Value | Lower 95% | Upper 95% | Lower 95% | Upper 95% |
|-------------|----------------|-----------------|-----------|-----------|-----------|-----------|
| | h_o | h_o | Mean | Mean | Predict | Predict |
| 1 | 14.6000 | 14.5915 | 14.1776 | 15.0054 | 13.9522 | 15.2308 |
| 2 | 14.6000 | 14.5206 | 14.2775 | 14.7636 | 13.9761 | 15.0651 |
| 3 | 14.3000 | 14.2481 | 14.0095 | 14.4866 | 13.7056 | 14.7905 |
| 4 | 13.9000 | 13.7762 | 13.5333 | 14.0191 | 13.2318 | 14.3206 |
| 5 | 13.3000 | 13.2240 | 12.9975 | 13.4504 | 12.6867 | 13.7613 |
| 6 | 12.7000 | 12.4902 | 12.2762 | 12.7042 | 11.9581 | 13.0224 |
| 7 | 11.6000 | 11.6891 | 11.3993 | 11.9789 | 11.1222 | 12.2560 |
| 8 | 15.4000 | 15.4875 | 15.2745 | 15.7006 | 14.9557 | 16.0193 |
| 9 | 15.0000 | 15.2308 | 15.0902 | 15.3714 | 14.7237 | 15.7379 |
| 10 | 14.5000 | 14.8866 | 14.7340 | 15.0392 | 14.3760 | 15.3971 |
| 11 | 14.1000 | 14.3492 | 14.1719 | 14.5264 | 13.8307 | 14.8676 |
| 12 | 13.5000 | 13.7571 | 13.5801 | 13.9342 | 13.2387 | 14.2755 |
| 13 | 12.9000 | 13.1412 | 12.9643 | 13.3181 | 12.6229 | 13.6595 |
| 14 | 12.0000 | 12.2708 | 11.9966 | 12.5450 | 11.7117 | 12.8299 |
| 15 | 16.2000 | 15.9624 | 15.7091 | 16.2158 | 15.4133 | 16.5116 |
| 16 | 15.9000 | 15.7292 | 15.5566 | 15.9019 | 15.2123 | 16.2462 |
| 17 | 15.4000 | 15.2511 | 15.0752 | 15.4271 | 14.7331 | 15.7691 |
| 18 | 15.1000 | 14.7620 | 14.5698 | 14.9541 | 14.2382 | 15.2857 |
| 19 | 14.4000 | 14.1689 | 13.9917 | 14.3462 | 13.6504 | 14.6874 |
| 20 | 13.9000 | 13.4621 | 13.2896 | 13.6346 | 12.9453 | 13.9789 |
| 21 | 12.8000 | 12.5486 | 12.3148 | 12.7825 | 12.0082 | 13.0890 |
| 22 | 16.4000 | 16.4258 | 16.1302 | 16.7214 | 15.8559 | 16.9957 |
| 23 | 16.0000 | 16.0827 | 15.8971 | 16.2682 | 15.5613 | 16.6040 |
| 24 | 15.4000 | 15.5777 | 15.3901 | 15.7653 | 15.0556 | 16.0998 |
| 25 | 15.1000 | 15.0791 | 14.8662 | 15.2920 | 14.5474 | 15.6108 |
| 26 | 14.4000 | 14.4726 | 14.1920 | 14.7532 | 13.9104 | 15.0348 |
| 27 | 13.6000 | 13.7407 | 13.4132 | 14.0682 | 13.1536 | 14.3278 |
| 28 | 12.7000 | 12.7742 | 12.3152 | 13.2331 | 12.1048 | 13.4435 |

Table E.9: Pure HFC-134a, Tu-B, square-pitch tube bundle, correlation results summary (Model 6)

| Observation | Measured Value | Predicted Value | Lower 95% | Upper 95% | Lower 95% | Upper 95% |
|-------------|----------------|-----------------|-----------|-----------|-----------|-----------|
| | h_o | h_o | Mean | Mean | Predict | Predict |
| 1 | 14.3000 | 14.2696 | 14.1370 | 14.4023 | 14.0116 | 14.5277 |
| 2 | 14.2000 | 14.0144 | 13.9324 | 14.0965 | 13.7784 | 14.2505 |
| 3 | 13.8000 | 13.7629 | 13.6587 | 13.8672 | 13.5183 | 14.0076 |
| 4 | 13.6000 | 13.5827 | 13.4778 | 13.6876 | 13.3377 | 13.8277 |
| 5 | 13.3000 | 13.3161 | 13.2173 | 13.4149 | 13.0737 | 13.5585 |
| 6 | 13.1000 | 13.0404 | 12.9287 | 13.1522 | 12.7925 | 13.2884 |
| 7 | 12.6000 | 12.6270 | 12.4834 | 12.7706 | 12.3631 | 12.8908 |
| 8 | 14.4000 | 14.5311 | 14.4227 | 14.6396 | 14.2846 | 14.7776 |
| 9 | 14.3000 | 14.4124 | 14.3474 | 14.4774 | 14.1817 | 14.6431 |
| 10 | 14.1000 | 14.2645 | 14.1944 | 14.3345 | 14.0323 | 14.4966 |
| 11 | 14.0000 | 14.0624 | 13.9926 | 14.1322 | 13.8303 | 14.2945 |
| 12 | 13.7000 | 13.8136 | 13.7510 | 13.8762 | 13.5836 | 14.0436 |
| 13 | 13.5000 | 13.4635 | 13.3848 | 13.5421 | 13.2286 | 13.6984 |
| 14 | 12.9000 | 12.9709 | 12.8207 | 13.1210 | 12.7034 | 13.2383 |
| 15 | 14.7000 | 14.7556 | 14.6589 | 14.8523 | 14.5141 | 14.9972 |
| 16 | 14.9000 | 14.7182 | 14.6541 | 14.7823 | 14.4878 | 14.9486 |
| 17 | 14.8000 | 14.6859 | 14.6242 | 14.7477 | 14.4561 | 14.9157 |
| 18 | 14.7000 | 14.6082 | 14.5402 | 14.6762 | 14.3766 | 14.8398 |
| 19 | 14.4000 | 14.3734 | 14.3003 | 14.4466 | 14.1403 | 14.6066 |
| 20 | 14.2000 | 14.0678 | 13.9891 | 14.1464 | 13.8328 | 14.3027 |
| 21 | 13.3000 | 13.3426 | 13.1963 | 13.4888 | 13.0772 | 13.6079 |
| 22 | 15.0000 | 14.9055 | 14.7890 | 15.0219 | 14.6554 | 15.1556 |
| 23 | 14.9000 | 14.9868 | 14.9109 | 15.0627 | 14.7528 | 15.2208 |
| 24 | 14.9000 | 15.0131 | 14.9350 | 15.0913 | 14.7784 | 15.2479 |
| 25 | 14.9000 | 14.9795 | 14.8860 | 15.0730 | 14.7392 | 15.2198 |
| 26 | 14.8000 | 14.8490 | 14.7433 | 14.9547 | 14.6037 | 15.0943 |
| 27 | 14.7000 | 14.5840 | 14.4827 | 14.6854 | 14.3406 | 14.8275 |
| 28 | 14.1000 | 14.0989 | 13.9090 | 14.2888 | 13.8072 | 14.3905 |

Table E.10: HFC-134a lubricant effects testing, plain-surface, triangular-pitch tube bundle, correlation results summary (Model 7)

| Observation | Measured Value | Predicted Value | Lower 95% | Upper 95% | Lower 95% | Upper 95% |
|-------------|----------------|-----------------|-----------|-----------|-----------|-----------|
| | h_o | h_o | Mean | Mean | Predict | Predict |
| 1 | 3.8300 | 3.8012 | 3.7032 | 3.8992 | 3.6237 | 3.9788 |
| 2 | 3.8700 | 3.7997 | 3.7342 | 3.8653 | 3.6378 | 3.9616 |
| 3 | 3.8400 | 3.7666 | 3.7071 | 3.8260 | 3.6070 | 3.9261 |
| 4 | 3.7800 | 3.7231 | 3.6603 | 3.7860 | 3.5623 | 3.8840 |
| 5 | 3.7000 | 3.6719 | 3.6070 | 3.7369 | 3.5103 | 3.8336 |
| 6 | 3.5600 | 3.5915 | 3.5169 | 3.6661 | 3.4257 | 3.7573 |
| 7 | 3.3700 | 3.4514 | 3.3399 | 3.5628 | 3.2660 | 3.6367 |
| 8 | 4.5800 | 4.6560 | 4.5537 | 4.7584 | 4.4761 | 4.8360 |
| 9 | 4.5100 | 4.5114 | 4.4461 | 4.5767 | 4.3496 | 4.6732 |
| 10 | 4.4300 | 4.4332 | 4.3714 | 4.4950 | 4.2727 | 4.5936 |
| 11 | 4.2800 | 4.2962 | 4.2328 | 4.3597 | 4.1351 | 4.4573 |
| 12 | 4.1100 | 4.1384 | 4.0753 | 4.2015 | 3.9775 | 4.2994 |
| 13 | 3.9000 | 3.8810 | 3.8107 | 3.9513 | 3.7171 | 4.0449 |
| 14 | 3.6700 | 3.5591 | 3.4471 | 3.6712 | 3.3734 | 3.7448 |
| 15 | 5.6500 | 5.6514 | 5.5650 | 5.7378 | 5.4800 | 5.8228 |
| 16 | 5.5800 | 5.5527 | 5.4871 | 5.6183 | 5.3907 | 5.7146 |
| 17 | 5.4600 | 5.4483 | 5.3952 | 5.5013 | 5.2910 | 5.6055 |
| 18 | 5.3300 | 5.3360 | 5.2838 | 5.3883 | 5.1790 | 5.4930 |
| 19 | 5.2000 | 5.2255 | 5.1675 | 5.2836 | 5.0665 | 5.3846 |
| 20 | 5.0100 | 5.0760 | 5.0075 | 5.1446 | 4.9129 | 5.2392 |
| 21 | 4.8000 | 4.8468 | 4.7655 | 4.9282 | 4.6779 | 5.0157 |
| 22 | 6.3100 | 6.4761 | 6.4013 | 6.5510 | 6.3102 | 6.6420 |
| 23 | 6.3500 | 6.3339 | 6.2734 | 6.3944 | 6.1740 | 6.4939 |
| 24 | 6.2000 | 6.1571 | 6.1071 | 6.2071 | 6.0008 | 6.3134 |
| 25 | 5.9600 | 5.9152 | 5.8732 | 5.9571 | 5.7613 | 6.0691 |
| 26 | 5.6600 | 5.7265 | 5.6772 | 5.7758 | 5.5705 | 5.8826 |
| 27 | 5.3800 | 5.4514 | 5.3820 | 5.5207 | 5.2879 | 5.6148 |
| 28 | 5.0300 | 4.9891 | 4.8825 | 5.0957 | 4.8067 | 5.1716 |
| 29 | 6.9200 | 7.0728 | 6.9747 | 7.1709 | 6.8952 | 7.2504 |
| 30 | 7.1400 | 7.2056 | 7.1385 | 7.2727 | 7.0430 | 7.3681 |
| 31 | 7.2800 | 7.2785 | 7.2175 | 7.3395 | 7.1183 | 7.4386 |
| 32 | 7.2800 | 7.2530 | 7.1886 | 7.3173 | 7.0915 | 7.4144 |
| 33 | 7.1600 | 7.1127 | 7.0459 | 7.1795 | 6.9502 | 7.2751 |
| 34 | 6.9800 | 6.9084 | 6.8317 | 6.9852 | 6.7417 | 7.0752 |
| 35 | 6.6300 | 6.6175 | 6.5093 | 6.7256 | 6.4341 | 6.8008 |
| 36 | 8.2800 | 8.1386 | 8.0404 | 8.2367 | 7.9609 | 8.3162 |
| 37 | 8.3500 | 8.2455 | 8.1788 | 8.3121 | 8.0831 | 8.4079 |
| 38 | 8.2800 | 8.2828 | 8.2195 | 8.3460 | 8.1218 | 8.4438 |
| 39 | 8.2300 | 8.2258 | 8.1600 | 8.2915 | 8.0638 | 8.3878 |
| 40 | 8.0800 | 8.0936 | 8.0283 | 8.1589 | 7.9318 | 8.2555 |
| 41 | 7.7800 | 7.7837 | 7.7143 | 7.8531 | 7.6202 | 7.9472 |
| 42 | 7.3100 | 7.3648 | 7.2471 | 7.4825 | 7.1757 | 7.5539 |

Table E.11: HFC-134a lubricant effects testing, W-40 fpi, triangular-pitch tube bundle, correlation results summary (Model 8)

| Observation | Measured Value | Predicted Value | Lower 95% | Upper 95% | Lower 95% | Upper 95% |
|-------------|----------------|-----------------|-----------|-----------|-----------|-----------|
| | h_o | h_o | Mean | Mean | Predict | Predict |
| 1 | 9.4900 | 7.9913 | 5.6426 | 10.3400 | 3.8692 | 12.1134 |
| 2 | 9.7100 | 8.5284 | 6.9626 | 10.0942 | 4.7965 | 12.2604 |
| 3 | 9.8800 | 8.9496 | 7.4065 | 10.4927 | 5.2271 | 12.6721 |
| 4 | 9.8800 | 9.3800 | 7.7430 | 11.0170 | 5.6176 | 13.1424 |
| 5 | 9.6000 | 9.5286 | 7.9358 | 11.1214 | 5.7852 | 13.2720 |
| 6 | 8.7700 | 9.4900 | 7.8109 | 11.1691 | 5.7091 | 13.2709 |
| 7 | 7.4000 | 9.0015 | 6.4480 | 11.5549 | 4.7593 | 13.2436 |
| 8 | 10.5000 | 12.1185 | 9.8740 | 14.3630 | 8.0548 | 16.1822 |
| 9 | 10.6000 | 11.8027 | 10.2441 | 13.3614 | 8.0738 | 15.5317 |
| 10 | 10.5000 | 11.4650 | 9.9199 | 13.0101 | 7.7417 | 15.1883 |
| 11 | 10.4000 | 10.7240 | 9.0718 | 12.3761 | 6.9550 | 14.4930 |
| 12 | 9.8600 | 9.7323 | 8.1706 | 11.2940 | 6.0021 | 13.4625 |
| 13 | 8.8700 | 8.1212 | 6.4464 | 9.7960 | 4.3422 | 11.9002 |
| 14 | 7.3300 | 5.9570 | 3.4413 | 8.4727 | 1.7375 | 10.1766 |
| 15 | 13.1000 | 13.8610 | 12.0086 | 15.7134 | 10.0000 | 17.7220 |
| 16 | 13.3000 | 13.8795 | 12.5369 | 15.2221 | 10.2356 | 17.5235 |
| 17 | 13.4000 | 13.8068 | 12.7868 | 14.8268 | 10.2690 | 17.3446 |
| 18 | 13.4000 | 13.6098 | 12.6521 | 14.5676 | 10.0895 | 17.1302 |
| 19 | 13.1000 | 13.1992 | 12.0456 | 14.3528 | 9.6206 | 16.7778 |
| 20 | 12.1000 | 12.4525 | 11.0156 | 13.8895 | 8.7728 | 16.1323 |
| 21 | 9.7300 | 11.2703 | 9.5585 | 12.9821 | 7.4748 | 15.0658 |
| 22 | 17.7000 | 16.3839 | 14.7126 | 18.0551 | 12.6065 | 20.1613 |
| 23 | 16.1000 | 15.6047 | 14.2987 | 16.9107 | 11.9741 | 19.2353 |
| 24 | 14.8000 | 14.6688 | 13.5879 | 15.7498 | 11.1129 | 18.2247 |
| 25 | 13.0000 | 13.2802 | 12.3262 | 14.2341 | 9.7608 | 16.7995 |
| 26 | 11.4000 | 11.5918 | 10.5721 | 12.6116 | 8.0541 | 15.1296 |
| 27 | 9.8000 | 9.3904 | 8.0339 | 10.7469 | 5.7413 | 13.0395 |
| 28 | 7.9700 | 5.9010 | 3.7336 | 8.0684 | 1.8793 | 9.9226 |
| 29 | 23.2000 | 23.9108 | 21.6686 | 26.1531 | 19.8484 | 27.9733 |
| 30 | 23.1000 | 24.4210 | 22.8618 | 25.9803 | 20.6918 | 28.1502 |
| 31 | 21.6000 | 23.3589 | 21.8210 | 24.8967 | 19.6386 | 27.0792 |
| 32 | 19.6000 | 21.2341 | 19.6285 | 22.8397 | 17.4852 | 24.9829 |
| 33 | 16.0000 | 17.3246 | 15.7429 | 18.9063 | 13.5860 | 21.0633 |
| 34 | 12.6000 | 12.6668 | 10.9397 | 14.3939 | 8.8643 | 16.4692 |
| 35 | 9.4500 | 5.6903 | 3.0932 | 8.2873 | 1.4217 | 9.9588 |
| 36 | 31.7000 | 31.6826 | 29.3528 | 34.0124 | 27.5712 | 35.7940 |
| 37 | 33.5000 | 32.0999 | 30.5609 | 33.6390 | 28.3791 | 35.8207 |
| 38 | 33.6000 | 31.1012 | 29.5432 | 32.6592 | 27.3725 | 34.8299 |
| 39 | 32.0000 | 28.2690 | 26.6622 | 29.8758 | 24.5196 | 32.0183 |
| 40 | 24.6000 | 24.1306 | 22.6466 | 25.6146 | 20.4322 | 27.8290 |
| 41 | 16.4000 | 19.5889 | 17.9112 | 21.2665 | 15.8086 | 23.3691 |
| 42 | 10.4000 | 12.2714 | 9.6171 | 14.9257 | 7.9678 | 16.5750 |

Table E.12: HFC-134a lubricant effects testing, W-SC, triangular-pitch tube bundle, correlation results summary (Model 9)

| Observation | Measured Value | Predicted Value | Lower 95% | Upper 95% | Lower 95% | Upper 95% |
|-------------|----------------|-----------------|-----------|-----------|-----------|-----------|
| | h_o | h_o | Mean | Mean | Predict | Predict |
| 1 | 13.3000 | 11.9582 | 10.6086 | 13.3078 | 9.3505 | 14.5659 |
| 2 | 13.9000 | 13.5613 | 12.6224 | 14.5003 | 11.1405 | 15.9822 |
| 3 | 14.7000 | 14.6656 | 13.7424 | 15.5889 | 12.2508 | 17.0804 |
| 4 | 14.8000 | 15.2058 | 14.2461 | 16.1656 | 12.7769 | 17.6348 |
| 5 | 15.0000 | 15.1474 | 14.2047 | 16.0902 | 12.7251 | 17.5697 |
| 6 | 13.6000 | 14.4886 | 13.4607 | 15.5165 | 12.0319 | 16.9453 |
| 7 | 11.0000 | 12.7171 | 11.1930 | 14.2412 | 10.0149 | 15.4193 |
| 8 | 14.4000 | 15.0503 | 13.6652 | 16.4353 | 12.4240 | 17.6765 |
| 9 | 14.8000 | 16.1262 | 15.1577 | 17.0946 | 13.6937 | 18.5586 |
| 10 | 15.3000 | 16.4070 | 15.5026 | 17.3115 | 13.9994 | 18.8147 |
| 11 | 15.3000 | 16.1167 | 15.1376 | 17.0959 | 13.6800 | 18.5534 |
| 12 | 15.1000 | 14.8254 | 13.9049 | 15.7460 | 12.4117 | 17.2392 |
| 13 | 14.2000 | 13.2830 | 12.3205 | 14.2456 | 10.8530 | 15.7131 |
| 14 | 11.2000 | 9.6683 | 8.0999 | 11.2367 | 6.9409 | 12.3957 |
| 15 | 15.4000 | 14.8687 | 13.9221 | 15.8153 | 12.4449 | 17.2925 |
| 16 | 16.8000 | 16.3649 | 15.6507 | 17.0791 | 14.0221 | 18.7077 |
| 17 | 18.6000 | 17.4489 | 16.7948 | 18.1031 | 15.1237 | 19.7741 |
| 18 | 18.5000 | 17.5331 | 16.8811 | 18.1850 | 15.2084 | 19.8577 |
| 19 | 18.3000 | 17.0671 | 16.4589 | 17.6754 | 14.7544 | 19.3799 |
| 20 | 16.8000 | 15.6570 | 14.9560 | 16.3580 | 13.3181 | 17.9958 |
| 21 | 12.9000 | 13.3514 | 12.3175 | 14.3852 | 10.8922 | 15.8106 |
| 22 | 19.1000 | 19.0420 | 18.1002 | 19.9838 | 16.6201 | 21.4639 |
| 23 | 19.8000 | 20.4386 | 19.7824 | 21.0948 | 18.1128 | 22.7644 |
| 24 | 20.5000 | 20.6434 | 20.0552 | 21.2316 | 18.3359 | 22.9510 |
| 25 | 20.5000 | 20.2924 | 19.6835 | 20.9012 | 17.9795 | 22.6053 |
| 26 | 19.6000 | 19.0478 | 18.4797 | 19.6158 | 16.7453 | 21.3502 |
| 27 | 16.8000 | 16.6909 | 16.0927 | 17.2892 | 14.3808 | 19.0010 |
| 28 | 12.6000 | 13.0774 | 12.0548 | 14.0999 | 10.6229 | 15.5318 |
| 29 | 18.1000 | 18.6460 | 17.2491 | 20.0430 | 16.0135 | 21.2785 |
| 30 | 18.5000 | 20.3373 | 19.3603 | 21.3143 | 17.9015 | 22.7731 |
| 31 | 19.1000 | 21.0734 | 20.1163 | 22.0306 | 18.6455 | 23.5014 |
| 32 | 19.3000 | 20.7976 | 19.7997 | 21.7956 | 18.3533 | 23.2419 |
| 33 | 19.6000 | 19.5530 | 18.5708 | 20.5352 | 17.1151 | 21.9909 |
| 34 | 18.9000 | 17.4805 | 16.4262 | 18.5348 | 15.0126 | 19.9483 |
| 35 | 14.1000 | 13.7017 | 12.0963 | 15.3071 | 10.9529 | 16.4505 |
| 36 | 26.3000 | 24.7334 | 23.2654 | 26.2014 | 22.0625 | 27.4043 |
| 37 | 27.0000 | 26.1714 | 25.2152 | 27.1276 | 23.7438 | 28.5989 |
| 38 | 27.0000 | 26.6569 | 25.7110 | 27.6028 | 24.2334 | 29.0804 |
| 39 | 26.3000 | 26.2367 | 25.2323 | 27.2410 | 23.7897 | 28.6836 |
| 40 | 25.2000 | 24.6734 | 23.6851 | 25.6618 | 22.2330 | 27.1138 |
| 41 | 22.3000 | 21.7250 | 20.6893 | 22.7607 | 19.2650 | 24.1850 |
| 42 | 15.6000 | 17.5692 | 15.9097 | 19.2286 | 14.7884 | 20.3499 |

Table E.13: HFC-134a lubricant effects testing, Tu-B, triangular-pitch tube bundle, correlation results summary (Model 10)

| Observation | Measured Value | Predicted Value | Lower 95% | Upper 95% | Lower 95% | Upper 95% |
|-------------|----------------|-----------------|-----------|-----------|-----------|-----------|
| | h_o | h_o | Mean | Mean | Predict | Predict |
| 1 | 14.6000 | 13.5142 | 11.8450 | 15.1834 | 10.4758 | 16.5526 |
| 2 | 14.6000 | 13.3747 | 12.2261 | 14.5233 | 10.5881 | 16.1612 |
| 3 | 14.3000 | 13.2632 | 12.1402 | 14.3862 | 10.4871 | 16.0394 |
| 4 | 13.9000 | 13.1811 | 12.0073 | 14.3550 | 10.3840 | 15.9782 |
| 5 | 13.3000 | 13.0740 | 11.9200 | 14.2279 | 10.2852 | 15.8628 |
| 6 | 12.7000 | 12.8924 | 11.6471 | 14.1377 | 10.0646 | 15.7202 |
| 7 | 11.6000 | 12.4920 | 10.6459 | 14.3380 | 9.3529 | 15.6310 |
| 8 | 16.2000 | 17.3170 | 15.6033 | 19.0306 | 14.2539 | 20.3801 |
| 9 | 15.9000 | 17.0551 | 15.8900 | 18.2201 | 14.2617 | 19.8485 |
| 10 | 15.4000 | 16.3612 | 15.2383 | 17.4841 | 13.5852 | 19.1373 |
| 11 | 15.1000 | 15.7093 | 14.5336 | 16.8849 | 12.9114 | 18.5071 |
| 12 | 14.4000 | 14.8962 | 13.7596 | 16.0329 | 12.1145 | 17.6779 |
| 13 | 13.9000 | 13.7061 | 12.4939 | 14.9183 | 10.8927 | 16.5195 |
| 14 | 12.8000 | 11.8636 | 9.9411 | 13.7862 | 8.6790 | 15.0483 |
| 15 | 23.4000 | 23.2599 | 21.5161 | 25.0037 | 20.1799 | 26.3399 |
| 16 | 26.7000 | 28.4291 | 27.3158 | 29.5424 | 25.6569 | 31.2013 |
| 17 | 30.3000 | 32.0764 | 30.9885 | 33.1643 | 29.3143 | 34.8385 |
| 18 | 33.8000 | 34.3650 | 33.2524 | 35.4777 | 31.5931 | 37.1370 |
| 19 | 36.4000 | 35.7082 | 34.6651 | 36.7514 | 32.9634 | 38.4530 |
| 20 | 36.9000 | 35.9129 | 34.7951 | 37.0307 | 33.1389 | 38.6870 |
| 21 | 33.4000 | 34.9313 | 33.2046 | 36.6580 | 31.8609 | 38.0016 |
| 22 | 31.5000 | 29.8231 | 28.1699 | 31.4762 | 26.7935 | 32.8527 |
| 23 | 33.9000 | 33.6889 | 32.5831 | 34.7948 | 30.9197 | 36.4582 |
| 24 | 36.4000 | 36.9162 | 35.8582 | 37.9742 | 34.1657 | 39.6667 |
| 25 | 39.3000 | 38.8044 | 37.7052 | 39.9035 | 36.0378 | 41.5709 |
| 26 | 40.9000 | 39.7388 | 38.7072 | 40.7704 | 36.9984 | 42.4792 |
| 27 | 40.6000 | 39.2560 | 38.1784 | 40.3336 | 36.4979 | 42.0141 |
| 28 | 36.6000 | 37.1897 | 35.4135 | 38.9659 | 34.0913 | 40.2882 |
| 29 | 20.3000 | 19.9503 | 18.2002 | 21.7004 | 16.8667 | 23.0339 |
| 30 | 23.4000 | 24.5615 | 23.3998 | 25.7232 | 21.7695 | 27.3535 |
| 31 | 27.1000 | 28.0824 | 26.9181 | 29.2467 | 25.2893 | 30.8755 |
| 32 | 31.2000 | 31.0377 | 29.8167 | 32.2586 | 28.2205 | 33.8548 |
| 33 | 35.0000 | 33.7929 | 32.6041 | 34.9818 | 30.9895 | 36.5964 |
| 34 | 37.4000 | 35.8360 | 34.5591 | 37.1128 | 32.9941 | 38.6778 |
| 35 | 36.7000 | 37.3788 | 35.4825 | 39.2751 | 34.2100 | 40.5477 |
| 36 | 29.2000 | 27.7728 | 26.0844 | 29.4611 | 24.7238 | 30.8217 |
| 37 | 31.4000 | 31.4927 | 30.3836 | 32.6019 | 28.7222 | 34.2633 |
| 38 | 34.4000 | 35.7555 | 34.5992 | 36.9117 | 32.9657 | 38.5452 |
| 39 | 38.3000 | 39.0886 | 37.8558 | 40.3213 | 36.2663 | 41.9109 |
| 40 | 41.4000 | 40.8827 | 39.7406 | 42.0248 | 38.0988 | 43.6666 |
| 41 | 44.2000 | 42.3602 | 41.1778 | 43.5425 | 39.5595 | 45.1608 |
| 42 | 41.9000 | 43.9080 | 41.9853 | 45.8307 | 40.7233 | 47.0928 |

Table E.14: HCFC-123 lubricant effects testing, plain-surface, triangular-pitch tube bundle, correlation results summary (Model 11)

| Observation | Measured Value | Predicted Value | Lower 95% | Upper 95% | Lower 95% | Upper 95% |
|-------------|----------------|-----------------|-----------|-----------|-----------|-----------|
| | h_o | h_o | Mean | Mean | Predict | Predict |
| 1 | 2.0200 | 2.0365 | 2.0099 | 2.0631 | 1.9886 | 2.0844 |
| 2 | 1.9200 | 1.9219 | 1.9052 | 1.9386 | 1.8787 | 1.9651 |
| 3 | 1.8200 | 1.8295 | 1.8124 | 1.8466 | 1.7862 | 1.8729 |
| 4 | 1.7500 | 1.7604 | 1.7408 | 1.7800 | 1.7160 | 1.8048 |
| 5 | 1.7100 | 1.7065 | 1.6865 | 1.7265 | 1.6620 | 1.7511 |
| 6 | 1.7000 | 1.6754 | 1.6545 | 1.6962 | 1.6304 | 1.7203 |
| 7 | 1.6800 | 1.6834 | 1.6556 | 1.7112 | 1.6348 | 1.7320 |
| 8 | 2.0900 | 2.0716 | 2.0468 | 2.0963 | 2.0247 | 2.1185 |
| 9 | 1.9800 | 1.9740 | 1.9568 | 1.9911 | 1.9306 | 2.0174 |
| 10 | 1.9000 | 1.8949 | 1.8760 | 1.9138 | 1.8508 | 1.9390 |
| 11 | 1.8200 | 1.8202 | 1.8014 | 1.8390 | 1.7761 | 1.8642 |
| 12 | 1.7800 | 1.7832 | 1.7648 | 1.8016 | 1.7393 | 1.8271 |
| 13 | 1.7600 | 1.7650 | 1.7456 | 1.7843 | 1.7207 | 1.8093 |
| 14 | 1.7600 | 1.7676 | 1.7402 | 1.7950 | 1.7193 | 1.8159 |
| 15 | 1.8900 | 1.9046 | 1.8684 | 1.9408 | 1.8508 | 1.9584 |
| 16 | 2.0400 | 2.0124 | 1.9910 | 2.0337 | 1.9672 | 2.0576 |
| 17 | 2.1100 | 2.1157 | 2.0837 | 2.1476 | 2.0646 | 2.1667 |
| 18 | 2.1300 | 2.1322 | 2.1088 | 2.1555 | 2.0860 | 2.1784 |
| 19 | 2.1400 | 2.1545 | 2.1314 | 2.1777 | 2.1085 | 2.2006 |
| 20 | 2.1600 | 2.1514 | 2.1201 | 2.1827 | 2.1007 | 2.2020 |
| 21 | 2.2100 | 2.2093 | 2.1706 | 2.2480 | 2.1537 | 2.2649 |
| 22 | 1.5600 | 1.5730 | 1.5480 | 1.5981 | 1.5260 | 1.6201 |
| 23 | 1.7900 | 1.8023 | 1.7858 | 1.8187 | 1.7592 | 1.8454 |
| 24 | 2.0200 | 1.9794 | 1.9624 | 1.9965 | 1.9361 | 2.0227 |
| 25 | 2.1800 | 2.1586 | 2.1400 | 2.1771 | 2.1146 | 2.2025 |
| 26 | 2.3100 | 2.3107 | 2.2917 | 2.3296 | 2.2666 | 2.3548 |
| 27 | 2.4100 | 2.4414 | 2.4209 | 2.4620 | 2.3966 | 2.4863 |
| 28 | 2.5400 | 2.5367 | 2.5096 | 2.5638 | 2.4885 | 2.5849 |
| 29 | 1.6300 | 1.6058 | 1.5796 | 1.6320 | 1.5581 | 1.6534 |
| 30 | 1.8200 | 1.8420 | 1.8243 | 1.8596 | 1.7984 | 1.8855 |
| 31 | 2.0300 | 2.0554 | 2.0371 | 2.0736 | 2.0115 | 2.0992 |
| 32 | 2.2400 | 2.2395 | 2.2199 | 2.2590 | 2.1951 | 2.2838 |
| 33 | 2.4200 | 2.4117 | 2.3930 | 2.4305 | 2.3677 | 2.4558 |
| 34 | 2.5600 | 2.5710 | 2.5518 | 2.5902 | 2.5268 | 2.6152 |
| 35 | 2.7100 | 2.6927 | 2.6634 | 2.7220 | 2.6433 | 2.7421 |

Table E.15: HCFC-123 lubricant effects testing, Tu-Cii, triangular-pitch tube bundle, correlation results summary (Model 12)

| Observation | Measured Value | Predicted Value | Lower 95% | Upper 95% | Lower 95% | Upper 95% |
|-------------|----------------|-----------------|-----------|-----------|-----------|-----------|
| | h_o | h_o | Mean | Mean | Predict | Predict |
| 1 | 4.8200 | 5.2236 | 4.6398 | 5.8074 | 4.1669 | 6.2803 |
| 2 | 4.8700 | 5.7636 | 5.3649 | 6.1623 | 4.7968 | 6.7305 |
| 3 | 5.7600 | 6.5604 | 6.1528 | 6.9681 | 5.5899 | 7.5310 |
| 4 | 8.0900 | 7.6510 | 7.2133 | 8.0887 | 6.6675 | 8.6346 |
| 5 | 9.1200 | 8.5599 | 8.1446 | 8.9752 | 7.5861 | 9.5337 |
| 6 | 9.8900 | 9.6086 | 9.1536 | 10.0637 | 8.6172 | 10.6000 |
| 7 | 10.6000 | 10.4152 | 9.7916 | 11.0387 | 9.3360 | 11.4943 |
| 8 | 5.4500 | 4.7281 | 4.1336 | 5.3226 | 3.6654 | 5.7908 |
| 9 | 5.4900 | 4.9268 | 4.5178 | 5.3358 | 3.9557 | 5.8979 |
| 10 | 5.6500 | 5.4574 | 5.0584 | 5.8564 | 4.4904 | 6.4243 |
| 11 | 6.1900 | 6.2543 | 5.8355 | 6.6730 | 5.2790 | 7.2295 |
| 12 | 6.7500 | 6.8387 | 6.4341 | 7.2434 | 5.8695 | 7.8080 |
| 13 | 6.9500 | 7.2771 | 6.8290 | 7.7252 | 6.2889 | 8.2653 |
| 14 | 7.3700 | 7.7352 | 7.0732 | 8.3972 | 6.6334 | 8.8371 |
| 15 | 6.0800 | 5.7975 | 5.1731 | 6.4219 | 4.7178 | 6.8772 |
| 16 | 6.7600 | 6.5970 | 6.1161 | 7.0779 | 5.5935 | 7.6005 |
| 17 | 7.4300 | 7.5776 | 7.1637 | 7.9915 | 6.6044 | 8.5508 |
| 18 | 8.1100 | 8.4526 | 8.0255 | 8.8796 | 7.4737 | 9.4314 |
| 19 | 8.9500 | 9.1704 | 8.7398 | 9.6010 | 8.1900 | 10.1508 |
| 20 | 9.6800 | 9.6357 | 9.1758 | 10.0957 | 8.6421 | 10.6294 |
| 21 | 10.2000 | 9.9792 | 9.2348 | 10.7236 | 8.8260 | 11.1324 |
| 22 | 6.1900 | 5.8756 | 5.2933 | 6.4580 | 4.8197 | 6.9315 |
| 23 | 6.8400 | 6.4999 | 6.0945 | 6.9053 | 5.5303 | 7.4695 |
| 24 | 7.4100 | 7.2755 | 6.8837 | 7.6674 | 6.3115 | 8.2395 |
| 25 | 8.2100 | 8.2623 | 7.8432 | 8.6815 | 7.2869 | 9.2378 |
| 26 | 9.3300 | 9.4319 | 9.0058 | 9.8580 | 8.4535 | 10.4104 |
| 27 | 11.0000 | 11.0350 | 10.5672 | 11.5028 | 10.0377 | 12.0323 |
| 28 | 12.2000 | 12.4840 | 11.8452 | 13.1228 | 11.3960 | 13.5721 |
| 29 | 7.1700 | 7.4876 | 6.8797 | 8.0956 | 6.4174 | 8.5579 |
| 30 | 7.9100 | 8.0828 | 7.6903 | 8.4753 | 7.1185 | 9.0471 |
| 31 | 8.7100 | 8.9755 | 8.5703 | 9.3807 | 8.0060 | 9.9450 |
| 32 | 9.9300 | 10.0316 | 9.6091 | 10.4540 | 9.0547 | 11.0084 |
| 33 | 11.2000 | 11.1310 | 10.7229 | 11.5392 | 10.1603 | 12.1018 |
| 34 | 12.8000 | 12.4614 | 12.0505 | 12.8723 | 11.4895 | 13.4333 |
| 35 | 14.1000 | 13.9658 | 13.2722 | 14.6594 | 12.8447 | 15.0869 |

Table E.16: HCFC-123 lubricant effects testing, Tu-Bi, triangular-pitch tube bundle, correlation results summary (Model 13)

| Observation | Measured Value | Predicted Value | Lower 95% | Upper 95% | Lower 95% | Upper 95% |
|-------------|----------------|-----------------|-----------|-----------|-----------|-----------|
| | h_o | h_o | Mean | Mean | Predict | Predict |
| 1 | 21.7000 | 21.7594 | 21.4626 | 22.0563 | 21.2616 | 22.2572 |
| 2 | 22.7000 | 22.7186 | 22.5155 | 22.9218 | 22.2703 | 23.1669 |
| 3 | 23.3000 | 23.5816 | 23.3868 | 23.7763 | 23.1370 | 24.0261 |
| 4 | 24.0000 | 23.9083 | 23.7144 | 24.1023 | 23.4641 | 24.3525 |
| 5 | 24.0000 | 23.8477 | 23.6509 | 24.0444 | 23.4022 | 24.2931 |
| 6 | 23.2000 | 23.0025 | 22.7820 | 23.2231 | 22.5461 | 23.4590 |
| 7 | 20.6000 | 20.8584 | 20.5639 | 21.1529 | 20.3620 | 21.3548 |
| 8 | 22.8000 | 22.6422 | 22.3638 | 22.9205 | 22.1552 | 23.1292 |
| 9 | 23.9000 | 23.6852 | 23.4959 | 23.8745 | 23.2430 | 24.1274 |
| 10 | 24.4000 | 24.7472 | 24.5428 | 24.9516 | 24.2983 | 25.1961 |
| 11 | 25.0000 | 25.0567 | 24.8649 | 25.2485 | 24.6134 | 25.5000 |
| 12 | 24.9000 | 24.8357 | 24.6358 | 25.0356 | 24.3889 | 25.2826 |
| 13 | 24.0000 | 23.8102 | 23.5970 | 24.0235 | 23.3573 | 24.2632 |
| 14 | 21.4000 | 21.4462 | 21.1310 | 21.7615 | 20.9372 | 21.9552 |
| 15 | 17.2000 | 17.2178 | 16.9193 | 17.5164 | 16.7190 | 17.7167 |
| 16 | 18.1000 | 18.0619 | 17.8440 | 18.2799 | 17.6067 | 18.5171 |
| 17 | 18.7000 | 18.7683 | 18.5734 | 18.9631 | 18.3237 | 19.2129 |
| 18 | 19.3000 | 19.2415 | 19.0661 | 19.4169 | 18.8051 | 19.6779 |
| 19 | 19.4000 | 19.3206 | 19.1363 | 19.5050 | 18.8806 | 19.7607 |
| 20 | 18.7000 | 18.8415 | 18.6153 | 19.0677 | 18.3823 | 19.3007 |
| 21 | 17.2000 | 17.1483 | 16.8559 | 17.4408 | 16.6531 | 17.6436 |
| 22 | 13.7000 | 13.8748 | 13.5730 | 14.1766 | 13.3740 | 14.3756 |
| 23 | 15.1000 | 14.9498 | 14.7467 | 15.1529 | 14.5015 | 15.3981 |
| 24 | 15.9000 | 16.0167 | 15.8187 | 16.2147 | 15.5707 | 16.4627 |
| 25 | 17.3000 | 16.9372 | 16.7386 | 17.1357 | 16.4909 | 17.3834 |
| 26 | 17.6000 | 17.5339 | 17.3386 | 17.7292 | 17.0891 | 17.9787 |
| 27 | 17.4000 | 17.5176 | 17.2938 | 17.7413 | 17.0596 | 17.9756 |
| 28 | 16.4000 | 16.5023 | 16.2020 | 16.8026 | 16.0024 | 17.0022 |
| 29 | 15.3000 | 15.1650 | 14.8730 | 15.4571 | 14.6701 | 15.6600 |
| 30 | 16.5000 | 16.5238 | 16.3220 | 16.7256 | 16.0761 | 16.9715 |
| 31 | 17.7000 | 17.8416 | 17.6517 | 18.0316 | 17.3992 | 18.2841 |
| 32 | 18.7000 | 18.7216 | 18.5308 | 18.9123 | 18.2787 | 19.1644 |
| 33 | 18.9000 | 19.1399 | 18.9354 | 19.3445 | 18.6910 | 19.5889 |
| 34 | 19.0000 | 18.9680 | 18.7517 | 19.1843 | 18.5136 | 19.4225 |
| 35 | 17.8000 | 17.6078 | 17.2786 | 17.9369 | 17.0900 | 18.1255 |